

# Assessment of Occupant Response in Frontal Bus Crash Scenarios using Human Body Models to Improve Public Transportation Safety

by

Christopher Cameron Pastula

A thesis

presented to the University of Waterloo

in fulfillment of the

thesis requirement for the degree of

Master of Applied Science

in

Mechanical and Mechatronics Engineering

Waterloo, Ontario, Canada, 2022

© Christopher Cameron Pastula 2022

## **Author's Declaration**

I hereby declare that I am the sole author of this thesis. This is a true copy of the thesis, including any required final revisions, as accepted by my examiners.

I understand that my thesis may be made electronically available to the public.

## Abstract

There has been limited investigation regarding occupant safety in transit bus crash scenarios. Experimental testing and numerical modelling can provide the insight required to reduce injury risk to transit bus passengers. Transport Canada (TC) has conducted a series of full-scale bus crash and frontal impact deceleration sled experiments as part of a research program to inform the development of crashworthiness standards for transit buses. Anthropomorphic Test Devices (ATD) were used in the TC experiments to assess occupant injury. ATDs have known limitations in replicating the response of a human passenger, primarily due to an overly stiff neck and thorax. Finite element ATDs and Human Body Models (HBM) are biofidelic occupant surrogate models that can be used in numerical crash simulations to predict response and localized tissue injury. This study expanded on the TC experimental work by using numerical simulations to assess transit bus passenger response and injury risk using a contemporary detailed HBM in a frontal impact scenario.

A numerical model of the TC sled buck was developed and validated for a series of eight frontal impacts utilizing 50<sup>th</sup> and 5<sup>th</sup> percentile Hybrid III (HIII) ATD models as the occupants. The Global Human Body Models Consortium (GHBMC) male 50<sup>th</sup> percentile (M50) and female 5<sup>th</sup> percentile (F05) HBMs were seated in the test buck model and simulated for a 6.5g frontal impact pulse. The 50<sup>th</sup> percentile occupants impacted the forward handrail on the anterior side of the neck, which posed a risk of a crushing injury to the larynx cartilage. A crushing injury to the larynx could occlude airways and is a potentially fatal injury. The 5<sup>th</sup> percentile passenger showed a potential for impacting the forward handrail on the lower face instead of the anterior neck, resulting in a mandible and upper neck injury.

This study investigated passive safety designs that could minimize the potential for passenger injury on transit buses without implementing seat belts. A lowered handrail resulted in the passenger being impacted on the thorax instead of the neck, effectively eliminating the injuries of the larynx, mandible, and neck at the expense of increased chest compression. The chest compression of the small stature HBM predicted a sternum fracture, which was still preferable over the crushing larynx injury observed in the experimental test buck design.

This study demonstrated that the placement of rigid handrails could put passengers at risk of focal impact injuries during a crash. Simple design changes, such as lowering the handrail to engage the thorax instead of the face or neck, proved to be an effective way to avoid potentially lethal injury. Future work should investigate passenger injury using HBMs in other transit bus impact configurations, such as rear and side impacts with varying pulse severities.

## Acknowledgments

I would first like to thank my supervisor Dr. Duane Cronin for accepting me as a student in his research group and providing me with the opportunity to work on a project directly related to my previous employment. Dr. Cronin's guidance throughout my time in graduate school has been immeasurable. His advice regarding academic, industry, and overall professional development has really helped develop and improve my engineering skills.

I would like to thank Transport Canada for providing the opportunity to collaborate on this project and to build off their experimental work. I would like to specifically thank Kathy Tang who was the correspondent from Transport Canada for this project and provided all the necessary data and project details whenever requested. I would like to thank Kathy for devoting a considerable amount of time to meetings throughout the project duration and always providing valuable feedback on the results along the way.

I would like to thank the Global Human Body Models Consortium, the Natural Sciences and Engineering Research Council of Canada, Stellantis Canada, GM Canada, and Honda Development and Manufacturing of America for financial support of this research, and Compute Canada for providing the necessary computing resources.

I would like to thank Donata Gierczycka for providing me with guidance at the beginning of my master's degree, her advice on software use, planning, and document editing really made the whole degree go smoothly.

I would like to thank Jeffrey Barker for providing me with technical guidance throughout my degree, and particularly in the final stretch as he provided extensive editing of this thesis. The IMMC group is lucky to have someone like Jeff who is so knowledgeable and always willing to help.

Lastly, I would like to thank my family, including my parents and my girlfriend Danielle for always providing me with encouragement and support throughout this whole process. Succeeding at something new requires support from those closest to you, and without my family I don't think this would have been possible.

# Table of Contents

Author’s Declaration.....	ii
Abstract .....	iii
Acknowledgments.....	iv
List of Figures.....	x
List of Tables.....	xvii
List of Abbreviations.....	xix
1. Introduction.....	1
1.1. Research Motivation.....	1
1.1.1. Transport Canada Experimental Work and Collaboration.....	2
1.2. Research Objectives.....	2
1.3. Thesis Organization.....	3
2. Background.....	5
2.1. Public Transit Bus Design and Operational Characteristics.....	5
2.2. Government Initiatives to Improve Transit Bus Crashworthiness.....	5
2.3. Transit Bus Fatalities.....	6
2.4. Transit Bus Fatality Risk to Other Road Users.....	7
2.5. Transit Bus Injuries.....	8
2.6. The Direction of Travel of Transit Buses Prior to Impact.....	10
2.7. Transit Bus Interior Design Recommendations.....	11
2.8. Computational Models in Crashworthiness Research.....	11
2.8.1. Cross-Correlation and Objective Rating of Model Response.....	11
2.9. Hybrid III ATD .....	13
2.9.1. Passenger Stature and Crash Safety.....	14
2.9.2. HIII Model Instrumentation.....	14
2.9.3. Biofidelity of the HIII ATD.....	17
2.10. ATD Injury Metrics.....	17
2.10.1. Head Injury Criterion.....	18
2.10.2. Neck Injury Criterion.....	19
2.10.3. Peak Neck Tension and Compression.....	20
2.10.4. Thorax Compression and Peak Acceleration.....	20
2.10.5. Lower Extremity Injury Criterion.....	21
2.10.6. Combined Thoracic Injury Criteria (CTI).....	22
2.10.7. Viscous Criterion (VC).....	23
2.10.8. Brain Injury Criteria (BrIC).....	24
2.10.9. Mertz Neck Criteria.....	25

2.10.10.	Mandible Fracture Prediction Using Impact Force.....	25
2.10.11.	Larynx Cartilage Fracture.....	26
2.11.	Numerical Human Body Models .....	29
2.11.1.	Human Body Models in Transit Bus Crashworthiness Research .....	30
2.12.	Tissue Level Injury Assessment by Body Region.....	30
2.12.1.	Diffuse Axonal Injury.....	31
2.12.2.	Acute Subdural Hematoma.....	32
2.12.3.	Cerebral Contusion.....	33
2.12.4.	Neck Ligament Failure .....	33
2.12.5.	Intervertebral Disc Avulsion.....	35
2.12.6.	Hard Tissue Fracture .....	36
2.13.	Frontal Crashworthiness Standards by Region and Applicability to Transit Buses .....	39
2.13.1.	Federal Crashworthiness Standards in Canada and the United States.....	39
2.13.2.	Crashworthiness Standards in Europe and Australia .....	40
2.14.	American Public Transportation Association Bus Procurement Guidelines.....	41
2.15.	Transit Bus Crashworthiness Literature Review.....	42
2.16.	Full Transit Bus Model Impact Simulations.....	42
2.16.1.	Enhanced Coach and Bus Occupant Safety (ECBOS) .....	43
2.16.2.	Federal Transit Administration Research .....	43
2.16.3.	Transit Bus Sled Experiments Using Adult and Child ATDs.....	45
2.17.	Passenger Safety in School Buses, Motorcoaches, and Passenger Rail and the Implementation of Passive Safety.....	46
2.17.1.	School Bus Passenger Safety and Injury .....	46
2.17.2.	Motorcoach Passenger Safety and Injury .....	47
2.17.3.	Rail Transportation Passenger Safety and Injury .....	48
3.	Transport Canada Transit Bus Crashworthiness Research.....	50
3.1.	Full Scale Transit Bus Impact Tests .....	50
3.2.	Test Buck Fabrication for Replication of Full-scale Impact Conditions.....	52
3.3.	Test Matrix for Test Buck Series of Experiments .....	52
3.3.1.	Test Buck Parameter 1: ATD Posture.....	53
3.3.2.	Test Buck Parameter 2: Acceleration Pulse Magnitude.....	53
3.3.3.	Test Buck Parameter 3: ATD Seating Location.....	54
3.4.	HIII Initial Positioning Data.....	55
3.5.	Geometry of Test Buck Seats and Handrail.....	56
3.6.	HIII Sensors for Recording ATD Kinetics During Impact.....	56
3.7.	Test Buck Experiment Results: Highspeed Video of M50 and F05 ATDs (test case #1) .....	56

3.8.	Results of Varying Parameters in the Test Buck (ATD posture, pulse magnitude, and ATD seating location).....	58
4.	Methods.....	62
4.1.	Methodology Overview.....	62
4.2.	Development and Validation of HIII Coupled Test Buck Model.....	63
4.2.1.	Crushable Foam Material Model.....	66
4.2.2.	Friction of Passenger on Seat Foam.....	67
4.2.3.	Positioning of FE HIII Limbs and Posture to Match Experiment Initial Conditions.....	67
4.2.4.	Seating the HIII Prior to Applying Acceleration Pulse.....	68
4.2.5.	Applying the Acceleration Pulse to the Test Buck Model.....	69
4.2.6.	HIII Sensor Data Processing and CORA Analysis.....	70
4.2.7.	Calculation of Weights for CORA Analysis.....	71
4.3.	Test Buck Model Assessment Using HBM and HIII with 6.5 g Pulse, Upright Posture, and Inboard Seating Location.....	73
4.3.1.	Integration of the GHBM HBM and Test Buck Model.....	73
4.3.2.	Anterior Neck and Lower Face Force Measurement with HIII.....	78
4.3.3.	Injury Metrics.....	79
4.3.4.	HBM Tissue Level Injury Assessment.....	80
4.4.	Alternate Seat Configurations Assessment using M50 HIII for Development of Proposed Seat Design 82	
4.4.1.	Parametric Analysis Using Experimental Test Buck Model Seat Geometry.....	83
4.4.2.	Assessing Statistical Significance of Parameter Variation on Injury Metrics using Linear Regression Analysis.....	85
4.4.3.	Three Alternative Seat Geometries to Improve Passive Safety for the Passenger.....	86
4.4.4.	Generation of Proposed Seat Design.....	88
4.5.	Proposed Seat Design Assessment and Comparison with Experimental Test Buck Model Using HBMs and HIIs with 6.5g Pulse, Upright Posture, and Inboard Seating Location.....	89
5.	Results.....	90
5.1.	Results Overview.....	90
5.2.	Validation of HIII Coupled Test Buck Model.....	90
5.2.1.	Qualitative Assessment of HIII Model Using Highspeed Video (Sample Case #1: 6.5g Pulse, Upright Posture, Inboard Seat).....	90
5.2.2.	Kinematic Trace Comparison (Test Case #1: 6.5g Pulse, Upright Posture, Inboard Seat).....	92
5.2.3.	CORA Analysis Results for Test Buck Model Validation Using Eight Test Configurations	95
5.2.4.	Injury Metrics and Associated Injury Risks (Test Case #1: 6.5g Pulse, Upright Posture, Inboard Seat).....	96
5.2.5.	Injury Metrics Summary for the Eight Test Configurations.....	100

5.3.	Test Buck Model Assessment Using HBM and HIII with 6.5g Pulse, Upright Posture, and Inboard Seating Location.....	103
5.3.1.	Qualitative Comparison of HBM Motion with HIII in Experimental Test Buck Model..	103
5.3.2.	Kinematic Trace Comparison Between HBM and HIII.....	104
5.3.3.	HBM Injury Metrics Comparison with HIII.....	108
5.4.	Alternate Seat Configurations Assessment using HIII M50 for Development of Proposed Seat Design	111
5.4.1.	Parametric Analysis and Linear Regression Results.....	111
5.4.2.	Alternative Seat Geometry Models.....	112
5.4.3.	Combining Findings from Parametric Analysis and Alternative Seat Geometries into Proposed Seat Design.....	116
5.4.4.	Proposed Seat Design.....	116
5.5.	Proposed Seat Design Assessment and Comparison with Experimental Test Buck Model Using HBMs and HIIs with 6.5g Pulse, Upright Posture, and Inboard Seating Location .....	117
5.5.1.	Qualitative Assessment of Occupant Motion in Proposed Seat Design in Comparison with Experimental Test Buck Model.....	117
5.5.2.	Injury Metrics Comparison Between Proposed Seat Design and Experimental Test Buck Model	121
5.5.3.	Tissue Level Injury Assessment and Comparison with HBMs in the Experimental Test Buck Model and Proposed Seat Design.....	128
6.	Discussion .....	135
6.1.	HIII Test Buck Model Validation .....	136
6.1.1.	M50 HIII Test Buck Model Validation.....	136
6.1.2.	F05 HIII Test Buck Model Validation.....	138
6.2.	Potential for Injury in the Experimental Test Buck Model Using Injury Metrics and Tissue Level Assessment.....	140
6.3.	Effect of Occupant Surrogate Biofidelity on Kinematics and Injury Potential .....	142
6.3.1.	F05 HBM and HIII Comparison.....	145
6.4.	Effect of Passenger Stature on Injury Potential .....	146
6.5.	Effective Passive Safety Measures Found Through Parametric Analysis and Alternative Seat Geometries using the HIII M50 .....	148
6.6.	Potential for Injury in Proposed Seat Design in Comparison with Experimental Test Buck Model	150
7.	Conclusions.....	152
7.1.	Study Limitations and Recommendations.....	152
7.2.	Concluding Remarks.....	153
	Letters of Copyright Permissions.....	155
	References.....	169
	Appendices.....	183



Appendix A: Highspeed Video Comparison with Models for Test Cases #2 - #8..... 183  
Appendix B: Kinematic Trace Comparison Between Experiments and Models for Test Cases #2 - #8  
192

## List of Figures

Figure 1: Thesis Visual Summary.....	4
Figure 2: Typical transit bus interior (“Regina Transit Bus 833 Cabin September 2020” by Johnnyw3 is licensed under CC BY-SA 4.0) .....	5
Figure 3: Average annual fatalities by all transportation modes in a) Canada [15], [16] and b) the US [17] .....	6
Figure 4: Transportation mode fatality rates in the US and European Union Nations [18], [19] .....	7
Figure 5: Comparison of fatality rates of passengers and other road users between transit buses and cars in London, UK [21].....	7
Figure 6: Fatalities attributed to transit buses in a) Canada [22] and b) the US [17] .....	8
Figure 7: a) Injuries by Transport Mode in US (2010 to 2019) [17]; b) Transit Bus Injuries by User (2019) [17] .....	8
Figure 8: a) Contribution of non-collision events to total transit bus passenger injuries [23]; b) Type of non-collision event that led to transit bus passenger injury [26].....	9
Figure 9: Passenger position/action prior to non-collision injury in a) Israel (2004) [26] and b) UK (1999-2001) [27].....	9
Figure 10: a) Age distribution of injured passengers in non-collision transit bus events (Adapted from [27]) b) Site of secondary impact injuries on passengers [26].....	10
Figure 11: Bus impact direction prior to a) fatalities and b) injuries of bus passengers [29].....	10
Figure 12: a) CORA progression analysis; b) CORA phase shift analysis .....	13
Figure 13: CORA magnitude analysis .....	13
Figure 14: Left: Humanetics physical 50 <sup>th</sup> and 5 <sup>th</sup> HIII ATDs (Copyright [39]); Right: LSTC numerical 50 <sup>th</sup> and 5 <sup>th</sup> HIII models [37].....	14
Figure 15: Head, Chest, and Pelvis nodes for tracking kinematics.....	15
Figure 16: HIII upper neck cross-section for measuring forces and moments.....	15
Figure 17: HIII chest compression measurement via a deflecting bar .....	16
Figure 18: Location of Femur Cross Section in HIII.....	16
Figure 19: AIS risk curves for HIC <sub>15</sub> [55].....	18
Figure 20: N <sub>ij</sub> Risk Curve [60] .....	20
Figure 21: Chest Deflection Injury Risk Curves [60].....	20
Figure 22: Peak Chest acceleration AIS Curves [60].....	21
Figure 23: Femur Load AIS2 Injury Curve [60].....	22
Figure 24: CTI AIS risk curves [60].....	23
Figure 25: Viscous Criterion AIS-4 Injury Curve [62] .....	23

Figure 26: Injury risk of traumatic brain injury using BrIC [64] .....	24
Figure 27: GHBMC M50 skull.....	25
Figure 28: Injury risk curve for mandible fracture due to anterior-posterior impact, adapted from Daniel et al. [69].....	26
Figure 29: a) Larynx tissue in the GHBMC M50, b) Diagram of the human larynx tissues (Olek Remesz (wiki-pl: Orem, commons: Orem), CC BY-SA 2.5 < <a href="https://creativecommons.org/licenses/by-sa/2.5">https://creativecommons.org/licenses/by-sa/2.5</a> >, via Wikimedia Commons).....	27
Figure 30: Thyroid and Cricoid Cartilage fracture modes (Copyright Permission [72]).....	27
Figure 31: a) Focal impact on the larynx of a passenger in a car crash; b) Location of the cricoid and thyroid cartilages; c) Front view of the cricoid and thyroid cartilages (Copyright Permission [72]).....	28
Figure 32: Dynamic Compression response of large larynges (Copyright Permission [72]).....	28
Figure 33: GHBMC M50 Model V-5.1 a) Entire Model; b) Musculoskeletal; c) Skeleton .....	30
Figure 34: Bridging Veins in the GHBMC M50 Model.....	32
Figure 35: Coup and contrecoup injury to the brain.....	33
Figure 36: Neck Ligaments in the Cervical Spine of the GHBMC M50 Model .....	34
Figure 37: Upper Cervical Spine Ligaments.....	34
Figure 38: Stretch response of neck ligament with initial toe region, linear region, and reduction in stiffness corresponding to ligament failure (Figure adapted from [99]).....	35
Figure 39: Cervical spine superior and inferior endplates at the isolated C2 level.....	36
Figure 40: Cortical and trabecular bone (Copyright [104]).....	37
Figure 41: Elastic-plastic material stress-strain curve.....	37
Figure 42: Ribs and sternum in the GHBMC M50 model .....	38
Figure 43: Bones that make up the lower extremities which include the pelvis (coxal and sacrum), the upper leg (femur), and the lower leg (fibula and tibia) .....	39
Figure 44: FMVSS and CMVSS 208 Acceleration pulse corridors.....	40
Figure 45: ECE80 acceleration pulse corridors .....	40
Figure 46: Frontal impact pulse corresponding to bus impacting a minivan (Copyright Permission [118]) .....	44
Figure 47: a) Rear impact hyper extension of the neck; b) Frontal impact ATD contacts the forward seat on the anterior surface of the neck; c) Proposed new seat design with headrests (Copyright Permission [116]).....	45
Figure 48: a) Test buck with HIII 50 <sup>th</sup> percentile ATD and 6 YO ATD; b) Rear impact hyperextension of neck due to low seat back; c) Face of ATDs impact the top of the forward seat in the frontal impact (Copyright Permission [119]) .....	46

Figure 49: Motorcoach passenger fatalities in the US from 1996 to 2005 (Figure adapted from [131]) ...	47
Figure 50: Secondary impact velocity of a passenger in a rail car undergoing a collision (Figure adapted from [141]).....	48
Figure 51: a) Full-scale transit bus impact experimental setup (side view); b) 40% overlap (top view) [10] .....	50
Figure 52: Schematic of full-scale bus impact with locations of the seated HIII ATD's inside of striking bus [10].....	51
Figure 53: 5th percentile HIII ATD impacting the forward seatback and handrail during the frontal impact [10] .....	51
Figure 54: a) test buck (isometric view) b) test buck side view [10] .....	52
Figure 55: a) M50 HIII with upright posture; b) Reclined posture.....	53
Figure 56: 6.5 g and 5.7 g acceleration pulses scaled down from the 7 g recorded pulse recorded during the full-scale experiment.....	54
Figure 57: a) M50 HIII seated in the inboard seat Vs. b) Outboard seat in test buck.....	54
Figure 58: Handrail mounted on top of each seatback curved down lower on the outboard side.....	55
Figure 59 a) Positioning points for head, face, shoulders, and knees; b) Positioning points for the knee, pelvis, and ankles as recorded by TC (HIII Image Copyright Permission [39]) .....	55
Figure 60: 3D point capture of experimental test buck geometry for a single seat row.....	56
Figure 61: M50 HIII highspeed video (test case #1) .....	57
Figure 62: F05 highspeed video (test case #1) .....	58
Figure 63: a) M50 HIII chin clears the handrail with upright posture; b) M50 HIII chin impacts the handrail with the reclined posture.....	59
Figure 64: a) M50 impact location moves from the lower face with the 5.7g pulse to b) the anterior neck with the 6.5g pulse.....	60
Figure 65: a) M50 HIII impacted the handrail at the upper neck in the inboard seat and b) at the upper chest in the outboard seat; c) the F05 impacted the lower face in the inboard seat and d) at the neck in the outboard seat.....	61
Figure 66: a) forward and rear seat row support brackets; b) middle seat row support bracket .....	63
Figure 67: Support brackets under seat pan in a) experimental test buck and b) test buck model.....	64
Figure 68: Rear view of seatback meshed using quadrilateral shell elements .....	64
Figure 69: FE test buck model corresponding to the rear and middle rows of the experimental test buck and used with the M50 HIII.....	65
Figure 70: Polyurethane foam stress strain curve .....	66

Figure 71: a) M50 HIII with limbs in default positioning b) Spatial coordinates of head, face, shoulders, pelvis, knees, and ankles provided by TC for the physical ATD prior to the experiment c) M50 HIII model with limbs and posture adjusted to match the physical ATD positioning, arms of model were positioned to match pretest photos provided by TC .....	68
Figure 72: a) HIII positioned above seat at start of simulation; b) HIII compressing seat foam at the end of the 125 ms of gravity.....	69
Figure 73: Test buck acceleration direction (sled pulses from Figure 6 applied).....	69
Figure 74: Acceleration of test buck with fixed point of view relative to the ground.....	70
Figure 75: a) Weights are calculated for the response of the traces from the model and experiment based on area under curves; b) Weights are averaged between the model and experiment for each axis; c) The scores from all the traces are multiplied by their respective weights and combined to calculate the final CORA cross-correlation score.....	72
Figure 76: a) HBM with standard automotive seat positioning b) HBM with repositioned arms and legs for transit seating.....	74
Figure 77: Spine and pelvis of HBM constrained from all motion except vertical displacement for first 115 ms of simulation.....	75
Figure 78: HBM head and pelvis nodal output locations.....	76
Figure 79: M50 HBM Neck Cross-section levels.....	76
Figure 80: Chest Band Locations on M50 HBM.....	77
Figure 81: HBM Larynx compression assessment using nodes on anterior and posterior. ....	78
Figure 82: a) Front view of segment sets on HIII neck; b) Side view with labelled segment set levels ....	78
Figure 83: F05 lower face and anterior neck segment sets .....	79
Figure 84: Seat pitch and forward seat height were varied for the parametric analysis.....	83
Figure 85: Inboard and outboard seating locations in the test buck model .....	84
Figure 86: a) Linear equation fitted to the data, the errors between the data points and the line are minimized; b) Example calculation of the R-squared value.....	86
Figure 87: Forward handrail lowered from top of seat to eliminate impact with the anterior neck .....	87
Figure 88: Raised lip on seat pan to limit the forward sliding of the passenger .....	87
Figure 89: Forward seat with headrest and raised seatback .....	88
Figure 90: a) The HIII knees impact the forward seatback; b) The neck of the HIII contacts the forward handrail; c) The neck of the HIII reaches peak flexion; d) The HIII rebounds from the handrail and the head rotates in extension.....	91
Figure 91: a) F05 slides forward off seat and the knees impact the forward seatback; b) The torso of the F05 tilts forward at the pelvis and the lower face impacts the handrail; c) The forward momentum of the	

F05 causes severe flexion of the neck; d) Contact with the handrail is released and the ATD ends up in a semi standing position.....	92
Figure 92: a) Pelvis acceleration (x-axis); b) Right femur axial force; c) Left femur axial force.....	93
Figure 93: a) Head sagittal plane angular velocity; b) Neck shear force; c) Neck sagittal plane bending moment; d) Neck axial force.....	93
Figure 94: a) Head acceleration (x-axis); b) Chest acceleration (x-axis); c) Chest deflection.....	94
Figure 95: a) Pelvis acceleration; b) Right Femur Axial Force; c) Left Femur Axial Force .....	94
Figure 96: a) Head sagittal plane angular velocity; b) Upper Neck Shear Force; c) Upper neck sagittal moment; d) Upper neck axial force.....	95
Figure 97: a) Head acceleration (x-axis); b) Chest acceleration (x-axis); d) Chest deflection.....	95
Figure 98: a) HBM seated prior to initiation of pulse; b) HBM knees impact the forward seatback and torso pitches forward at the pelvis; c) the anterior of the neck strikes the forward handrail; d) the HBM thoracic spine in flexion after impact with forward handrail.....	103
Figure 99: a) HBM seated prior to pulse initiation; b) knees impact forward seatback; c) anterior neck of HBM impacts forward handrail; d) HBM face impacts forward side of seat frame .....	104
Figure 100: a) Pelvis acceleration (x-axis); b) Left femur axial force; c) Right femur axial force.....	105
Figure 101: a) Neck shear force; b) Neck axial force; c) Neck sagittal plane bending moment.....	105
Figure 102: (a) Head linear acceleration (x-axis); (b) Head sagittal plane angular velocity; (c) Chest deflection .....	106
Figure 103: a) Pelvis acceleration (x-axis); b) Left femur axial force; c) Right femur axial force.....	106
Figure 104: a) Upper neck shear force; b) Upper neck axial force; c) Upper neck sagittal plane bending moment.....	107
Figure 105: a) Head acceleration (x-axis); b) Head sagittal plane angular velocity; c) Chest displacement .....	107
Figure 106: a) Effect of seat pitch on LE; b) Effect of forward seat height on CTI; c) Effect of forward seat height on $N_{ij}$ ; d) Influence of inboard/outboard seating location on $HIC_{15}$ .....	112
Figure 107: Lowered handrail test buck model .....	113
Figure 108: Headrest test buck model .....	113
Figure 109: M50 HIII motions in bucket seat design.....	114
Figure 110: Proposed seat design with lowered handrail, raised lip on seat pan, and rubber pad on forward seatback .....	117
Figure 111: HIII M50 motion in the proposed seat design (left) and experimental test buck model with test case #1 parameters (right).....	118

Figure 112: HIII F05 Motion in proposed seat design (left) compared with motions in experimental test buck model for test case #1 (right).....	119
Figure 113: Comparison of the motion of the M50 HBM in the proposed seat design and experimental test buck model.....	120
Figure 114: Comparison of the F05 motion between the proposed seat design and experimental test buck model.....	121
Figure 115: Comparison of the MPS trend through the duration of the simulation in the Corpus Callosum of the M50 and F05 model in the experimental test buck model (Exp.) and the proposed seat design (PD) .....	129
Figure 116: Bridging veins axial strains comparison between the experimental test buck model (Exp.) and proposed seat design (PD) with the M50 and F05 HBMs .....	131
Figure 117: M50 cervical spine ligament distraction comparison between experimental test buck model (Exp.) and proposed seat design (PD).....	132
Figure 118: F05 cervical spine ligament distraction comparison between experimental test buck model (Exp.) and proposed seat design (PD).....	132
Figure 119: a) Test configuration #8, the HIII model chin misses the handrail while the physical HIII impacts it due to a more forward tilt of the torso; b) #2a, #2b, and #2c configurations show enough variation in head motion to cause the chin to impact the handrail in one case, and not in the other two cases.....	137
Figure 120: a) Fluctuations in chest displacement caused by inertia; b) Chest deflection of the F05 HIII in the model, F05 HIII does not exhibit any chest deflection in the experiment.....	138
Figure 121: Knee extension of the F05 HIII upon impacting the forward seatback, the legs of the HIII model appear to extend faster, due to the impact location with the forward seatback favoring extension of the knee instead of higher femur loads as observed with the physical HIII .....	139
Figure 122: a) Larynx tissue compression for the HBM; b) Pivot point between chin and handrail of the F05 results in a significant bending moment in the upper neck.....	141
Figure 123: a) The face of the HBM impacts the top of the forward seat frame due to the increased head excursion, which does not occur with the HIII; b) Comparison of the flexion of the spine-head complex of the HBM with the HIII showing the further forward and vertical excursion of the head.....	143
Figure 124: a) Lower neck bracket of HIII prevents further flexion of the neck; b) thoracic spine of HBM allows for a full range of spinal flexion in a biofidelic manner .....	143
Figure 125 a) Distance from head CG to the cross-section increases further down the cervical spine, causing increased bending moment arm; b) Peak angular velocities of the HBM and HIII head are similar	

in magnitude, which results in a similar value of BrIC, while the longer duration of sagittal plane rotation of the HBM head contributed to the face impacting the seat frame..... 144

Figure 126: a) Side-by-side comparison of F05 HBM and HIII head form showing that the HIII chin protrudes down 20 mm further than the HBM; b) The HBM chin clearance with the handrail is less than the additional size of the HIII chin c) Positioning of the F05 HBM and HIII after 125 ms seating phase of the simulation..... 146

Figure 127: a) The head of the F05 is closer to the handrail vertically due to the shorter seated stature; b) F05 HBM misses the handrail by a smaller margin than the M50 ..... 146

Figure 128: a) F05 HBM has thorax compression due to impacting the top of the seat frame, not observed with the M50; b) the F05 has a more upright posture as it impacts the forward seat, resulting in chest compression on the top of the seat frame ..... 147

Figure 129: a) Secondary impact velocity reduction is smaller for the F05 HBM compared with the M50 HBM; b) Initial separation between the knees and forward seatback is greater for the F05 HBM, resulting in greater secondary impact velocity ..... 148

Figure 130: Focal impact of the face on raised headrest causes high bending moment and shear forces in the upper neck and a high probability of neck injury..... 150

Figure 131: a) Focal impact of the lowered handrail on the thorax of F05 HBM; b) Isolated sternum and ribs of the F05 HBM; c) Close up of sternum with fracture along the manubrium joint ..... 151



## List of Tables

Table 1: CORA Biofidelity Ratings .....	12
Table 2: Abbreviated Injury Scale (AIS).....	17
Table 3: Head Injury AIS level description, adapted from [57].....	19
Table 4: Nij critical intercept values for 50th and 5th percentile ATDs [58], [59].....	19
Table 5: Lower Extremity Criteria critical values .....	21
Table 6: Critical intercepts for CTI based on ATD size .....	22
Table 7: Critical intercepts of angular velocity for calculating BrIC.....	24
Table 8: Mertz Neck injury criteria.....	25
Table 9: Impact Fracture loads for the maxilla and mandible .....	26
Table 10: Fracture thresholds for the larynx cartilages .....	29
Table 11: Brain Strains associated with concussion via FE modelling of concussive impacts.....	32
Table 12: Cervical Spine ligament high strain rate failure distraction [101].....	35
Table 13: Plastic strains measured at failure from experiments.....	38
Table 14: Experimental test matrix with varying ATD posture, pulse magnitude, and ATD seating location.....	53
Table 15: FE Mesh quality criteria.....	65
Table 16: FE model nodal rigid body connections (see Figure 69 for schematic).....	66
Table 17: Friction coefficients of floor and seat fabric .....	67
Table 18: Kinematic outputs for HIII with corresponding filters.....	71
Table 19: CORA metrics and weights, test case #1.....	73
Table 20: Injury Metrics and associated injury probability by body regions.....	80
Table 21: HBM tissue level injury assessment metrics by body region .....	81
Table 22: C2-T1 Neck Ligament Distraction Failure Levels .....	82
Table 23: OC/C1 Neck Ligament Distraction Levels .....	82
Table 24: Parametric analysis test matrix.....	85
Table 25: CORA ratings for all tests (M50 & F05).....	96
Table 26: Injury metrics and risk of injury for the M50 HIII model and experiment.....	97
Table 27: F05 HIII injury metrics comparison between experiment and model (test case #1) .....	99
Table 28: HIII M50 injury metrics for all experiments and test cases .....	101
Table 29: F05 Injury metrics for all experiments and test cases .....	102
Table 30: M50 HBM comparison with HIII injury metrics .....	108
Table 31: HBM F05 calculated injury metrics and comparison with HIII F05 (test case #1).....	110

Table 32: Linear Regression Analysis Results for Injury Metrics and Varied Parameter, Ranked by R-squared Value .....	111
Table 33: Injury Metric comparison between experimental test buck model (test case #1) and alternative geometry models .....	115
Table 34: M50 and F05 injury metric comparison between proposed seat design (PD) and experimental test buck model (Exp.).....	123
Table 35: HBM M50 injury metric comparison between experimental test buck model (Exp.) and proposed seat design (PD).....	125
Table 36: HBM F05 injury metric comparison between experimental test buck model and proposed seat design .....	127
Table 37: 95 <sup>th</sup> percentile MPS per brain region for the experimental test buck model (Exp.) and proposed seat design (PD) .....	128
Table 38: Peak average coup and countercoup pressures by brain region of interest.....	130
Table 39: F05 Rib and sternum EPS and potential for fracture in the experimental test buck model (Exp.) and the proposed seat design (PD) .....	133
Table 40: Effective plastic strain in the pelvis region for M50 HBM in experimental test buck (Exp.) and proposed seat design (PD).....	134
Table 41: Fracture in the legs of the M50 and F05 HBMs seated in the experimental test buck model (Exp.) and proposed seat design (PD).....	134

## List of Abbreviations

FE	Finite Element
FEM	Finite Element Model
TC	Transport Canada
HBM	Human Body Model
GHBMC	Global Human Body Models Consortium
ATD	Anthropomorphic Test Device
III	Hybrid III
CG	Center of Gravity
EPS	Effective Plastic Strain
M50	Male 50 <sup>th</sup> percentile
F05	Female 5 <sup>th</sup> percentile
DAI	Diffuse axonal injury
IARV	Injury Assessment Reference Values

# 1. Introduction

## 1.1. Research Motivation

Transit buses form an integral part of urban transportation networks. Canadians used an average of 153 million monthly passenger trips on public transit from 2017 to 2019 [1]. Governments and municipalities are investing in public transit buses to reduce transportation emissions and achieve carbon reduction targets [2], [3]. Passenger safety on transit buses has received little attention historically. Recent crashes that resulted in passenger fatalities have exposed the gap between perceived passenger safety and the actual risk of fatality [4], [5].

A research study conducted by Transport Canada was initiated following an incident involving a transit bus that resulted in multiple passenger fatalities. On September 18, 2013, an OC Transpo double-decker transit bus driving from Ottawa to Toronto collided with a VIA rail passenger train at a rail crossing. The bus was travelling at a speed of 8 kph with the brakes fully applied when it impacted the side of the train, which was travelling at a speed of 70 kph. The front of the bus was completely sheared off due to the impact, resulting in six bus passenger fatalities and nine serious injuries. The fatalities occurred predominantly to passengers on the second floor at the front of the bus.

An ensuing investigation by the Transportation Safety Board (TSB) of Canada identified that one of the factors contributing to the crash severity was the lack of structural and passenger crashworthiness standards applicable to transit buses. The TSB made the following recommendation directed to Transport Canada:

**“The Department of Transport develop and implement crashworthiness standards for commercial passenger buses to reduce the risk of injury.” [4]**

Crashworthiness describes the ability of a vehicle to protect passengers from fatality and severe injury during a crash event [6]. Over the last five decades, a combination of federally implemented crashworthiness standards and research conducted by the automotive industry have significantly reduced injury and fatalities of private automobile occupants [7]. Frontal impact crashworthiness standards in Canada and the US that govern the protection of passengers in small vehicles are not applicable to transit buses [8], [9]. Crashworthiness standards are only applicable to vehicles with a weight under 2495 kg, which transit buses far exceed. In addition, seat belts are not implemented on passenger seats of transit buses.

### **1.1.1. Transport Canada Experimental Work and Collaboration**

In response to TSB recommendation R15-02, Transport Canada (TC) has undertaken a multi-year research program to develop crashworthiness standards for transit buses [10]. TC initiated the research by conducting two full-scale transit bus impacts using decommissioned buses. Hybrid III (HIII) Anthropomorphic Test Devices (ATDs) were seated inside the bus and used to assess passenger injury. The motion of the unrestrained ATDs was captured using highspeed video.

TC fabricated a test buck to re-create the impact conditions of the full-scale impacts in a lab-controlled environment. HIII ATDs of the 5<sup>th</sup> and 50<sup>th</sup> percentile statures were used to assess passenger injury in the deceleration sled tests.

The current study used numerical modelling to expand on the findings from the experimental tests conducted by TC. A Finite Element (FE) model of the physical test buck was developed and validated using previously developed HIII ATD models. Developing a numerical model of the physical test buck allowed for the implementation of a Human Body Model (HBM, GHBMC M50 v5.1 and F05 v5.1) in place of the ATDs as occupant surrogates.

HBMs are high fidelity occupant models designed to replicate the response of a human passenger in automotive crash simulations. HBMs incorporate tissue geometry informed by medical imaging of a human subject and tissue material characterization based on experimental testing of biological tissues. HBMs serve a similar purpose as ATDs, which is to assess passenger injury in crashworthiness testing. HBMs provide increased biofidelic capabilities such as the prediction of localized tissue injury and the implementation of active musculature.

## **1.2. Research Objectives**

The aim of this study was to assess the potential for passenger injury using a biofidelic HBM in a transit bus frontal impact. The simulations were conducted using the explicit finite element software LS-DYNA version 9.2 on the Graham Cluster (Digital Research Alliance of Canada).

The research objectives of this study were:

**Objective 1:** Develop and validate a numerical model of the physical test buck used by Transport Canada. Assess the responses of the 50<sup>th</sup> and 5<sup>th</sup> percentile HIII ATDs for kinematics in eight test configurations that varied the acceleration pulse magnitude, ATD posture, and ATD seating location.

**Objective 2:** Incorporate the GHBMC M50 and F05 human body models into the test buck model. Assess the HBMs and ATDs motion and injury potential in the test buck model. Compare the responses of the biofidelic HBMs with the HIIIs to determine any differences in kinematics and injury resulting from

occupant surrogate biofidelity. Compare the responses of the small and mid-stature passengers to determine the effect of passenger size on kinematics and injury potential.

**Objective 3:** Investigate passive safety measures for a transit bus interior design using two simulation studies. The first study was a parametric analysis using the test buck model with varying seat pitch, seat height, and passenger seating location. The second study investigated three alternative seat and handrail geometries. Both studies assessed the occupant motion and injury potential in comparison with the baseline test buck model.

**Objective 4:** Investigate a proposed seat design based on the findings from Objective #3. Assess the potential for injury in the proposed seat design following the same procedure used with the experimental test buck model. Determine the effectiveness of the passive safety measures by comparing the results with those from the experimental test buck (Objective #2)

### **1.3. Thesis Organization**

This thesis begins with background information (section 2) that covers the safety statistics for public transit buses, federal crashworthiness regulations, ATD models, HBMs, injury metrics, and tissue level injury assessment. The background section demonstrates the gap in the current literature that this study will address, and the required information to understand the work that was done.

Section 3 covers the series of experimental tests conducted by Transport Canada for their research programme (Figure 1). The section will show the full-scale bus impacts and the series of experimental sled tests. A summary of the findings from the experiments is provided.

Section 4 covers the methodology of the current study, which begins with the development and validation of the numerical test buck model. The methods used to assess injury with the ATD and HBM models are presented. The methodology used to assess passive safety measures through a parametric analysis and the three alternative seat geometries is presented. The section concludes by showing how the proposed seat design was created by combining the results from the passive safety studies and the subsequent assessment in relation to the experimental test buck model.

Section 5 will present the results from the simulations, which includes the validation of the test buck model, assessment of passenger injury using the ATDs and HBMs, the passive safety investigation, and the assessment of passenger injury in the proposed seat design.

Section 6 discusses the findings from the study which begins with the validation of the test buck model and explaining any discrepancies with the experiments. The potential for injury in the test buck model using the ATDs and HBMs is then discussed. The effective, and non-effective passive safety measures

found through the series of simulations is discussed. The effectiveness of the proposed seat design is discussed by comparing with the results from the test buck model using all the occupant surrogates. The section concludes by discussing the effect that occupant surrogate (ATD vs HBM) has on injury potential, and the effect of occupant stature (small vs mid-sized) on injury.

Section 7 presents the concluding remarks of the study and some recommendations for future work.

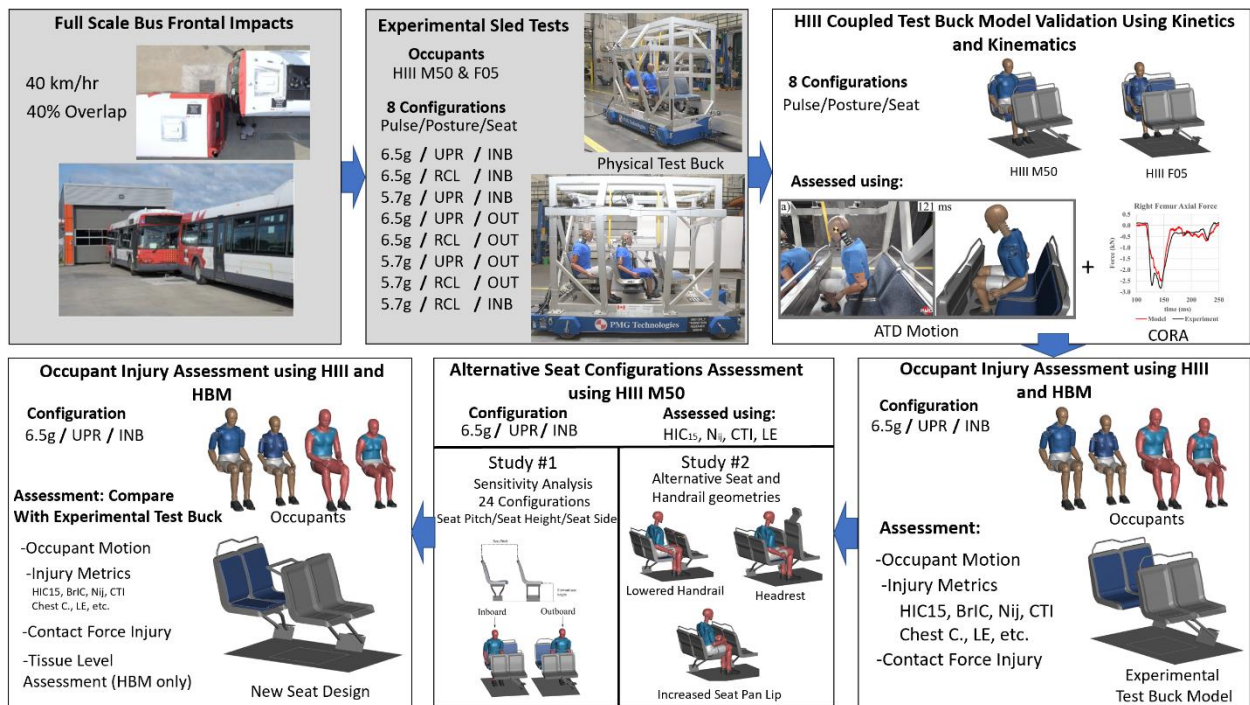


Figure 1: Thesis Visual Summary

## 2. Background

### 2.1. Public Transit Bus Design and Operational Characteristics

Transit buses service a fixed route in urban environments, frequently stopping to allow passengers to get on and off the bus. The interior design of a typical transit bus features a low floor profile with handrails and handholds for passengers to hold on to while the bus is moving. Bench style seats with forward-facing and side-facing configurations are standard (Figure 2). Seat belts are not implemented on transit buses.



**Figure 2: Typical transit bus interior (“Regina Transit Bus 833 Cabin September 2020” by Johnnyw3 is licensed under CC BY-SA 4.0)**

### 2.2. Government Initiatives to Improve Transit Bus Crashworthiness

Transit bus crashworthiness safety has not received the same level of attention as other modes of transport, such as small passenger cars and trucks. Cafiso et al. suggested that this is due to the assumption that adequate safety measures have already been implemented in public transit [11]. In recent years, municipal and federal agencies in Canada, the US, and the UK have expressed intentions of improving the crashworthiness of transit buses to address the issue of passenger safety.

- A 2019 Canadian House of Commons report on bus safety issues recommended developing crashworthiness standards applicable to transit buses [12].



- The Federal Transit Administration (FTA) made recommendations in a 2017 report for crashworthiness improvements to public transit buses [13].
- The "Mayor's Transportation Plan" for the city of London, UK, aims to eliminate all transportation deaths by 2041 [14]. The plan includes the improvement of transit bus crashworthiness.

### 2.3. Transit Bus Fatalities

The annual fatality data for various forms of transportation is made available in Canada by Transport Canada (TC) [15], [16] and in the US by the Federal Transit Administration (FTA) [17]. Transit buses account for less than 0.1% of annual transportation fatalities in both countries (Figure 3).

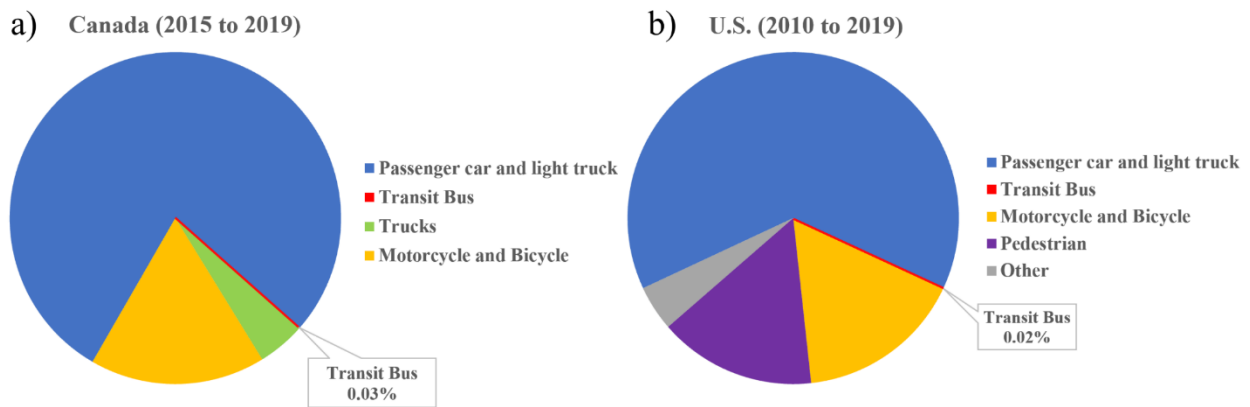


**Figure 3: Average annual fatalities by all transportation modes in a) Canada [15], [16] and b) the US [17]**

Fatality rates assess the relative risk of death for passengers among various transport modes. Data from the US [18] and Europe [19] show that bus passengers on transit and motorcoaches have 6% of the fatality rate as car passengers on a per km travelled basis (Figure 4).

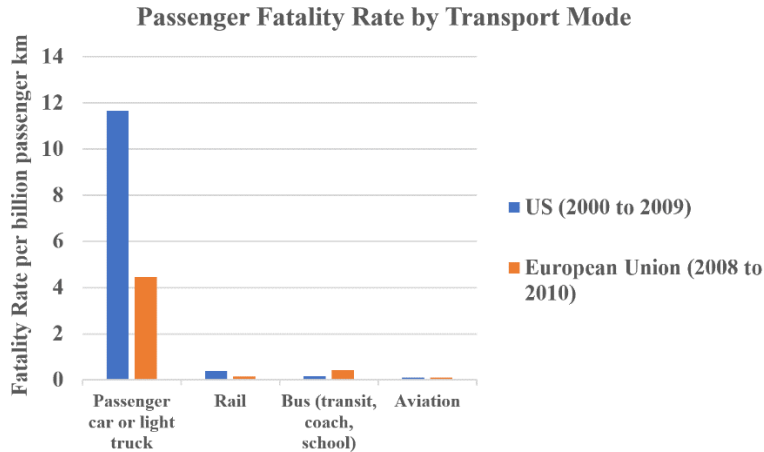


**Figure 4: Transportation mode fatality rates in the US and European Union Nations [18], [19]**

### 2.4. Transit Bus Fatality Risk to Other Road Users

Transit buses pose a high risk of fatality to other road users, such as pedestrians, because they are operated in dense urban environments [20]. Ensuring that the fatality data delineates the fatalities of the bus passengers and other road users is essential for determining the actual risk posed to passengers. Transport for London (TfL) [21] compared the fatality rates for transit buses and cars in the city of London, UK (Figure 5). The data showed that buses had a higher fatality rate for other road users, and a lower fatality rate for occupants when compared with cars.

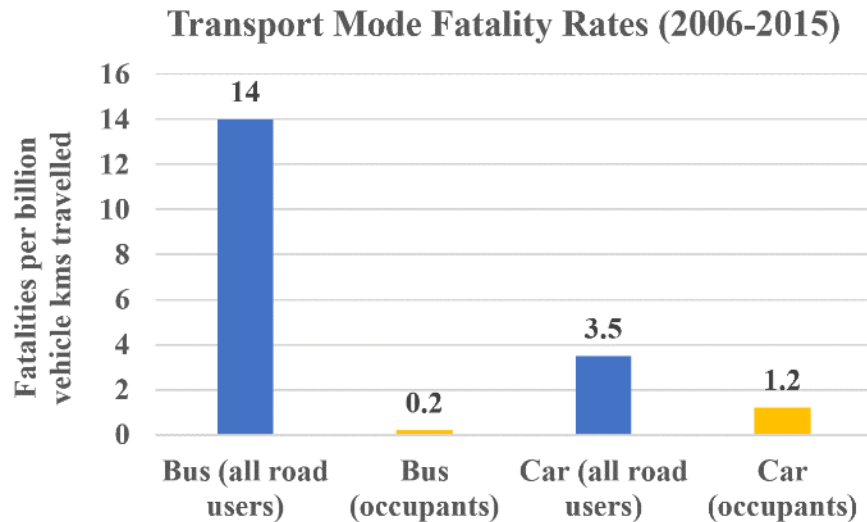


**Figure 5: Comparison of fatality rates of passengers and other road users between transit buses and cars in London, UK [21]**

TC reported the delineated transit bus fatality data in Canada from 1989 to 1999 [22] and showed that none of the deaths attributed to transit buses were passengers (Figure 6). Data from the Bureau of Statistics shows that passengers made up 3% of annual transit bus fatalities in the US in 2019 [17].

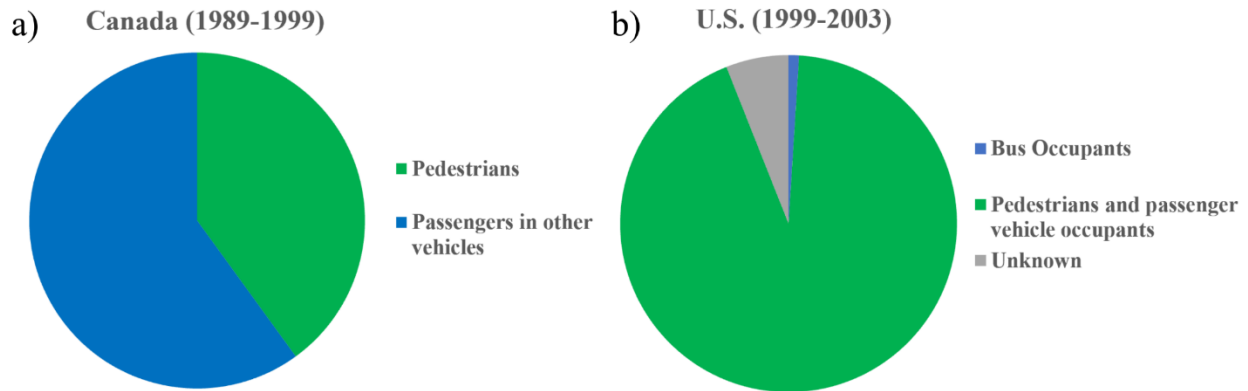


**Figure 6: Fatalities attributed to transit buses in a) Canada [22] and b) the US [17]**

## 2.5. Transit Bus Injuries

Injuries are more common than fatalities on buses as a transport mode [17]. In the US, transit buses account for 0.64% of all transport injuries compared with 0.02% of all transport fatalities (Figure 7a). The US data includes information about the user type for all the injuries attributed to transit buses (Figure 7b). Transit bus passengers accounted for 47% of total transit bus injuries in 2019.

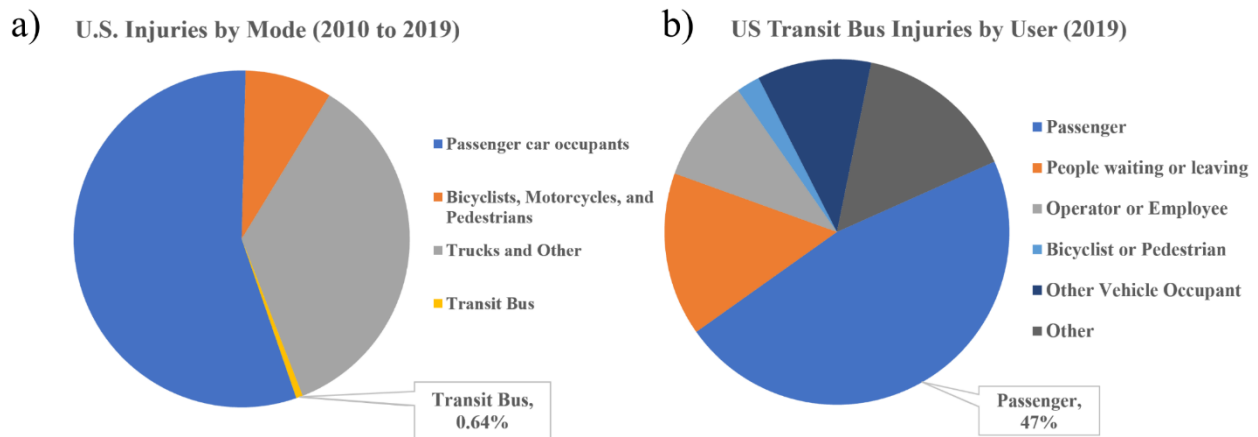


**Figure 7: a) Injuries by Transport Mode in US (2010 to 2019) [17]; b) Transit Bus Injuries by User (2019) [17]**

Transit buses allow passengers to remain standing, which maximizes occupant capacity and allows people to move around the bus while it is in motion. Transit bus drivers must account for unpredictable motorists and other road users, resulting in occasional rapid accelerations, decelerations, or sharp maneuvers [23].

Standing passengers risk tripping or falling during these situations, referred to as non-collision events [24]. A 1996 report from the US [25] showed that almost half of transit bus injuries occurred to passengers in non-collision events (Figure 8a). A 2004 study examined people admitted to Israeli hospitals with injuries from non-collision transit bus incidents [26]. Rapid acceleration and deceleration of the bus contributed to over half of all passenger injuries (Figure 8b).

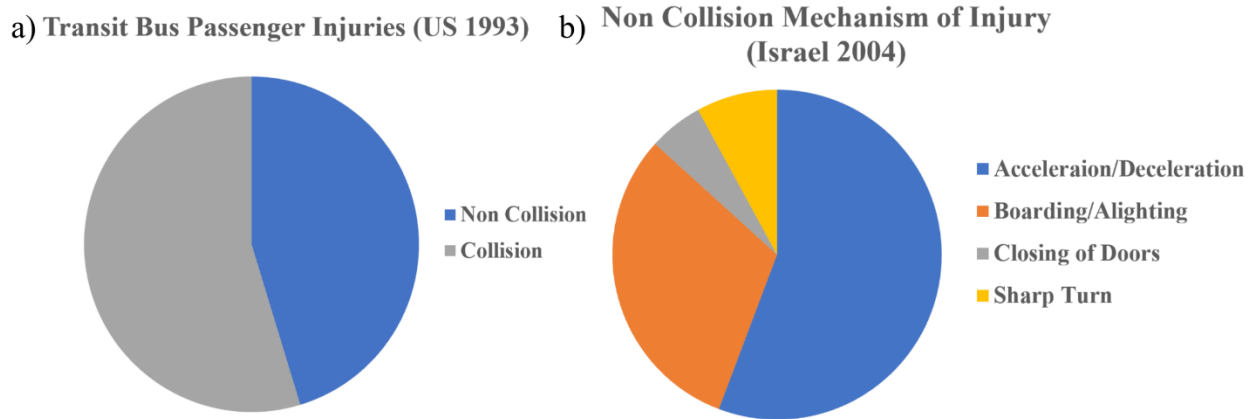


**Figure 8: a) Contribution of non-collision events to total transit bus passenger injuries [23]; b) Type of non-collision event that led to transit bus passenger injury [26]**

Passenger position/action data showed that more than half of the passengers were standing, and about a quarter were sitting at the time of injury (Figure 9a). A study in the UK [27] reported that almost half of all non-collision injuries were passengers seated before injury (Figure 9b). The data from both studies showed that seated passengers are still at risk of injury in a non-collision event.

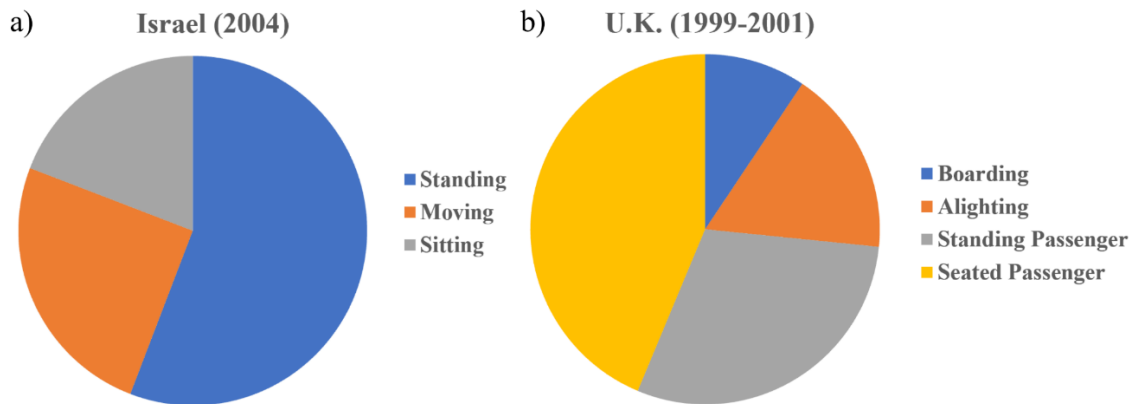


**Figure 9: Passenger position/action prior to non-collision injury in a) Israel (2004) [26] and b) UK (1999-2001) [27]**

The UK study also provided the age distribution of the injured passengers (Figure 10a). The data showed that elderly female passengers (>65 y/o) were at a higher risk of being injured when compared with other

age/gender groups. Injuries to the limbs, head, and spine accounted for more than three-quarters of all injuries in the Israeli study (Figure 10b).

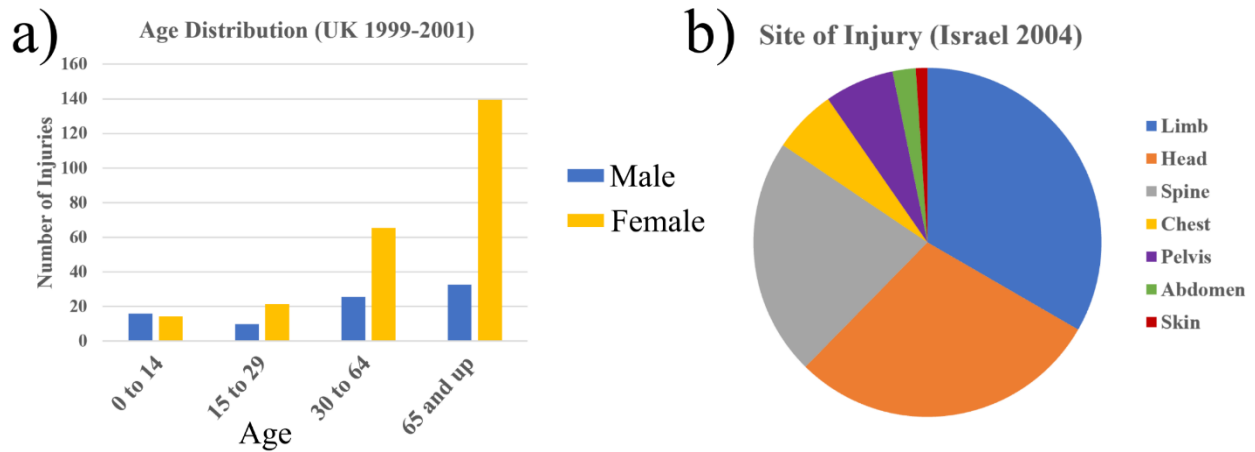


**Figure 10: a) Age distribution of injured passengers in non-collision transit bus events (Adapted from [27]) b) Site of secondary impact injuries on passengers [26]**

A 2019 study investigated non-collision injuries of UK bus passengers from 2016 to 2017. Seated passengers had one-third the risk of a non-collision injury as standing passengers [28]. The most frequent parts of the bus impacted by seated passengers were the vertical handrails (27%) and the forward seat (27%). For the seated passengers who were injured from impacting interior structures, they were caused by vertical handrails 31% of the time and horizontal handrails 20% of the time.

### 2.6. The Direction of Travel of Transit Buses Prior to Impact

A 2005 report by the National Institute for Aviation Research (NIAR) investigated transit bus impact direction that resulted in passenger injuries and fatalities [29]. Frontal impacts resulted in more than half of all bus passenger fatalities, while there was an even distribution for crashes that resulted in injuries (Figure 11).

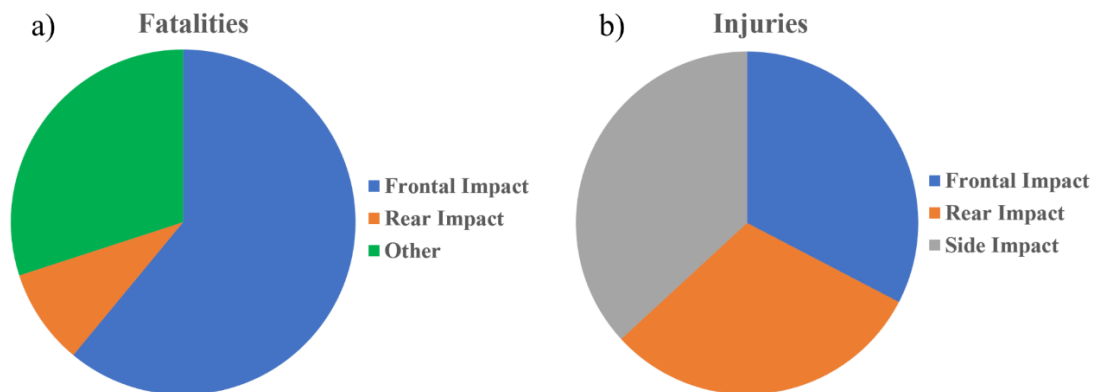


**Figure 11: Bus impact direction prior to a) fatalities and b) injuries of bus passengers [29]**

## **2.7. Transit Bus Interior Design Recommendations**

Previous reports have concluded that improving the design of transit bus interiors can reduce the potential for passenger injury [25], [30]. Recommendations have included improving the design of handrails, seats, and ticket machines to prevent serious injury when impacted by passengers. Transport for London (TfL) identified the challenge of changing the rigidity and geometry of handrails to reduce injury potential while still maintaining the functionality [31].

A 2019 study detailed a design improvement session for transit bus interiors that included bus manufacturers and stakeholders in the transit industry [32]. Despite the acknowledged effectiveness, the designers expressed concerns about retrofitting buses with seat belts due to the legal responsibility of the bus driver to check that every passenger uses them correctly. Adding to this, requiring seatbelts could imply that standing is not a safe way to ride the bus. High seat backs were suggested as a potential design to mitigate the risk of whiplash.

## **2.8. Computational Models in Crashworthiness Research**

Numerical modelling utilizes mathematical equations to describe a physical phenomenon, such as electromagnetism, fluid flow, or a car crash. The Finite Element Method (FEM) is a form of numerical modelling which describes a physical body in a computational environment using discretized elements. Differential equations are used to describe the motion of the finite element body when boundary conditions (force, acceleration, displacement, etc.) are applied [33]. Materials characterization and boundary conditions play an integral role in the accuracy of the response of a FE model.

Numerical models are cost-effective relative to experimental testing and allow for the use of biofidelic occupant surrogates in crashworthiness research. Validation is the process where a numerical model is compared against a series of experimental tests to evaluate how accurately the model reproduces the experimental response [34]. Comprehensive validation of a model includes a qualitative and quantitative component. The qualitative assessment visually compares the highspeed video of the experiment with the simulation to check for visual agreement. The quantitative assessment involves comparing signals from the experiment and model response, such as acceleration or force traces. Quantitative assessments use cross-correlation software to objectively rate how well the signal responses from a model compare with an experiment.

### **2.8.1. Cross-Correlation and Objective Rating of Model Response**

Correlation and Analysis Software (CORA) compares and rates the correlation between two temporal signals (i.e. time history and model response) [35]. CORA generates an objective rating between 0 and 1 that corresponds to a level of biofidelity (Table 1).

**Table 1: CORA Biofidelity Ratings**

<b>Biofidelity Level</b>	<b>CORA Rating</b>
<b>Excellent</b>	<b>0.86&lt;rating&lt;1</b>
<b>Good</b>	<b>0.65&lt;rating&lt;0.86</b>
<b>Fair</b>	<b>0.44&lt;rating&lt;0.65</b>
<b>Marginal</b>	<b>0.26&lt;rating&lt;0.44</b>
<b>Unacceptable</b>	<b>0&lt;rating&lt;0.22</b>

CORA employs the cross-correlation method, combining three sub-ratings, *progression* ( $V$ ), *phase shift* ( $P$ ), and *magnitude* ( $G$ ) into the final rating ( $C$ ) (Eq. 1). Each sub rating  $V$ ,  $P$ , and  $G$  is between 0 and 1, with 0 corresponding to no agreement and 1 corresponding to perfect agreement. The terms  $g_V, g_P, g_G$  are the weights assigned to progression, size, and magnitude.

$$C = g_V \cdot V + g_P \cdot P + g_G \cdot G \quad (1)$$

The weights attributed to progression, phase shift, and magnitude can be adjusted when calculating the final cross-correlation score. Each of the weights must be between 0 and 1 (Eq. 2) and must all sum to a value of 1 (Eq. 3).

$$0 \leq (g_V, g_P, g_G) \leq 1 \quad (2)$$

$$g_V + g_P + g_G = 1 \quad (3)$$

When the signal from a model and experiment starts at the same time (i.e.  $t=0$ ), the phase shift ( $g_P$ ) is omitted from the cross-correlation analysis to avoid an artificially high rating. The progression analyzes the shape of the two signals (Figure 12a), and the phase shift analyzes the degree of overlap of the signals (Figure 12b).

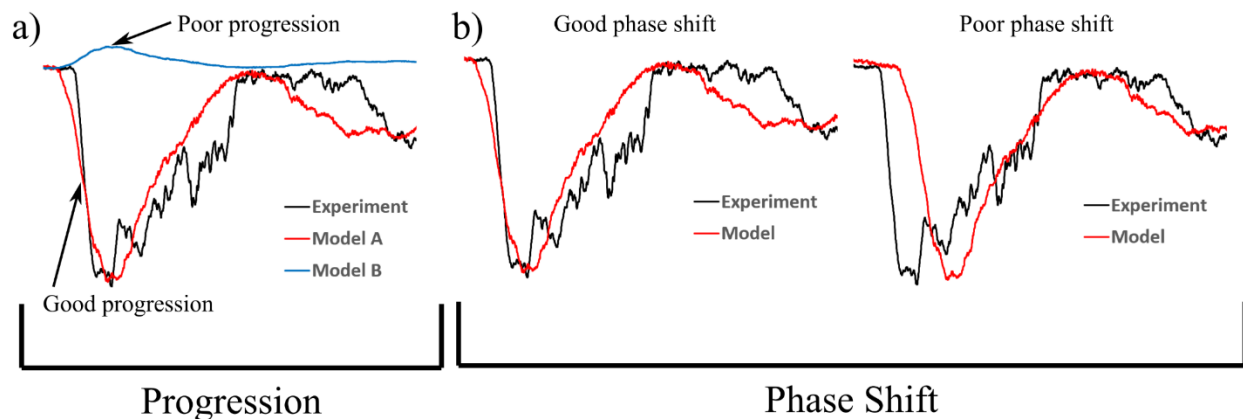


**Figure 12: a) CORA progression analysis; b) CORA phase shift analysis**

The magnitude analyzes the agreement between the area under the curve from both signals (Figure 13).

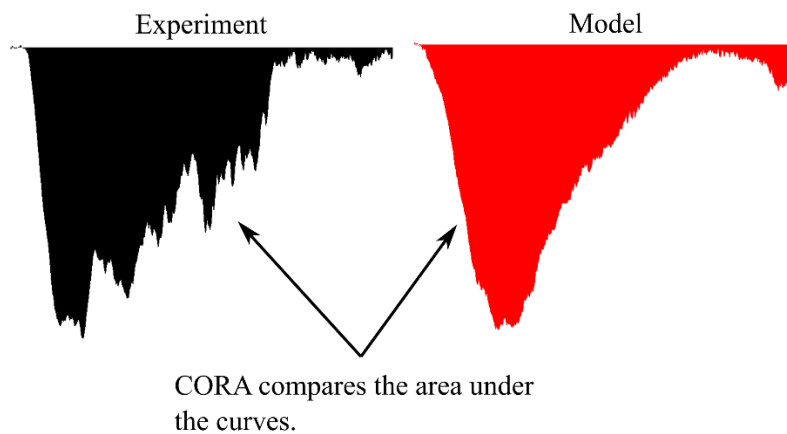


**Figure 13: CORA magnitude analysis**

## 2.9. Hybrid III ATD

The Hybrid III (HIII) is a family of Anthropomorphic test devices (ATD) and is the primary test device used to ensure compliance with frontal impact safety standards. The HIII is available in various sizes, including a 50<sup>th</sup> percentile male and a 5<sup>th</sup> percentile female. The 50<sup>th</sup> male represents an average-sized male passenger [36], while the 5<sup>th</sup> percentile represents a small stature female. Livermore Software Technology Company (LSTC) provides free-to-use FE models of the HIIIs for explicit FE simulations (Figure 14). The M50 model is validated for neck flexion/extension and thorax deflection response [37]. The HIII model is also available in the smaller stature 5<sup>th</sup> percentile female, validated for head, neck, thorax, and femur load response [38].



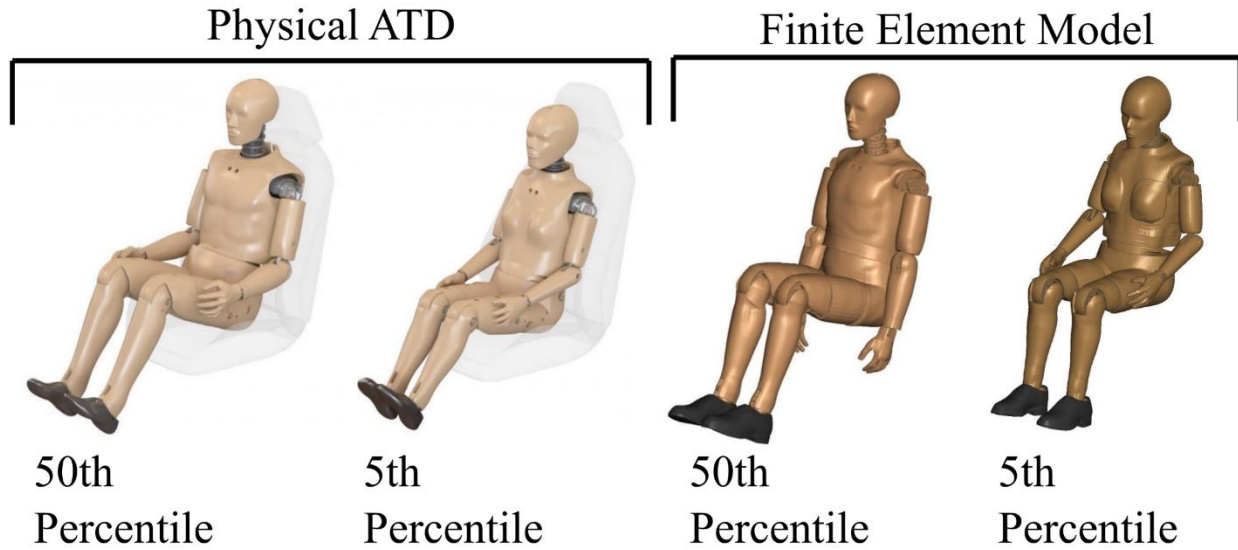


**Figure 14: Left: Humanetics physical 50<sup>th</sup> and 5<sup>th</sup> HIII ATDs (Copyright [39]); Right: LSTC numerical 50<sup>th</sup> and 5<sup>th</sup> HIII models [37]**

### 2.9.1. Passenger Stature and Crash Safety

Previous studies have shown that smaller stature female passengers are at an increased risk of injury in automobile accidents [40]. Physiological differences between males and females, such as bone geometry and density can place females at an increased risk [41]. Non physiological risks are related to vehicle design, such as the height of handholds or seatbacks and their effect on passenger kinematics and injury [42]. When airbags were first implemented in production vehicles, the head of a small stature female sitting close to the steering wheel could be in the deployment zone of the airbag, where the power of the deployment could cause a fatal blow to the head [43]. Improving the crashworthiness of transportation systems requires the assessment of different stature passengers to ensure that safety improvements benefit all.

### 2.9.2. HIII Model Instrumentation

The nodes located at the center of gravity of the head, chest, and pelvis of the HIII model monitor the kinematics (Figure 15). The nodes correspond to accelerometers in the physical HIII.

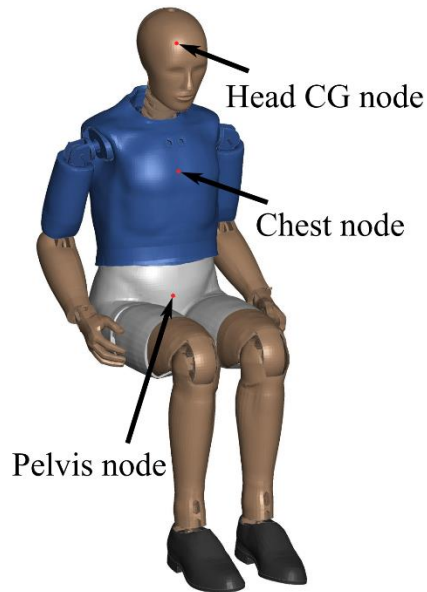


**Figure 15: Head, Chest, and Pelvis nodes for tracking kinematics**

The HIII model monitors the forces and moments in the upper neck via an element set corresponding to a load cell in the physical HIII (Figure 16).

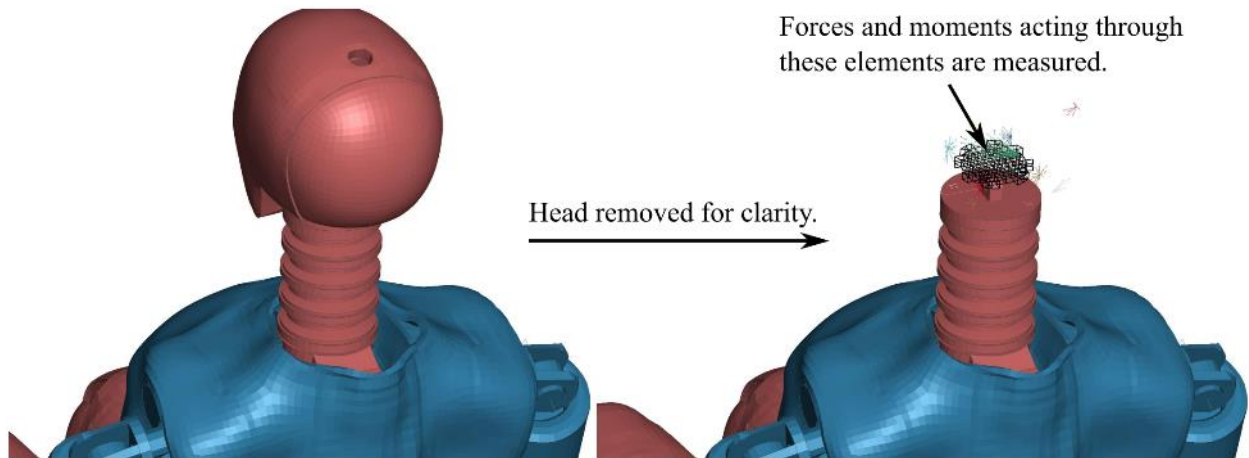


**Figure 16: HIII upper neck cross-section for measuring forces and moments**

A rotating bar element in the chest cavity of the HIII model measures the chest deflection (Figure 17).

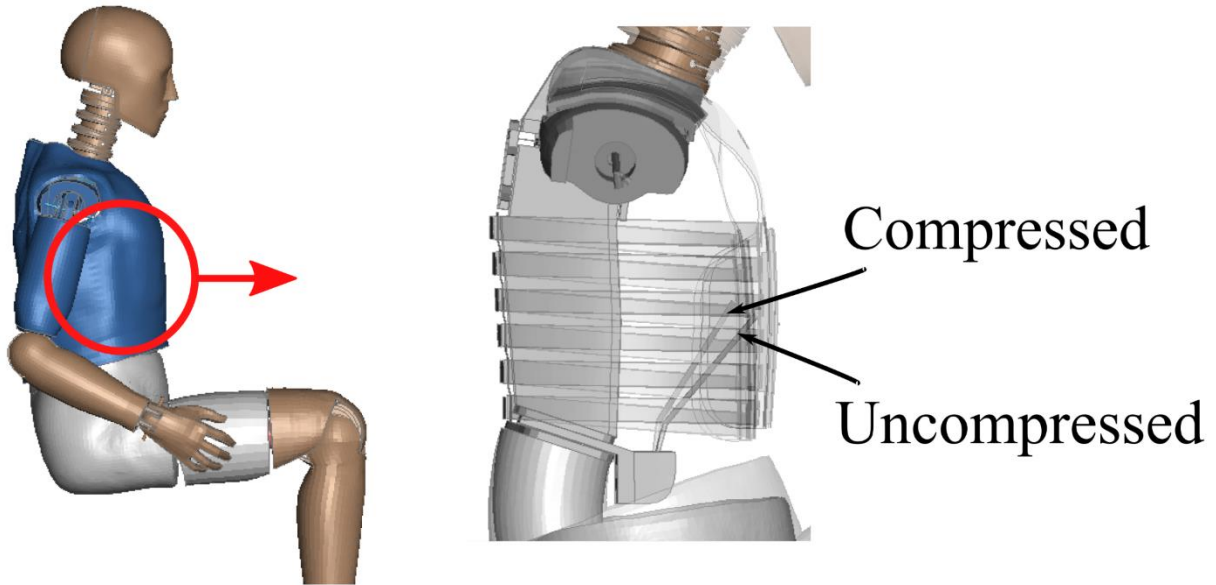


**Figure 17: HIII chest compression measurement via a deflecting bar**

The femur axial load is measured in the HIII model using an element cross-section in the upper leg (Figure 18).

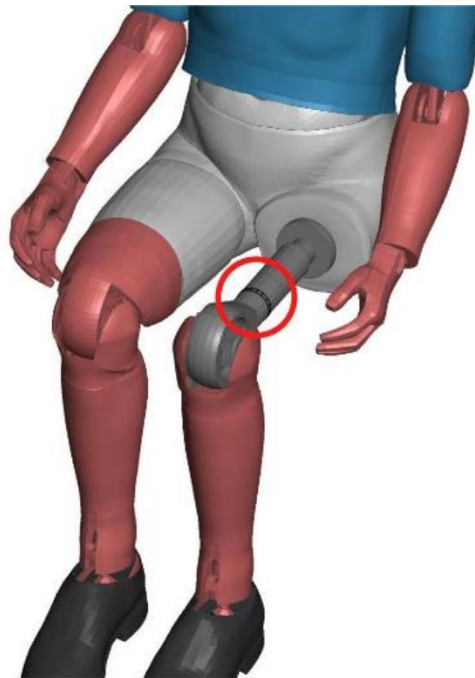


**Figure 18: Location of Femur Cross Section in HIII**

### 2.9.3. Biofidelity of the HIII ATD

The biofidelity of the HIII refers to how accurately it replicates the response of a biological surrogate (PMHS or human volunteer). The HIII demonstrates excellent biofidelity at the head region and femur region and an overly stiff response of the neck and thorax regions [44], [45].

The overly stiff neck and thorax of the HIII results in reduced forward head excursion in frontal impacts compared with PMHS [46]. Agaram et al. demonstrated that the artificially stiff design of the HIII neck resulted in higher bending moments in the upper neck from airbag loading [47]. The stiffness of the HIII neck is partly due to the design, which uses multiple metal discs joined by rubber inserts, with a single metal cable running down the center [48].

The thorax of the HIII exhibits less peak thorax deflection under belt loading in frontal impacts compared with PMHS [49]. The HIII thorax was developed using pendulum impact loading and lacked validation for the response of focal belt loading [50], [51], [52], [53]. The lack of validation for focal impacts on the thorax results in an overly stiff response of the HIII under low-rate loading.

### 2.10. ATD Injury Metrics

Crashworthiness researchers use ATDs to assess the probability of an occupant sustaining an injury during a crash. The Abbreviated Injury Scale (AIS) describes the injury severity of a given tissue or body region. The AIS ranges from AIS-1 being a minor injury to AIS-6 being a maximal (fatal) injury (Table 2) [54]. The AIS codebook provides descriptions and an AIS score for various types of injuries throughout the body.

**Table 2: Abbreviated Injury Scale (AIS)**

AIS level	Injury Severity
AIS-1	Minor
AIS-2	Moderate
AIS-3	Serious
AIS-4	Severe
AIS-5	Critical
AIS-6	Maximal

Injury metrics correlate peak accelerations, forces, and displacements measured with an ATD during a crash to the probability of sustaining a specific AIS level injury (e.g., Peak femur force and probability of AIS-2 femur injury). Some injury metrics involve comparing a maximum value with a reference limit (e.g., peak head linear acceleration). Other metrics use functions to calculate the risk from multiple kinematic inputs (e.g., Neck injury criteria is a combination of neck moments and axial forces to determine neck injury potential). Injury Assessment Reference Values (IARV) are thresholds for injury

potential set by industry regulators to minimize passenger injury during crash events. The IARV values correspond to a specific probability of sustaining a given AIS level injury. The following sections detail the method of calculating each injury metric and the injury risk curves for determining the injury probability.

### 2.10.1. Head Injury Criterion

The Head Injury Criterion ( $HIC_{15}$ ) measures the maximum head injury potential using a 15 ms integral of head linear acceleration (Eq. 4).

$$HIC = \max \left( (t_2 - t_1) \cdot \left[ \frac{1}{t_2 - t_1} \cdot \int_{t_1}^{t_2} a(t) dt \right]^{2.5} \right) \quad (4)$$

Prasad and Mertz [55] formulated injury risk curves for  $HIC_{15}$  (Figure 19). A  $HIC_{15}$  of 700 indicates a 31% risk of an AIS-2 skull fracture or a less than 5% risk of an AIS-4 brain injury for the 50<sup>th</sup> percentile male [56].

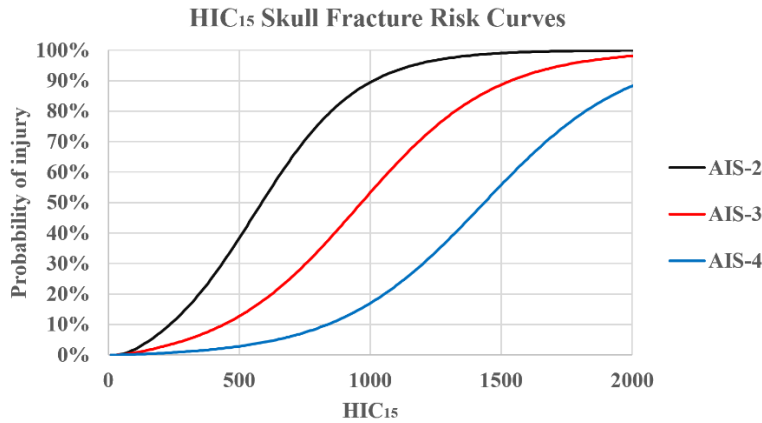


**Figure 19: AIS risk curves for  $HIC_{15}$  [55]**

The related head injury for different levels of AIS head injuries has been summarized in the literature [57] (Table 3).

**Table 3: Head Injury AIS level description, adapted from [57]**

AIS code	Description
1	Skin and scalp: abrasions, superficial lacerations. Face: fracture of the nose.
2	Leather: more abrasions. Simple or decomposed fractures to the face, open fractures or displacements of the jaw, fractures of the jaw.
3	Different fractures, total loss of scalp, bruises to the cerebellum.
4	Complex facial fractures, exposure or loss of brain tissue, small epidural or subdural hematoma.
5	Greater penetration of brain injuries, damage and hematoma to the trunk, epidural or subdural compression, and axonal damage spread.
6	Mass destruction of both the skull and the brain

### 2.10.2. Neck Injury Criterion

The neck injury criterion ( $N_{ij}$ ) is calculated by summing the ratio of axial loading (tension/compression) to a critical intercept with the ratio of sagittal bending moment (flexion/extension) to a critical intercept (Eq.5).

$$N_{ij} = \frac{N_{Moment}}{N_{Mc}} + \frac{N_{Axial Force}}{N_{CF}} \quad (5)$$

The Critical intercepts,  $N_{mc}$  and  $N_{cf}$ , are dependent on ATD size (Table 4). The IARV value of 1 for  $N_{ij}$  corresponds to a 22% chance of an AIS-3 neck injury.

**Table 4:  $N_{ij}$  critical intercept values for 50th and 5th percentile ATDs [58], [59]**

ATD	Sagittal Plane Bending Moment (Nm) (Flexion/Extension)	Axial Force (N) (Compression/Tension)
HIII 50th	310/135	6160/6806
HIII 5th	155/67	3880/4287

The value of  $N_{ij}$  determines the probability of an AIS-2 to AIS-5 injury using the associated risk curves (Figure 20).

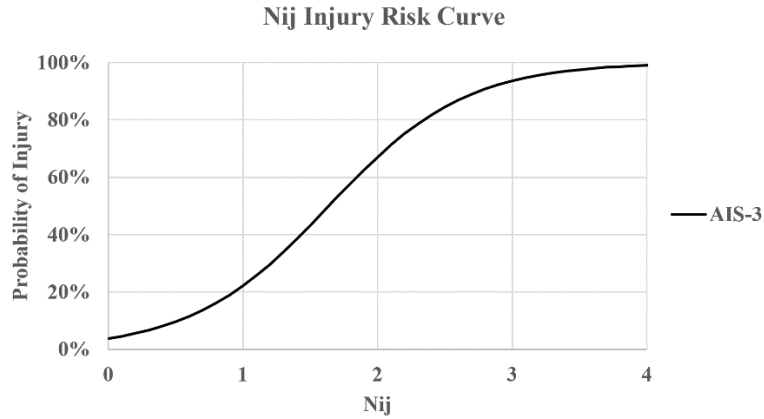


**Figure 20: Nij Risk Curve [60]**

### 2.10.3. Peak Neck Tension and Compression

The IARV of 4170 N for peak neck tension and 4000 N for peak neck compression corresponds to a 50% risk of an AIS-3 neck injury.

### 2.10.4. Thorax Compression and Peak Acceleration

Thorax compression can result in damage to vital organs, such as the heart and lungs. Rib fracture from excessive compression can result in a puncture to the vital organs and can be fatal if not treated immediately [61]. The risk of associated thoracic injuries can be calculated based on the total deflection of the chest (Figure 21). The IARV for chest deflection is 63 mm and corresponds to a 30% risk of an AIS-3 injury.

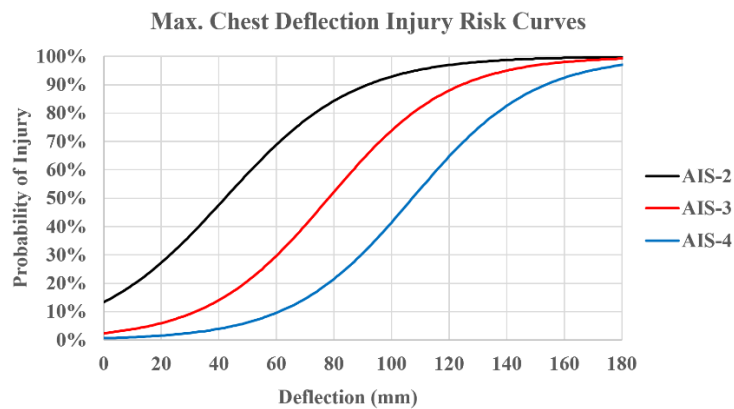


**Figure 21: Chest Deflection Injury Risk Curves [60]**

The peak acceleration measured at the chest can also be used to assess the potential for thorax injury. An IARV of 60 g is set for the 50<sup>th</sup> percentile male for the FMVSS 208 standard and corresponds to a 37% risk of an AIS-4 chest injury (Figure 22).

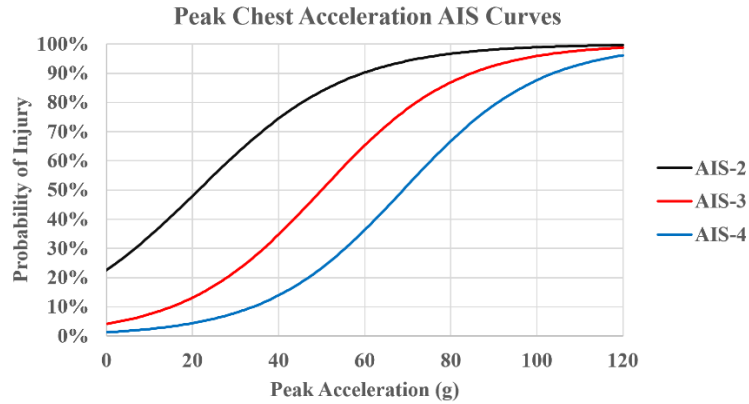


**Figure 22: Peak Chest acceleration AIS Curves [60]**

### 2.10.5. Lower Extremity Injury Criterion

The Lower Extremity (LE) criterion uses the femur axial force to determine the risk of femur fracture (Table 5).

**Table 5: Lower Extremity Criteria critical values**

Passenger	IARV
50 <sup>th</sup> percentile male	10 000 N
5 <sup>th</sup> percentile female	6800 N

The IARVs for femur loads correspond to a 35% risk of an AIS-2 femur injury (Figure 23).



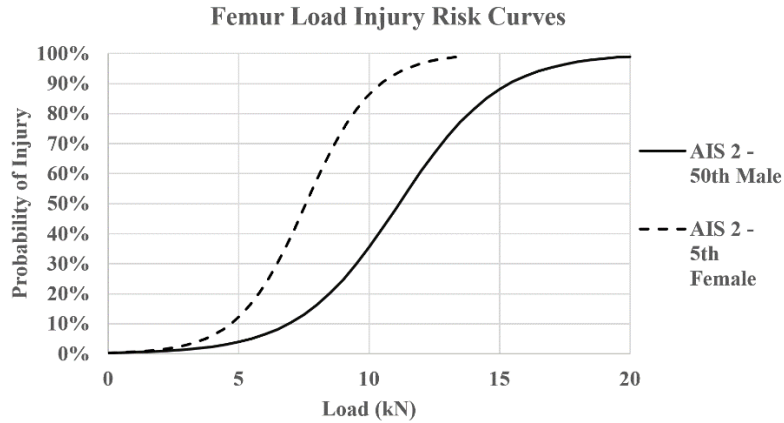


**Figure 23: Femur Load AIS2 Injury Curve [60]**

### 2.10.6. Combined Thoracic Injury Criteria (CTI)

The Combined Thoracic Criteria (CTI) calculates the probability of an injury to the thorax using a combination of chest acceleration and deflection (Eq. 6) [60]. Each HIII stature has specific critical intercepts used to calculate CTI (Table 6).

$$CTI = \frac{A_{max}}{A_{int}} + \frac{D_{max}}{D_{int}} \quad (6)$$

**Table 6: Critical intercepts for CTI based on ATD size**

Dummy Type	Mid-Sized Male	Small Female
Chest Deflection Intercept for CTI ( $D_{int}$ )	103 mm	84 mm
Chest Acceleration Intercept for CTI ( $A_{int}$ )	90 g	90 g

A CTI value of 1 is associated with a 25% risk of an AIS-3 thoracic injury for the 50<sup>th</sup> percentile male (Figure 24).

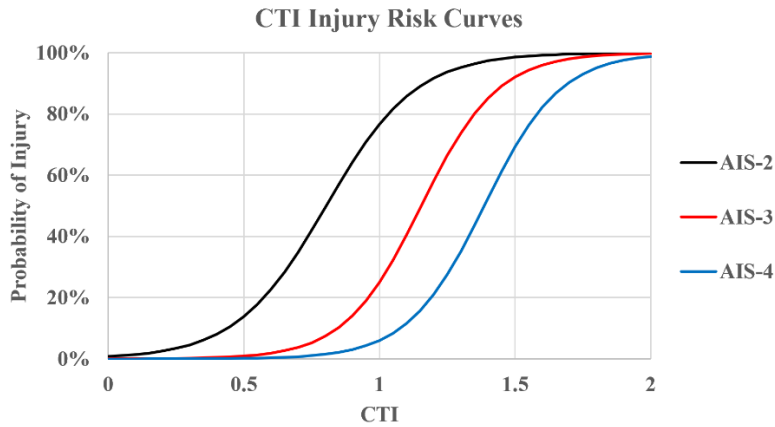


Figure 24: CTI AIS risk curves [60]

### 2.10.7. Viscous Criterion (VC)

The Viscous Criterion (VC) measures the potential for thoracic injury using a combination of normalized chest compression and chest compression rate (Eq. 7). The VC accounts for experimental findings that lower chest compression at very high deflection rates can still lead to thoracic injury [62].

$$VC = V(t) \times C(t) \quad (7)$$

The calculated value of VC can be used with the associated injury risk curve to calculate the probability of an AIS-4 thoracic injury (Figure 25).

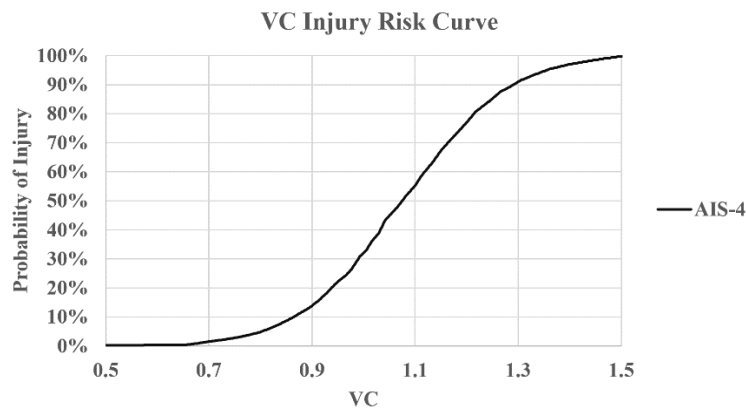


Figure 25: Viscous Criterion AIS-4 Injury Curve [62]

### 2.10.8. Brain Injury Criteria (BrIC)

The Brain Injury Criteria (BrIC) measures the potential for brain injury using the angular velocity components of the head CG [63], [64]. The BrIC equation divides the peak angular velocity of the head in the x, y, and z-axis by critical intercepts (Eq. 8) (Table 7).

$$BrIC = \sqrt{\frac{\omega_x}{\omega_{xc}} + \frac{\omega_y}{\omega_{yc}} + \frac{\omega_z}{\omega_{zc}}} \quad (8)$$

**Table 7: Critical intercepts of angular velocity for calculating BrIC**

Axis of Rotation	Rads/sec
$\omega_x$	66.3
$\omega_y$	53.8
$\omega_z$	41.5

The value of BrIC correlates with a risk of traumatic brain injury (TBI) (Figure 26).

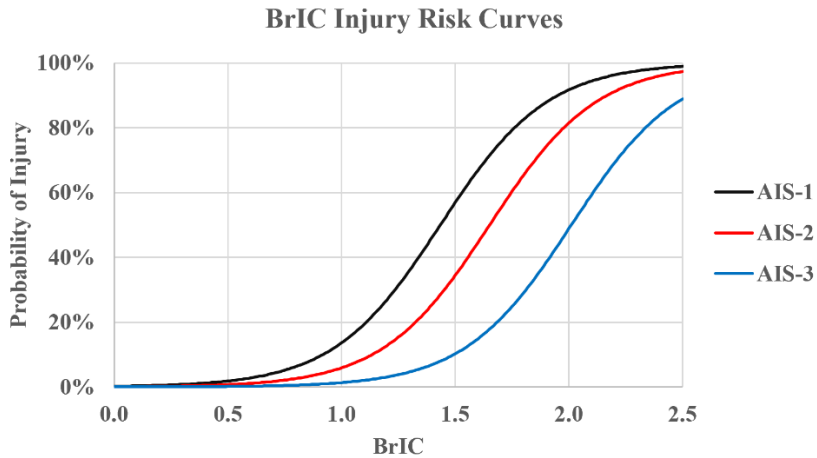


**Figure 26: Injury risk of traumatic brain injury using BrIC [64]**

### 2.10.9. Mertz Neck Criteria

Mertz reported additional IARVs for the peak neck flexion, extension, and shear force (Table 8). The IARV for the peak extension moment corresponds to a 20% risk of an AIS-3 neck injury, and the neck flexion moment and shear force corresponds to a 5% AIS-4 neck injury risk.

**Table 8: Mertz Neck injury criteria**

Neck Load Metric	IARV
Neck Sagittal Bending Flexion Moment (Nm)	190
Neck Sagittal Bending Extension Moment (Nm)	96
Neck Shear Force (N)	3100

### 2.10.10. Mandible Fracture Prediction Using Impact Force

Impacts to the face of passengers, from steering wheels and other structures located in the driver space, posed a risk of fracture to the mandible and maxilla prior to the widespread implementation of 3-point belts and airbags [65]. Experimental drop tower tests on PMHS subjects generate impact tolerances for the mandible and maxilla of the human face (Figure 27).

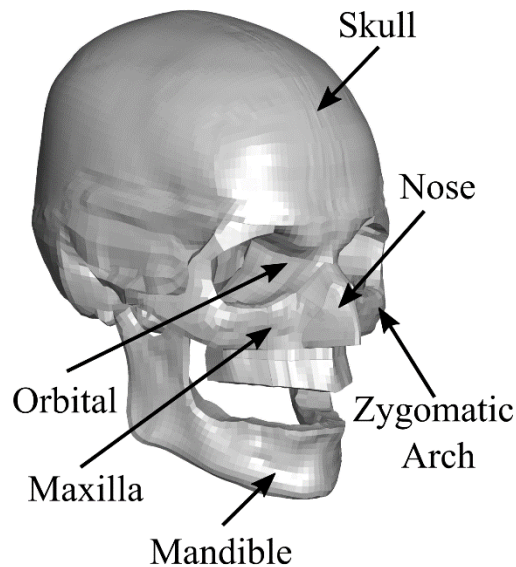


**Figure 27: GHBMC M50 skull**

A drop weight impactor is aimed at the bone of interest on the PMHS, and fracture occurrence is monitored for varying impact velocities. Experiments generate mean or minimum fracture thresholds for the maxilla and mandible (Table 9).

**Table 9: Impact Fracture loads for the maxilla and mandible**

Study	Experiment type	Region	Fracture Load
Nyquist (1986) [66]	Impactor, PMHS (unembalmed), Nose impact	Maxilla	3000 N (Mean)
Allsop (1988) [67]	Impactor, PMHS (unembalmed)	Maxilla	1000 – 1800 N
Schneider (1972) [68]	Drop tower, supine PMHS (unembalmed)	Mandible	1779 N (Minimum)
Daniel (2021) [69]	Drop tower, PMHS (unembalmed)	Mandible	2834 N (50% risk of fracture)

Daniel et al. [69] generated an injury risk curve for the impact force on the mandible and the corresponding risk of fracture (Figure 28). The AIS codebook states that a fracture to the mandible is an AIS-1 injury.

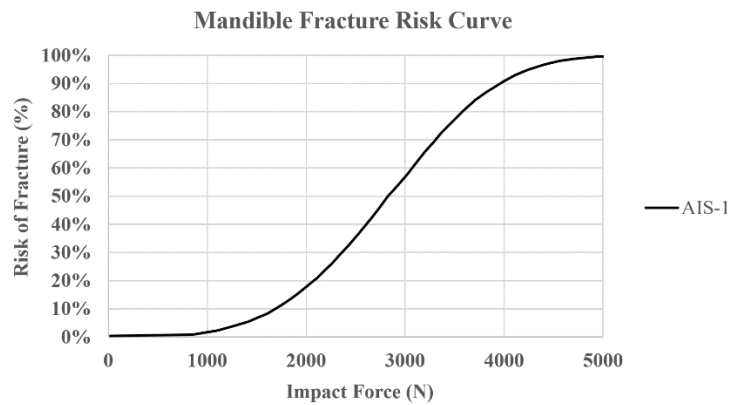


**Figure 28: Injury risk curve for mandible fracture due to anterior-posterior impact, adapted from Daniel et al. [69]**

### 2.10.11. Larynx Cartilage Fracture

The larynx (voice box) is a hollow tissue located along the anterior of the neck that allows for breathing and voice production (Figure 29).

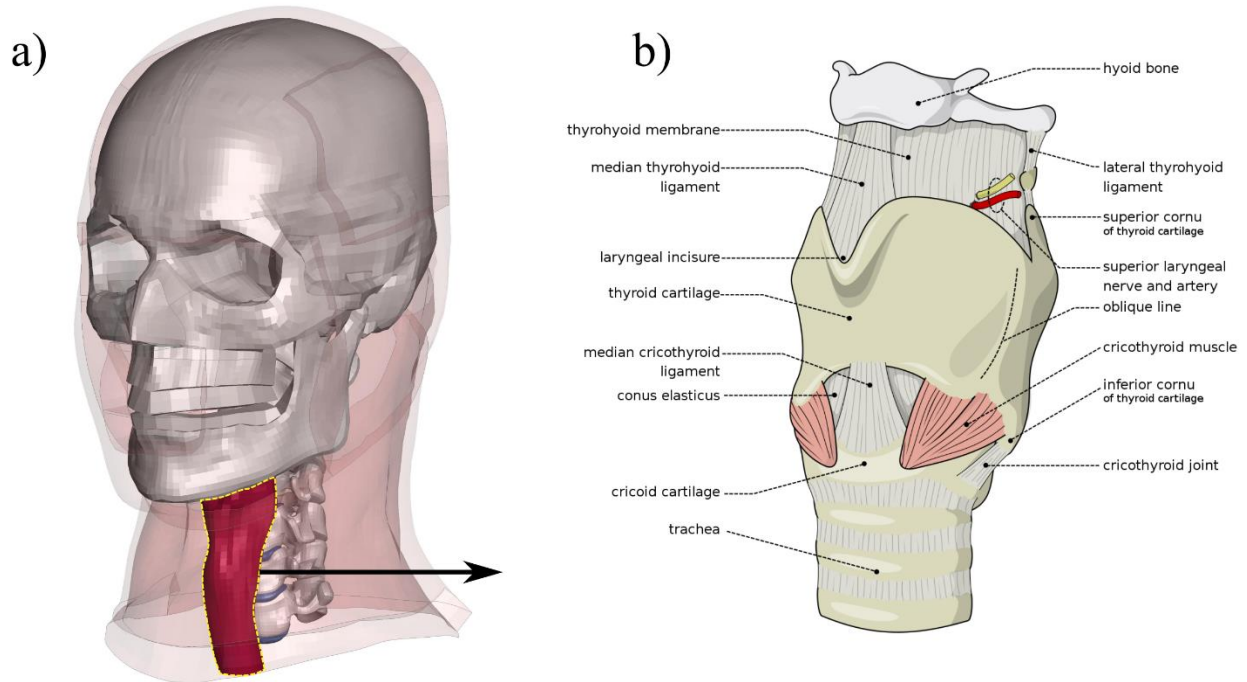


**Figure 29: a) Larynx tissue in the GHBMCM50, b) Diagram of the human larynx tissues (Olek Remesz (wiki-pl: Orem, commons: Orem), CC BY-SA 2.5 <<https://creativecommons.org/licenses/by-sa/2.5>>, via Wikimedia Commons)**

Focal impact on the anterior neck can result in fractures to the cartilages of the larynx, which are critical for maintaining open airways (Figure 30) [70]. Severe damage to the larynx cartilages has a prehospital fatality rate of 80% [71].

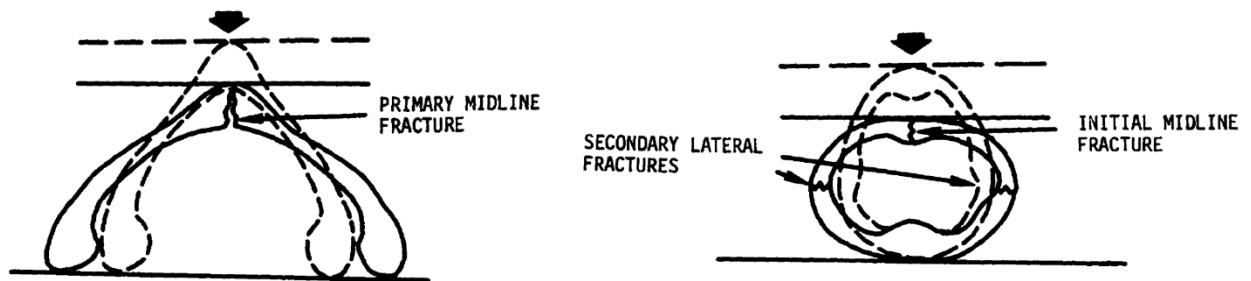


**Figure 30: Thyroid and Cricoid Cartilage fracture modes (Copyright Permission [72])**

Prior to the widespread adoption of seatbelts and airbags, passenger impacts with the dashboard or steering wheel (Figure 31a) led to larynx trauma, or even cervical spine fracture, referred to as the "padded dash syndrome" [73], [74]. The widespread adoption of 3-point belts in the automotive industry has mostly eliminated the issue of focal impact on the anterior neck [75].

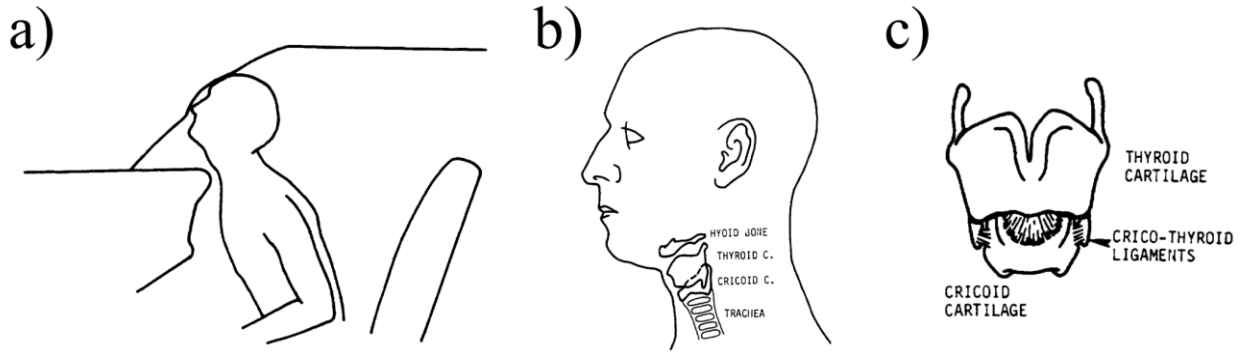


**Figure 31: a) Focal impact on the larynx of a passenger in a car crash; b) Location of the cricoid and thyroid cartilages; c) Front view of the cricoid and thyroid cartilages (Copyright Permission [72])**

Impact testing of PMHS generates fracture tolerances for the thyroid and cricoid cartilages (Figure 31b,c) of the larynx. Melvin reported that loading of the larynx initially increases until the thyroid cartilage fractures. At that point, there is a slight decrease in the load before increasing as the cricoid cartilage bears all the load (Figure 32).

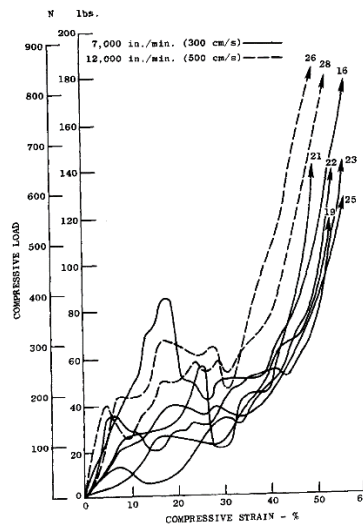


**Figure 32: Dynamic Compression response of large larynges (Copyright Permission [72])**

The AIS codebook states that a crushing injury to the larynx cartilage is an AIS-5 injury (Table 10).

**Table 10: Fracture thresholds for the larynx cartilages**

Study	Test Subject	Bone/cartilage	Fracture Force
Bockholdt [76]	Extracted Tissue Sample	Thyroid Horns	29 N
Gadd [77]	PMHS (Embalmed)	Thyroid, Cricoid Cartilages	200-250 lbs, 175-225 lbs
Gadd [78]	PMHS (unembalmed)	Thyroid, Cricoid Cartilages	90-100 lbs (both cartilages)
Melvin [72]	PMHS (unembalmed)	Thyroid, Cricoid Cartilage	180 N, 248 N (Average)

### **2.11. Numerical Human Body Models**

Researchers have primarily used physical ATDs and post mortem human subjects (PMHS) for crash safety testing. ATDs are made from non-biological tissues, such as rubber and metal, which makes them less biofidelic than PMHS [79]. PMHS provides a more accurate assessment of tissue-level injury but suffer from limited supply, tissue degradation, and a lack of muscle activation.

Human Body Models (HBM) replicate the tissue geometry and material properties of a live human for use in numerical simulations. There are numerous computational HBMs in use today. Three of the most widely used HBMs are the Global Human Body Models Consortium (GHBMC) model (Figure 33), the Total Human Model for Safety (THUMS) model, and the VIVA+ model [80].



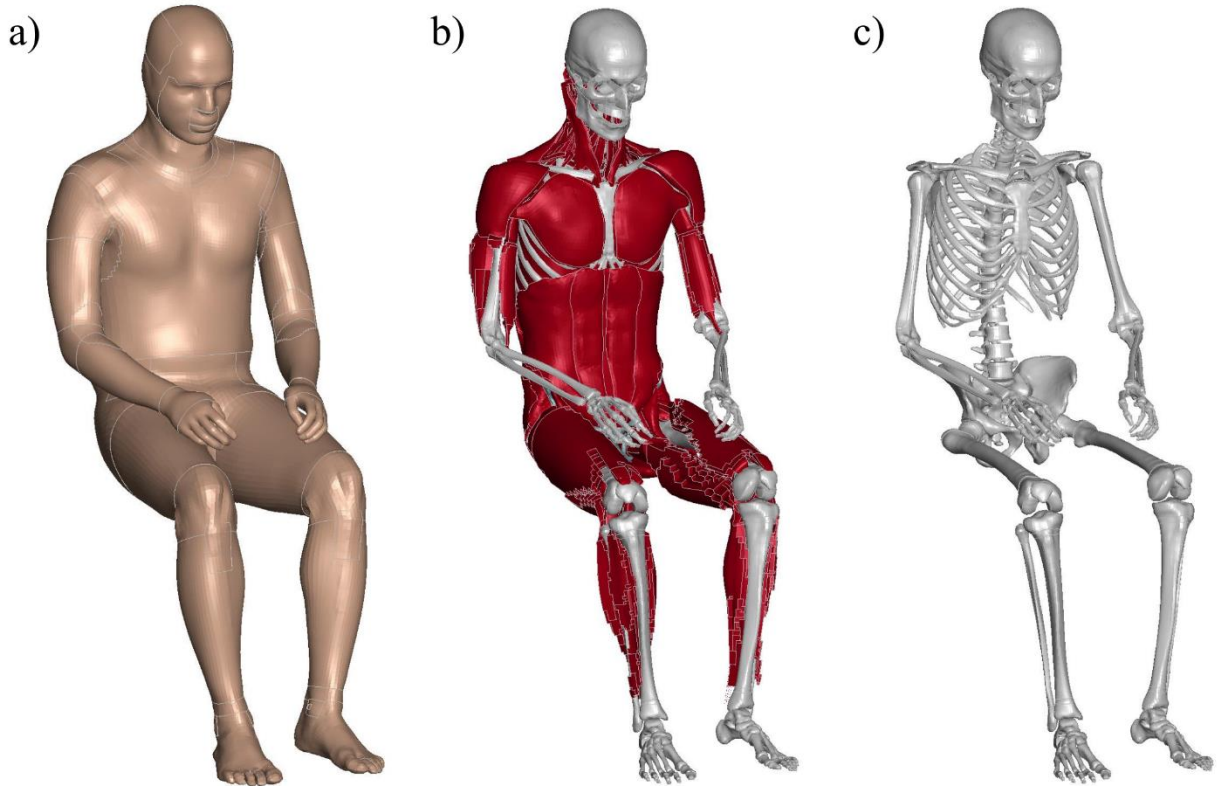


**Figure 33: GHBMC M50 Model V-5.1 a) Entire Model; b) Musculoskeletal; c) Skeleton**

The GHBMC consolidates the work of multiple Centers of Excellence (COE) that each focus on the development of a specific body region [81]. The GHBMC full-body model combines the separate body regions developed by the COEs [82]. Version 5-1 of the GHBMC M50 model is made up of 2,473,387 elements and 1,355,605 nodes. The model uses various materials to characterize the behaviour of tissues such as muscle, adipose tissue, ligaments, bone, vasculature, and organs.

### **2.11.1. Human Body Models in Transit Bus Crashworthiness Research**

The safety risks posed to standing passengers in transit buses was investigated using an active Human Body Model (Madmyo-HBM) in a 2007 study [83]. The passenger model was positioned in a transit bus model and subjected to a crash pulse. The potential for severe head injury was identified based on the impact severity between the head and the rigid handrails. The HBM was not used in a seated configuration in bus model.

### **2.12. Tissue Level Injury Assessment by Body Region**

Human Body Models provide the ability to assess localized tissue injury. Predicting injury at the tissue level requires comparing element level metrics such as stress, strain, and pressure with the thresholds

provided in the user GHBM user manual [84]. This section will detail the tissue injuries assessed in this study and the corresponding injury thresholds.

### **2.12.1. Diffuse Axonal Injury**

Traumatic brain injury (TBI) is brain tissue damage that can lead to permanent neurocognitive impairment. TBIs are common in vehicular crashes and can result from a direct blow, impulse, or rapid head movement [85]. Axons are long thin cells arranged throughout the brain in the form of a network that conducts signals to facilitate brain activity [86]. A Diffuse Axonal Injury (DAI) is a form of TBI caused by the damage to the axonal structures during the rapid deformation of brain tissue [87].

Researchers generate injury thresholds for DAI using measured head accelerations from concussive impacts suffered by athletes during training and competition. Accelerometers embedded in the athlete helmets and mouthguards in sports such as American Football, boxing, and mixed martial arts record the peak head accelerations that lead to physician-diagnosed concussions. The accelerations are applied to FE brain models to correlate brain strains at the element level with concussive symptoms (Table 11).

The GHBM currently uses a threshold of 0.48 for maximum principal strain in a given brain region to predict a DAI. Typically, the 95<sup>th</sup> percentile maximum principal strain in the brain region is used to determine the severity of brain tissue deformation while filtering out distorted elements with excessive strain.

**Table 11: Brain Strains associated with concussion via FE modelling of concussive impacts**

Study	Brain Region	Sport	Metric	Value predicting concussion
Viano (2005) [88]	Midbrain, Thalamus,	Football	Strain (mean)	0.344 (SD 0.14), 0.376 (SD 0.193)
Hernandez (2015) [89]	Corpus Callosum	American Football, boxing, MMA	Peak Strain	0.498 (loss of consciousness),
Beckwith (2018) [90]	Cerebrum, Cerebellum, brain stem, corpus callosum	Football	MPS (Median)	0.18, 0.09, 0.14, 0.13
Patton (2013) [91]	Midbrain, Corpus Callosum, Thalamus, Gray Matter	Australian football, rugby	MPS (mean)	0.25, 0.31, 0.26, 0.47
GHBMC User Manual	All brain regions			0.48

### 2.12.2. Acute Subdural Hematoma

Acute subdural hematoma (ASDH) occurs when the bridging veins that connect the cerebral cortex to the superior sagittal sinus rupture during an impact event (Figure 34) [92] [93]. Bridging veins from cadavers have been loaded to failure experimentally with a resulting failure strain of  $18 \pm 7\%$  [94]. The GHBMC implements a failure strain of 25% for an ASDH.

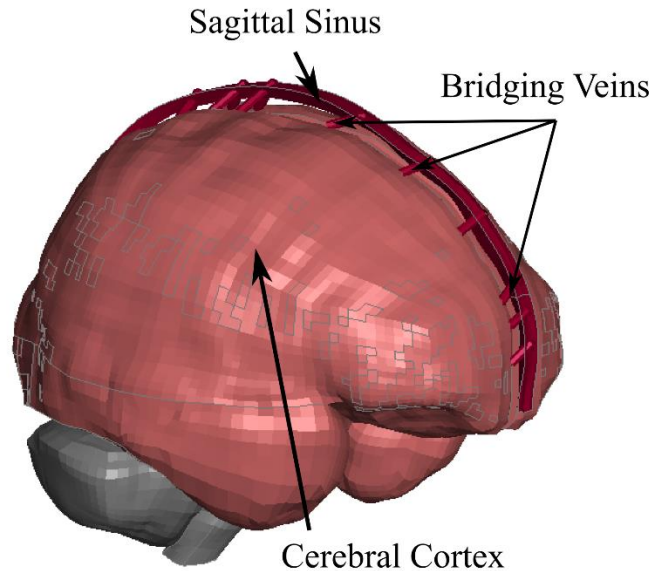


**Figure 34: Bridging Veins in the GHBMC M50 Model**

### 2.12.3. Cerebral Contusion

A cerebral contusion is the localized tissue damage to the brain that occurs during head impacts. As the brain moves within the skull during impact, a high positive pressure develops at the site of impact between the brain and the anterior skull, which is called a "coup injury." A pressure wave is generated at the coup injury location which travels through the brain and reflects off the skull on the opposite side of the brain, generating localized negative pressure [95] The negative pressure can cause localized damage to the brain tissue called a "contrecoup injury" (Figure 35).

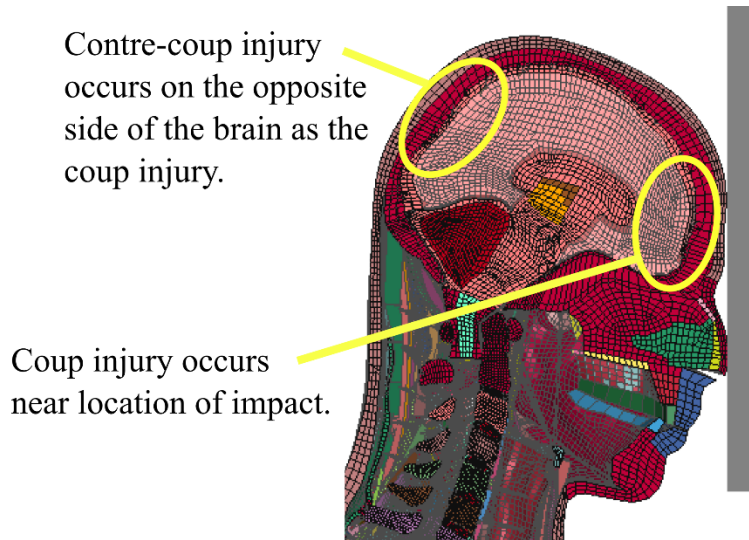


**Figure 35: Coup and contrecoup injury to the brain**

PMHS head impacts with recorded intracranial pressure are subsequently assessed for contusion injury by researchers to generate injury thresholds [96], [97]. The experimental data was then used with FE modelling to develop an injury tolerance for a positive pressure of 234 kPa [98]. Element pressures throughout the brain regions of interest allow the prediction of cerebral contusion with the GHBMC model using positive/negative pressure thresholds of 237/-104 kPa.

### 2.12.4. Neck Ligament Failure

Injuries to the ligaments in the cervical spine can result in long-lasting pain and disability. Multiple ligaments connect the ascending cervical spine vertebrae from the base of the skull (occipital condyle) down to the thoracic spine. These include the Anterior Longitudinal Ligament (ALL), Posterior Longitudinal Ligament (PLL), Ligamentum Flavum (LF), Interspinous Ligaments (ISL), and the Cervical Capsular Ligament (CL) (Figure 36).

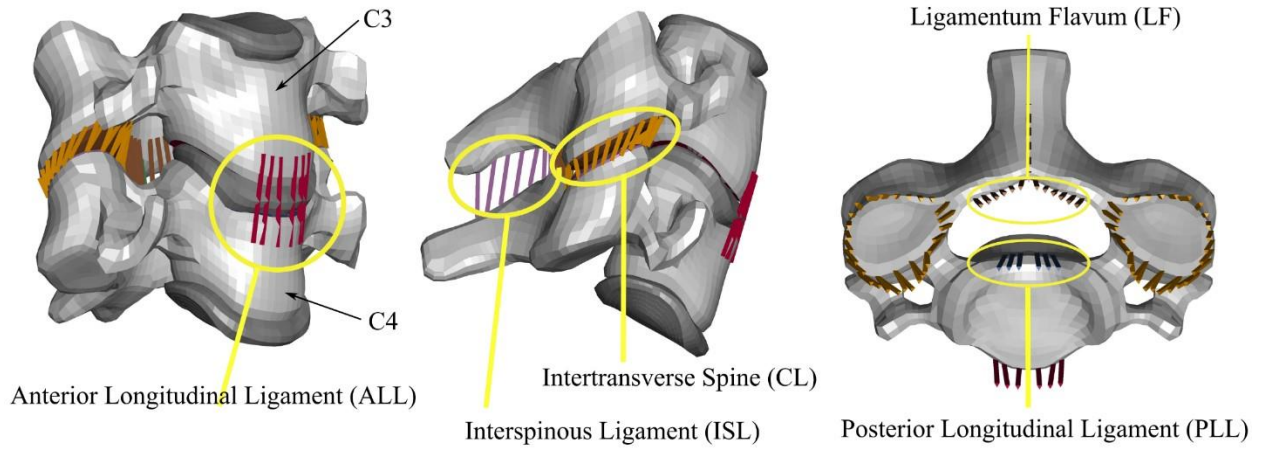


**Figure 36: Neck Ligaments in the Cervical Spine of the GHBMC M50 Model**

There are ligaments specific to the upper cervical spine connecting C2, C1, and the Occipital Condyle (Figure 37).

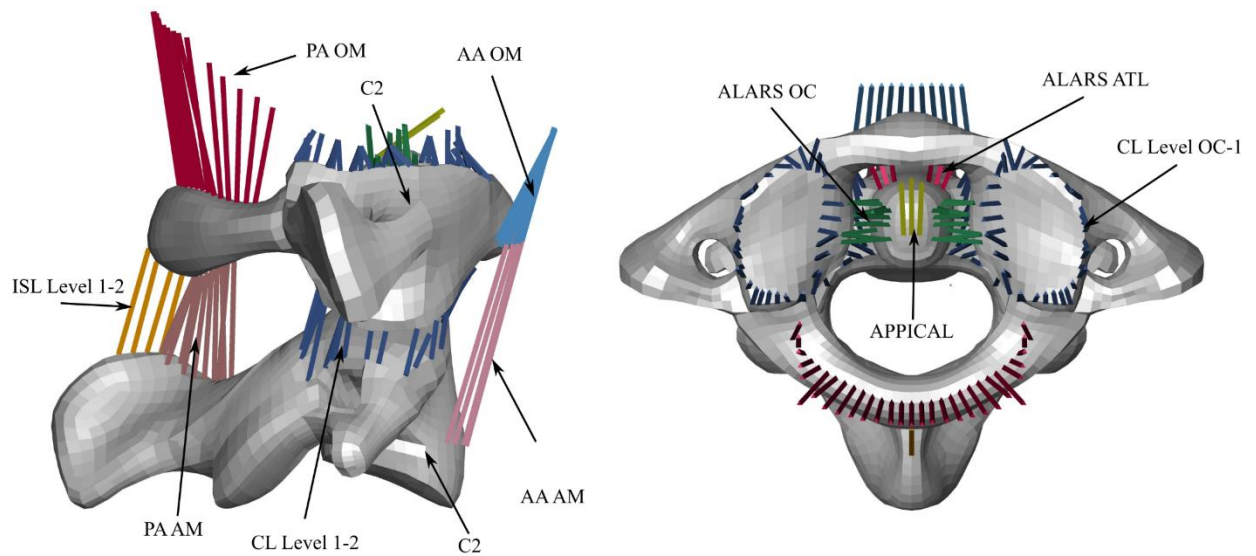


**Figure 37: Upper Cervical Spine Ligaments**

Yoganandan found that ligaments in the cervical spine displayed a nonlinear behaviour under loading that initiates with a toe region where the fibres of the ligaments are initially engaged [99]. As the displacement increases, the stress response exhibits a linear elastic response. At a certain point the ligament begins to fail, causing a drop in stress (Figure 38).

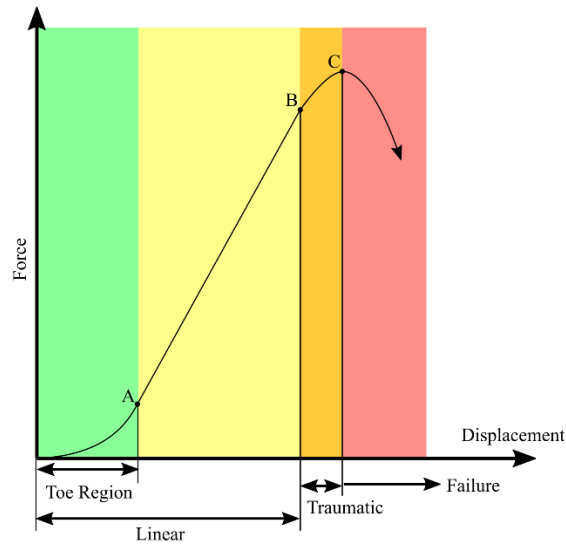


**Figure 38: Stretch response of neck ligament with initial toe region, linear region, and reduction in stiffness corresponding to ligament failure (Figure adapted from [99])**

Mattucci et al. performed a series of quasi-static and high strain rate tensile tests on cervical spine ligaments from PMHS to measure the stretch-stiffness response and failure limit [100]. The experimental data was curve fit for implementation in HBM neck models, including the predicted failure distraction for each ligament (Table 12) [101]. The GHBMC model implements ligament failure by deleting elements once the tensile displacement of the element surpasses a threshold.

**Table 12: Cervical Spine ligament high strain rate failure distraction [101]**

Ligament	High Strain Rate Failure (mm)	SD
ALL	3.65	0.81
PLL	2.85	0.76
LF	4.08	1.51
CL	4.39	1.8
ISL	4.8	1.12

### 2.12.5. Intervertebral Disc Avulsion

Intervertebral disc avulsion (IDA) occurs when the disc tissue separates from the bone due to high stresses. The GHBMC model sets a failure limit for the tied connection between the disc endplates and the cervical spine vertebrae to predict an IDA injury. DeWitt demonstrated that a cervical spine segment model implementing avulsion accurately predicted injury observed in experiments [102]. Tied

connections between the endplates and the vertebral body (Figure 39) get deleted when the tensile stress in the connection surpasses 30 MPa.

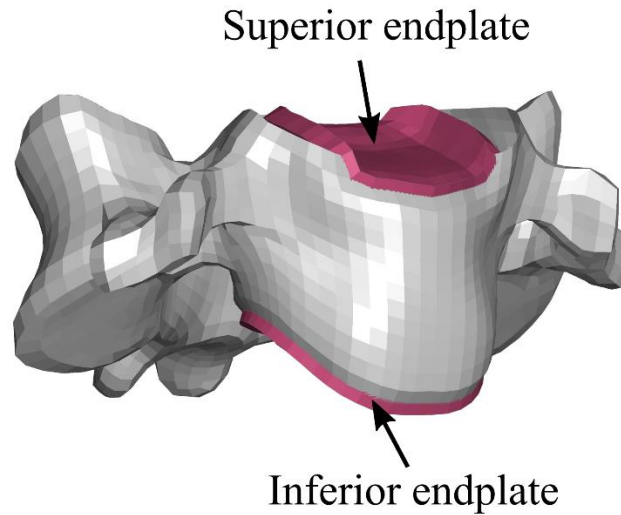


**Figure 39: Cervical spine superior and inferior endplates at the isolated C2 level**

#### **2.12.6. Hard Tissue Fracture**

Bone is a rigid tissue made up of collagen and calcium phosphate which functions to support the human body and protects vital organs [103]. Cortical bone makes up the dense outer layer of a bone and does the primary load-bearing. The interior of the bone is a sponge-like structure called trabecular (cancellous) bone (Figure 40). When bones are loaded past their ultimate strength, cracks can develop and eventually lead to fractures.

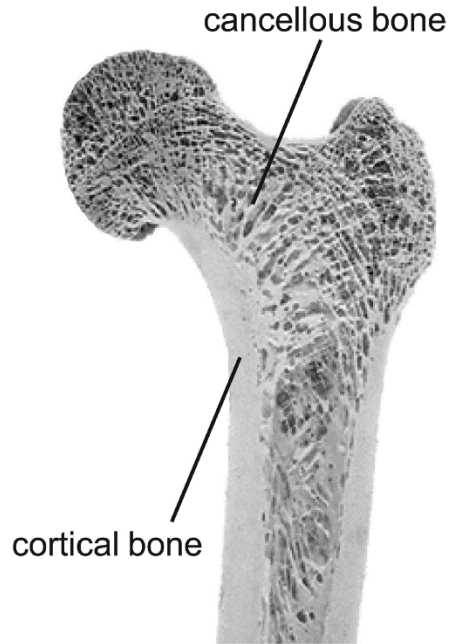


**Figure 40: Cortical and trabecular bone (Copyright [104])**

Bone is modelled as an elastic-plastic material in the GHBM model. Elastic-plastic material models allow for permanent deformation to develop once the stress in the material surpasses the yield stress (Figure 41). Effective plastic strain describes the amount of permanent deformation in an element modelled with an elastic-plastic material. Bone failure is modelled in the GHBM HBM by deleting elements that have surpassed a limit for effective plastic strain.

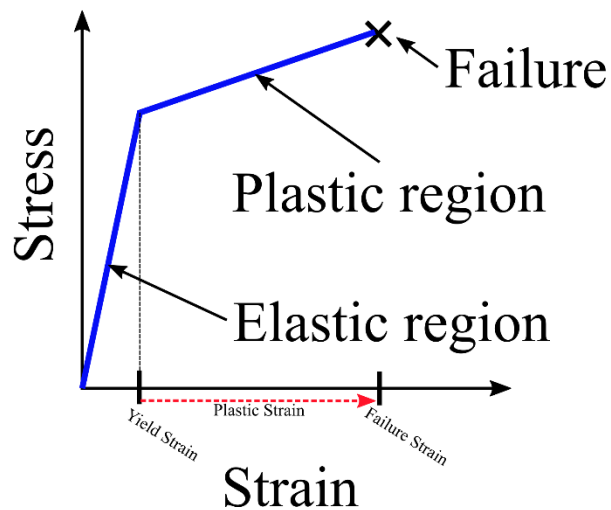


**Figure 41: Elastic-plastic material stress-strain curve**



Failure strains are typically determined experimentally using PMHS bone samples loaded to failure (Table 13). The yield strain and failure strain (ultimate strain) have been reported in the literature for various bones throughout the body.

**Table 13: Plastic strains measured at failure from experiments**

Study	Bone	Failure Strain	GHBMC User Manual
McElhaney	Cervical body (Cortical)	1.78%	1.78%
Lindhahl	Cervical Body (Trabecular)	9.5% male, 9% female	9.5%
Kemper	Ribs (Cortical)	1.82%	1.8%
Duma	Ribs (Cortical)	1.1-2.5 %	
Keller et al. 1990, Currey et al. 1997	Femur (Cortical)	0.85%	0.88%
Burnstein 1976	Tibia and Femur (cortical)	0.89%	
Song 2005	Pelvis (Cortical)	3%	3%

### 2.12.6.1. Ribs and Sternum

The human ribcage consists of twelve levels of ribs (left and right) which attach at the anterior side of the body at the costal cartilage and sternum (Ribs 1-10), and on the posterior side at the spine (Figure 42).

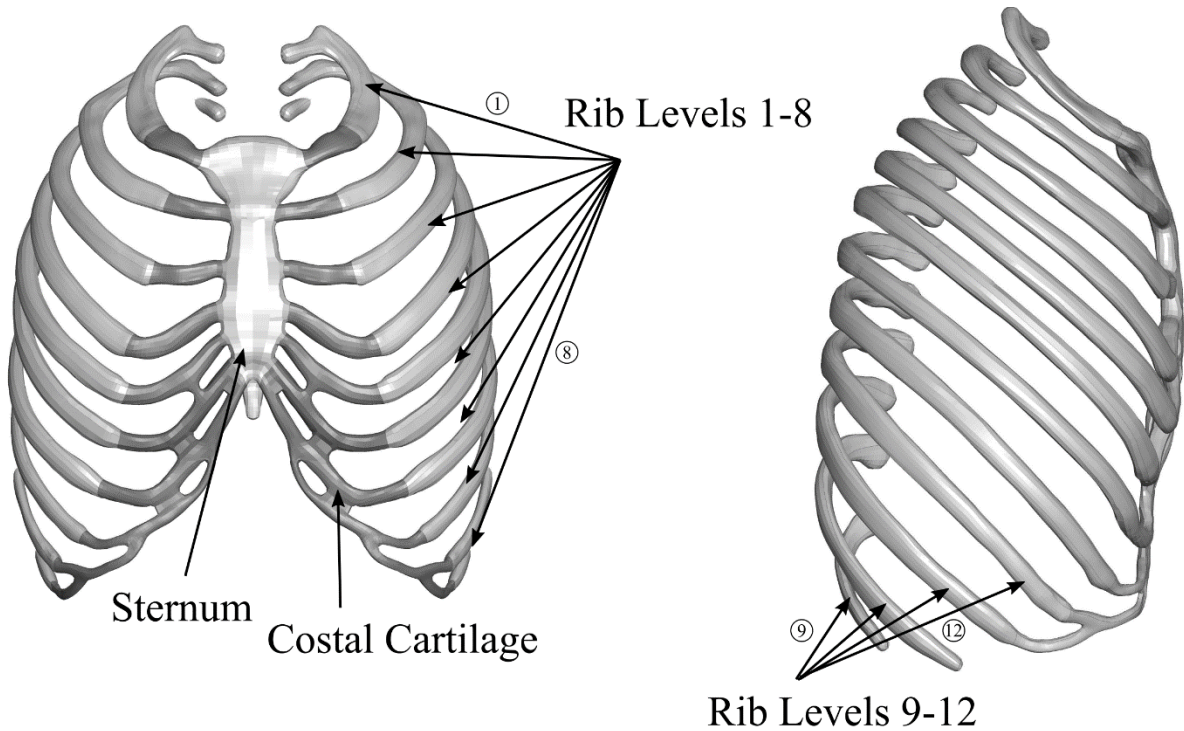


**Figure 42: Ribs and sternum in the GHBMC M50 model**

### 2.12.6.2. Lower Extremities

The major bones in the lower extremities consist of the coxal and sacrum in the pelvis region, and the femur, tibia, and fibula in both the left and right legs (Figure 43).

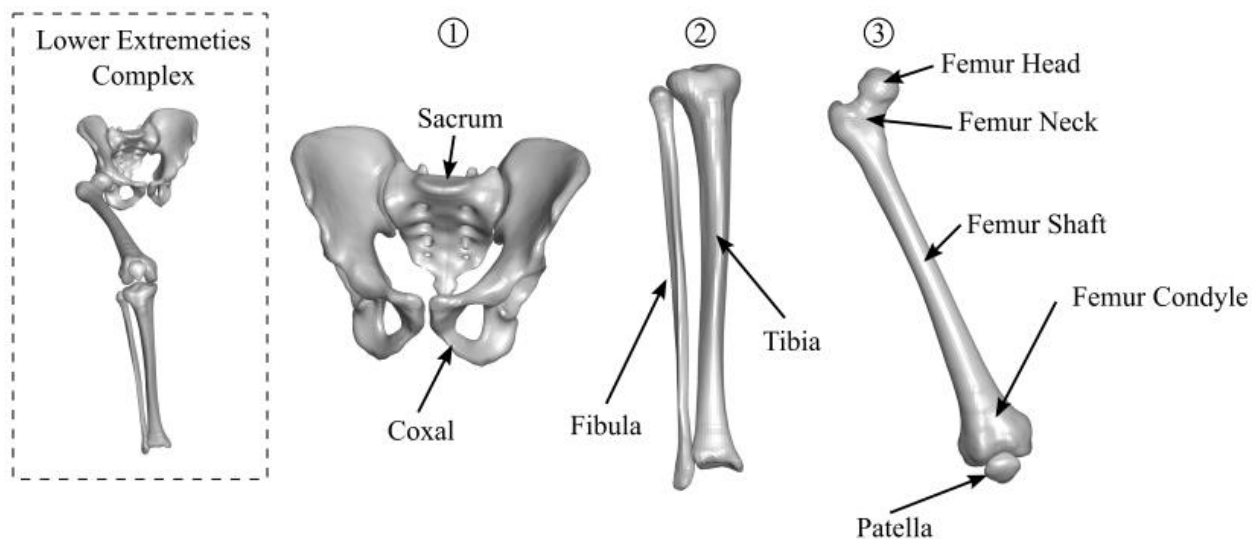


**Figure 43: Bones that make up the lower extremities which include the pelvis (coxal and sacrum), the upper leg (femur), and the lower leg (fibula and tibia)**

## 2.13. Frontal Crashworthiness Standards by Region and Applicability to Transit Buses

This section will cover the frontal automotive crashworthiness regulations in various regions and discuss the application, if any, to transit buses.

### 2.13.1. Federal Crashworthiness Standards in Canada and the United States

The Canadian Federal Motor Vehicle Safety Standards (CMVSS) and the Federal Motor Vehicle Safety Standards (FMVSS) set the safety regulations for the automotive industry in Canada and the US. Standard 208 (CMVSS & FMVSS) covers the protection of occupants in passenger vehicles in frontal impacts [8], [9]. The standard sets limits for injury metrics measured at the head, neck, chest, and lower extremities during a crash. The crash pulse for the sled testing procedure for standard 208 must be within specified bounds (Figure 44).

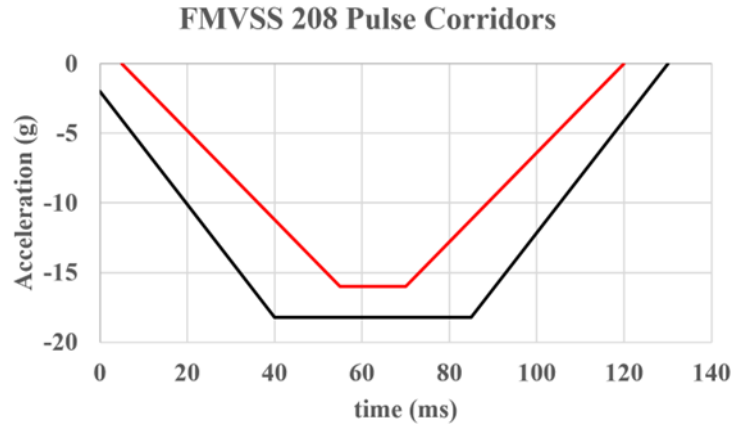


**Figure 44: FMVSS and CMVSS 208 Acceleration pulse corridors**

Standard 208 only applies to passengers in vehicles weighing less than 2495 kg. The weight of a typical transit bus is in the range of 9500-13500 kg, excluding it from standard 208 [105]. The weight restriction for standard 208 is only applicable for passenger seats, thus the driver seat of transit buses is required to be equipped with a 3-point belt.

### 2.13.2. Crashworthiness Standards in Europe and Australia

The United Nations Economic Commission for Europe (UNECE) implements regulation ECE 80, which regulates the crashworthiness of large passenger buses [106], [107]. ECE 80 requires that seat structures withstand the load generated from a passenger impacting it from the rear during sled tests that utilize an acceleration pulse that falls within specified corridors (Figure 45). ECE 80 sets maximum thresholds for injury metrics at the head, chest, and lower extremities in frontal impacts (HIC<sub>15</sub> under 500, Thoracic Acceptability Criteria (ThAC) under 30 g, Lower Extremity (LE) under 10 kN). ECE 80 only applies to passenger vehicles weighing 4 534 kg or less and thus excludes transit buses.

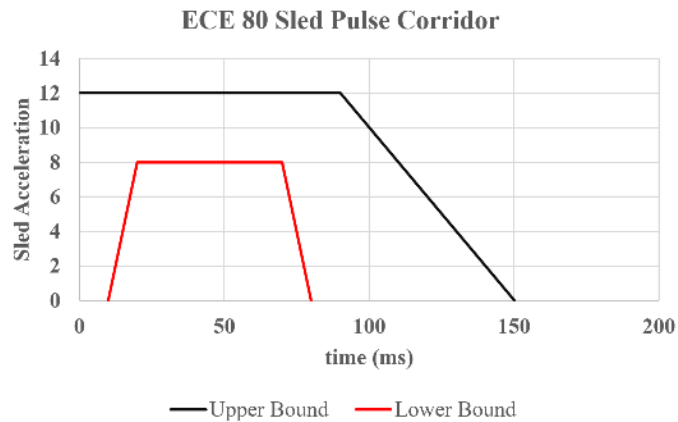


**Figure 45: ECE80 acceleration pulse corridors**

Australia implemented safety regulations mandating 3-point belts for motorcoaches following two mass casualty events in 1989 that resulted in 56 fatalities [108]. Australia implements a similar standard to ECE 80 for large buses called Australian Design Rule (ADR) 68 [109]. The standard uses a more severe pulse than ECE 80, which requires a change in velocity of 49 km/hr and 20 g of deceleration within the first 30 milliseconds. ADR 68 sets the minimum requirement for protection of the head, thorax, and lower extremities, with higher thresholds than ECE 80 due to the increased pulse severity (HIC<sub>36</sub> under 1000, ThAC under 60, LE under 10 kN). ADR 68 explicitly omits transit buses from its regulations.

#### **2.14. American Public Transportation Association Bus Procurement Guidelines**

The American Public Transportation Association (APTA) is an international non-profit association that advocates for and conducts research on behalf of the public transit industry. The APTA releases bus procurement guidelines created in collaboration between the public and private sectors. The guidelines cover many aspects of bus design and performance standards, including some related to bus crashworthiness [110].

The transit bus crashworthiness standards state that the bus must be able to withstand a 25-mph side impact by a 4000 lb. automobile with no more than 3 inches of deformation at the passenger hip height and cannot result in protrusions into the passenger compartment. The roof structure of the bus can deflect no more than 6-inches when subjected to a 150% curb weight load.

The guidelines also cover the design of the passenger compartment, including seats and handrails. The passenger seats must be cantilevered to provide adequate cleaning room and have at least 27 in. separating two rows of seats in the transverse direction. A minimum seat height from the floor (17+- 1 in.), seat width (35 in.), and seat depth (17 +-1 in.) are all specified. Each transverse seat row must incorporate a 7/8 in. handhold along its top edge. The guidelines also state that the handrail should not be hazardous to passengers during a severe deceleration. The transverse seat rows are required to deflect no more than 2 in. if two 95<sup>th</sup> percentile passengers impact the forward seat during a 10 g deceleration.

There are two passenger crashworthiness requirements included in the guideline. The femur axial loads cannot exceed 4500 N, and the Head Injury Criterion (HIC<sub>15</sub>) cannot exceed 400 for passengers ranging in size from the 5<sup>th</sup> percentile female to the 95<sup>th</sup> percentile male. The test condition is for a 10 g deceleration that peaks between 0.05 and 0.150 seconds from initiation.

The guideline states that new transit buses should pass the Altoona bus testing procedure conducted at Penn State University to assess vehicle performance. The tests assess rapid lane-changing capabilities and

braking strength of new bus models [111], [112]. The Altoona tests do not include any assessment of the crashworthiness or protection of passengers for new bus models.

### **2.15. Transit Bus Crashworthiness Literature Review**

This section will cover the previous research investigating the crashworthiness of transit buses and the potential for injury to passengers. The key findings from each study will be shown, along with the test conditions tested, and the occupant surrogates tested. This section will identify the gaps in the current literature that the current study will seek to address.

### **2.16. Full Transit Bus Model Impact Simulations**

Kumbhar and Joshi utilized a full transit bus FE model provided by the bus manufacturer Optima Bus Corporation to assess passenger injury in frontal and rear impacts [113] [114]. Both studies validated the bus model for a frontal, rear, and side-impact using experimental data from tests conducted by the manufacturer to comply with the APTA bus crashworthiness guidelines (see section 2.9). Following validation, Kumbhar assessed passenger injury in rear impacts, and Joshi assessed the potential for injury to passengers in frontal impacts,

Kumbhar reported bus CG accelerations under varying rear impact conditions. The impacts included a 100% and 60% overlap with another transit bus at initial speeds of 0, 5, and 15 mph. Additional simulations included the bus impacting a midsize car, a minivan, and a pickup truck, with both vehicles having initial speeds of either 20 or 30 mph. The maximum bus acceleration occurred during the 100% overlap impact with another transit bus.

The second stage of the Kumbhar study assessed passenger injury under the Insurance Institute for Highway Safety (IIHS) test condition. The IIHS test condition required a rear impact by a vehicle of equivalent weight (transit bus) at 20 mph. The bus model incorporated Madymo HIII ATD models (5<sup>th</sup>, 50<sup>th</sup>, and 95<sup>th</sup> percentiles) in various seating locations for the rear impact injury assessment. The results showed minimal potential for head, neck, chest, and lower extremity injury under the IIHS rear impact test condition.

Joshi reported the resulting center of gravity (CG) acceleration for a full transit bus model under varying frontal impacts. The impact conditions included a rigid barrier impact at 18.6 mph, impacting a small car at 30 mph, and impacting a minivan at 30 mph. An acceleration sled model consisting of four forward-facing and one side-facing seat taken from the full bus model was used to assess passenger injury in frontal impacts. HIII ATDs of varying sizes (5<sup>th</sup>, 50<sup>th</sup>, and 95<sup>th</sup> percentile) were seated in the forward-facing seats, and a 50<sup>th</sup> male was seated in the side-facing seat.

Acceleration pulses from the full bus model impacts were applied to the acceleration sled model. The injury assessment with the rigid barrier pulse showed that the 5<sup>th</sup> percentile ATD impacted the forward handrail on the lower face. The axial forces and bending moments measured in the upper neck of the 5<sup>th</sup> percentile female predicted a severe neck injury as a result. The forward-facing 50<sup>th</sup> male ATD showed a potential for a head injury in the car and minivan impact pulses due to the head impacting the forward seatback. In general, the results showed a low potential for injury to the thorax and the lower extremities and a high potential for head and neck injury if the face of the passenger impacted the forward handrail.

The Joshi and Kumbhar studies were limited because the ATD models were simplified. The simple Madymo occupant models did not have the capabilities to analyze the focal impact injuries of passengers on transit buses.

### **2.16.1. Enhanced Coach and Bus Occupant Safety (ECBOS)**

A 2004 study out of Europe investigated rapid transit bus decelerations and the potential for passenger injury [115]. Multibody HIII models were seated in a bay-style seating arrangement in a full-scale bus model facing the front of the bus.

The unrestrained ATDs were thrown forward under the rapid deceleration and impacted the forward seat. The passenger stature determined the impact location between the ATD and the forward seat. The small stature female impacted the forward seat headfirst, while the 95<sup>th</sup> percentile ATD impacted the forward seat with its lower extremities. The most significant injury source was the focal impact of the head with the forward seat, which resulted in a severe neck injury for the small stature female. The report recommended 3-point belts on transit buses to reduce the potential for injury in a frontal impact scenario.

One of the limitations of this study was that the passenger models used were rudimentary multibody models that lacked the detail required to capture all of the injury potential. The report did not include the pulse magnitude used to simulate the rapid deceleration.

### **2.16.2. Federal Transit Administration Research**

From 2005 to 2010, the National Institute for Aviation Research (NIAR) at Wichita State University conducted a research program into passenger injury on transit buses on behalf of the Federal Transit Administration (FTA) [116], [117], [118].

The study used an acceleration sled with two rows of forward-facing transit bus seats and a side-facing seat. Frontal, side, and rear impacts were conducted with the sled buck using 5<sup>th</sup>, 50<sup>th</sup>, and 95<sup>th</sup> percentile HIII ATD models. The 95<sup>th</sup> male ATD was seated in the front seat facing a knee-high panel, the 50<sup>th</sup> male and 5<sup>th</sup> female were seated in the row behind, and a 50<sup>th</sup> male was seated in the side-facing seat. The

frontal impact pulse was sourced from the Joshi study where the bus impacted a minivan at 30 mph (Figure 46) [114]. The rear impact pulse was taken from the Kumbhar study and corresponded to a rear transit bus impact at 20 mph [113]. The side impact pulse corresponded to a large truck impacting the side of the transit bus at 25 mph. A FE model of the test buck was developed and validated using the experimental data from the sled tests.

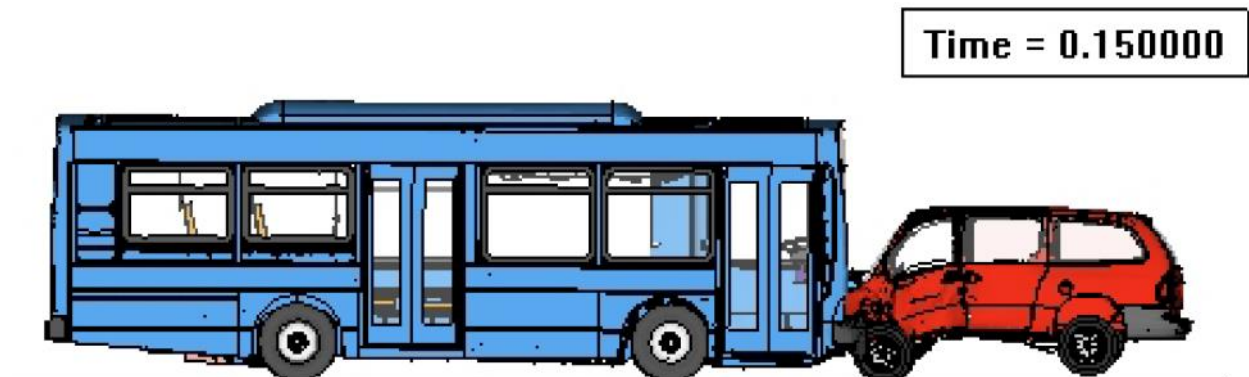


**Figure 46: Frontal impact pulse corresponding to bus impacting a minivan (Copyright Permission [118])**

The ATDs impacted the forward handrail on the face during the frontal impacts, which resulted in the upper neck bending moment surpassing the injury thresholds for the small stature ATD. In some instances, the ATDs impacted the forward handrail on the anterior surface of the neck, but the study did not report the resulting impact forces or injury assessment.

The rear impact caused severe hyperextension of the neck and predicted a high probability of neck injury. The side impact showed that ATDs seated in the side-facing seats were thrown across the aisle into passengers on the other side of the bus, resulting in a high probability of neck and femur injuries.

The test buck model was used to conduct a parametric analysis to investigate safety improvements for the bus seat design. The seat pitch, height, handrail, and headrest design were varied and assessed separately with ATDs of varying sizes. An optimal design was identified based on ATD injury assessment for each impact direction. The optimized design for the frontal impact increased the seat pitch and maintained a low seat back. The optimized design for the rear impact included raised headrests to prevent hyperextension injury to the neck.

The final FTA report included a proposed new seat design that incorporated raised headrests (Figure 47). The headrest design aimed to eliminate the risk of a hyperextension neck injury, deemed the most injurious loading source to the passengers. The report did not include any experimental tests or numerical

simulations with the new seat design to test its effectiveness. The report recommended using human body models with muscle activation to further improve transit seat design.

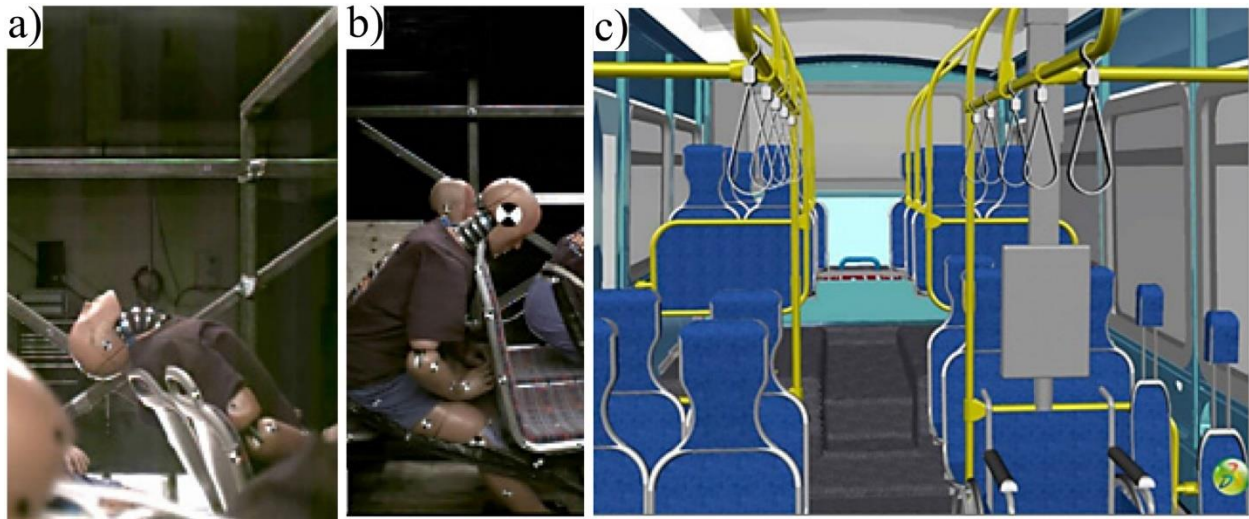


**Figure 47: a) Rear impact hyper extension of the neck; b) Frontal impact ATD contacts the forward seat on the anterior surface of the neck; c) Proposed new seat design with headrests (Copyright Permission [116])**

### **2.16.3. Transit Bus Sled Experiments Using Adult and Child ATDs**

Martinez et al. [119] investigated the passive safety features of public transit seating using an acceleration sled comprised of two rows of forward-facing seats (Figure 48). The ATDs used in the experiment included a HIII 50<sup>th</sup>, 95<sup>th</sup>, 6-year-old, 3-year-old, and 18-month-old seated in the sled buck. A 12 g pulse corresponding to a 50 km/hr head-on collision between a bus and car was applied to the test buck model to replicate frontal and rear impacts. The 3-year-old dummy suffered a severe upper neck injury in the frontal impact from impacting the forward seat with the face. The 50<sup>th</sup> percentile ATD impacted the forward handrail on the neck or the lower face but did not predict a head or neck injury. In the rear impact simulation, the 50<sup>th</sup> male reported neck extension moments that surpassed the threshold for a hyperextension injury. The peak femur loads surpassed the lower threshold for femur fracture in elderly passengers, highlighting the risk of a lower extremity injury for elderly passengers. Martinez recommended implementing a raised headrest seat design to prevent the risk of neck hyperextension injury, identified as the most significant risk of injury.





**Figure 48: a) Test buck with HIII 50<sup>th</sup> percentile ATD and 6 YO ATD; b) Rear impact hyperextension of neck due to low seat back; c) Face of ATDs impact the top of the forward seat in the frontal impact (Copyright Permission [119])**

## **2.17. Passenger Safety in School Buses, Motorcoaches, and Passenger Rail and the Implementation of Passive Safety**

Other forms of mass transit, such as school buses, motor coaches, and passenger rail, implement passenger safety mechanisms in various ways. This section will review the safety features implemented on these vehicles, including active safety (seat belts) and passive safety. Passive safety refers to the orientation of seats, placement of rigid structures such as handrails, and seat geometry to improve safety without requiring seat belts.

### **2.17.1. School Bus Passenger Safety and Injury**

NHTSA considers school buses one of the safest forms of travel for students, stating that it is eight times safer than commuting by private automobile [120]. An average of two passenger fatalities occur during school bus frontal crashes each year [121]. Fatalities of school bus passengers typically occur during rollover events where ejection and roof crush injuries are likely [122].

School buses include several safety features, including a raised frame, bright reflective exterior paint, and stop signs that allow children to cross the street safely [123]. FMVSS and CMVSS 222 set crashworthiness standards for school buses, including performance standards for protecting the head and the lower extremities. The most recent update to the standard in 2009 requires equipping small school buses (under 4536 kg) with seatbelts at all passenger seating locations and for seat back height to be increased by 10 cm [124]. Large school buses (over 4536 kg) are not mandated to provide 3-point belts for passengers.

School buses implement compartmentalization as a means of passenger crash protection.

Compartmentalization functions by maintaining the passenger in their seating zone during a crash event

with high seat backs and minimal seat row spacing [125]. Seat backs absorb energy and reduce the potential for impact injuries to passengers.

NHTSA undertook a series of full-scale crash experiments with school buses in the early 2000s to investigate the effectiveness of compartmentalization [126], [127]. NHTSA impacted a school bus into a rigid barrier at 48.3 kph with ATDs of various sizes (adult male, small female, child) seated throughout the bus. None of the ATDs showed a potential for head or chest injury. There was a risk of severe neck hyperextension injury for the small female and child ATDs due to the face impacting the forward seat. Further investigation by NHTSA demonstrated that implementing a lap belt could pose a head and neck injury risk. Lap belts are effective at restraining the pelvis of an ATD from sliding forward, but allow the torso to rotate forward, resulting in the head striking the forward seat and causing severe head and neck injury [128], [129], [130]. The study also showed that using a 3-point belt significantly mitigated all passenger injuries in a frontal impact.

### 2.17.2. Motorcoach Passenger Safety and Injury

Motorcoaches operate primarily on highways at elevated speeds. A single collision involving a motorcoach can result in numerous fatalities, as was the case in 1999, 2004, and 2005 in the US (Figure 49) [131].

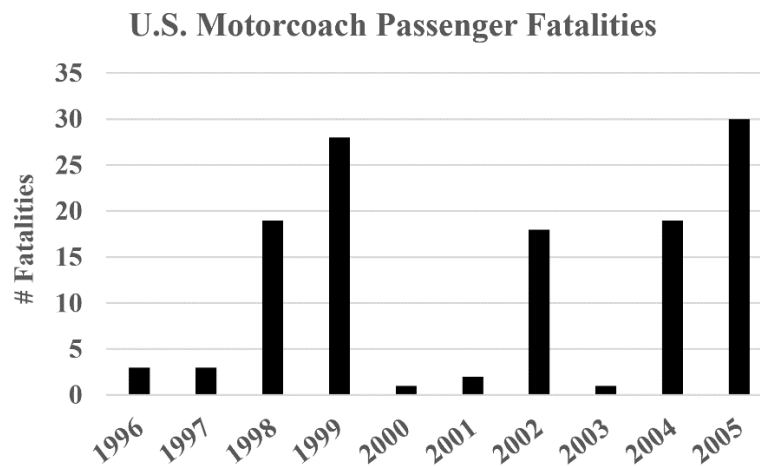


**Figure 49: Motorcoach passenger fatalities in the US from 1996 to 2005 (Figure adapted from [131])**

Motorcoaches typically have high-backed forward-facing seats. Unrestrained passengers have shown a potential for injuries to the head, neck, and lower extremities in frontal collisions [132], [133]. Similar to what was observed in school buses, the head of the passenger impacts the forward seat back and can cause severe neck hyperextension.

Research investigating the improvement of crash safety for motorcoaches has demonstrated that optimizing seat pitch, height, and seatback stiffness are effective passive safety measures [134]. Peng demonstrated that, in general, having a decreased seat pitch resulted in a lower potential for a head, neck, and femur injury due to the improved compartmentalization [135].

Due to the elevated operating speeds of motorcoaches, most research into safety improvement has focused on the implementation of seatbelts. Experiments have shown that lap belts tend to result in the head impacting the forward seatback due to the torso pitching forward, similar to school buses [136]. Implementing 3-point belts is recommended because they effectively eliminate contact with the forward seat [134]. Recent regulation updates in Canada and the US now require 3-point belts at every passenger seat in motor coaches [137], [138]. The operating characteristics of motorcoaches facilitate 3-point belt usage for passengers since trips are often long-distance and do not involve passengers continuously getting on and off the bus.

### 2.17.3. Rail Transportation Passenger Safety and Injury

Passenger rail operates at high speeds, and passengers are not required to wear seatbelts in the US or Canada [139]. A "secondary impact" describes how unrestrained passengers impact the surrounding seats or structures during a crash, which is the primary source of injury for passengers [140], [141]. An unrestrained passenger will continue their forward motion during an impact at a constant velocity until they impact the forward seat (Figure 50). The distance separating seat rows determines the free-flight time of the passenger and the secondary impact velocity. The longer the free flight time, the greater the velocity differential between the passenger and the surrounding seat structures.

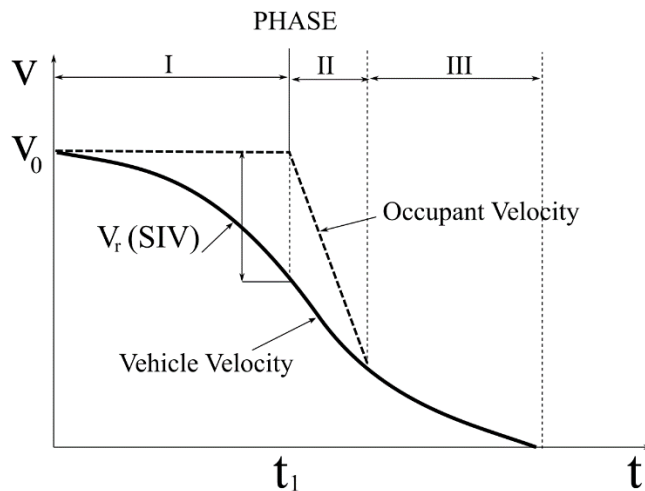


**Figure 50: Secondary impact velocity of a passenger in a rail car undergoing a collision (Figure adapted from [141])**

Carvalho et al. demonstrated that unrestrained, small-stature passengers are at an increased risk of neck hyperextension injuries when they impact the forward seat back with their face [142]. Improvement of the design of the upper portion of the seatback mitigated the risk of head and neck injury. The potential for head and neck injuries with passengers using lap belts has also been observed in the passenger rail industry [143].

Multiple studies have investigated methods of passive safety for reducing passenger injury. One study found that implementing swivel seatbacks reduced the potential for head and neck injury to passengers [144]. Another study used a numerical model to develop an improved table design that incorporated a crushable honeycomb structure to reduce the potential for a chest injury as the passenger impacted it [145], [146]. Like motorcoaches, the most effective means of protecting passengers on rail is by implementing 3-point belts [147].

### 3. Transport Canada Transit Bus Crashworthiness Research

Transport Canada (TC) has initiated a research program to investigate transit bus crashworthiness [10]. Their research is intended to inform the development of crashworthiness standards for transit buses as per recommendation by the Transportation Safety Board of Canada (TSB) [4]. TC's research has progressed in multiple phases. The first phase involved full scale collisions using two retired low floor transit buses. Two separate impacts were conducted where one bus impacted the rear end of the other at 40 km/hr. The second phase of the research involved lab impact tests using a test buck on a deceleration sled designed to replicate the kinematics observed during the full-scale transit bus impacts. HIII ATDs were used in both the full-scale impacts and test buck impacts to observe passenger kinematics.

Development and validation of a numerical model of the test buck in the current study depended on the experimental data generated in TC's experiments. The experimental data included the deceleration pulse of the test buck, the highspeed video of the HIII motions, and the kinematic responses of the HIII's.

#### 3.1. Full Scale Transit Bus Impact Tests

The full-scale bus impacts involved impacting one bus into the rear of the other at 40 km/hr with a 40% overlap (Figure 51). The bus positions were reversed for the second test, with the impacting bus from the first test being impacted in the second test. Both crash tests utilized the same initial velocity and overlap. The second test incorporated reinforcements to the front frame of the impacting bus to measure the change in response. The accelerations at the centers of gravity of each bus, as well as under the seats in each bus were recorded during both tests.

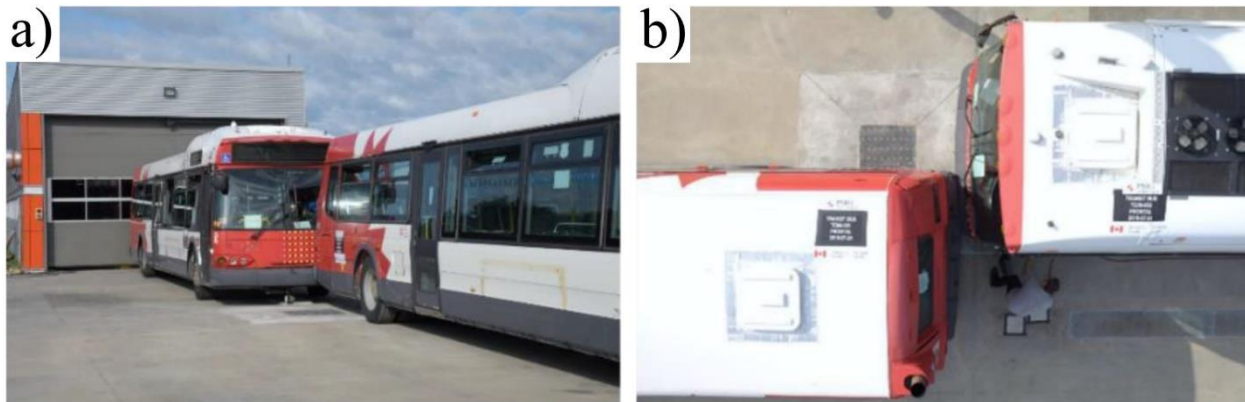


**Figure 51: a) Full-scale transit bus impact experimental setup (side view); b) 40% overlap (top view) [10]**

HIII ATD's of various sizes, including a 50<sup>th</sup> percentile male, 5<sup>th</sup> percentile female, and child dummies were placed at various locations throughout the striking bus (Figure 52).

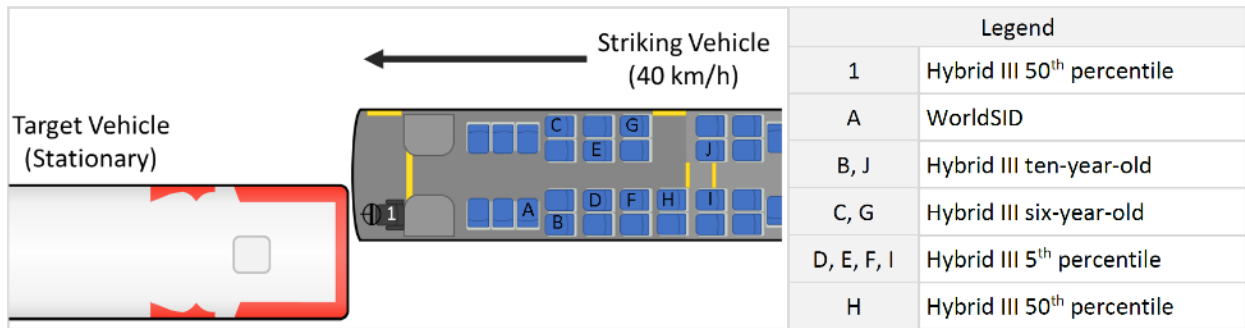


**Figure 52: Schematic of full-scale bus impact with locations of the seated HIII ATD's inside of striking bus [10]**

Highspeed video captured the motion of the ATDs during the impact. The unrestrained ATDs were observed to impact the interior structures of the bus as they were thrown in the forward direction during the collision (Figure 53).

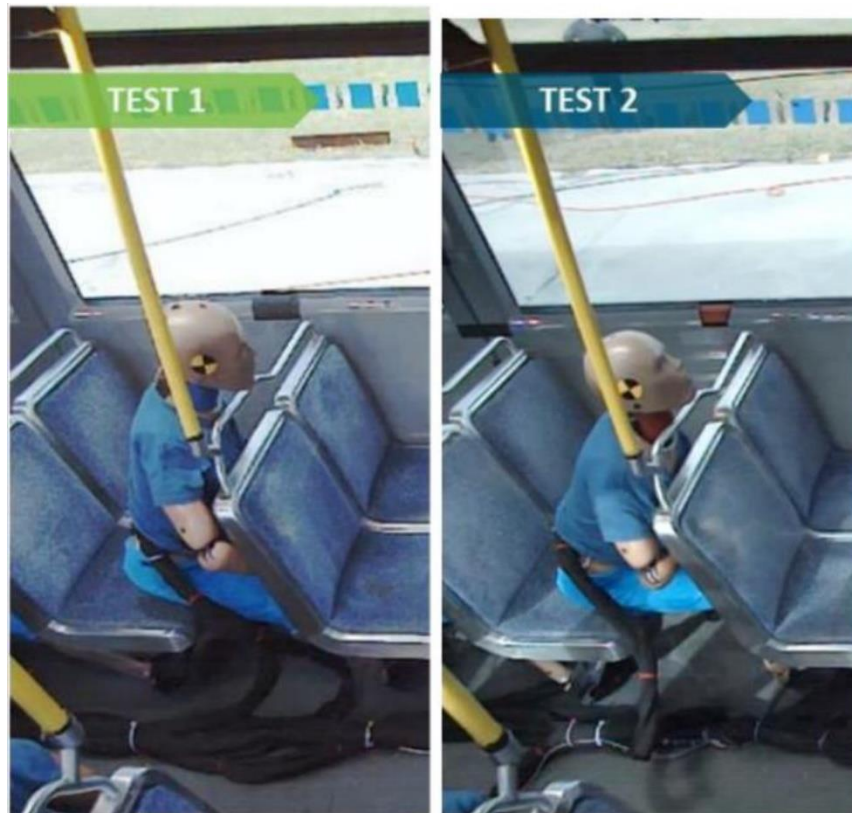


**Figure 53: 5th percentile HIII ATD impacting the forward seatback and handrail during the frontal impact [10]**

The HIII ATDs were instrumented with accelerometers and load cells. Accelerometers recorded kinematics in the head, chest, and pelvis. Load cells recorded forces in the upper neck and femurs. Peak accelerations and forces for each HIII were included in TCs interim report.

### 3.2. Test Buck Fabrication for Replication of Full-scale Impact Conditions

TC fabricated a test buck to replicate the frontal impact of the full-scale experiments in a repeatable, lab-controlled environment. The deceleration pulse recorded during the first full-scale impact with no structural reinforcement was applied to the test buck. The test buck included three rows of seats taken from the buses used in the full-scale experiments. A HIII 50<sup>th</sup> percentile male ATD was seated in the rear row of the test buck, and a HIII 5<sup>th</sup> percentile female ATD was seated in the middle row (Figure 54).

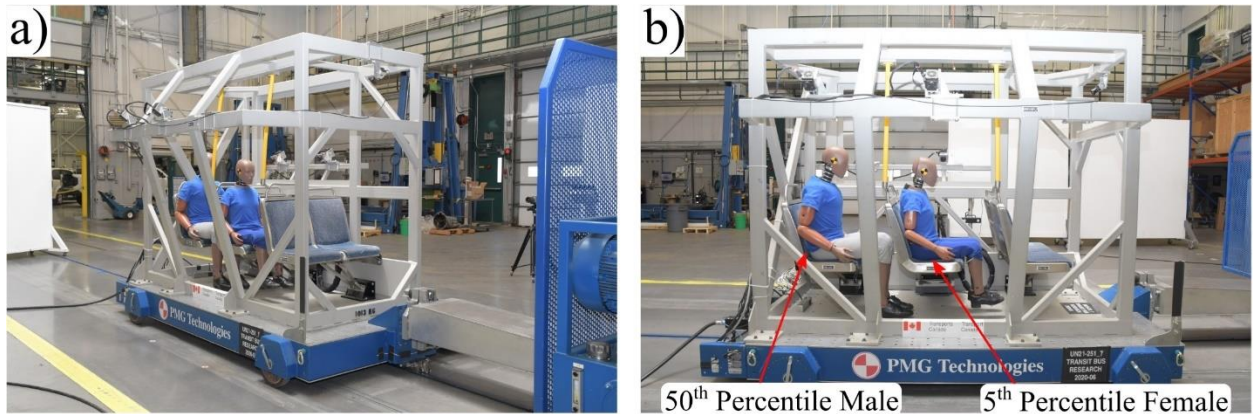


**Figure 54: a) test buck (isometric view) b) test buck side view [10]**

### 3.3. Test Matrix for Test Buck Series of Experiments

TC conducted 10 frontal impact tests using the test buck (Table 14). Three parameters were varied among the tests to observe the change in response of the ATDs. The varied parameters included the initial ATD posture, acceleration pulse magnitude, and ATD seating location. There were eight unique tests based on selected parameters. The parameters used for Test #2 was repeated three times to observe the repeatability of the HIII tests. The posture and seating location of the 5<sup>th</sup> percentile HIII was matched to the seating location and posture of the 50<sup>th</sup> percentile HIII for each test.

**Table 14: Experimental test matrix with varying ATD posture, pulse magnitude, and ATD seating location**

Test Name	Posture	Acceleration Pulse Magnitude (g)	Inboard/Outboard
Test 1	Upright	6.5	Inboard
Test 2a	Reclined	6.5	Inboard
Test 2b	Reclined	6.5	Inboard
Test 2c	Reclined	6.5	Inboard
Test 3	Upright	5.7	Inboard
Test 4	Upright	6.5	Outboard
Test 5	Reclined	6.5	Outboard
Test 6	Upright	5.7	Outboard
Test 7	Reclined	5.7	Outboard
Test 8	Reclined	5.7	Inboard

**3.3.1. Test Buck Parameter 1: ATD Posture**

The ATD posture was varied between upright and reclined for the test buck experiments. The upright posture eliminated contact between the back of the HIII and the seatback cushion. The reclined posture resulted in contact between the back of the HIII and the seatback cushion (Figure 55).

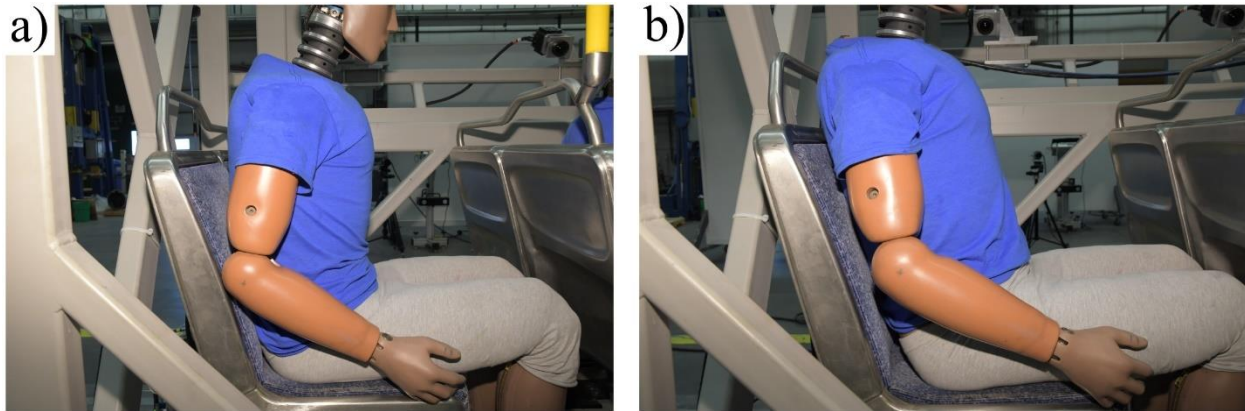


**Figure 55: a) M50 HIII with upright posture; b) Reclined posture**

**3.3.2. Test Buck Parameter 2: Acceleration Pulse Magnitude**

The test buck acceleration pulse magnitude was set at a peak of either 6.5g or 5.7g. The two acceleration pulses were scaled down from the 7g pulse recorded using an accelerometer located under one of the seats in the full-scale experiment (Figure 56). There was concern by TC that the ATDs could be damaged after initial testing with the 7g pulse. Through additional testing it was found that the responses of the ATDs in the 6.5g pulse did not indicate the potential for damage with repeated testing.



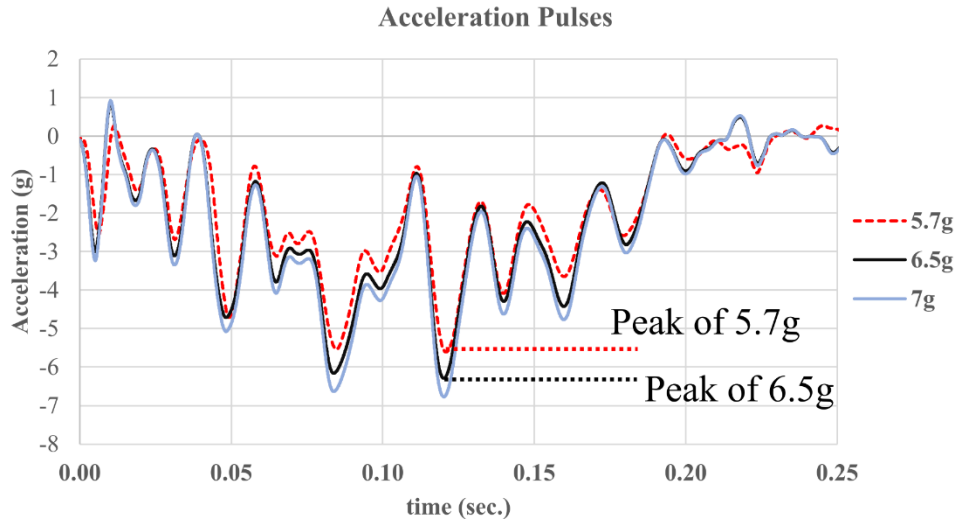


**Figure 56: 6.5 g and 5.7 g acceleration pulses scaled down from the 7 g recorded pulse recorded during the full-scale experiment**

### 3.3.3. Test Buck Parameter 3: ATD Seating Location

The passenger seating location was varied between the inboard and outboard seats (Figure 57). The inboard seat was located closest to the aisle, while the outboard seat was located closest to the window. The handrail curved down lower to the top of the seat on the outboard side which created a potential difference in impact location with the ATD (Figure 58).

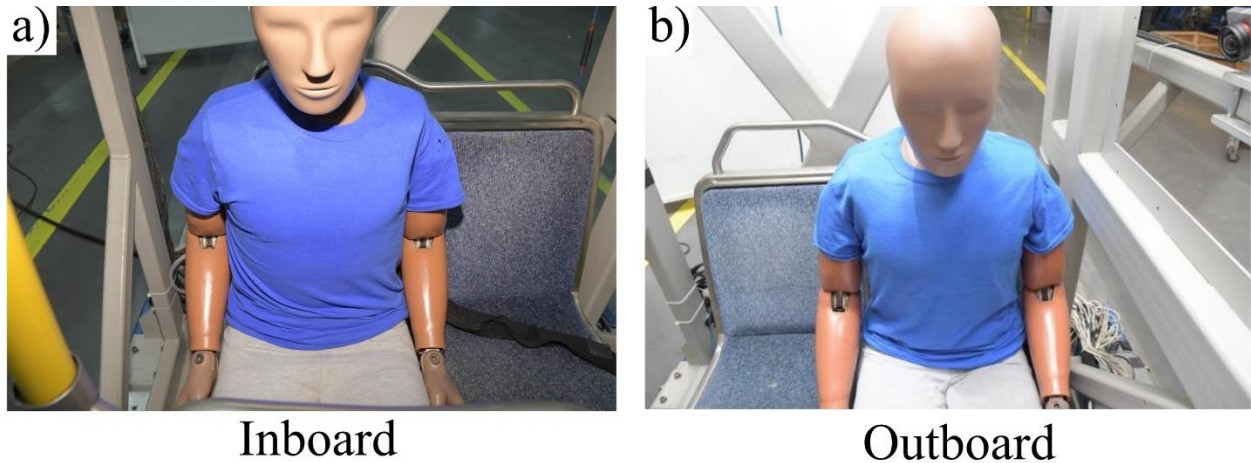


**Figure 57: a) M50 HIII seated in the inboard seat Vs. b) Outboard seat in test buck**

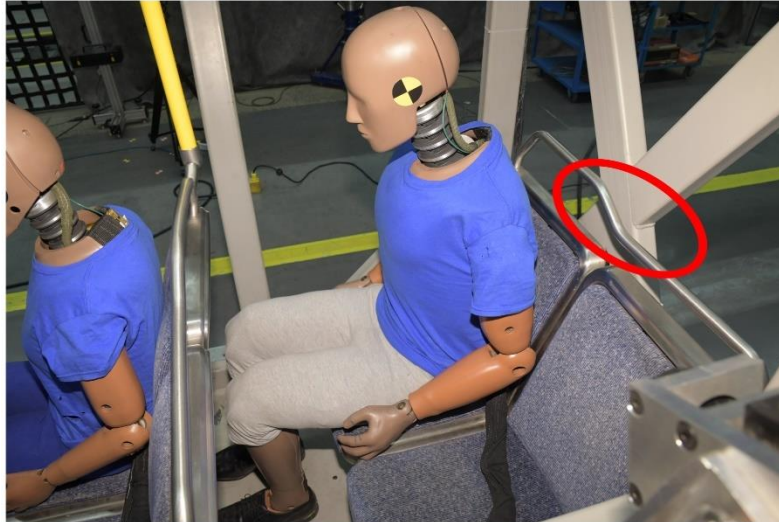


**Figure 58: Handrail mounted on top of each seatback curved down lower on the outboard side**

### 3.4. HIII Initial Positioning Data

The positioning of the HIIs seated in the test buck were recorded prior to each test. Locations of the hip centre point, limb joints, and the location of the forward handrail relative to the HIII was recorded by TC (Figure 59).

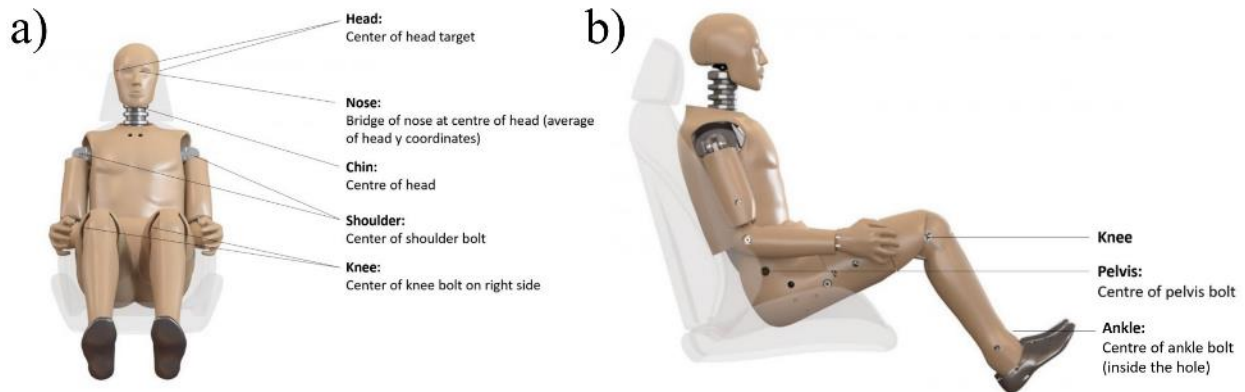


**Figure 59 a) Positioning points for head, face, shoulders, and knees; b) Positioning points for the knee, pelvis, and ankles as recorded by TC (HIII Image Copyright Permission [39])**

### 3.5. Geometry of Test Buck Seats and Handrail

Measurements of the seat geometry in the test buck were recorded using a 3D coordinate measurement tool (Quantum Max FaroArm® Series, Faro Industries, Florida). Coordinates were captured on multiple surfaces on the seats including the seat foam, seat back, seat shell, handrail, and support brackets (Figure 60). Measurements were taken with a targeted separation of 1 cm. The coordinates were written to an .xlsx file using in house software at TC.

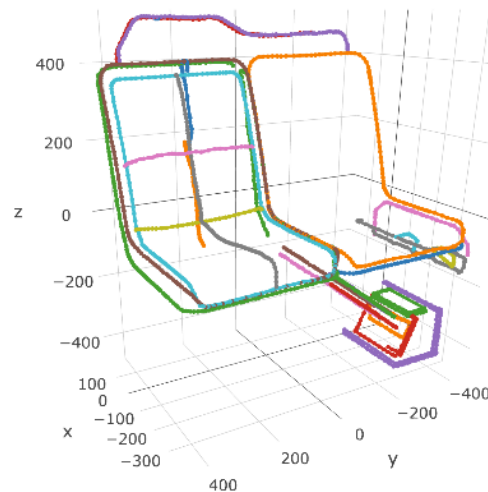


**Figure 60: 3D point capture of experimental test buck geometry for a single seat row**

### 3.6. HIII Sensors for Recording ATD Kinetics During Impact

The HIIs were fitted with sensors to record kinematics and kinetics throughout the duration of the impact. There were accelerometers located in the head, chest, pelvis, as well as load cells in the upper neck and femurs. A potentiometer located in the thorax allowed for the measurement of chest deflection. The sensor data for the experiments was presented along with the corresponding results from the models in the results section (Section 5.1).

### 3.7. Test Buck Experiment Results: Highspeed Video of M50 and F05 ATDs (test case #1)

Highspeed video freeze frames (1000 FPS) of the HIII motions presented in the following section was limited to a single sample (test case #1).

Highspeed video of the M50 HIII in the test buck showed that as the test buck decelerated, the HIII slid forward off the seat. The knees impacted the forward seatback, causing the HIII to swivel forward at the hip. The anterior portion of the neck subsequently impacted the forward handrail. The impact with the

handrail first caused flexion of the neck, which was followed by extension as the forward motion of the HIII stopped. The kinematics led to the HIII rebounding from the forward seat (Figure 61).

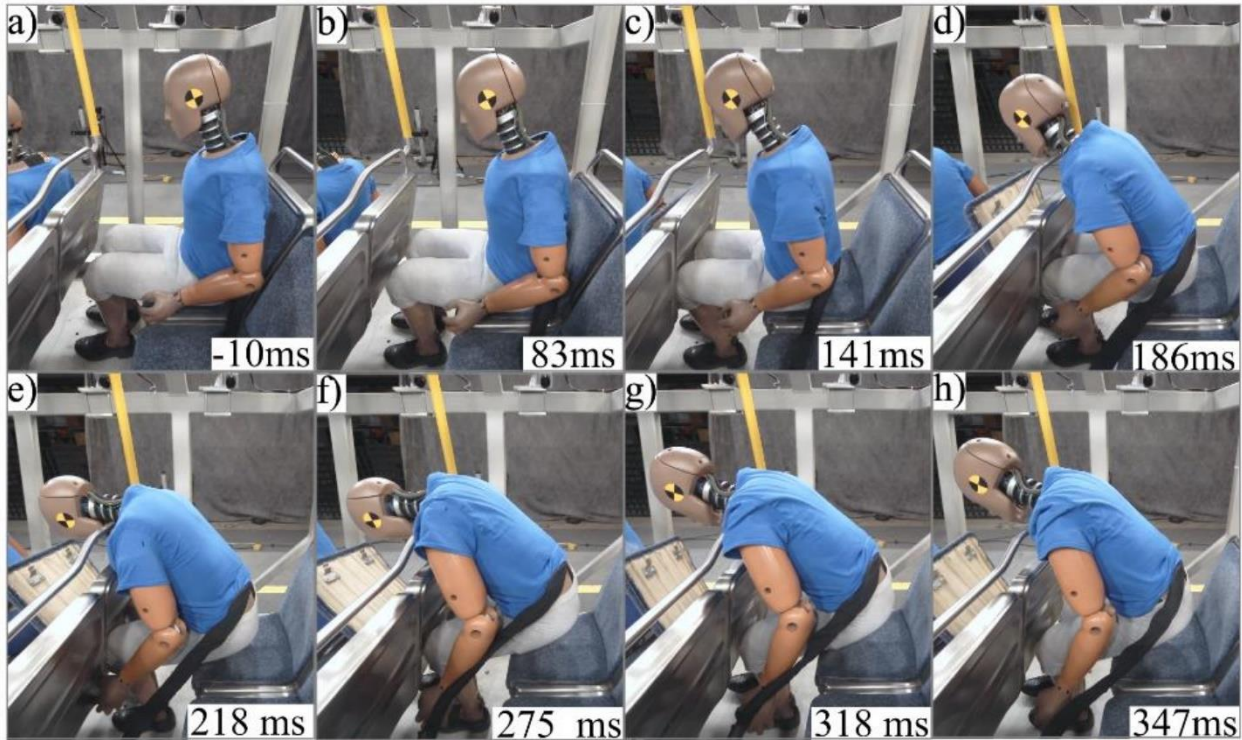


**Figure 61: M50 HIII highspeed video (test case #1)**

The highspeed video of the HIII F05 showed that the smaller stature of the ATD resulted in the lower face impacting the forward handrail instead of the neck (Figure 62). The impact with the lower face resulted in flexion of the upper neck as the HIII F05 continued forward. Eventually, the lower face lost contact with the handrail, causing the neck to extend. The HIII F05 finished the kinematic sequence with the pelvis raised up off the seat and the legs extended under the forward seat.

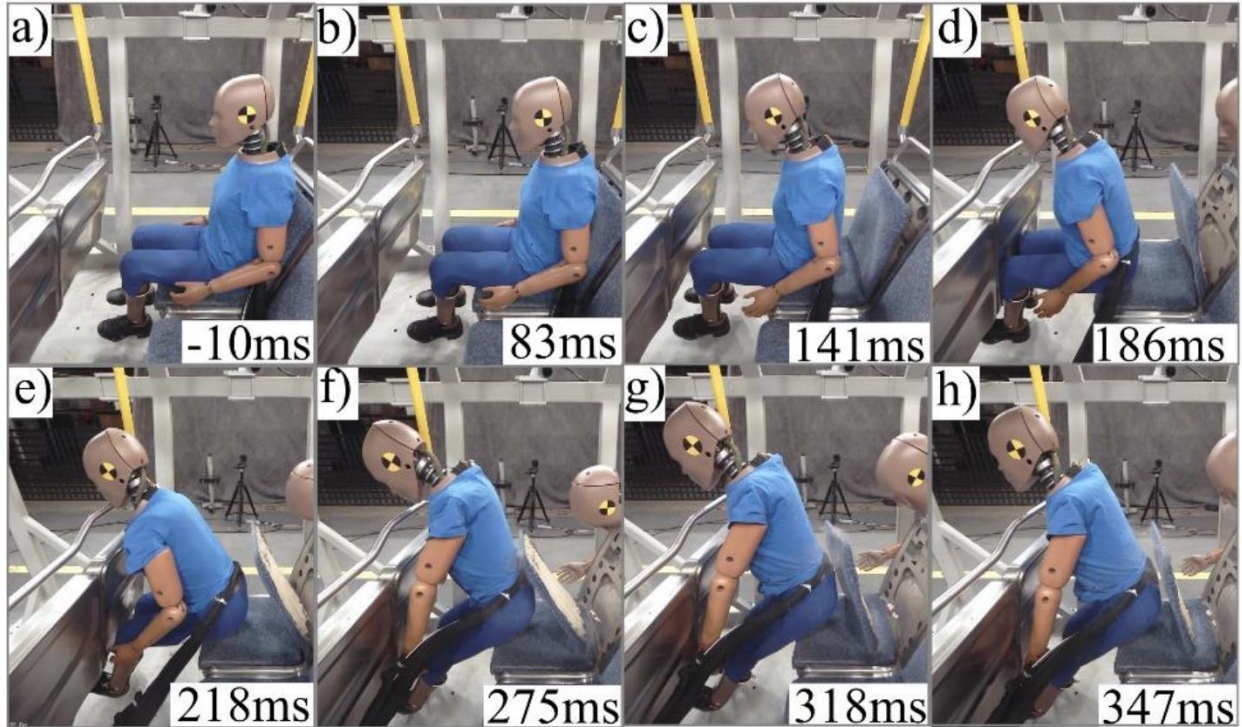
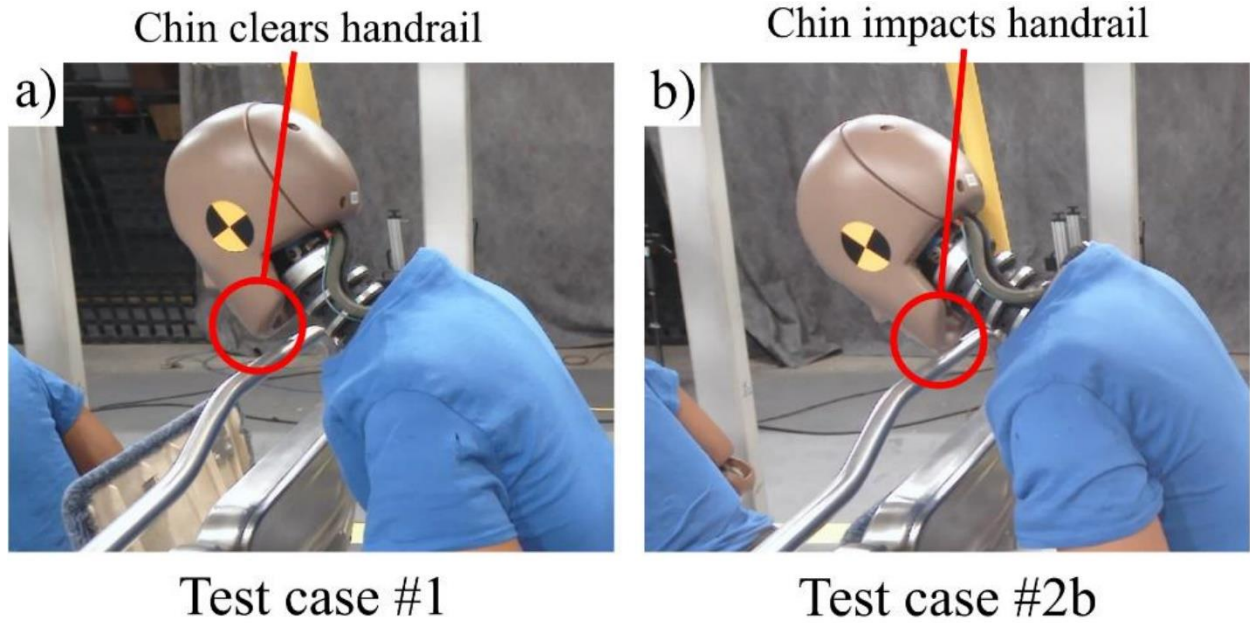


Figure 62: F05 highspeed video (test case #1)

### 3.8. Results of Varying Parameters in the Test Buck (ATD posture, pulse magnitude, and ATD seating location)

The results from the 10 tests showed that the ATDs tended to slide forward off the seat and impact the forward handrail. Varying the ATD posture, sled pulse magnitude, and ATD seating location had the effect of changing the impact location of the handrail with the ATD.

Results showed that varying the posture of the ATDs affected the impact location with the handrail. With the M50 HIII in the reclined posture, one of the tests resulted in the chin impacting the handrail, while in the upright posture the ATD cleared the handrail and impacted the neck with the handrail (Figure 63).



**Figure 63: a) M50 HIII chin clears the handrail with upright posture; b) M50 HIII chin impacts the handrail with the reclined posture**

When the pulse magnitude was increased from 5.7g to 6.5g, it was observed that the location of impact between the ATD and the forward handrail was lower (Figure 64). With the higher magnitude pulse, the impact location between the M50 and the handrail was on the neck, whereas with the 5.7g pulse the face of the M50 impacted the handrail. The higher magnitude pulse resulted in the HIII maintaining a more upright posture as it slid forward off the seat, causing the difference in impact location with the handrail.

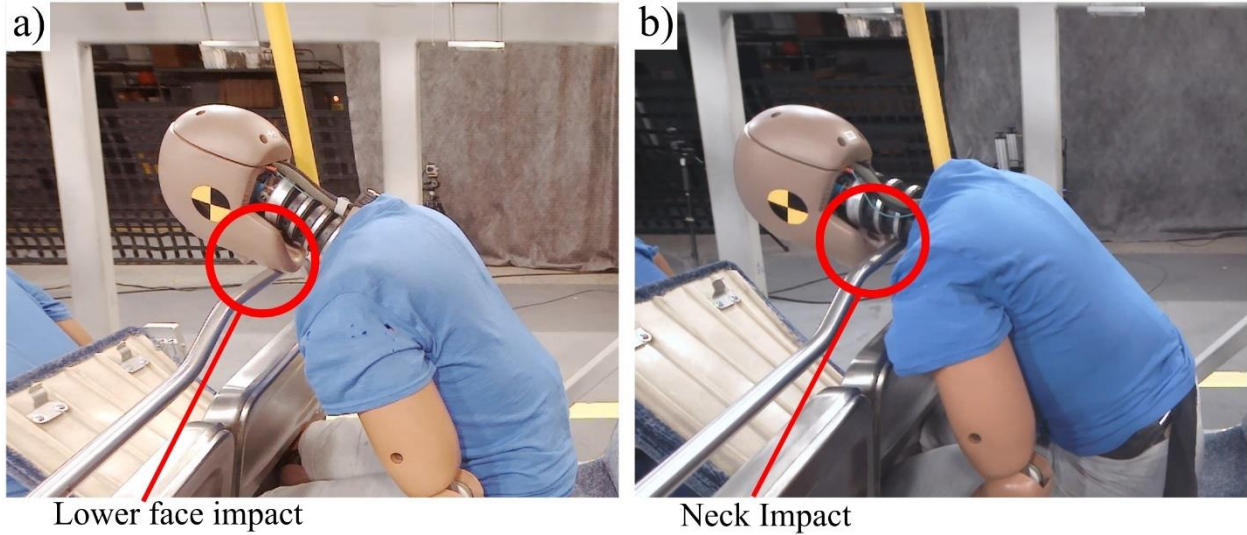


**Figure 64: a) M50 impact location moves from the lower face with the 5.7g pulse to b) the anterior neck with the 6.5g pulse**

Varying the seating location from inboard to outboard consistently resulted in an impact between the handrail at a lower location with the HIII for both the M50 and the F05. For the M50, the outboard seating location resulted in the impact with the handrail being lowered from the neck to the upper chest. When the F05 was moved to the outboard seat it resulted in the handrail impacting the neck instead of the face (Figure 65).

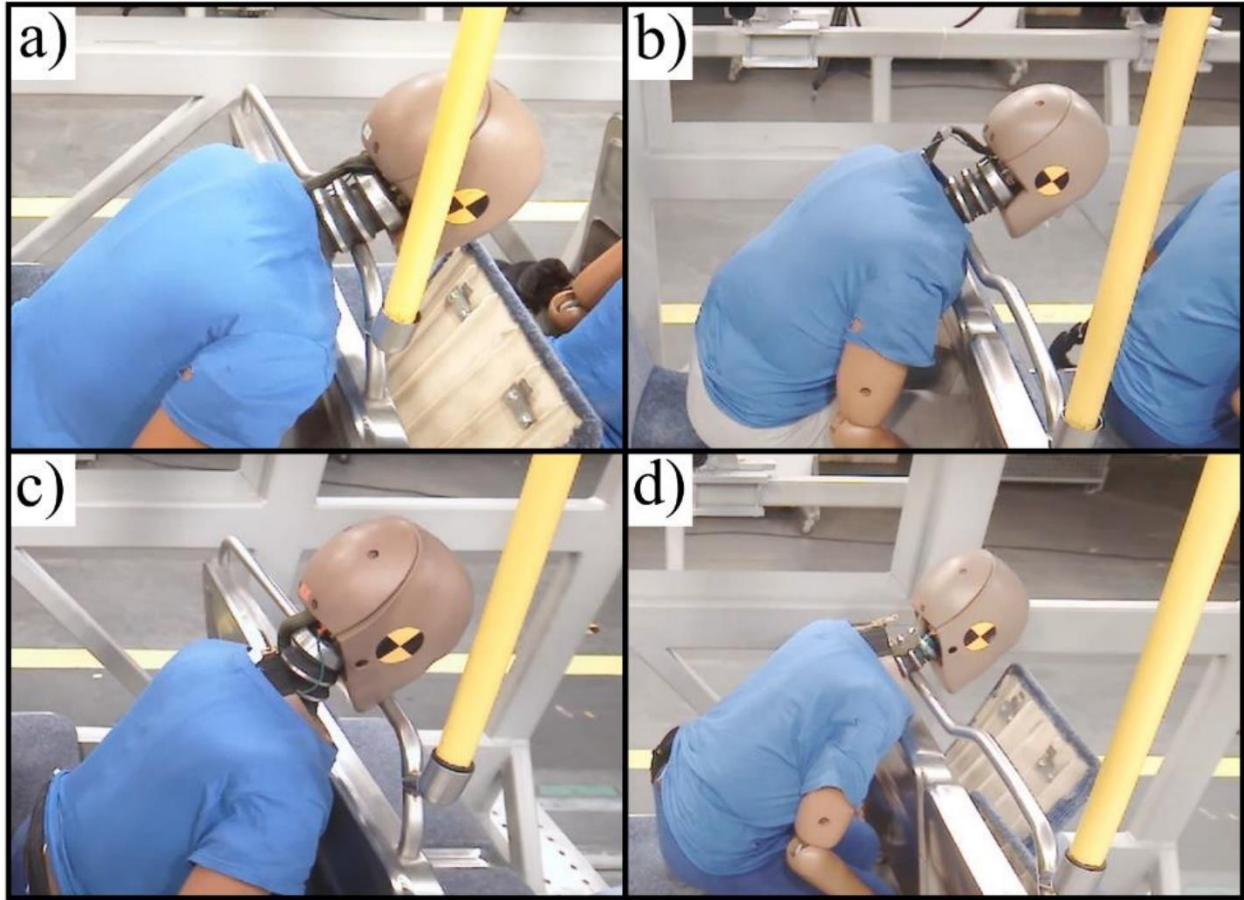


**Figure 65: a) M50 HIII impacted the handrail at the upper neck in the inboard seat and b) at the upper chest in the outboard seat; c) the F05 impacted the lower face in the inboard seat and d) at the neck in the outboard seat.**



## 4. Methods

### 4.1. Methodology Overview

The aim of this study was to incorporate a numerical human body model (HBM) into a test buck model to assess passenger injury. Prior to incorporating the HBM, the ATD coupled test buck model was validated using experimental data.

A FE mesh was generated to replicate the seats, handrails, and other components of the experimental test buck. Commercially available and validated FE models of the 50th percentile male and 5th percentile female HIII ATDs were implemented as the passengers. The motions and kinematics of the FE ATDs in the test buck model were compared with the experiments for the purpose of validation.

The GHBMC HBM M50-O v5.1, 50<sup>th</sup> percentile male, and the GHBMC HBM F05-O v5.1, 5<sup>th</sup> percentile female models were implemented into the test buck model with the 6.5g pulse, upright posture, and inboard seating location. Results with the HBMs were compared with the HIII ATDs for kinematics and injury metrics.

The injury potential for the HIIs and HBMs were assessed in the test buck model using established injury metrics at the head, neck, chest, and lower extremities. The potential for a focal injury to the larynx and lower face of the passenger was assessed using tissue fracture forces and strains reported in the literature. A tissue level injury assessment was conducted with both HBM models at the head, neck, thorax, and lower extremities.

Potential design improvements to the test buck seats were investigated with the aim of reducing passenger injury. Creation of the improved seat design was informed through two studies, both of which utilized the M50 HIII as the passenger surrogate due to increased computational efficiency. The first study was a parametric analysis using the original geometry of the test buck seats and handrails. The parametric analysis investigated modified positioning of the seats and ATD in the test buck to observe the effect on injury metrics. The second study assessed three alternative seat and handrail geometries to assess the effect on injury metrics. The findings from the parametric analysis and alternative seat and handrail geometries were incorporated into a new seat and handrail design.

The new seat and handrail design was assessed using the HIIs and the GHBMC HBMs, both M50 and F05, using the same methods applied to the experimental test buck model. The motion of each occupant surrogate, and potential for injury using the injury metrics, was compared with the results from the experimental test buck. The tissue level injury risk for both HBMs was compared between the responses in the experimental test buck and the improved seat design to determine if there was a reduction in injury.

## 4.2. Development and Validation of HIII Coupled Test Buck Model

Development of the test buck model involved meshing individual parts and combining them into a single assembly. Material properties and element formulations were then applied to each part in the assembly.

Development of the test buck model took eight iterations of development. The test buck modeling detail was increased progressively which included adding parts such as the lower bracket, improving mesh quality, and updating friction and material properties based on values obtained from the literature.

The experimental test buck included three rows of seats. Each row had identical seats and handrails. The support brackets were different between the three seat rows, with the rear and front rows having curved lower brackets and the middle row having straight support brackets (Figure 66). The spacing between the rear and middle rows was 29.5 in. and the spacing between the middle and forward rows was 30.5 in.

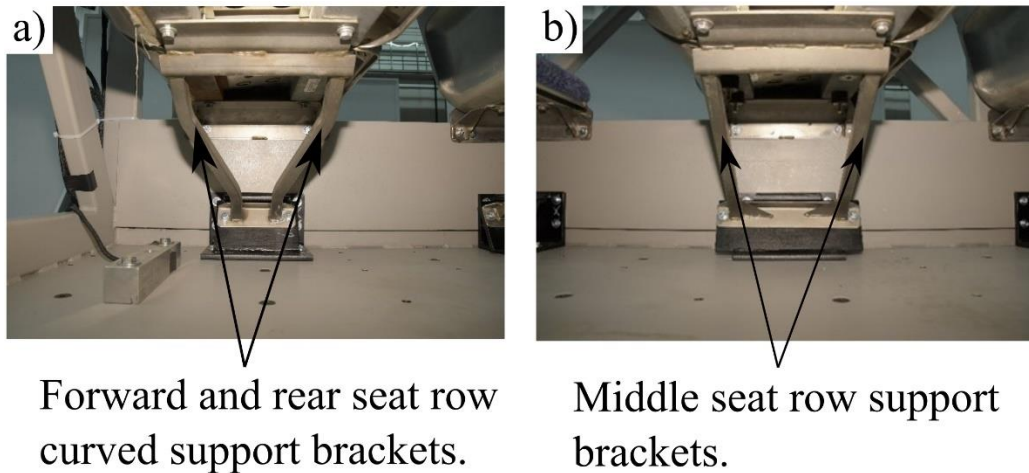


**Figure 66: a) forward and rear seat row support brackets; b) middle seat row support bracket**

The undersides of the seats were reinforced with rectangular brackets that provided structural integrity and prevented buckling (Figure 67).

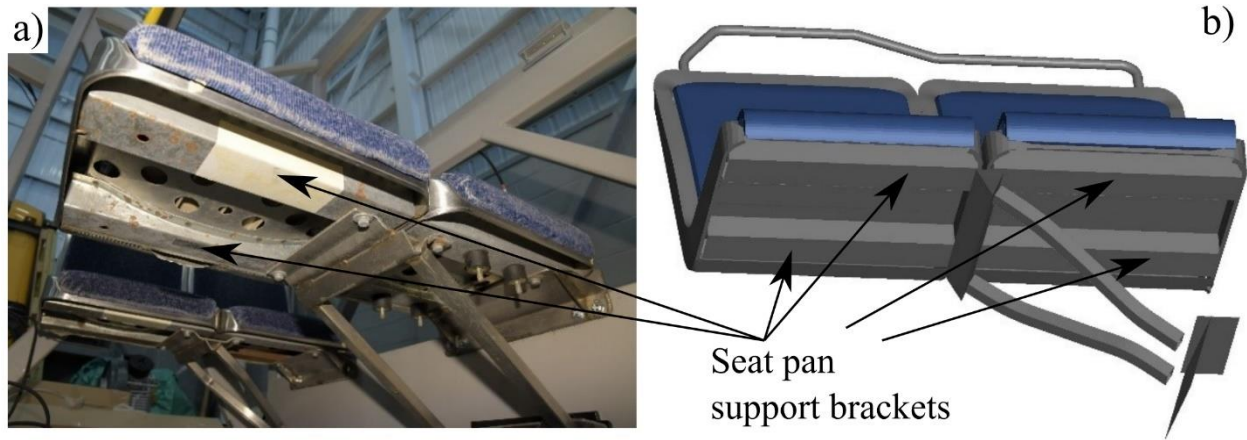


**Figure 67: Support brackets under seat pan in a) experimental test buck and b) test buck model**

The 3D point measurements of the experimental test buck provided by TC were used to create the geometry of the test buck model parts. The 3D points were loaded from an .xlsx file into FE meshing software (Altair Hyperworks, Altair Engineering, Michigan) and used as a guide to generate the geometry of the test buck parts. The geometry was then used to generate the mesh for the seat shells (Figure 68), handrails, seat foam, and lower support brackets. The mesh had a targeted size of 5 mm and was adjusted to accommodate corners and bends. All parts were meshed with quadrilateral elements.

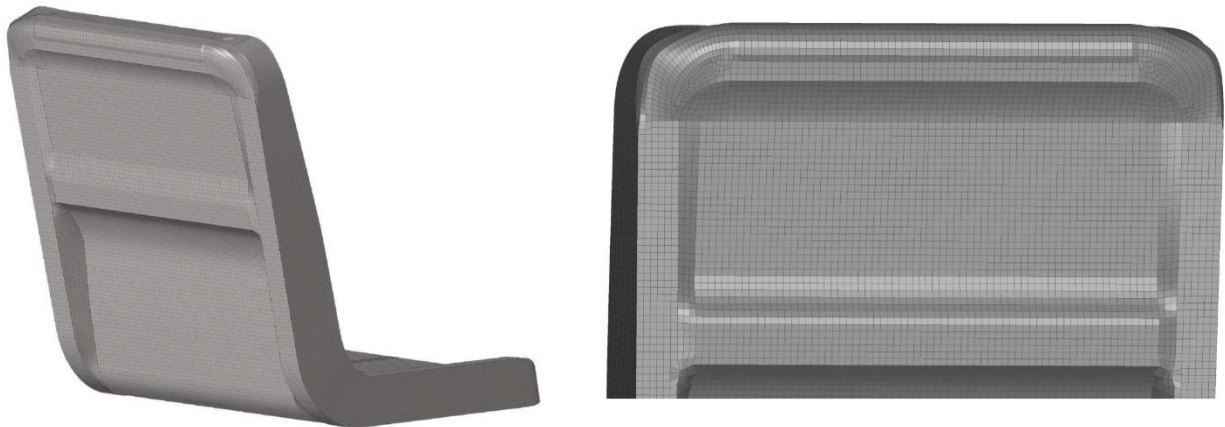


**Figure 68: Rear view of seatback meshed using quadrilateral shell elements**

Mesh quality was reported using the mesh quality checking tool in the pre/post processing software LS-PrePost (Livermore Software Technology Corporation, Ansys, Pennsylvania). The relative simplicity of the geometry of the parts in the model resulted in all elements passing the set criteria (Table 15).

**Table 15: FE Mesh quality criteria**

Hard Target, All elements	
Warpage	< 30
Aspect Ratio	< 6
Skew	< 60
Jacobian	> 0.4
Quad min. angle	> 30
Quad max. angle	< 150

The test buck model was assembled from all the meshed parts (Figure 69). The spacing between seat rows and the configuration of the lower brackets was adjusted depending on whether the M50 or F05 HIII was seated in the model.

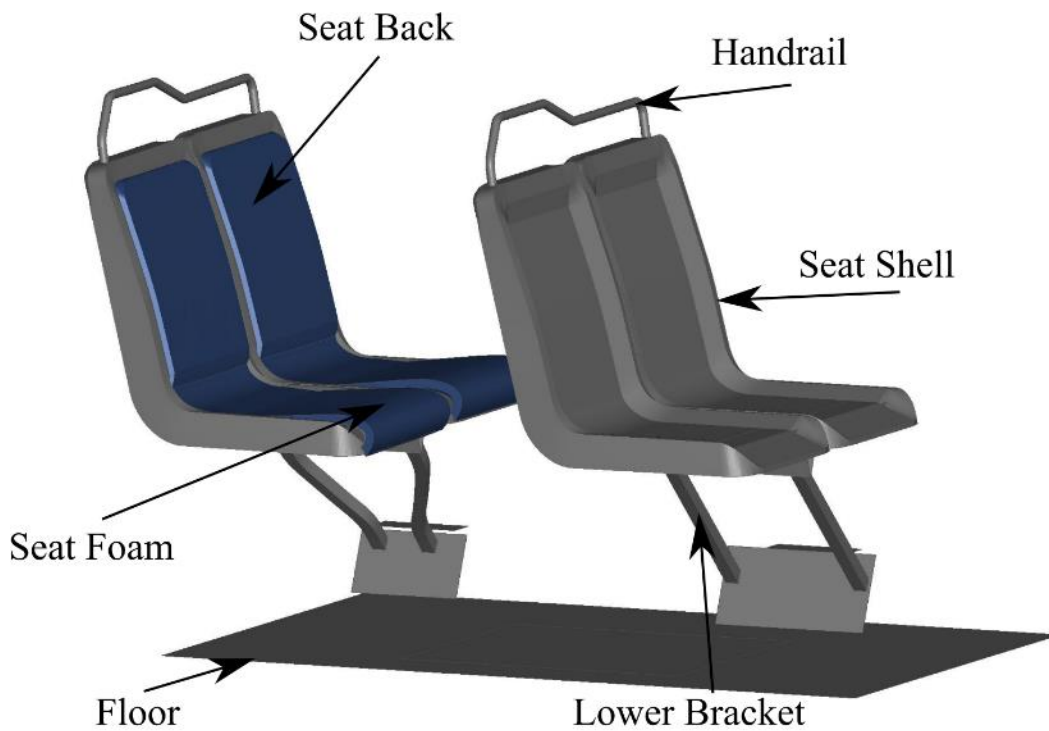


**Figure 69: FE test buck model corresponding to the rear and middle rows of the experimental test buck and used with the M50 HIII**

Connections between parts were achieved by kinematically constraining the adjacent nodes (CONSTRAINED\_NODAL\_RIGID\_BODY in LS-DYNA) (Table 16).

**Table 16: FE model nodal rigid body connections (see Figure 69 for schematic)**

Connection #	Connection Description
1	Handrail connection to seat shells.
2	Seat pan support bracket attachments to seat shells.
3	Support bracket arms to triangular bracket (upper & lower)
4	Triangular bracket to lower seat shells.
5	Left seat shell rigid connection to test buck side.

#### 4.2.1. Crushable Foam Material Model

Public transit seating typically has a low-density crushable foam layer to provide comfort for the passenger while sitting. Implementation of a low-density foam material model in a numerical model requires material characterization for density, stiffness, and a nominal stress strain curve to define the increase in material stiffness as it is compressed.

Krishan [148] conducted material testing on polyurethane foam samples from automotive seats for the purpose of modeling in FE. The material density was measured as  $63 \frac{kg}{m^3}$ , Young's Modulus was measured to be 90kPa, and the nominal stress strain curve was generated through compression testing (Figure 70). Once the material surpasses a strain value of 0.6, the material behaves elastically.

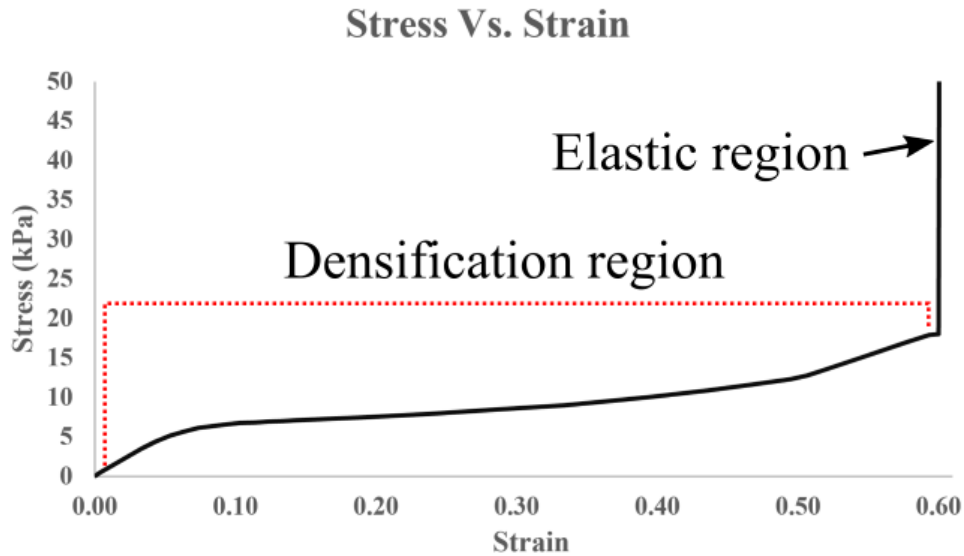


**Figure 70: Polyurethane foam stress strain curve**

#### 4.2.2. Friction of Passenger on Seat Foam

The unrestrained motion of a passenger in a public transit bus exhibits friction between the ATD and the seat as well as between the shoes and the floor. A 2011 paper [149] reported friction coefficients for rubber soled shoes on ceramic tiles with a range of 0.82-1.15 (Table 17). The floor of the experimental test buck is observed to be a painted metal surface, and thus would not exhibit the same level of friction as nonslip flooring used in a transit bus. A value of 0.9 for static and dynamic friction was selected for the model based on the range provided in the report. Values for friction of the passenger on the seat fabric were sourced from a study where a passenger form was slid across various automotive seat fabrics [150].

**Table 17: Friction coefficients of floor and seat fabric**

Part	Static Friction	Dynamic Friction
Seat Foam	0.9	0.75
Floor	0.9	0.9

#### 4.2.3. Positioning of FE HIII Limbs and Posture to Match Experiment Initial Conditions

TC recorded the spatial coordinates of the lower extremities, shoulders, head (left and right side), and face (bridge of nose and chin) while positioning the physical HIII prior to the experimental tests. The spatial coordinates of the physical ATD joints were loaded into the commercial preprocessor (LS-PrePost) as nodal points. The FE ATD was repositioned in the preprocessor to match the physical ATD coordinates (Figure 71). The arms and hands of the FE ATDs were repositioned to match the pre-test positioning photos because there was no positioning data provided for the arms and hands of the physical ATDs

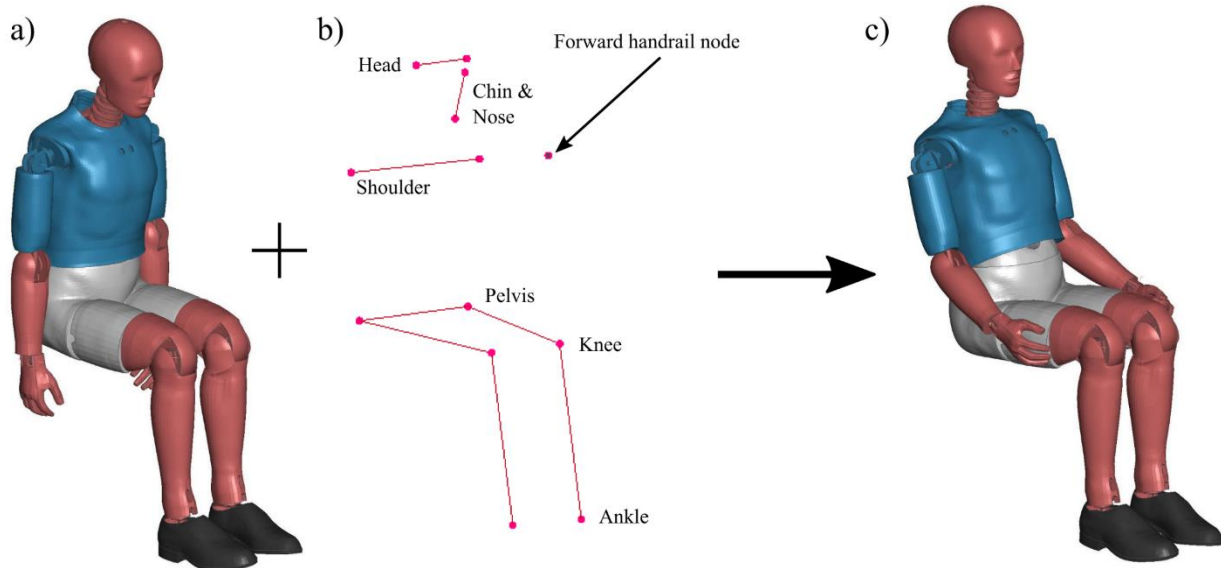


**Figure 71: a) M50 HIII with limbs in default positioning b) Spatial coordinates of head, face, shoulders, pelvis, knees, and ankles provided by TC for the physical ATD prior to the experiment c) M50 HIII model with limbs and posture adjusted to match the physical ATD positioning, arms of model were positioned to match pretest photos provided by TC**

#### **4.2.4. Seating the HIII Prior to Applying Acceleration Pulse**

The HIII model was integrated with the seat prior to applying the acceleration pulse, using a method known as settling. The HIII model was positioned slightly above the surface of the seat foam and gravity (1g vertical down) was applied to achieve an equilibrium seating position over a duration of 125 ms. After achieving equilibrium (125 ms) the sled acceleration pulse was applied (Figure 72) to the test buck.

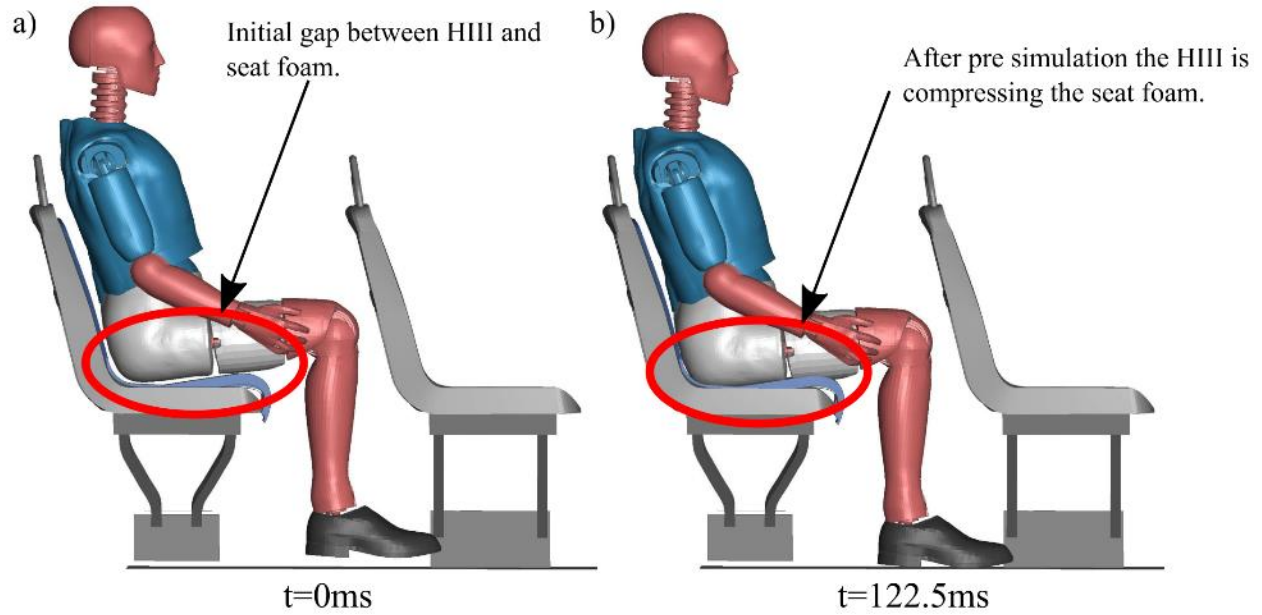


**Figure 72: a) HIII positioned above seat at start of simulation; b) HIII compressing seat foam at the end of the 125 ms of gravity**

#### 4.2.5. Applying the Acceleration Pulse to the Test Buck Model

The acceleration pulse was applied to the test buck model as a prescribed motion to the floor (Figure 73, Figure 74).

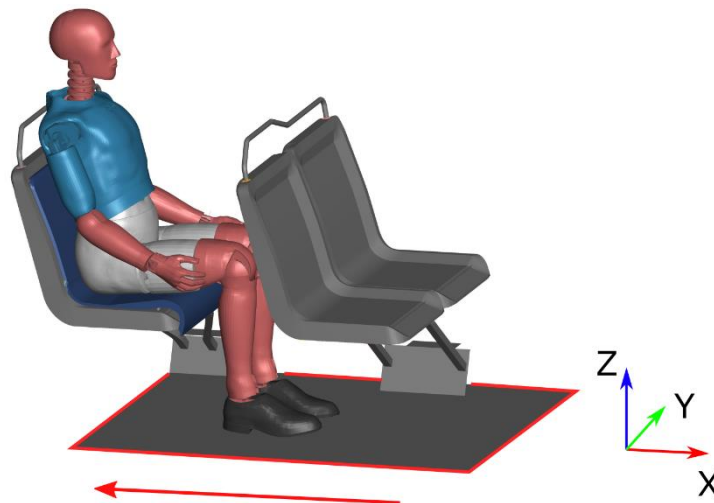


**Figure 73: Test buck acceleration direction (sled pulses from Figure 6 applied)**



Applying the acceleration pulse to the test buck model from rest had the same dynamic effect as applying it to the test buck with an initial velocity. The required condition at the beginning of the simulation was that the HIII and test buck were not moving relative to each other.

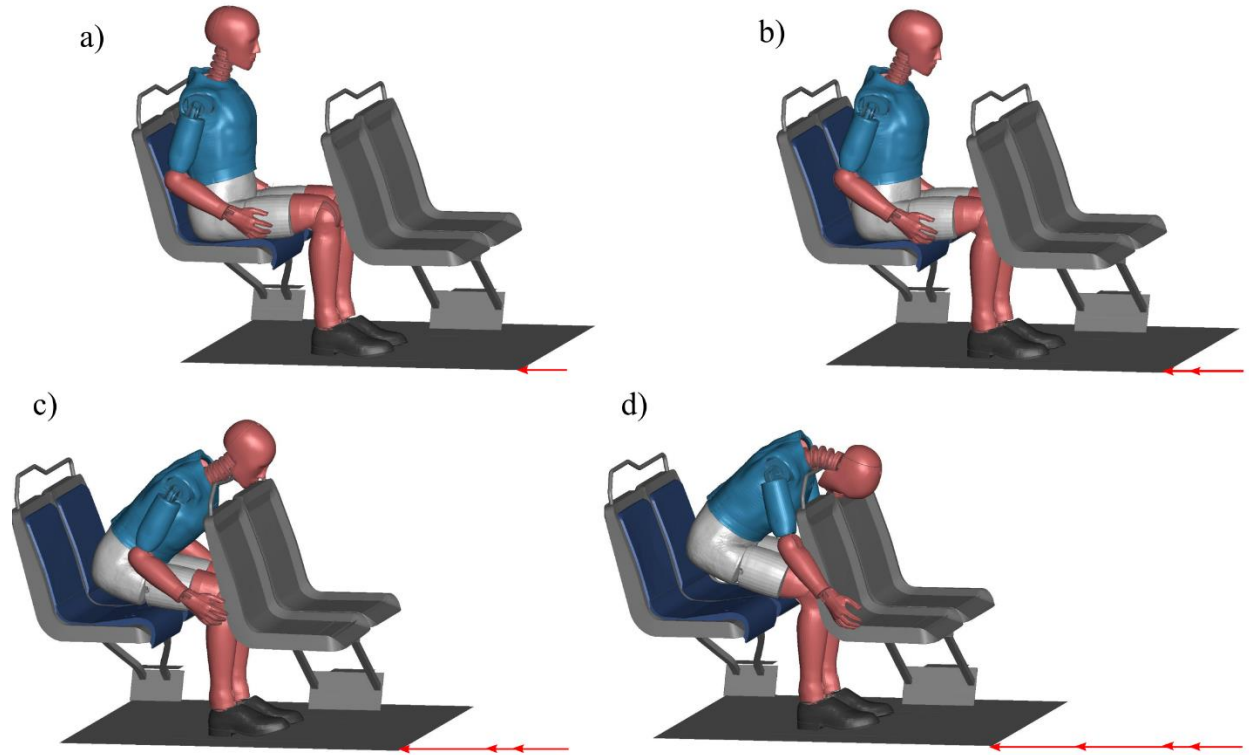


**Figure 74: Acceleration of test buck with fixed point of view relative to the ground**

#### **4.2.6. HIII Sensor Data Processing and CORA Analysis**

The acceleration, force, and displacement traces from the HIIs were filtered using industry standards [151] (Table 18).

**Table 18: Kinematic outputs for HIII with corresponding filters**

Metric	Axis	Unit	Filter
Head Acceleration	X,Y,Z	g	SAE 1000
Chest Acceleration	X,Y,Z	g	SAE 1000
Pelvis Acceleration	X,Y,Z	g	SAE 1000
Upper Neck Forces	X,Y,Z	kN	SAE 1000
Upper Neck Moments	X,Y,Z	Nm	SAE 600
Left & Right Femur Force	Z	kN	SAE 600
Chest Deflection	X	mm	SAE 600

#### **4.2.7. Calculation of Weights for CORA Analysis**

CORA generated a final numerical score for cross-correlation to determine the biofidelity of the model in comparison with the experiment for each test case. The CORA score was an equal combination of the responses from each sensor. The response of each sensor was a weighted combination of the responses from the experiment and model (Figure 75). The weights for a given sensor were calculated based on the area under the curve for each axial response (x-axis, y-axis, and z-axis).

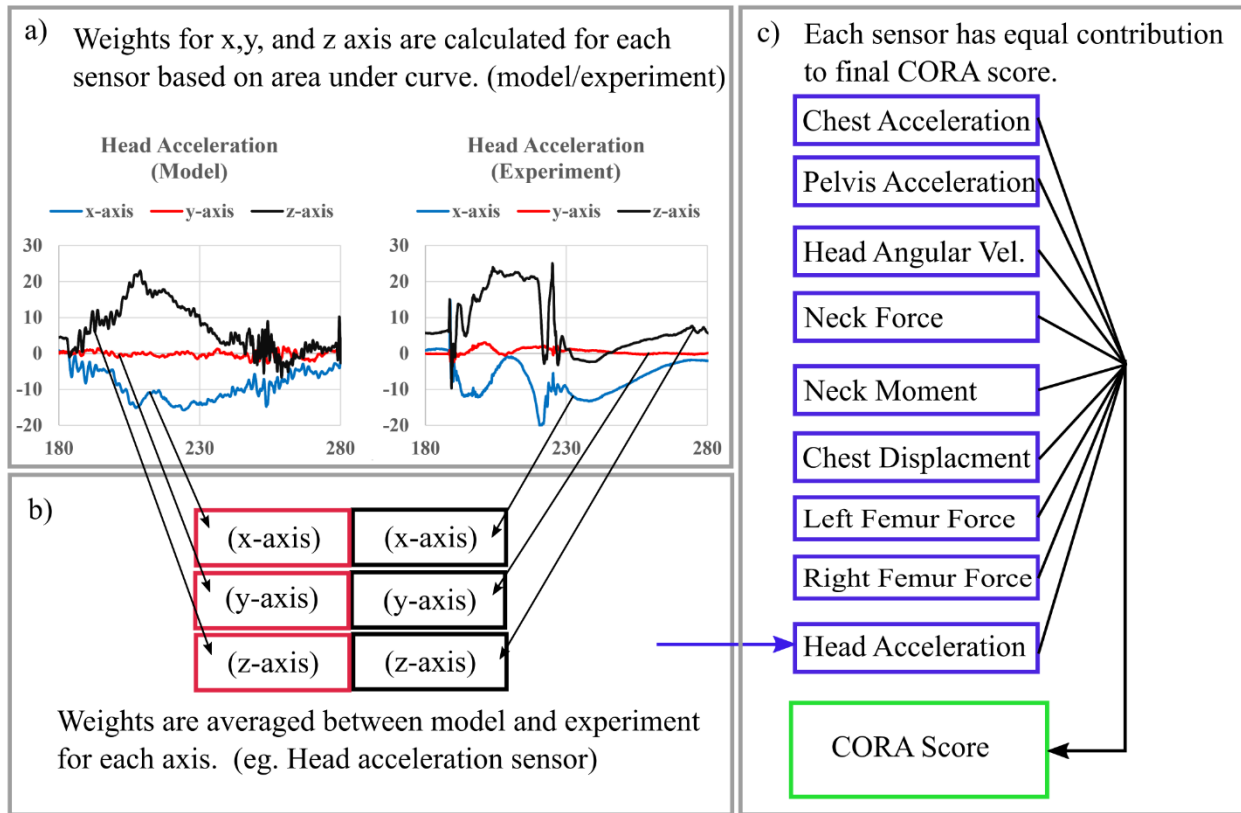


**Figure 75: a) Weights are calculated for the response of the traces from the model and experiment based on area under curves; b) Weights are averaged between the model and experiment for each axis; c) The scores from all the traces are multiplied by their respective weights and combined to calculate the final CORA cross-correlation score**

The table below presents an example of the calculated weights for the load case of 6.5g upright inboard for the M50 HIII (Table 19).

**Table 19: CORA metrics and weights, test case #1**

Output No.	Output ID	Resultant Weight	Experimental Weights	Simulation Weights	Load Case Weights
1	Head X-Acceleration	1	0.045	0.04868	0.046600
2	Head Y-Acceleration		0.005	0.00429	0.004721
3	Head Z-Acceleration		0.061	0.05813	0.059790
4	Chest X-Acceleration	1	0.062	0.05366	0.058065
5	Chest Y-Acceleration		0.006	0.00759	0.006689
6	Chest Z-Acceleration		0.043	0.04986	0.046357
7	Pelvis X-Acceleration	1	0.063	0.05399	0.058711
8	Pelvis Y-Acceleration		0.008	0.01643	0.012104
9	Pelvis Z-Acceleration		0.040	0.04069	0.040296
10	Head X Rotational Velocity	1	0.008	0.00665	0.007450
11	Head Y Rotational Velocity		0.095	0.10010	0.097445
12	Head Z Rotational Velocity		0.008	0.00435	0.006216
13	Neck X Moment	1	0.010	0.01207	0.011079
14	Neck Y Moment		0.095	0.09424	0.094517
15	Neck Z Moment		0.006	0.00480	0.005515
16	Neck X Force	1	0.043	0.04954	0.046247
17	Neck Y Force		0.006	0.00337	0.004746
18	Neck Z Force		0.062	0.05821	0.060118
19	Left Femur Force- Z axis	1	0.111	0.11111	0.111111
20	Right Femur Force- Z axis	1	0.111	0.11111	0.111111
21	Chest Displacement- X axis	1	0.111	0.11111	0.111111
Sum			1.0	1.0	1.0

### **4.3. Test Buck Model Assessment Using HBM and HIII with 6.5 g Pulse, Upright Posture, and Inboard Seating Location**

#### **4.3.1. Integration of the GHMCM HBM and Test Buck Model**

The second phase of the study focused on incorporating the GHMCM M50 and F05 detailed human models into the test buck. The responses of the HBM models were compared with the HIII responses using kinematics and injury metrics. The HBMs were also used to conduct a tissue level injury assessment of the passenger.

### 3.1.1.1. Repositioning of HBM for Seating in the Test Buck Model

The first step in implementing the HBM in the test buck model was to reposition it from the standard automotive seating position to the transit seating position. A simulation based repositioning technique was implemented to move the hands and feet of the HBM from the initial positioning to the required positioning for the test buck model (Figure 76) [152]. A boundary prescribed motion was applied to the hands and feet to displace them the required distance. The remaining body regions of the HBM, including the torso, head, and neck were rigidized during the repositioning simulation. Once the hands and feet of the HBM reached the desired locations the simulation was terminated. The repositioned HBM was then used as the starting position for the proceeding simulations.

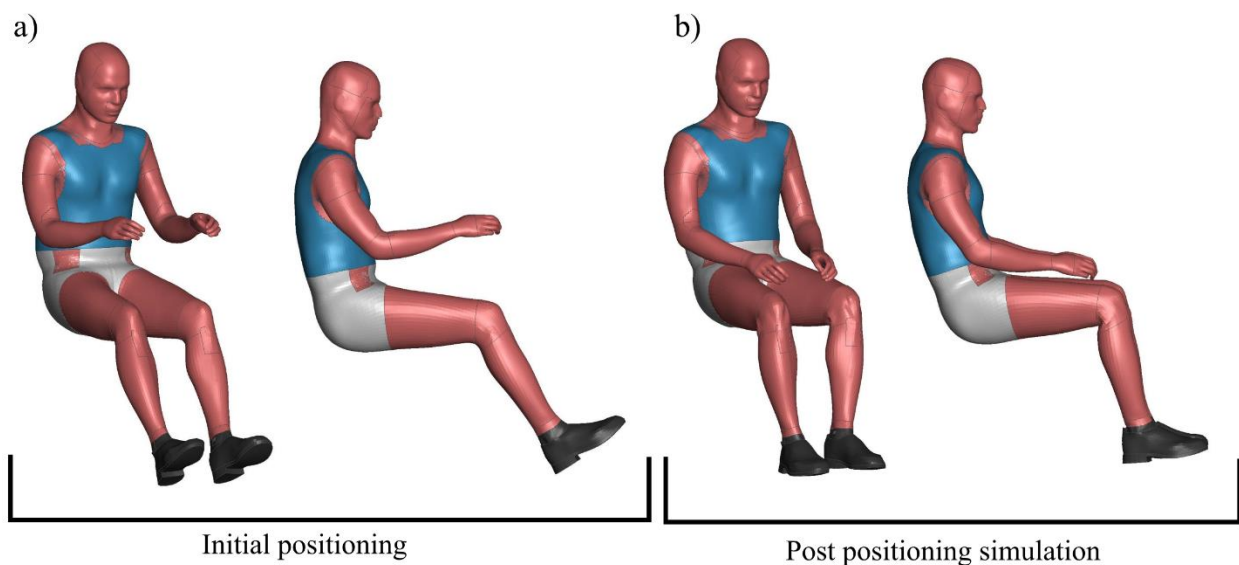


**Figure 76: a) HBM with standard automotive seat positioning b) HBM with repositioned arms and legs for transit seating**

### 3.1.1.2. Maintaining HBM Posture While Settling in the Sled Buck Seat

The first 125 ms of the simulation was used to settle the HBM in the seat, as was done with the HIII. In early attempts, a lack of muscle activation in the HBM resulted in a loss of initial upright posture while being seated under the load of gravity, as would happen with an actual human without muscle tone. The upper spine of the HBM began to round which led to the loss of upright posture needed to replicate the initial positioning used with the HIII. To address this issue, the spine and pelvis of the HBM were rigidized to maintained the upright posture during the seating process (DEFORMABLE\_TO\_RIGID in LS-DYNA) (Figure 77) [153].

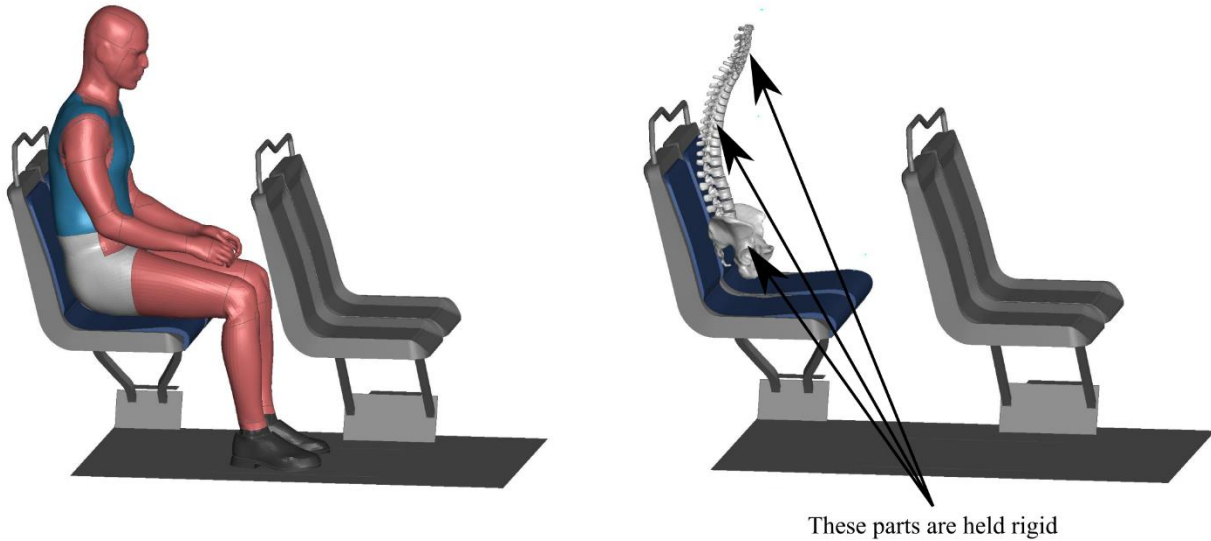


**Figure 77: Spine and pelvis of HBM constrained from all motion except vertical displacement for first 115 ms of simulation**

The spine was maintained as rigid for the first 115 ms, coinciding with most of the seating phase of the simulation. The spine was then transformed to deformable at the 115 ms mark in preparation for the dynamic phase of the simulation where the acceleration pulse was applied, allowing the spine of the HBM to deform in a biofidelic manner.

### **3.1.1.3. Extracting Kinematics from the Head and Pelvis of the HBM**

Linear accelerations for the head and pelvis of the HBM were extracted from the model via a node located at the center of gravity (CG) of each region (Figure 78). The accelerations were filtered with an SAE 1000 filter as per industry standard [151]. Both the head and pelvis accelerations were directly compared with the equivalent outputs from the HIII.

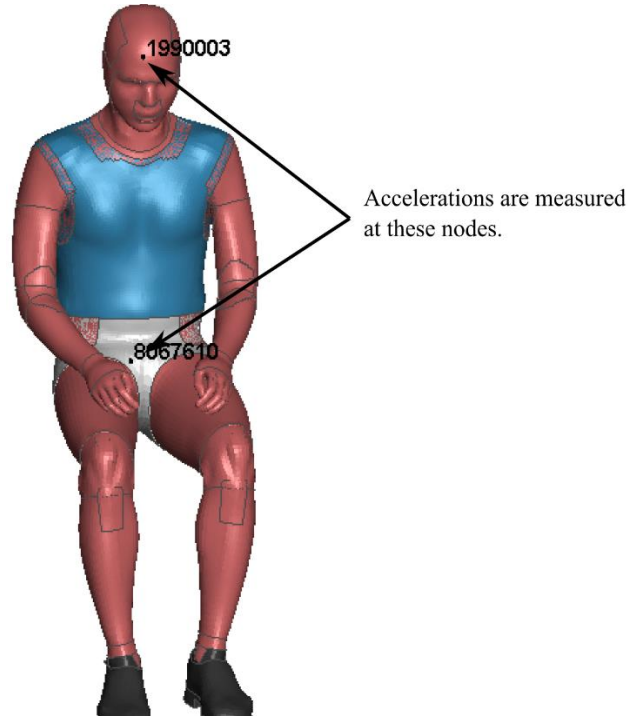


**Figure 78: HBM head and pelvis nodal output locations**

### 3.1.1.4. Extracting neck cross section forces and moments

The M50 HBM was capable of reporting forces and moments acting through five cross-section levels in the cervical spine that ranged from the base of the skull to the lower cervical spine. These cross-sections included the occipital condyle (OC), Cervical 1 (C1), C2, C4, and C7 (Figure 79) [154]. The cross-sections included the forces and moments acting in the bone and surrounding tissues.

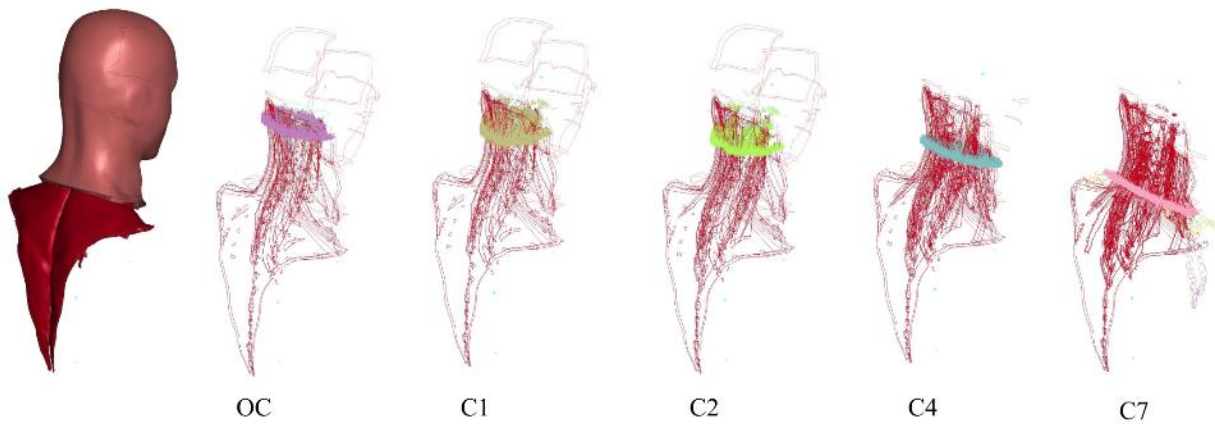


**Figure 79: M50 HBM Neck Cross-section levels**

The OC level cross-section was comparable with that of the upper neck load cell in the HIII. The F05 HBM reported forces and moments acting through four cross-section levels which included the C1, C2, C4, and C7 levels. The C1 level was selected as the cross section for the F05 HBM for comparing with the upper neck load cell of the F05 HIII, as there is no OC cross section level available in the F05 model.

### 3.1.1.5. Chest Band Displacement to Measure Chest Compression

Chest compression was measured in the HBM via three levels of chest bands that reported the displacement of nodes relative to a local origin located along the spine [155](Figure 80).

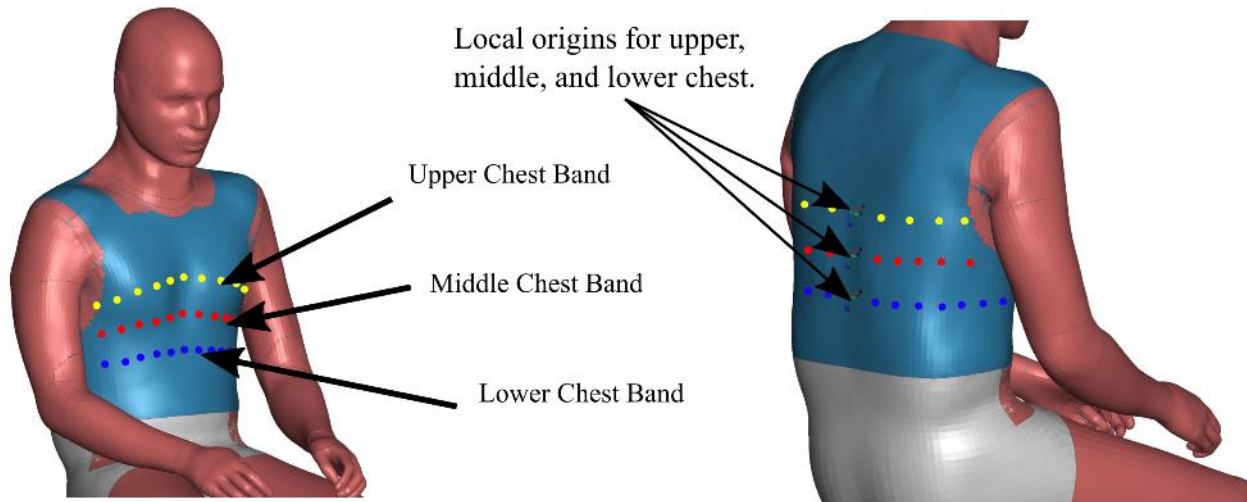


**Figure 80: Chest Band Locations on M50 HBM**

The middle chest band of the HBM was comparable with the location of measured chest compression in the HIII. The velocities of each node of the chest bands were extracted and used for calculating the VC.

### 3.1.1.6. Compression of Larynx Cartilage in the HBM

Compression of the larynx cartilage of the HBM was measured via the change in distance of nodes on the anterior and posterior of the larynx structure (Figure 81). The peak magnitude of larynx compression was compared with values of cartilage strain associated with fracture that were reported in the literature [72].



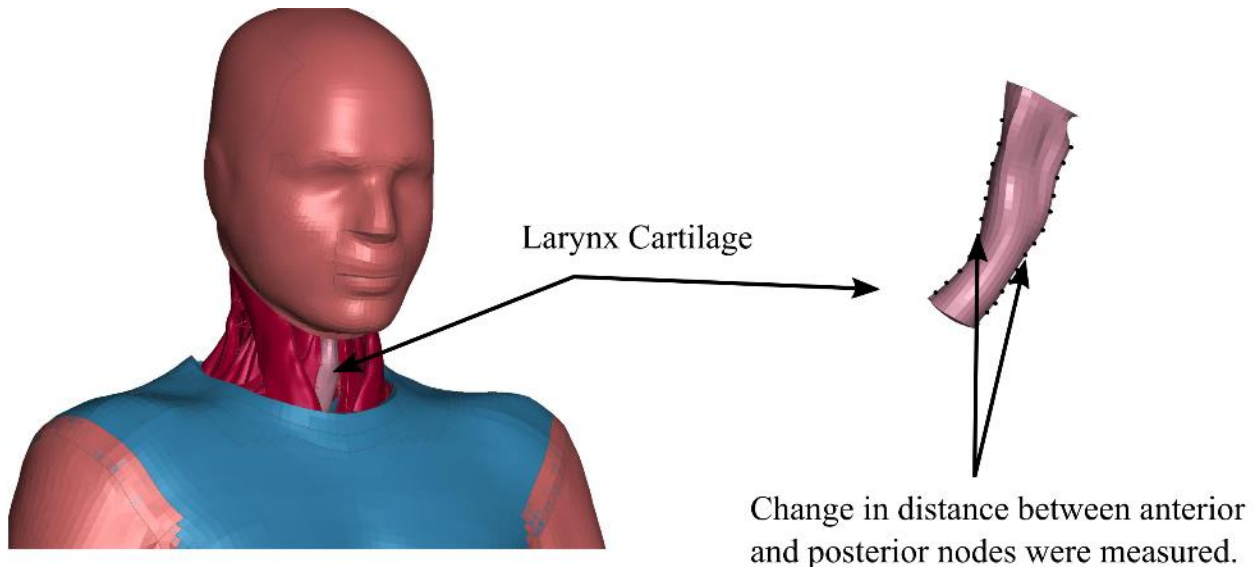


**Figure 81: HBM Larynx compression assessment using nodes on anterior and posterior.**

#### 4.3.2. Anterior Neck and Lower Face Force Measurement with HIII

Impact forces on the anterior of the neck of the HIII models were measured by defining a series of segment sets that ascended the front of the neck (Figure 82). There was an individual segment set for each metal disc and rubber layer that made up the neck of the HIII.

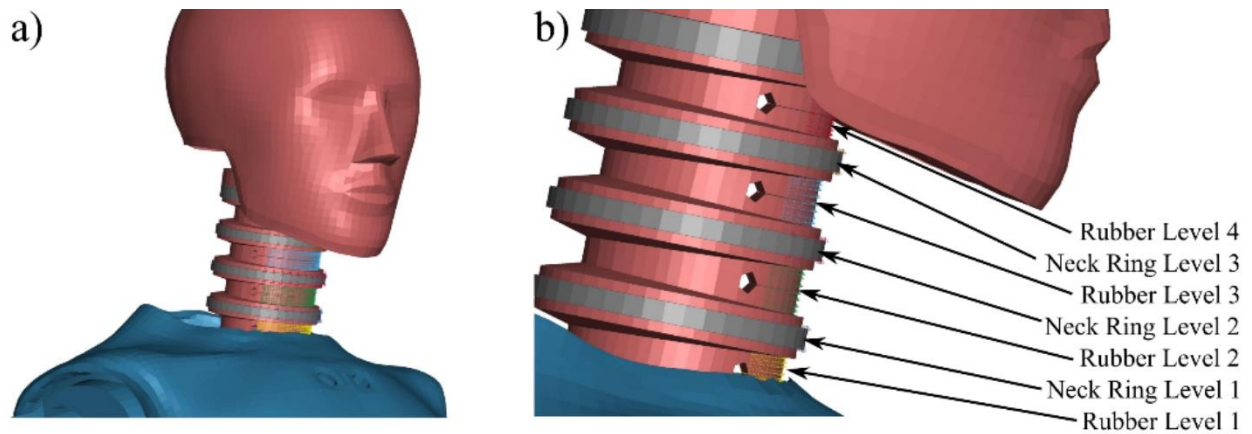


**Figure 82: a) Front view of segment sets on HIII neck; b) Side view with labelled segment set levels**

The F05 HIII included a segment set to measure impact forces on the lower face in addition to segment sets on the anterior neck (Figure 83).

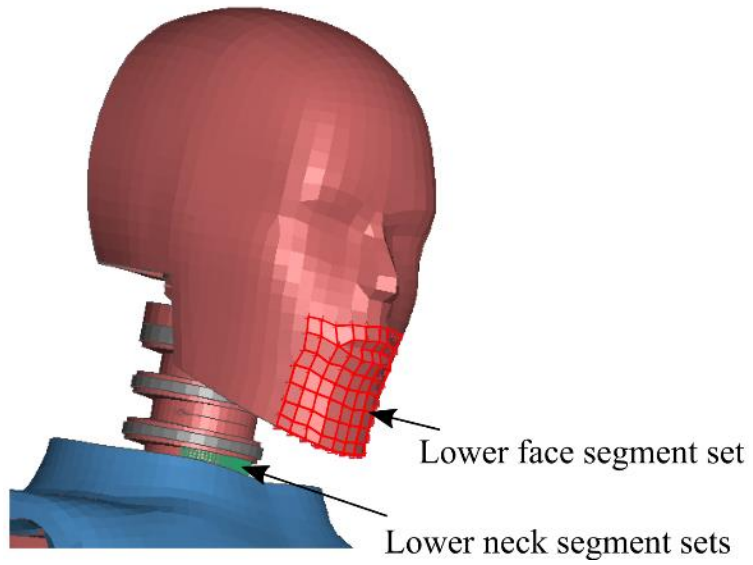


**Figure 83: F05 lower face and anterior neck segment sets**

### **4.3.3. Injury Metrics**

Injury metrics were calculated using the HIII kinematics and kinetics for comparison with the IARVs from the literature (Table 20). Each IARV corresponded to a probability of injury level, as ranked on the AIS.

**Table 20: Injury Metrics and associated injury probability by body regions**

Injury Metric	IARV		Associated Injury Probability
	M50	F05	
Head			
HIC <sub>15</sub>	700	700	31% AIS ≥ 2 skull fracture <sup>a</sup> 5% AIS ≥ 4 brain injury <sup>a</sup>
BrIC	2	2	49% AIS ≥ 3 Injury <sup>e</sup>
Neck			
Nij	1	1	22% AIS 3 <sup>a</sup>
Pk. Upper Neck Moment, Extension (Nm)	96	49	20% AIS ≥ 3 <sup>c</sup>
Pk. Upper Neck Moment, Flexion (Nm)	190	95	<5% risk AIS 4 <sup>c</sup>
Pk. Upper Neck Axial Force, Tension (N)	4170	2620	50% AIS ≥ 3 <sup>c</sup>
Pk. Upper Neck Axial Force, Compression (N)	4000	2520	50% AIS ≥ 3 <sup>c</sup>
Pk. Upper Neck Shear Force (N)	3100	1950	<5% risk AIS 4 <sup>c</sup>
Larynx Crush, Thyroid cartilage (N)**	180	180	N/A <sup>f</sup>
Larynx Crush, Cricoid cartilage (N)**	248	248	N/A <sup>f</sup>
Larynx Crush, Thyroid and Cricoid (Strain)***	50%	50%	N/A <sup>f</sup>
Maxillofacial Fracture (anterior-posterior) (N)**	2834	2834	50% AIS 1 <sup>b</sup>
Thorax			
CTI*	1	1	25% AIS ≥ 3 <sup>a</sup>
Pk. Chest Acceleration (g)*	60	60	37% AIS ≥ 4 <sup>a</sup>
Pk. Chest Deflection (mm)	50	41	30% AIS ≥ 3 <sup>a</sup>
Viscous Criterion (VC)	1	1	25% AIS 4 <sup>d</sup>
Pk. Chest Deflection Rate (m/s)	8.2	8.2	50% AIS 3, 15% AIS 4 <sup>a</sup>
Lower Extremity			
Pk. Femur Axial Force (N)	10000	6800	35% AIS ≥ 2 <sup>a</sup>

a. NHTSA (1999) [60]

b. Daniel 2021 [69]

c. Mertz (2003) [56]

d. Viano 1988 [62]

e. Laituri (2016) [64]

\* HIII specific

f. Melvin 1973 [72]

\*\* Segment set force assessment

\*\*\* HBM Specific

#### 4.3.4. HBM Tissue Level Injury Assessment

The initial injury assessment with the HBM was done using the same injury metrics and IARVs that were used with the HIII and outlined in section 4.4. The CTI and peak chest acceleration was not assessed with the HBM due to excessive noise in the chest CG node.

The biofidelic nature of the GHBM HBM allowed for an injury assessment at the tissue level. The GHBM user manual listed the available Crash Induced Injury (CII) metrics and the corresponding model assessment method (Table 21). Extracting the strains, pressures, and deformations of elements in regions of interest allowed for the assessment of injury.

**Table 21: HBM tissue level injury assessment metrics by body region**

Injury Type	GHBMC model assessment metric	Injury Threshold
Head		
Diffuse Axonal Injury	Maximum Principal Strains	0.48
Cerebral Contusion	Pressure in solid elements	237kPa coup/-104kPa countercoup
Acute Subdural Hematoma	Axial strain in beam elements	0.25
Skull Bone Fracture	Maximum Principal Stress/Strain	20 MPa/0.0042
Neck		
Ligament Distraction	Change in length of beam element	Table 22, Table 23
Intervertebral Disc Avulsion	Tensile stress in elements	30 MPa
Cervical Spine Bone Fracture	Effective plastic strain in elements	(Cortical/Trabecular) 0.0178/0.095
Thorax		
Rib Fracture	Effective plastic strain in elements	(Cortical/Trabecular) 0.018/0.13
Lower Extremity		
Pelvic Fracture	Effective plastic strain in elements	(Cortical/Trabecular) 0.03/0.25
Leg Fracture (Thigh-knee-leg)	Effective plastic strain in elements	(Cortical) 0.0088

The change in length of the beam elements that modeled the neck ligaments in the HBM were extracted from the simulation and compared with values provided in the GHBMC user manual to determine the potential for ligament failure (Table 22). The distraction level of each ligament was reported based on the classification of the peak distraction and whether it corresponded to the toe region, linear region, traumatic region, or failure region (Figure 38).

**Table 22: C2-T1 Neck Ligament Distraction Failure Levels**

Ligament	Average Failure Distraction (mm)			Average - 1 S.D. Failure Distraction (mm)		
	C2C3/C3C4	C4C5/C5C6	C6C7/C7T1	C2C3/C3C4	C4C5/C5C6	C6C7/C7T1
ALL	3.8	3.3	4.2	2.8	2.2	3.3
PLL	3.3	2.8	2.8	2.1	1.9	1.7
CL	4	4.9	5.1	2.5	3	2.7
LF	4.5	5.5	7.5	2.6	3.5	4.7
ISL	5.9	6.6	8.1	3.4	3.4	4.1

The strains in the ligaments in the upper neck were compared with the corresponding failure distraction limits listed in the GHBMC user manual (Table 23).

**Table 23: OC/C1 Neck Ligament Distraction Levels**

Ligament	Average Failure Distraction (mm)	Average - 1 S.D. Failure Distraction (mm)
AAOM	18.9	16.2
AAAM	11.8	4.8
CL OC-C1	9.9	1.5
CL C1-C2	9.3	4.8
PAOM	18.1	2.7
PAAM	9.6	5.3
TM	11.9	9.4
Apical	8	2.7
Alar	14.1	6.9
SC	12.5	7.6

#### **4.4. Alternate Seat Configurations Assessment using M50 HIII for Development of Proposed Seat Design**

Development of an improved test buck seat was conducted in two separate studies. The first study was a parametric analysis utilizing the experimental test buck seat geometry. The parametric analysis varied the seat pitch, forward seat height, and passenger seating location. The second study assessed three alternative seat /handrail designs. Both studies utilized the HIII M50 as the passenger surrogate with the 6.5g pulse and the ATD in the upright posture. The HIII was utilized as the passenger surrogate for the

development of the new seat geometry due to its reduced computation time when compared with the HBM.

Injury metrics ( $HIC_{15}$ ,  $N_{ij}$ , CTI, and LE) were assessed for each simulation of the parametric analysis and alternative seat designs. A linear regression analysis was conducted with the results from the parametric analysis to determine how varying parameters affected injury metrics. For the alternative seat designs the injury metrics were compared with the original model to determine which designs improved injury. The results from the two studies helped inform the creation of the final improved seat design incorporating the most effective measures.

#### 4.4.1. Parametric Analysis Using Experimental Test Buck Model Seat Geometry

A parametric analysis was conducted with the experimental test buck model by varying the forward seat pitch, forward seat height, and the passenger seating location (inboard/outboard) for a total of 24 simulations (Table 24). The seat pitch was varied from its original distance of 745 mm by a magnitude of 50 mm to distances of 715 mm, 795 mm, and 845 mm (Figure 84). The 50 mm variation was based on a similar parametric analysis done for motorcoach seat optimization [135]. The forward seat height was varied from its original height of 365 mm to heights of 335 mm and 415 mm. A seat height of 335 mm was identified by TC as the minimum height for the forward seat due to limitations imposed by the seat mounting bracket.

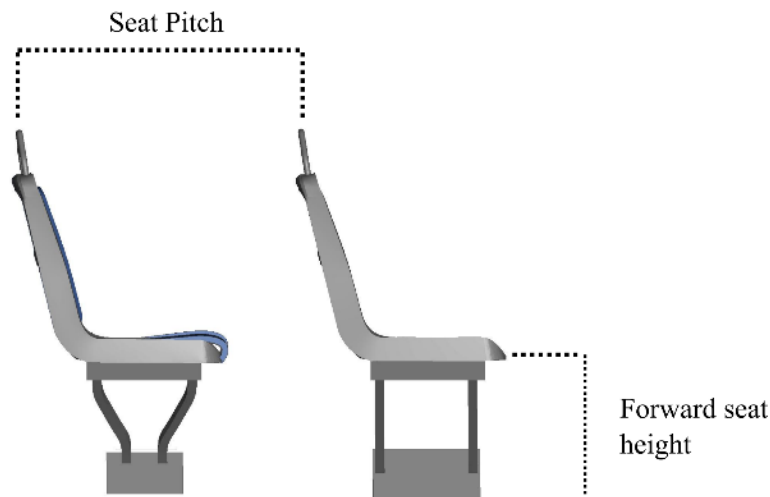


**Figure 84: Seat pitch and forward seat height were varied for the parametric analysis**

The passenger seating location was varied using the inboard and outboard seats (Figure 85). The two seating configurations were included as a means of testing the effect of the lower handrail height on the outboard side.

Inboard



Outboard



**Figure 85: Inboard and outboard seating locations in the test buck model**

**Table 24: Parametric analysis test matrix**

Test ID	Pitch	Forward Seat Height	Inboard/Outboard
Test #1	745 mm	365 mm	Inboard
Test #2	795 mm	365 mm	Inboard
Test #3	745 mm	415 mm	Inboard
Test #4	795 mm	415 mm	Inboard
Test #5	745 mm	365 mm	Outboard
Test #6	795 mm	365 mm	Outboard
Test #7	745 mm	415 mm	Outboard
Test #8	795 mm	415 mm	Outboard
Test #9	845 mm	365 mm	Inboard
Test #10	845 mm	415 mm	Inboard
Test #11	845 mm	365 mm	Outboard
Test #12	845 mm	415 mm	Outboard
Test #13	715 mm	365 mm	Inboard
Test #14	715 mm	335 mm	Inboard
Test #15	715 mm	365 mm	Outboard
Test #16	715 mm	335 mm	Outboard
Test #17	745 mm	335 mm	Inboard
Test #18	795 mm	335 mm	Inboard
Test #19	845 mm	335 mm	Inboard
Test #20	745 mm	335 mm	Outboard
Test #21	795 mm	335 mm	Outboard
Test #22	845 mm	335 mm	Outboard
Test #23	715 mm	415 mm	Inboard
Test #24	715 mm	415 mm	Outboard

#### **4.4.2. Assessing Statistical Significance of Parameter Variation on Injury Metrics using Linear Regression Analysis**

A linear regression analysis was used to determine the effect of varying each parameter in the parametric analysis on each given injury metric (e.g. the effect of varying seat pitch on  $HIC_{15}$ ). A linear regression analysis creates a linear equation to describe the relation between the dependant (injury metric) and explanatory variable. A linear equation is fit to the data by minimizing the error between the data points and the line (Figure 86).



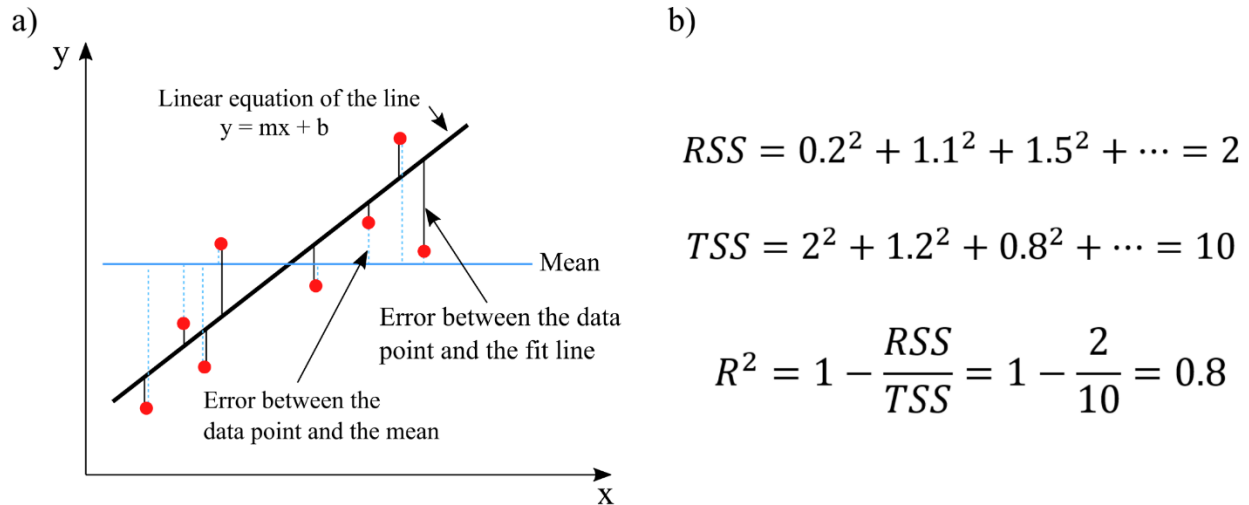


**Figure 86: a) Linear equation fitted to the data, the errors between the data points and the line are minimized; b) Example calculation of the R-squared value**

The coefficient of determination (R-squared) is then calculated to determine how much of the variation is explained by the explanatory variable. The variation between each data point and the fit line is calculated, squared, and summed to find the Sum of the Residuals (RSS). The variation of each data point in relation to the mean is calculated, squared, and summed to find the Total Sum of Squares (TSS). R-squared is then calculated from the ratio of the Sum of Residuals and the Total Sum of Squares.

In this study, the explanatory variables were the seat pitch, forward seat height, and seating location. A linear equation and R-squared was calculated for each explanatory variable in relation to each dependant variable (HIC<sub>15</sub>, Nij, CTI, LE), for a total of 12 linear relationships.

#### **4.4.3. Three Alternative Seat Geometries to Improve Passive Safety for the Passenger**

Three alternative seat and handrail geometries were created to assess the effectiveness of implementing passive safety for transit bus seating. The focus on passive safety features was maintained for this research due to the relative ease of implementation when compared with active safety features such as seat belts which would require various design and operational changes. Passive safety measures operate on the assumption that the passenger will be free to impact surrounding structures during a crash event. Implementation of passive safety required these structures to be designed to minimize the potential for injury to the passenger upon impact. Several mechanisms of injury were identified and addressed in the alternative seat geometries based on the results of the experimental test buck model (section 5.1).

The focal impact of the neck on the handrail was addressed by incorporating a lowered handrail to move the impact location from the anterior neck to the thorax (Figure 87). The handrail diameter was increased to spread the impact force over a greater area.

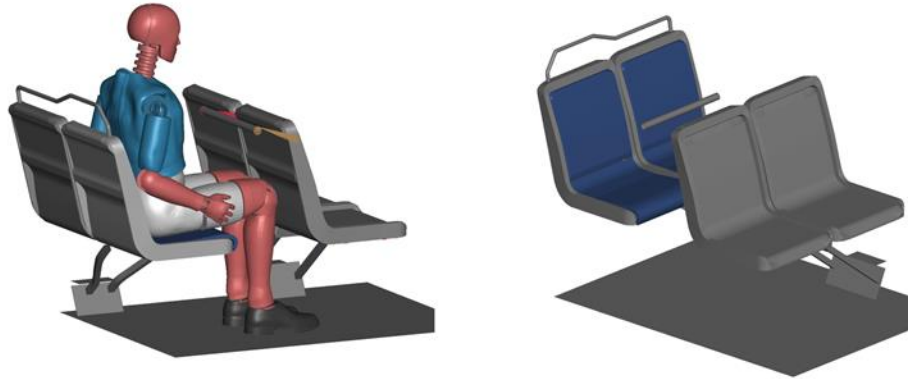


**Figure 87: Forward handrail lowered from top of seat to eliminate impact with the anterior neck**

The second seat geometry design addressed the forward pelvis sliding of the passenger by incorporating a raised lip on the seat pan (Figure 88).



**Figure 88: Raised lip on seat pan to limit the forward sliding of the passenger**

The third alternative seat geometry was based on recommendations made in the literature. It was suggested by Olivares [116] and Martinez [119] that including a raised headrest would prevent hyperextension of the neck during a rear impact. A model that incorporated a raised headrest was created and assessed in the frontal impact scenario (Figure 89).



**Figure 89: Forward seat with headrest and raised seatback**

The results of the simulations with the alternative designs were first assessed using the motions to observe the difference in contact locations with the test buck parts. In addition, each of the three designs were assessed using the injury metrics HIC<sub>15</sub>, Nij, CTI, and LE. The injury metrics were compared with the experimental test buck model to determine if there was a reduction in injury.

#### **4.4.4. Generation of Proposed Seat Design**

The findings from the parametric analysis and alternative seat geometries were combined to generate a final improved seat design.

The linear regression model was used to determine the effect of varying a parameter on a given injury metric. For example, whether increasing seat pitch had a positive or negative impact on HIC<sub>15</sub>. The linear regressions with the strongest correlations were used to inform the creation of the new design.

The alternative geometries were initially assessed for the ability to limit the focal impact on the anterior neck or face of the passenger, as this was identified as the most injurious aspect of the experimental design. The design aspects of the alternative geometries that were shown to reduce injury metrics were considered for the final improved design.

Combining the results of the parametric and alternative seat designs, a proposed seat design was created. The proposed seat design incorporated multiple improvements while ensuring that the model would still be practical.

#### **4.5. Proposed Seat Design Assessment and Comparison with Experimental Test Buck Model Using HBMs and HIIIs with 6.5g Pulse, Upright Posture, and Inboard Seating Location**

The proposed seat design was initially assessed by repeating the steps that were done with the experimental test buck model (Section 4.3). The motions and injury metrics for the HIII and HBM were assessed in the proposed seat design and compared with the results of the experimental test buck model. The aim was to determine if there was any improvement in injury outcome for the passenger in the proposed seat design.

The second stage of the assessment of the proposed seat design was done using the tissue level injury assessment. Results were compared at each body region for the tissue level injury assessment for the responses of the HBMs in the experimental test buck and proposed seat design.

## **5. Results**

### **5.1. Results Overview**

The results for this study are presented in the same four step sequence that was presented in the methods section. The first section (5.2) covers the validation of the test buck model using the HIII M50 and F05 models. The comparison of the motion of the ATDs between the experiment and model, along with the kinematic trace comparison are only presented for a sample test case #1. The highspeed video motion and kinematic trace comparison for test cases #2 - #8 are available in appendices A and B.

Section 5.3 presents the GHBM models response in the test buck and the comparison with the HIIs. The motion, kinematic traces, and injury metrics are all compared between the HBMs and HIIs. The tissue level assessment with the HBMs in the experimental test buck model was not presented until section 5.5 for the comparison with the results with the proposed seat design.

Section 5.4 presents the results of the parametric analysis and alternative seat geometry models.

Section 5.5 concludes the results by presenting the responses of all four occupant surrogates seated in the proposed seat design model and the comparison with the results from the experimental test buck model.

The motion, injury metrics, and tissue level injury assessment are presented as a comparison of the response of the occupant surrogates in the experimental test buck model and the proposed seat design.

### **5.2. Validation of HIII Coupled Test Buck Model**

This section presents the results for the validation of the HIII (M50 & F05) coupled test buck model using the experimental data from the eight TC experimental test configurations. A sample test case (#1) was selected to present the qualitative comparison of ATD motion and the kinematic traces for both the M50 and F05 HIIs. In general, the results for the eight test configurations were comparable with the sample test case #1. Section 5.2.5 will present the notable findings from test configurations #2-#8 that did not align with the sample test case.

#### **5.2.1. Qualitative Assessment of HIII Model Using Highspeed Video (Sample Case #1: 6.5g Pulse, Upright Posture, Inboard Seat)**

##### **5.2.1.1. M50 HIII**

The highspeed video of the experiment provided by TC was compared with the simulation (Figure 90).

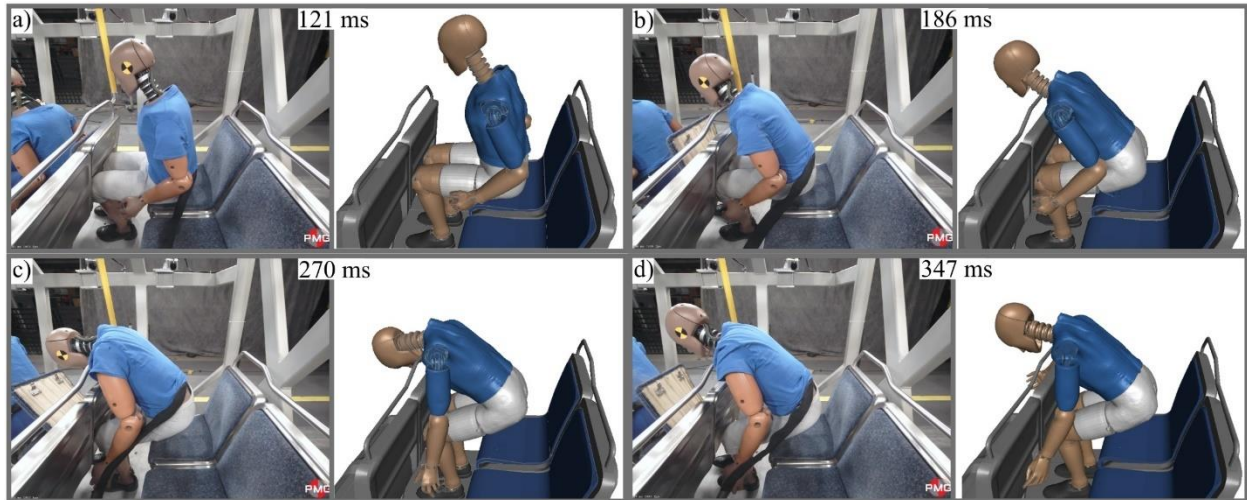


**Figure 90: a) The HII knees impact the forward seatback; b) The neck of the HII contacts the forward handrail; c) The neck of the HII reaches peak flexion; d) The HII rebounds from the handrail and the head rotates in extension**

The knees of the HII in the model and experiment both impacted the forward seatback at 121 ms. The HII in the experiment impacted the handrail on the rubber between the first and second discs in the neck (186 ms). The HII in the model impacted the handrail on the rubber between the second and third discs in the neck (186 ms). The neck of the HII transitioned from flexion to extension at 270 ms in both the model and experiment. The HII rebounded from the forward seat with the pelvis displaced vertically at a height of 16 cm in the model and 31 cm in the experiment (347 ms).

### 5.2.1.2. F05 HIII

The highspeed video of the experiment provided by TC was compared with the simulation (Figure 91).

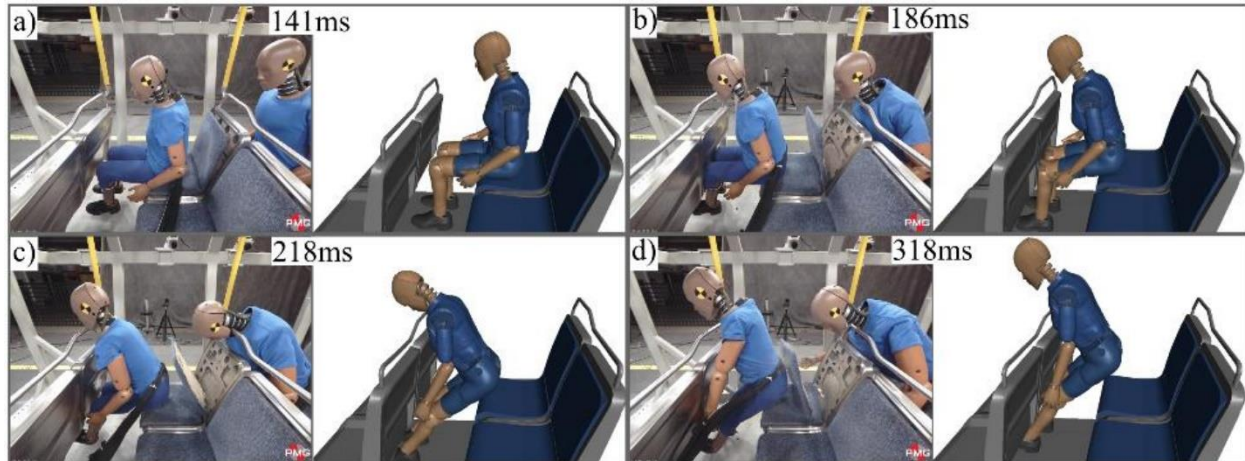


**Figure 91: a) F05 slides forward off seat and the knees impact the forward seatback; b) The torso of the F05 tilts forward at the pelvis and the lower face impacts the handrail; c) The forward momentum of the F05 causes severe flexion of the neck; d) Contact with the handrail is released and the ATD ends up in a semi standing position**

The impact between the lower face and the handrail in the model (218 ms) exhibited increased sagittal rotation (63 deg.) of the HIII head when compared with the experiment (45 deg.). The HIII pelvis was displaced 20 cm vertically in both the model and experiment as it rebounded from the forward seat at 318 ms.

## 5.2.2. Kinematic Trace Comparison (Test Case #1: 6.5g Pulse, Upright Posture, Inboard Seat)

### 5.2.2.1. M50 HIII Kinematic Traces

The acceleration, velocity, displacement, force, and moment traces from the HIII in the experiment and model were plotted. The kinematics quantitatively compared were the head x-axis acceleration, head sagittal angular velocity, neck axial and shear forces, neck sagittal bending moment, chest deflection, chest x-axis acceleration, pelvis x-axis acceleration, and femur axial forces. In general, the plots showed good agreement between the model and the experiment.

The increase and peak values for the pelvis acceleration and femur forces showed good response synchronization between the model and experiment (Figure 92).

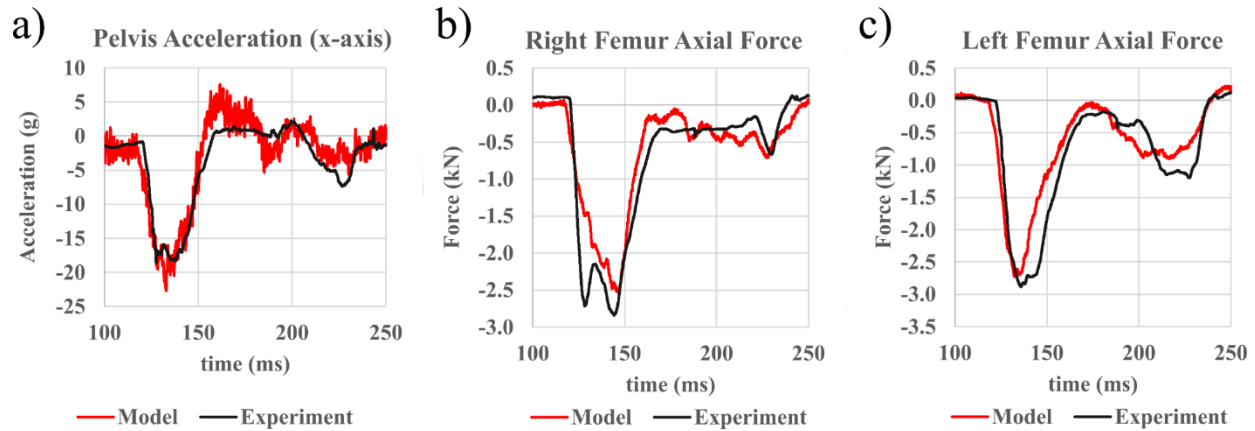


**Figure 92: a) Pelvis acceleration (x-axis); b) Right femur axial force; c) Left femur axial force**

The increase in neck forces/moments and the maximum values (positive/negative) showed that the impact between the anterior neck and handrail resulted in similar head and neck kinematics for the model and experiment (Figure 93).

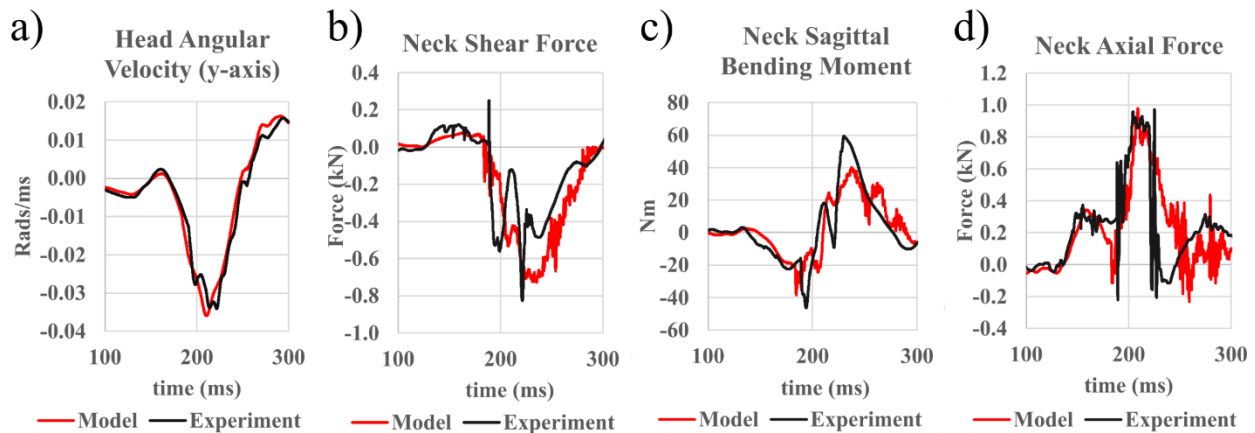


**Figure 93: a) Head sagittal plane angular velocity; b) Neck shear force; c) Neck sagittal plane bending moment; d) Neck axial force**

The head and chest acceleration traces showed good agreement between the model and experiment. A negative value for the chest deflection sensor corresponded to compression of the thorax of the HIII (Figure 94). The results showed primarily positive values for chest deflection which did not correspond to a reduction in thorax volume. The peak chest compression, which was shown via a negative chest deflection value, was less than 1% of initial thorax depth.



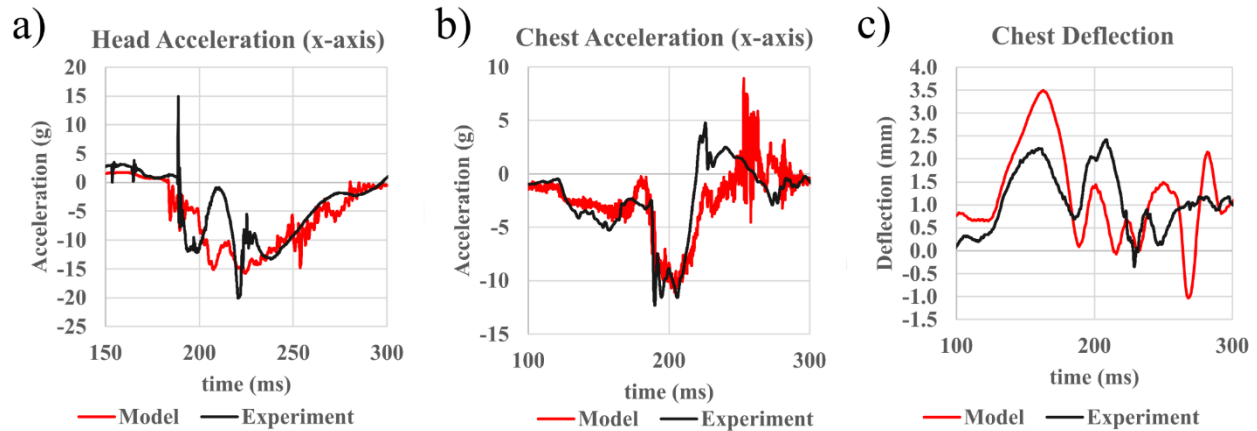


**Figure 94: a) Head acceleration (x-axis); b) Chest acceleration (x-axis); c) Chest deflection**

### 5.2.2.2. F05 HIII Kinematic Traces

The acceleration, velocity, displacement, force, and moment traces outputted from the HIII in the experiment and model were plotted. The kinematics quantitatively compared included the head x-axis acceleration, head sagittal angular velocity, neck axial and shear forces, neck sagittal bending moment, chest deflection, chest x-axis acceleration, pelvis x-axis acceleration, and femur axial forces.

The pelvis acceleration and femur force plots showed that the impact between the knees and the forward seatback occurred 10 ms earlier in the model than in the experiment (Figure 95). The femur loads and pelvis acceleration in the model peaked at approximately half (average 47%) the maximum values in the experiment.

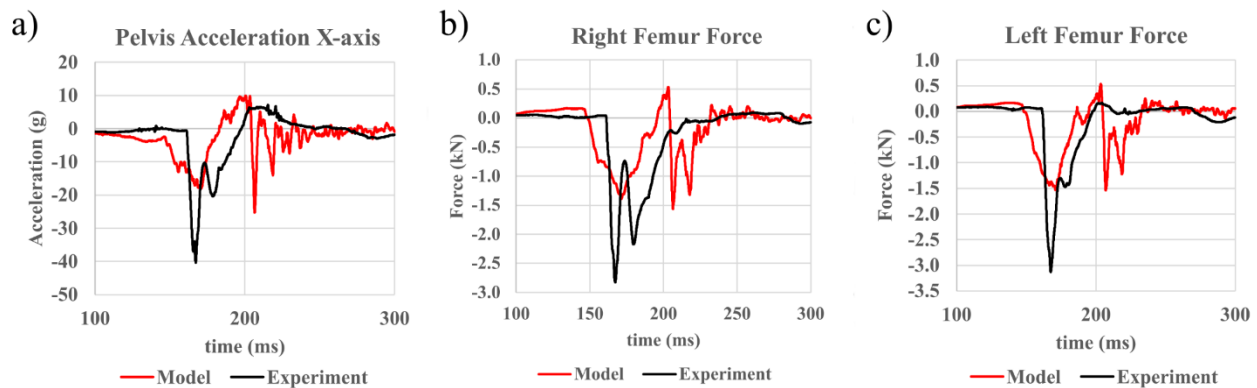


**Figure 95: a) Pelvis acceleration; b) Right Femur Axial Force; c) Left Femur Axial Force**

The neck shear force, sagittal bending moment, and head angular velocity plots showed good agreement between the model and experiment (Figure 96). The plots showed that the head and neck kinematics peaked 10 ms earlier in the model. The neck axial forces in the experiment peaked in the range of 1 kN

for tension and compression compared with peaks of 500 N tension and 400 N compression for the model.

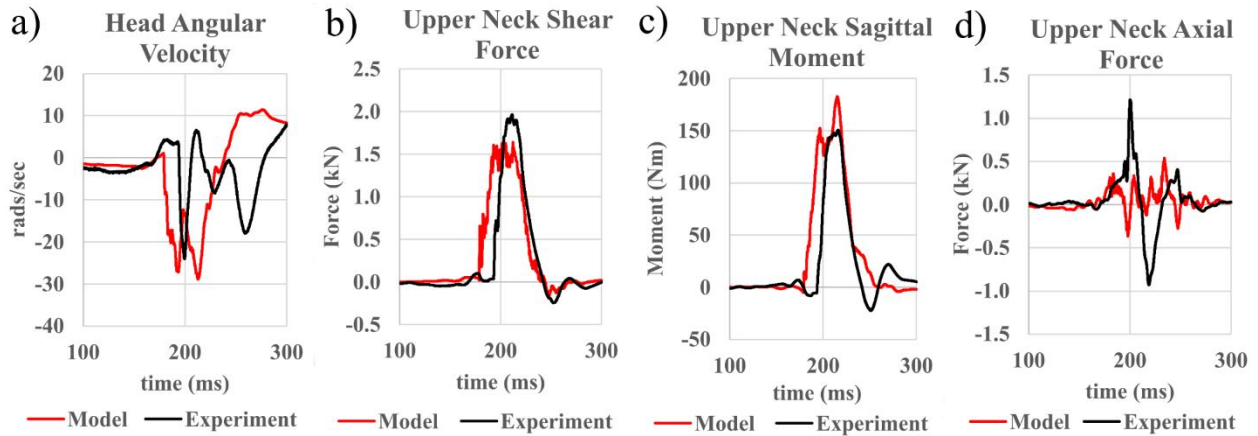


**Figure 96: a) Head sagittal plane angular velocity; b) Upper Neck Shear Force; c) Upper neck sagittal moment; d) Upper neck axial force**

The head and chest accelerations showed good agreement between the model and the experiment (Figure 97). The chest deflection in the model peaked at 3 mm whereas in the experiment it peaked at 0.5 mm.

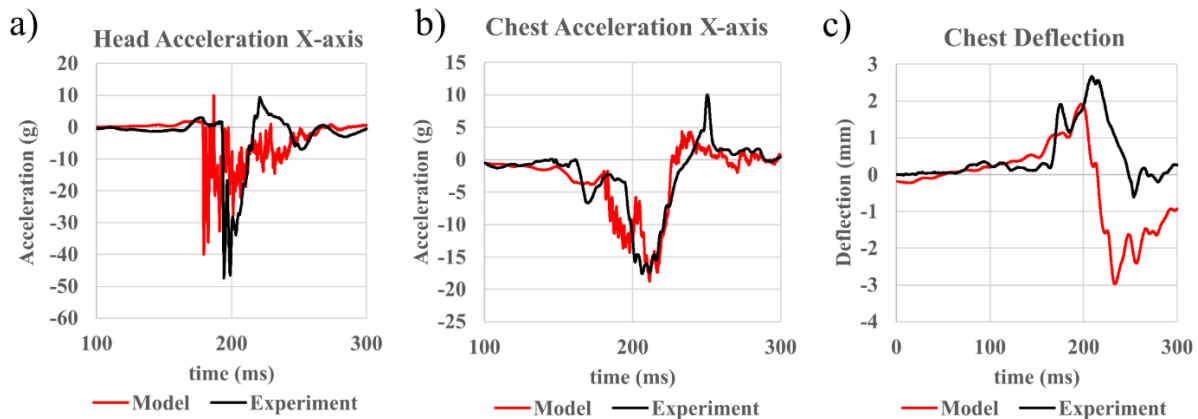


**Figure 97: a) Head acceleration (x-axis); b) Chest acceleration (x-axis); d) Chest deflection**

### 5.2.3. CORA Analysis Results for Test Buck Model Validation Using Eight Test Configurations

The CORA ratings for each experimental test and corresponding model were calculated and averaged to generate a final score for the M50 and F05 coupled test buck models (Table 25).

**Table 25: CORA ratings for all tests (M50 & F05)**

Test Case	CORA score	
	M50	F05
Test #1 (6.5g, Upright, Inboard)	0.913	0.677
Test #2a (6.5g, Reclined, Inboard)	0.792	0.665
Test #2b (6.5g, Reclined, Inboard)	0.782	0.719
Test #2c (6.5g, Reclined, Inboard)	0.763	0.694
Test #3 (5.7g, Upright, Inboard)	0.86	0.595
Test #4 (6.5g, Upright, Outboard)	0.819	0.642
Test #5 (6.5g, Reclined, Outboard)	0.802	0.713
Test #6 (5.7g, Upright, Outboard)	0.866	0.45
Test #7 (5.7g, Reclined, Outboard)	0.751	0.577
Test #8 (5.7g, Reclined, Inboard)	0.674	0.695
<b>Average</b>	<b>0.779</b>	<b>0.634</b>

The average among all M50 tests was 0.779, which classified it in the good biofidelity rating. The average among the F05 tests was 0.634 which placed it in the fair category.

#### **5.2.4. Injury Metrics and Associated Injury Risks (Test Case #1: 6.5g Pulse, Upright Posture, Inboard Seat)**

##### **5.2.4.1. M50 HIII Injury Metrics**

The injury metrics were assessed for the experiment and model for test case #1 (Table 26). Injury assessment reference values (IARV) were listed in the table as a reference for the probability of injury. The injury metrics for the remaining test cases (#2 - #8) were presented in section 5.3.

**Table 26: Injury metrics and risk of injury for the M50 HIII model and experiment**

Metric	Model	Experiment	IARV	Injury Risk Model	Injury Risk Experiment	Associated Risk
<b>Head</b>						
HIC <sub>15</sub>	35.5	36.8	700	0%	0%	AIS 3 Skull Fracture
BrIC	0.87	0.94	2	1%	1%	AIS 3 Brain Injury
<b>Neck</b>						
Nij	0.38	0.51	1	8%	10%	AIS 3 Injury
Pk. Upper Neck Moment, Extension (Nm)	38.5	46.3	96	0%	0%	AIS 3 Injury
Pk. Upper Neck Moment, Flexion (Nm)	40.2	59.6	190	<5%	<5%	AIS 4 Injury
Pk. Upper Neck Axial Force, Tension (N)	977.7	973.0	4170	0%	0%	AIS 3 Injury
Pk. Upper Neck Axial Force, Compression (N)	233.7	220.2	4000	0%	0%	AIS 3 Injury
Pk. Upper Neck Shear Force (N)	726.0	826.2	3100	<5%	<5%	AIS 4 Injury
Pk. Larynx Force, Cricoid	300	N/A	248	Fracture	N/A	Cartilage Fracture
Pk. Larynx Force, Thyroid	300	N/A	180	Fracture	N/A	Cartilage Fracture
<b>Thorax</b>						
CTI	0.15	0.15	1	0%	0%	AIS 3 Injury
Pk. Chest Acceleration (g)	11.57	13.14	60	7%	7%	AIS 3 Injury
Pk. Chest Deflection (mm)	1.03	0.35	50	2%	2%	AIS 3 Injury
VC	0	N/A	1	0%	N/A	AIS 4 Injury
Pk. Chest Deflection Rate (m/s)	0.42	N/A	8.2	0%	N/A	AIS 3 Injury
<b>Lower Extremity</b>						
Pk. Left Femur Axial Force (N)	2722	2880	1	0%	0%	AIS 2 Injury
Pk. Right Femur Axial Force (N)	2529	2837	1	0%	0%	AIS 2 Injury

The injury metrics showed good agreement between the model and experiment for  $HIC_{15}$ , and BrIC.  $HIC_{15}$  was well below the IARV and predicted zero probability of an AIS 3 skull fracture. The low probability of skull fracture injury was due to the lack of a direct impact on the head of the HIII in combination with the overall low severity test buck pulse. The value of BrIC showed a negligible risk of a brain injury based off the head CG angular velocities. Overall, the results showed very low probability of head injury to the passenger in test case #1.

The neck injury metrics showed good agreement between the model and experiment. The values of  $N_{ij}$  were well below the IARV of 1, predicting an 8% and 10% probability of an AIS3 neck injury for the model and experiment respectively. The risk of neck injury predicted by  $N_{ij}$  was the highest probability of injury for all the upper neck injury metrics. Peak values for the neck bending moments in both flexion and extension were well below the IARV, thus predicting a low probability of an AIS3 neck injury. The peak values of neck tension, compression, and shear forces were well below the IARV and showed a low probability of neck injury.

The peak force measured on the segment sets of the anterior neck of the HIII model (300 N) surpassed the experimental thresholds that resulted in larynx cartilage fracture (180 N Thyroid cartilage, 248 N Cricoid cartilage). As a result, fracture to the larynx cartilages is probable in this impact scenario.

The injury metrics for the thorax showed good agreement between the model and the experiment. The highest probability of injury at the thorax was the peak chest acceleration which predicted a 7% probability of an AIS 3 injury for both the model and experiment. All the other thorax injury metrics predicted a less than 2% risk of injury.

Results for the lower extremity injury metrics showed good agreement between the model and the experiment. The potential for a femur fracture based on the peak axial loads in both the left and right femurs was less than 1%.

#### **5.2.4.2. F05 HIII Injury Metrics**

The injury metrics were assessed for the experiment and model (Table 27). Injury assessment reference values (IARV) were listed in the table as a reference for a probability of injury.

**Table 27: F05 HIII injury metrics comparison between experiment and model (test case #1)**

Metric	Model	Experiment	IARV-F05	Injury Risk Model	Injury Risk Experiment	Associated Risk
<b>Head</b>						
HIC <sub>15</sub>	25.8	82.0	700	0%	0%	AIS 3 Skull Fracture
BrIC	0.89	0.02	2	1%	0%	ASI 3 Brain Injury
<b>Neck</b>						
N <sub>ij</sub>	1.21	1.2	1	10%	22%	AIS 4 Injury
Pk. Upper Neck Moment, Extension (Nm)	5.1	22.31	49	0%	0%	AIS 3 Injury
Pk. Upper Neck Moment, Flexion (Nm)	182.7	150.6	95	>5%	>5%	AIS 4 Injury
Pk. Upper Neck Axial Force, Tension (N)	538.0	150.6	2620	0%	0	AIS 3 Injury
Pk. Upper Neck Axial Force, Compression (N)	365.7	22.3	2520	0%	0	AIS 3 Injury
Pk. Upper Neck Shear Force (N)	1647.5	1967.8	1950	<5%	<5%	AIS 4 Injury
Pk. Lower Face Force (N)	2404	N/A	2834	30.1%	N/A	AIS 1 Injury
<b>Thorax</b>						
CTI	0.25	0.24	1	0%	0%	AIS 3 Injury
Pk. Chest Acceleration (g)	19.1	18.55	60	13%	13%	AIS 3 Injury
Pk. Chest Deflection (mm)	3.0	0.62	41	2%	2%	AIS 3 Injury
VC	0.0	N/A	1	0%	0%	AIS 4 Injury
Pk. Chest Deflection Rate (m/s)	0.2	N/A	8.2	0%	0%	AIS 3 Injury
<b>Lower Extremity</b>						
Pk. Left Femur Axial Force (N)	1543	0.46	1	0%	0%	AIS 2 Injury
Pk. Right Femur Axial Force (N)	1563	0.42	1	0%	0%	AIS 2 Injury

A negligible probability of injury was predicted for the head and lower extremity. The N<sub>ij</sub> peaked above the IARV of 1 in both the model and experiment, predicting a 22% probability of an AIS 3 neck injury. The peak upper neck sagittal flexion moment of 150 Nm in the model and experiment were well above the IARV of 95 Nm and predicted a greater than 5% risk of an AIS 4 neck injury. The peak neck shear force in the experiment was above the IARV of 1950 N and predicted at >5% risk of an AIS 4 neck injury. The peak force of 2404 N on the lower face in the model surpassed the experimental fracture

threshold of 1779 N. In this impact scenario a fracture to the mandible of the passenger would be probable.

The highest probability of injury in the thorax was due to the peak linear chest acceleration of 18 g in both the model and experiment which predicted a 13% probability of an AIS 3 thorax injury. All other injury metrics in the thorax predicted little or no probability of injury.

### **5.2.5. Injury Metrics Summary for the Eight Test Configurations**

Injury metrics were calculated for all test cases (#2-8) for the M50 and F05 and tabulated (Table 28, Table 29).

In general, the injury metrics agreed well between the M50 models and experiments and predicted little to no injury when compared with the IARV. All the M50 models predicted forces on the anterior neck that exceeded the threshold found experimentally to result in larynx cartilage fracture. The experiment and model for test case #8 resulted in different impact locations between the M50 and the handrail. The model for test case #8 resulted in the anterior neck impacting the handrail, as was the case with every other model. The experiment for test case #8 resulted in the lower face of the M50 impacting the handrail instead of the anterior neck. The lower face impact resulted in an  $N_{ij}$  value of 1.27 which corresponded to a 32% probability of an AIS 3 neck injury. The remaining injury metrics for the head and neck of the M50 in experiment test case #8 did not predict a high probability of injury. The difference in handrail impact location between the model and experiment for test case #8 resulted in the biggest discrepancy between all M50 models and corresponding experiments.

The injury metrics for the F05 models and experiments showed good agreement and predicted a low probability of injury throughout the ATD except at the neck. The test cases with the F05 seated in the inboard seat resulted in the lower face impacting the forward handrail which caused  $N_{ij}$ , neck flexion, and lower face force to predict injury. When the F05 was seated on the outboard seat it impacted the forward handrail on the anterior neck which resulted in forces that surpassed the larynx cartilage fracture threshold.

**Table 28: HIII M50 injury metrics for all experiments and test cases**

	IAR V	Mod.	Exp	Mod	Exp	Exp	Exp	Mod	Exp	Mod	Exp	Mod	Exp	Mod	Exp	Mod	Exp	Mod	Exp
		#1	#1	#2	#2a	#2b	#2c	#3	#3	#4	#4	#5	#5	#6	#6	#7	#7	#8	#8
Head																			
HIC <sub>15</sub>	700	35.5	36.8	17.8	31.4	13.2	28.0	20.2	14.5	40.6	25.2	10.8	22.1	18.3	17.3	5.4	6.8	8.4	56.0
BrIC	2	0.87	0.94	0.70	0.86	0.74	0.82	0.80	0.88	0.82	0.86	0.66	0.69	0.69	0.75	0.63	0.62	0.66	0.84
Neck																			
N <sub>ij</sub>	1	0.38	0.51	0.31	0.55	0.46	0.46	0.39	0.46	0.36	0.43	0.23	0.29	0.26	0.37	0.34	0.57	0.26	1.27
Pk. Upper Neck Moment, Extension (Nm)	96	38.5	46.3	21.9	21.7	31.9	20.2	36.8	33.8	23.8	31.4	22.7	16.7	21.7	17.1	19.5	15.6	19.3	17.6
Pk. Upper Neck Moment, Flexion (Nm)	190	40.2	59.6	29.3	46.7	47.1	49.2	37.7	47.9	33.4	30.8	19.6	35.0	28.7	44.4	16.3	56.1	26.1	144.5
Pk. Upper Neck Axial Force, Tension (N)	4170	977	973	641	882	1372	921	687	633	1013	855	584	780	723	711	355	764	452	1267
Pk. Upper Neck Axial Force, Compression (N)	4000	233.7	220.2	119.5	157.1	120.8	244.6	154.3	272.7	80.3	47.2	156.8	119.9	56.5	110.1	116.1	72.2	84.8	369.8
Pk. Upper Neck Shear Force (N)	3100	726	826	604	667	575	683	813	757	692	485	475	469	576	480	427	382	476	1370
Pk. Larynx Force, Cricoid	248	300	N/A	318	N/A	N/A	N/A	738	N/A	435	N/A	240	N/A	278	N/A	198	N/A	298	N/A
Pk. Larynx Force, Thyroid	180	300	N/A	318	N/A	N/A	N/A	738	N/A	435	N/A	240	N/A	278	N/A	198	N/A	298	N/A
Thorax																			
CTI	1	0.15	0.15	0.12	0.15	0.11	0.14	0.12	0.12	0.20	0.14	0.11	0.11	0.14	0.11	0.15	0.08	0.10	0.13
Pk. Chest Acceleration (g)	60	11.6	13.1	9.6	12.8	8.6	11.9	9.6	10.3	16.3	12.4	8.1	9.1	11.7	8.7	6.4	6.3	8.3	11.0
Pk. Chest Deflection (mm)	50	1.0	0.3	3.8	0.0	0.0	0.2	0.5	0.3	5.5	3.2	10.9	3.1	4.5	1.3	6.3	1.7	1.4	0.4
VC	1	0.0	0.0	0.0	0.0	0.0	0.0	0.1	0.0	0.1	0.0	0.4	0.0	0.1	0.0	0.1	0.0	0.0	0.0
Pk. Chest Deflection Rate (m/s)	8.2	0.4	0.5	3.3	0.5	0.4	0.5	0.2	0.3	0.4	0.4	0.3	0.5	0.6	0.6	0.3	0.3	0.3	0.3
Lower Extremity																			
Pk. Left Femur Axial Force (N)	1000	2722	2880	3316	2529	2477	2832	2535	2992	3087	3233	3800	3218	3205	3636	3313	2964	2960	2365
Pk. Right Femur Axial Force (N)	1000	2529	2837	3060	2971	2694	3079	2278	2785	2942	2845	3743	2778	3147	3228	3290	2648	2724	2525



**Table 29: F05 Injury metrics for all experiments and test cases**

	IAR V	Mod	Exp	Mod	Exp	Exp	Exp	Mod	Exp	Mod	Exp	Mod	Exp	Mod	Exp	Mod	Exp	Mod	Exp
		#1	#1	#2	#2a	#2b	#2c	#3	#3	#4	#4	#5	#5	#6	#6	#7	#7	#8	#8
Head																			
HIC <sub>15</sub>	700	25.8	82.0	50.8	116	96.1	93.8	31.9	67.9	68.5	48.4	48.0	42.7	40.9	36.8	17.2	21.9	37.3	66.5
BrIC	2	0.89	0.80	0.78	0.96	0.80	0.83	0.80	0.73	0.95	0.95	0.86	0.89	0.84	0.91	0.77	0.85	0.72	0.75
Neck																			
N <sub>ij</sub>	1	1.21	1.20	0.91	1.00	0.86	0.92	1.03	0.83	0.78	0.74	0.68	0.68	0.69	0.59	0.49	0.54	0.72	0.73
Pk. Upper Neck Moment, Extension (Nm)	49	5.1	22.3	16.2	50.4	34.8	32.7	3.6	9.1	34.7	37.2	27.7	36.8	28.6	28.6	22.8	25.2	11.9	13.9
Pk. Upper Neck Moment, Flexion (Nm)	95	182	150	126	114	95	98	150	102	35	41	35	28	32	30	21	27	102	91
Pk. Upper Neck Axial Force, Tension (N)	2620	538	1213	603	1853	1305	1414	587	941	984	1016	850	920	800	975	561	716	479	996
Pk. Upper Neck Axial Force, Compression (N)	2520	365	932	387	364	36	204	600	637	8	219	124	120	115	68	120	84	359	453
Pk. Upper Neck Shear Force (N)	1950	1647	1967	1479	1592	136	1375	1529	1427	577	589	454	500	498	444	336	382	1242	1148
Pk. Lower Face Force	1779	2404	N/A	2460	N/A	N/A	N/A	2236	N/A	0	N/A	0	N/A	0	N/A	0	N/A	1994	N/A
Pk. Larynx Force (Cricoid, Thyroid)	248, 180	0.0	N/A	0	N/A	N/A	N/A	0	N/A	347	N/A	305	N/A	291	N/A	190	N/A	0	N/A
Thorax																			
CTI	1	0.25	0.24	0.16	0.22	0.16	0.19	0.22	0.17	0.43	0.20	0.31	0.24	0.31	0.16	0.34	0.18	0.12	0.15
Pk. Chest Acceleration (g)	60	19.1	18.5	13.0	16.5	12.3	14.7	17.5	12.8	20.3	14.6	12.4	17.8	16.7	11.3	10.5	12.7	10.1	11.1
Pk. Chest Deflection (mm)	41	3.0	0.6	1.7	2.1	0.8	0.6	1.0	0.0	17.3	3.0	14.3	3.0	10.7	2.6	18.4	2.2	1.0	0.1
VC	1	0.0	0.0	0.0	0.0	0.0	0.0	0.0	0.0	0.0	0.0	0.0	0.0	0.0	0.0	0.1	0.0	0.0	0.0
Pk. Chest Deflection Rate (m/s)	8.2	0.2	0.4	0.2	0.4	0.3	0.4	0.2	0.3	0.8	0.6	0.4	0.5	0.5	0.5	0.4	0.4	0.2	0.4
Lower Extremity																			
Pk. Left Femur Axial Force (N)	6800	1543	3129	1453	3245	2511	2951	695	2827	1225	3474	1302	3536	1857	4122	1218	3520	1468	3049
Pk. Right Femur Axial Force (N)	6800	1563	2828	1601	2832	2803	3219	985	2493	1203	3747	1491	3814	1366	3280	576	3018	1046	2749

### 5.3. Test Buck Model Assessment Using HBM and HIII with 6.5g Pulse, Upright Posture, and Inboard Seating Location

This section will present the results of the HBMs (M50 and F05) seated in the test buck model with the 6.5g pulse, upright posture, and inboard seating location. The HBM response was compared with the HIII from the TC case #1, which had the same test configuration.

#### 5.3.1. Qualitative Comparison of HBM Motion with HIII in Experimental Test Buck Model

##### 5.3.1.1. GHBMCM50 Qualitative Comparison with HIII

The motion of the HBM M50 was qualitatively compared with the HIII motion (Figure 98).

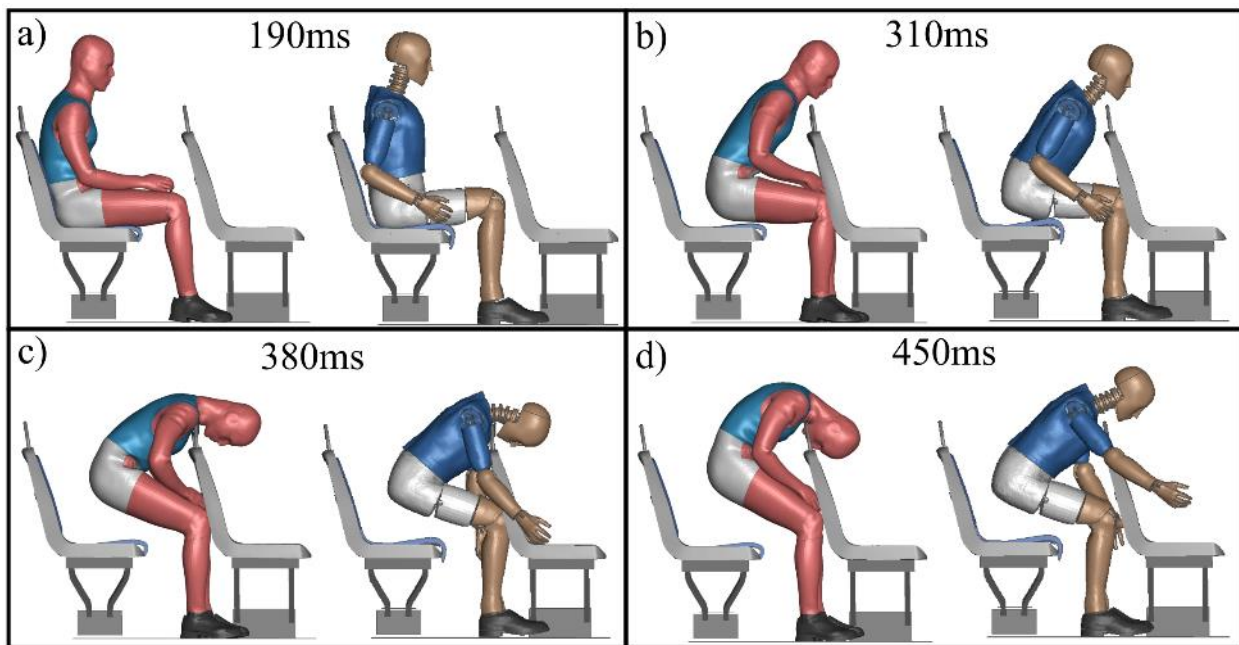


**Figure 98: a) HBM seated prior to initiation of pulse; b) HBM knees impact the forward seatback and torso pitches forward at the pelvis; c) the anterior of the neck strikes the forward handrail; d) the HBM thoracic spine in flexion after impact with forward handrail**

The response of the HBM was comparable with the HIII prior to impact with the handrail. The HBM exhibited thoracic spine flexion after impacting the handrail which was not observed with the HIII. The flexion of the spine resulted in the face of the HBM impacting the top of the forward seat. The HBM neck was in flexion throughout the impact and did not transition to extension as was observed with the HIII. The pelvis of the HBM was displaced 19 cm vertically from the seat while the HIII was displaced 16 cm from the seat. The HBM remained positioned above the forward handrail at the end of the simulation, instead of rebounding horizontally as was observed with the HIII.

### 5.3.1.2. GHBMC F05 Qualitative Comparison with HIII

The motion of the F05 HBM was qualitatively compared with the results for the F05 HIII for TC test case #1 (Figure 99).

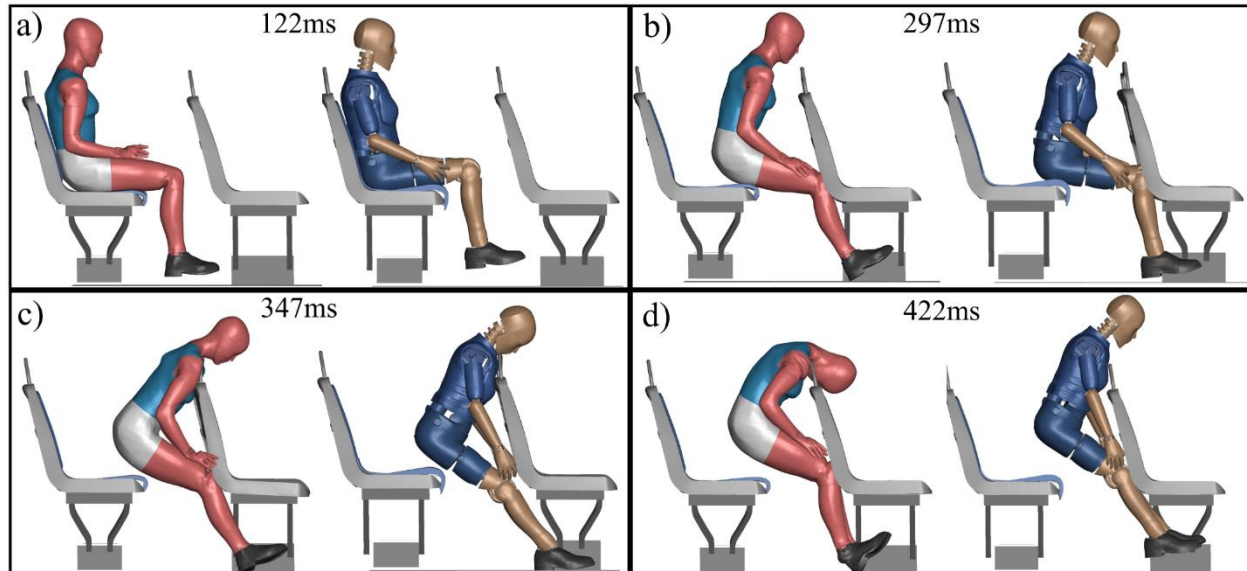


**Figure 99: a) HBM seated prior to pulse initiation; b) knees impact forward seatback; c) anterior neck of HBM impacts forward handrail; d) HBM face impacts forward side of seat frame**

The chin of the HBM cleared the forward handrail which resulted in the lower anterior neck impacting the handrail (347 ms). There was no impact between the face of the HBM and handrail as was observed with the HIII. The spine of the HBM went into flexion following the impact with the handrail. The HIII was displaced 20 cm vertically from the seat at 420 ms while the HBM was displaced vertically 13 cm from the seat.

## 5.3.2. Kinematic Trace Comparison Between HBM and HIII

### 5.3.2.1. GHBMC M50 Kinematics Traces

The pelvis acceleration and femur force of the HBM showed a 26 ms delay in the impact between the knees and seatback compared with the HIII (Figure 100). The pelvis acceleration of the HBM and HIII showed the same peak magnitude of 23 g. The femur force was comparable between the HBM and HIII models for peak force which was in the range of 2500 N for both the right and left femurs.

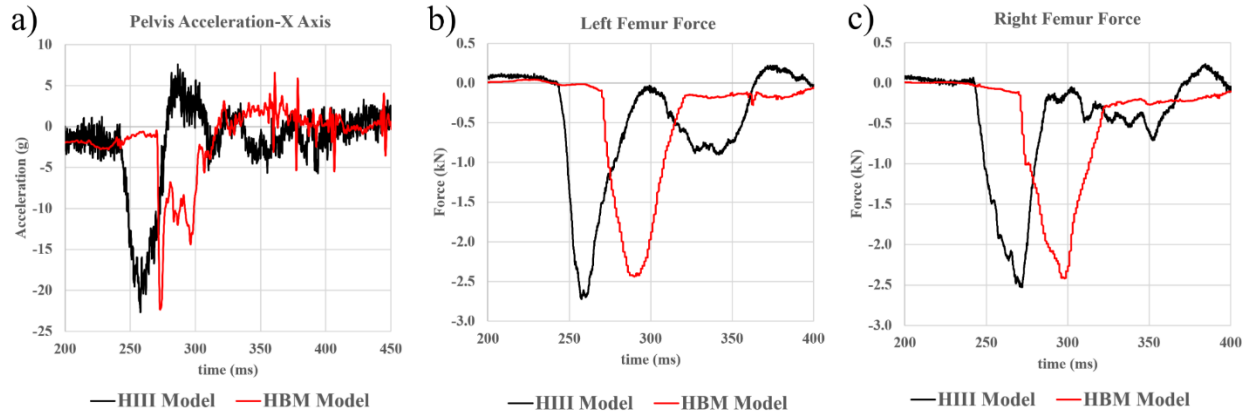


**Figure 100: a) Pelvis acceleration (x-axis); b) Left femur axial force; c) Right femur axial force**

The OC cross section of the HBM neck measured a maximum shear force of 150 N compared with 700 N for the HIII upper neck (Figure 101). The shear force in the lower neck (C7) cross section of the HBM had a peak of 600 N which was more comparable with the HIII model.

The tension force at the OC level in the HBM peaked at 500 N compared with 1000 N for the HIII. The C4 cross section of the HBM neck peaked at a magnitude of 1000 N, which was comparable with the HIII.

The sagittal plane bending moment at the OC cross section of the HBM neck registered a peak extension moment of 15 Nm compared with 30 Nm for the HIII. Following the impact with the handrail at 325 ms, there was no flexion moment at the OC cross section of the HBM, whereas the HIII saw a 40 Nm peak in flexion in the upper neck. The C7 cross section of the neck was again more comparable with the upper neck of the HIII, seeing a peak extension moment of 30 Nm and a peak flexion moment of 60 Nm.

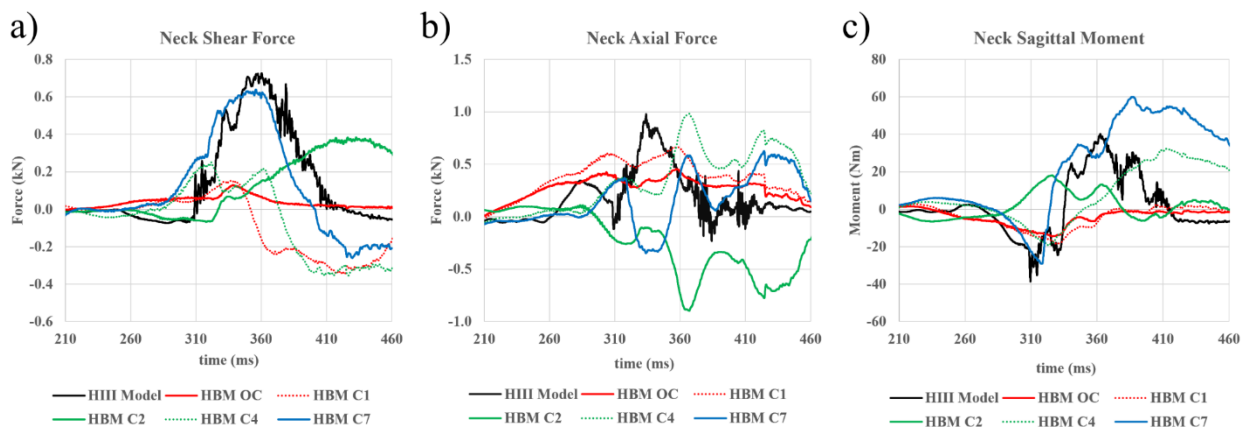


**Figure 101: a) Neck shear force; b) Neck axial force; c) Neck sagittal plane bending moment**

The HBM head acceleration peaked at 4 g during the impact with the handrail from 320 ms-370 ms while the HIII peaked at 15 g (Figure 102). The 20 g peak head acceleration for the HBM occurred at 420 ms when the face impacted the forward side of the seat. The head angular velocity was comparable between the HBM and HIII after accounting for the 15 ms delay in response with the HBM.

The response of the chest bands of the HBM did not show any thorax compression. The positive deflection with the middle and lower chest bands was the result of the thorax expanding as the HBM lost posture prior to impacting the forward handrail.

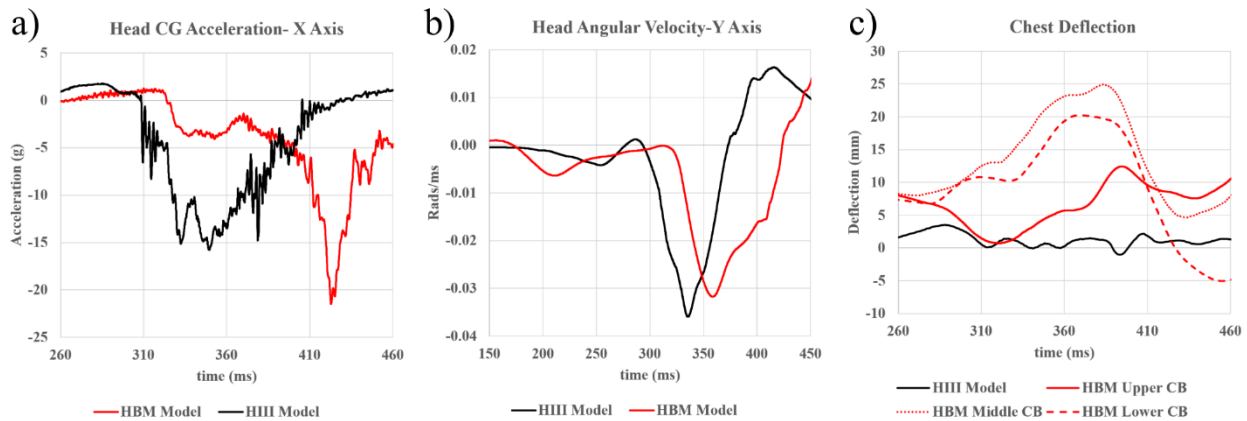


**Figure 102: (a) Head linear acceleration (x-axis); (b) Head sagittal plane angular velocity; (c) Chest deflection**

### 5.3.2.2. GHBM F05 Kinematics Traces

The pelvis acceleration peaked at 10 g for the HBM upon impacting the forward seatback with the knees compared with a peak of 18 g for the HIII (Figure 103). The femur loads showed that the initial impact between the knees and the forward seatback occurred at 156 ms with the HBM, 10 ms after the HIII impacted the seat.

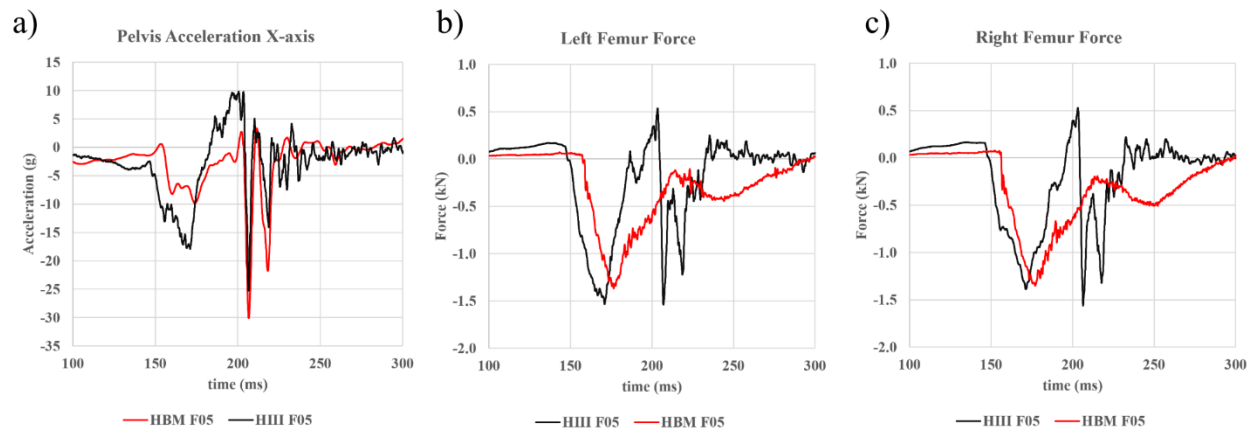


**Figure 103: a) Pelvis acceleration (x-axis); b) Left femur axial force; c) Right femur axial force**

The lack of focal impact on the face of the HBM resulted in significantly lower shear forces and bending moments throughout the cross sections of the HBM neck (Figure 104). The HBM peak neck shear force was less than 300 N compared with the peak shear of 1600 N for the HIII. The sagittal bending moment in the neck of the HBM peaked at 20 Nm flexion compared with 150 Nm flexion for the HIII. The HBM exhibited a peak compression force of 1100 N in the lower neck (C7) cross section because of the focal impact on the handrail with the anterior neck.

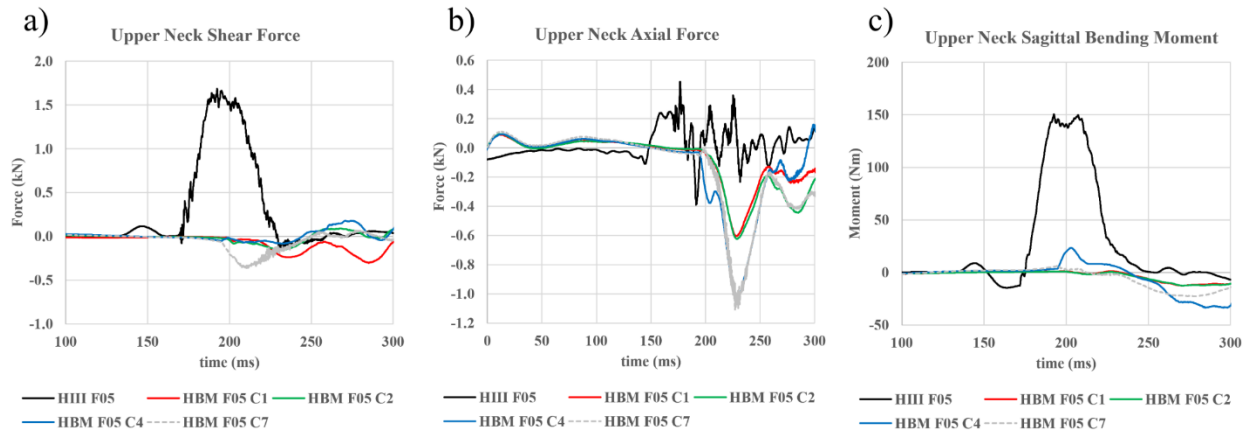


**Figure 104: a) Upper neck shear force; b) Upper neck axial force; c) Upper neck sagittal plane bending moment**

The HBM head acceleration peaked between 260 ms-300 ms as a result of the face impacting the top of the forward seat frame (Figure 105). The angular velocity of the head for the F05 exhibited a longer duration of negative rotation due to the head not coming in direct impact with the handrail. The chest of the HBM ended up impacting the top part of the forward seatback which resulted in a peak deflection of 25 mm (13% chest compression).

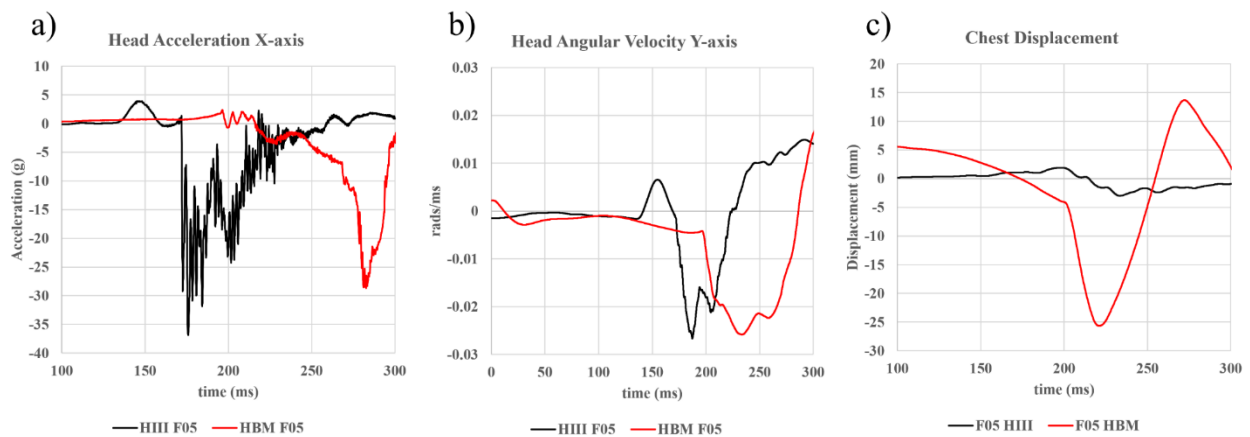


**Figure 105: a) Head acceleration (x-axis); b) Head sagittal plane angular velocity; c) Chest displacement**

### 5.3.3. HBM Injury Metrics Comparison with HIII

#### 5.3.3.1. GHBMC M50 Injury Metrics

The injury metrics for the M50 HBM were calculated and compared with the M50 HIII (Table 30). The OC neck cross section of the HBM was compared with the HIII upper neck load cell. The middle chest band of the HBM was compared with the HIII thorax compression.

**Table 30: M50 HBM comparison with HIII injury metrics**

Metric	HIII	HBM	IARV	Injury Risk HIII Model	Injury Risk HBM	Associated Risk
<b>Head</b>						
HIC <sub>15</sub>	35.5	23.2	700	0%	0%	AIS 3 Skull Fracture
BrIC	0.87	0.81	1	1%	1%	ASI 3 Brain Injury
<b>Neck</b>						
N <sub>ij</sub>	0.38	0.16	1	8%	5%	AIS 3 Injury
Pk. Upper Neck Bending Moment, Extension (Nm)	38.5	14.4	96	0%	0%	AIS 3 Injury
Pk. Upper Neck Bending Moment, Flexion (Nm)	40.2	5.6	190	<5%	<5%	AIS 3 Injury
Pk. Upper Neck Axial Load, Tension (N)	977.7	454.0	4170	0%	0%	AIS 3 Injury
Pk. Upper Neck Axial Load, Compression (N)	233.7	129.8	4000	0%	0%	AIS 3 Injury
Pk. Upper Neck Shear Load (N)	726.0	128.8	3100	<5%	<5%	AIS 4 Injury
Pk. Larynx Force Compression	N/A	75%	50%	N/A	Fracture	Cartilage Fracture
<b>Thorax</b>						
Pk. Chest Deflection (mm)	1.03	4.80	50	0%	2%	AIS 3 Injury
VC	0	0	1	0%	0%	AIS 4 Injury
Pk. Chest Deflection Rate (m/s)	0.42	0.29	8.2	0%	0%	AIS 3 Injury
<b>Lower Extremity</b>						
Pk. Left Femur Axial Force (kN)	2722	2440	1	0%	0%	AIS 2 Injury
Pk. Right Femur Axial Force (kN)	2529	2420	1	0%	0%	AIS 2 Injury

In general, the ATD injury metrics for the HBM were comparable to those with the HIII. The highest predicted probability of injury for the HBM was the N<sub>ij</sub> criteria which showed a 5% risk of an AIS3 neck injury. All other ATD injury metrics with the HBM predicted a negligible probability of injury.

The larynx compression with the M50 HBM peaked at a value of 75% which showed a potential for larynx cartilage fracture when compared with the 50% compression fracture threshold reported in the literature.

#### **5.3.3.2. GHBMC F05 Injury Metrics**

The injury metrics calculated for the F05 HBM were calculated and compared with the F05 HIII (Table 31).



**Table 31: HBM F05 calculated injury metrics and comparison with HIII F05 (test case #1)**

Metric	HIII	HBM	IARV	Injury Risk HIII Model	Injury Risk HBM	Associated Risk
<b>Head</b>						
HIC <sub>15</sub>	25.8	57.9	700	0%	0%	AIS 3 Skull Fracture
BrIC	0.89	0.74	2	1%	0%	ASI 3 Brain Injury
<b>Neck (OC)</b>						
N <sub>ij</sub>	1.21	0.26	1	30%	6%	AIS 3 Injury
Pk. Upper Neck Moment, Extension (Nm)	5.1	1.2	49	0%	0%	AIS 3 Injury
Pk. Upper Neck Moment, Flexion (Nm)	182.7	12.7	95	<5%	<5%	AIS 3 Injury
Pk. Upper Neck Axial Force, Tension (N)	538.0	91.8	2620	0%	0%	AIS 3 Injury
Pk. Upper Neck Axial Force, Compression (N)	365.7	605.1	2520	0%	0%	AIS 3 Injury
Pk. Upper Neck Shear Force (N)	1674.5	304.7	1950	<5%	<5%	AIS 4 Injury
Larynx Compression	N/A	80%				Cartilage Fracture
<b>Thorax</b>						
Pk. Chest Deflection (mm)	2.97	25.67	41	2%	1%	AIS 3 Injury
VC	0.00	0.10	1	0%	0%	AIS 4 Injury
Pk. Chest Deflection Rate (m/s)	0.3	1.56	8.2	0%	5%	AIS 3 Injury
<b>Lower Extremity</b>						
Pk. Left Femur Axial Force (N)	1543.00	1368.00	1	0%	0%	AIS 2 Injury
Pk. Right Femur Axial Force (N)	1563.00	1351.00	1	0%	0%	AIS 2 Injury

N<sub>ij</sub> did not predict a neck injury for the HBM as was the case with the HIII. Due to the focal impact on the anterior neck of the HBM there was an 80% total compression of the larynx tissue in the HBM. Based on the 50% strain threshold presented in the literature, a larynx cartilage fracture would be probable with the HBM. The peak chest deflection of 25.7 mm and deflection rate of 1.6 m/s for the HBM were significantly higher than the HIII (3mm, 0.3 m/s). All the other injury metrics were comparable between the F05 HBM and HIII.

## 5.4. Alternate Seat Configurations Assessment using HIII M50 for Development of Proposed Seat Design

This section presents the results from the parametric analysis and alternative seat geometry models.

### 5.4.1. Parametric Analysis and Linear Regression Results

The injury metrics  $HIC_{15}$ ,  $N_{ij}$ , CTI, and LE were calculated for all 24 simulations in the parametric analysis. Plots were created comparing the influence of the parameters (seat pitch, seat height, and seating location) on each injury metric. A linear regression model was created for each plot and ranked based on the R-squared value (Table 32).

**Table 32: Linear Regression Analysis Results for Injury Metrics and Varied Parameter, Ranked by R-squared Value**

Injury Metric	Parameter	R <sup>2</sup>
LE	Seat Pitch	0.86
CTI	Seat Height	0.56
$N_{ij}$	Seat Height	0.47
$HIC_{15}$	Inboard/Outboard	0.37
$HIC_{15}$	Seat Height	0.26
$N_{ij}$	Inboard/Outboard	0.22
CTI	Inboard/Outboard	0.13
$HIC_{15}$	Seat Pitch	0.12
CTI	Seat Pitch	0.09
LE	Seat Height	0.05
$N_{ij}$	Seat Pitch	0.04
LE	Inboard/Outboard	0.01

The highest R-squared value was for the effect of varying seat pitch on the LE criteria. The parameter/injury metrics that had an R-squared above 0.3 were selected for further analysis. The injury metrics in each group were averaged for a given variable and replotted (Figure 106). The linear equation was recalculated with the averaged data to determine the magnitude of the effect each variable had on a given injury metric.

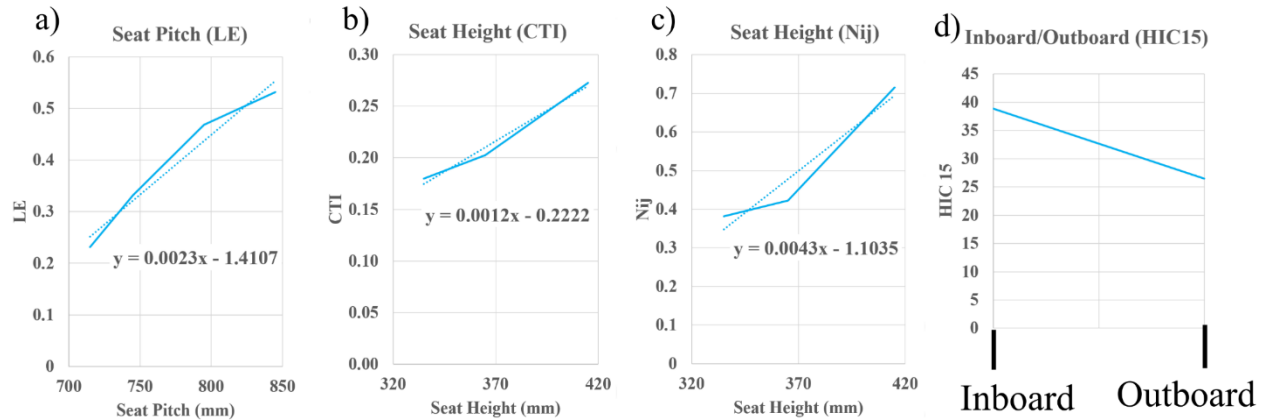


**Figure 106: a) Effect of seat pitch on LE; b) Effect of forward seat height on CTI; c) Effect of forward seat height on  $N_{ij}$ ; d) Influence of inboard/outboard seating location on  $HIC_{15}$**

The linear regression analysis with the average values showed an increase in LE of 0.23 for every increase of seat pitch of 100 mm. An increase in seat height of 50 mm resulted in an increase in CTI of 0.06, and an increase of  $N_{ij}$  of 0.22. Moving the passenger from the inboard to outboard seat resulted in an average decrease in  $HIC_{15}$  of 12.5.

The linear regression models showed that:

- Moving from the inboard to outboard seat resulted in a decrease in head injury potential.
- Decreasing the forward seat height resulted in a decrease in neck injury potential.
- Decreasing the forward seat height resulted in a decrease in thorax injury potential.
- Decreasing the seat pitch resulted in a decrease in femur injury potential.

#### 5.4.2. Alternative Seat Geometry Models

This section will present the qualitative assessment of the HIII motion in the three alternative geometry models.

##### 5.4.2.1. HIII Motion in Lowered Handrail Model

Lowering the handrail resulted in the HIII impacting the handrail on the thorax as opposed to the anterior neck (Figure 107).

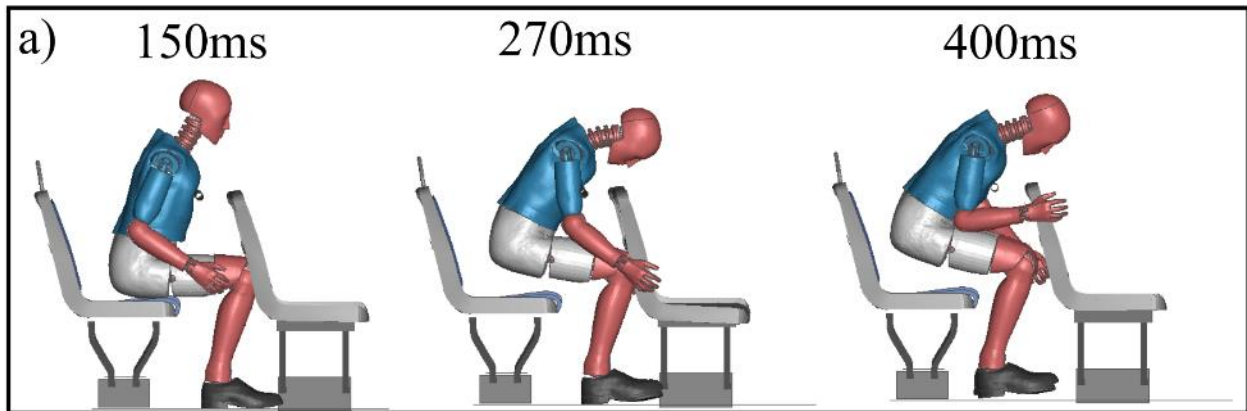


**Figure 107: Lowered handrail test buck model**

#### 5.4.2.2. HIII Motion in Headrest Model

The headrest model resulted in the face of the HIII impacting the rear side of the seat frame/headrest (Figure 108).

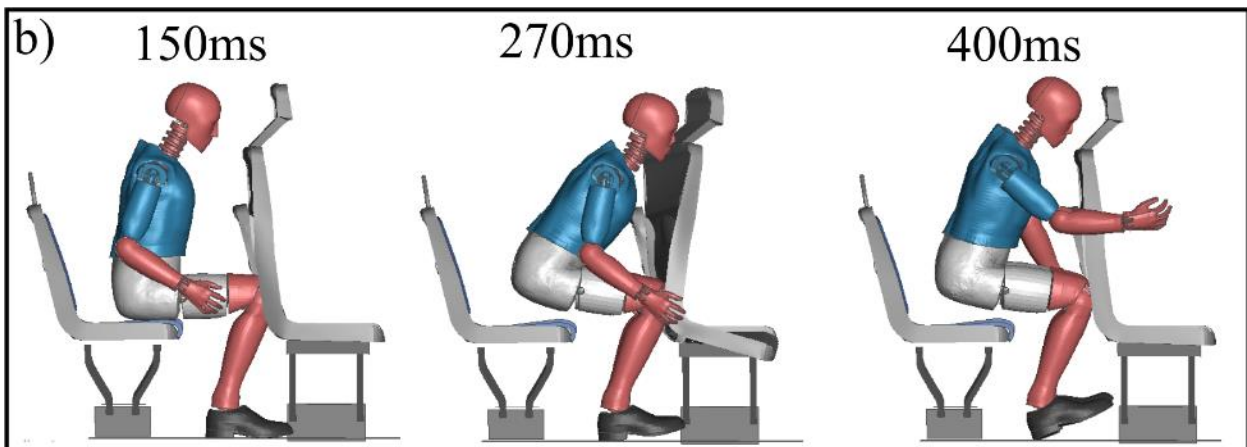


**Figure 108: Headrest test buck model**

#### 5.4.2.3. HIII Motion in Bucket Seat Model

The forward sliding of the pelvis of the HIII was reduced in the bucket seat model (Figure 109). The friction interaction between the feet and the floor prevented the feet from sliding forward. This resulted in the knees of the HIII locking and prevented them from impacting the forward seatback. The anterior neck impacted the handrail as was observed in the experimental test buck model.

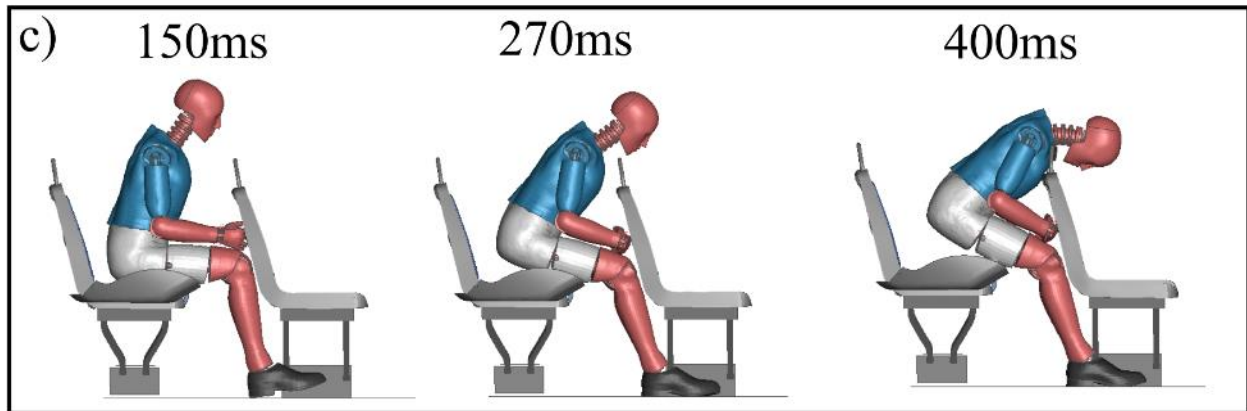


**Figure 109: M50 HIII motions in bucket seat design**

#### **5.4.2.4. Injury Metric Comparison Between Alternative Geometry Models**

The injury metrics were calculated for each of the three alternative seat geometries and compared with the experimental test buck model (Table 33). The results of the test buck model were compared with the alternative geometries as the baseline for injury.

**Table 33: Injury Metric comparison between experimental test buck model (test case #1) and alternative geometry models**

Metric	Experimental Test Buck Model	Lowered Handrail Design	Headrest Design	Bucket Seat Design
<b>Head</b>				
HIC <sub>15</sub>	36	10	100	22
BrIC	0.87	0.82	0.72	0.60
<b>Neck</b>				
N <sub>ij</sub>	0.38	0.40	1.34	0.28
Pk. Upper Neck Moment, Extension (Nm)	39	42	7	11
Pk. Upper Neck Moment, Flexion (Nm)	40	28	151	32
Pk. Upper Neck Axial Force, Tension (N)	978	583	683	758
Pk. Upper Neck Axial Force, Compression (N)	234	125	1061	99
Pk. Upper Neck Shear Force (N)	726	493	1796	568
Pk. Larynx Force, Cricoid	300	80	103	275
<b>Thorax</b>				
CTI	0.15	0.18	0.19	0.16
Pk. Chest Acceleration (g)	11.57	15.41	16.12	13.62
Pk. Chest Deflection (mm)	1.03	28.52	0.28	0.94
VC	0.00	0.12	0.00	0.01
Pk. Chest Deflection Rate (m/s)	0.42	1.88	0.23	0.36
<b>Lower Extremity</b>				
Pk. Left Femur Axial Force (N)	2722	2754	2527	1517
Pk. Right Femur Axial Force (N)	2529	2641	1934	2012

The peak force on the anterior neck in the lowered handrail model was below the threshold for a larynx crushing injury. The lowered handrail model resulted in 28 mm of chest deflection due to the focal impact of the handrail with the thorax. For comparison, the second largest chest deflection was in the baseline model with 1 mm peak deflection. None of the thorax injury metrics for the lowered handrail model surpassed the IARV. The femur loads with the lowered handrail model were comparable to the baseline model.

There was no impact on the anterior neck of the HIII in the headrest model, which eliminated the potential for larynx injury. The headrest model saw a HIC<sub>15</sub> value of 102 due to the direct impact on the head, which was below the threshold of 700 to predict a skull fracture. The second largest HIC<sub>15</sub> value was 27 for the baseline model. The headrest model resulted in a N<sub>ij</sub> value of 1.34, which surpassed the

IARV of 1 to predict a high probability of neck injury. The high  $N_{ij}$  value was due to the increased flexion moment in the upper neck due to the focal impact between the face and headrest.

The bucket seat model resulted in a focal impact on the anterior neck with the handrail. The peak force of 275 N on the anterior neck surpassed the threshold for a larynx crushing injury. The neck and chest injury metrics were comparable between the bucket seat model and the baseline model. The bucket seat model resulted in peak femur loads that were comparable with the other models despite not having an impact between the knees and the forward seatback. The legs of the ATD in the bucket model straightened out during the impact which caused the feet to become firmly planted on the floor. The axial force through the feet of the ATD prevented the forward motion of the pelvis of the ATD and caused an equivalent level of femur axial load as the other models.

#### **5.4.3. Combining Findings from Parametric Analysis and Alternative Seat Geometries into Proposed Seat Design**

Several key findings were made from the parametric analysis and the alternative geometry models. It was found that lowering the handrail resulted in contact with the thorax instead of the neck. Moving the impact location to the thorax eliminated the potential for a larynx crush injury. Having any structure directly in the path of the head of the passenger resulted in an increase in head and neck injury potential. Having a raised lip on the seat pan limited the forward sliding motion of the passenger and prevented impact between the knees and forward seatback. Reducing the seat pitch minimized injury by coupling the passenger with the forward seatback and extending the duration under which the passenger was decelerated, which reduced the forces exerted on the femurs.

#### **5.4.4. Proposed Seat Design**

The proposed seat design included a lowered handrail connected to the forward seatback with arms that extended down to the base of the seat (Figure 110). This allowed for the handrail to swivel forward when the passenger impacted it, reducing the impact rigidity. The redesigned seat pan had a raised lip at the front of the seat to prevent the forward sliding motion of the passenger. A rubber pad was attached to the surface of the forward seatback to reduce the contact force with the knees. The seat pitch was reduced by 30 mm to minimize the distance that the passenger would slide forward before impacting the forward seatback.

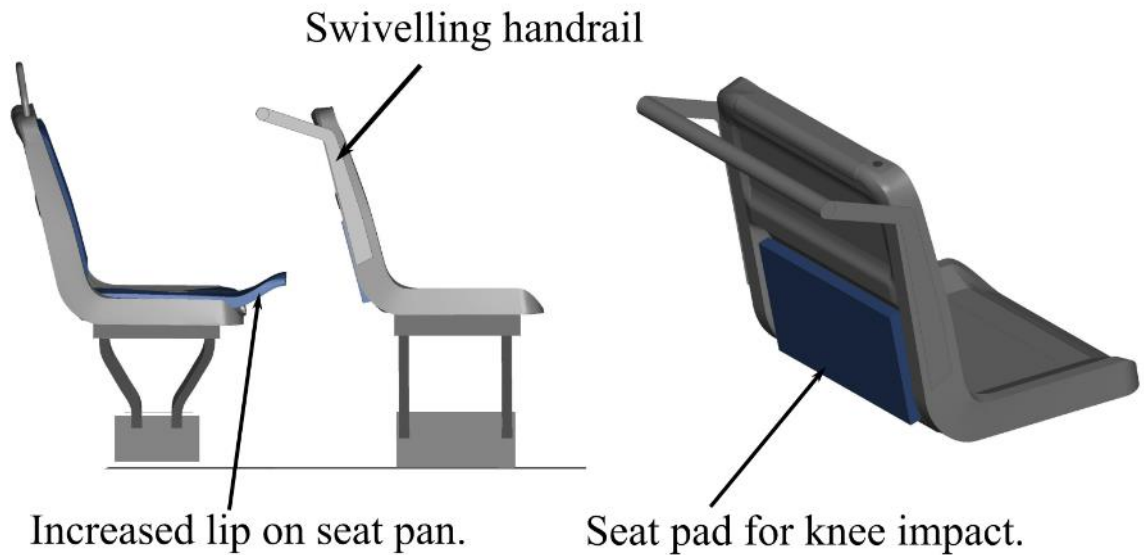


**Figure 110: Proposed seat design with lowered handrail, raised lip on seat pan, and rubber pad on forward seatback**

### **5.5. Proposed Seat Design Assessment and Comparison with Experimental Test Buck Model Using HBMs and HIIIs with 6.5g Pulse, Upright Posture, and Inboard Seating Location**

The 6.5g pulse, upright posture, and inboard seating location were used as the test configuration for the proposed seat design for the simulations with all occupant surrogates (HIII and HBM, 50<sup>th</sup> and 5<sup>th</sup> percentile). The response of each occupant surrogate seated in the experimental test buck model and the proposed seat design were compared using motion, injury metrics, and tissue level assessment (HBM only) to determine if there was a reduction in injury potential with the proposed seat design.

#### **5.5.1. Qualitative Assessment of Occupant Motion in Proposed Seat Design in Comparison with Experimental Test Buck Model**

##### **5.5.1.1. M50 HIII Motion in Proposed Seat Design**

The motion of the M50 HIII in the proposed seat design and experimental test buck model were compared (Figure 111).



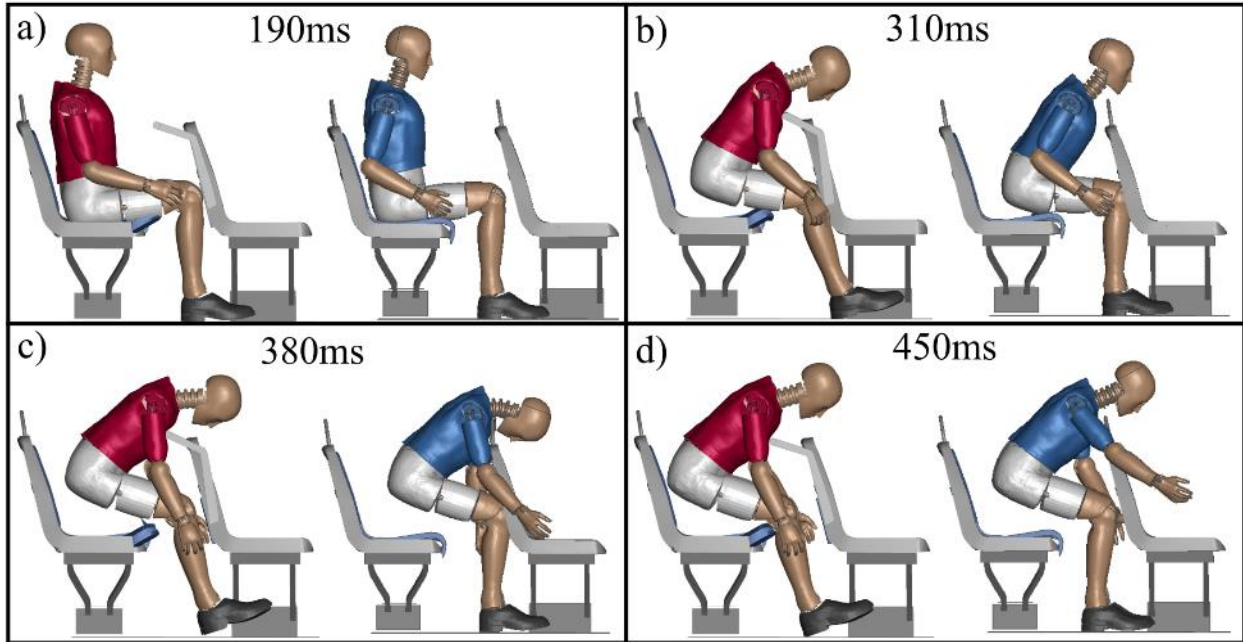


**Figure 111: HIII M50 motion in the proposed seat design (left) and experimental test buck model with test case #1 parameters (right)**

The focal impact with the handrail occurred at the mid thorax in the proposed seat design which eliminated the focal impact on the anterior neck. The proposed seat design resulted in 3 cm of horizontal separation between the HIII pelvis and the seatback at 450 ms compared with 13 cm for the experimental test buck model.

#### **5.5.1.2. F05 HIII Motion in Proposed Seat Design**

The motion of the F05 HIII was compared between the proposed seat design and experimental test buck model (Figure 112).

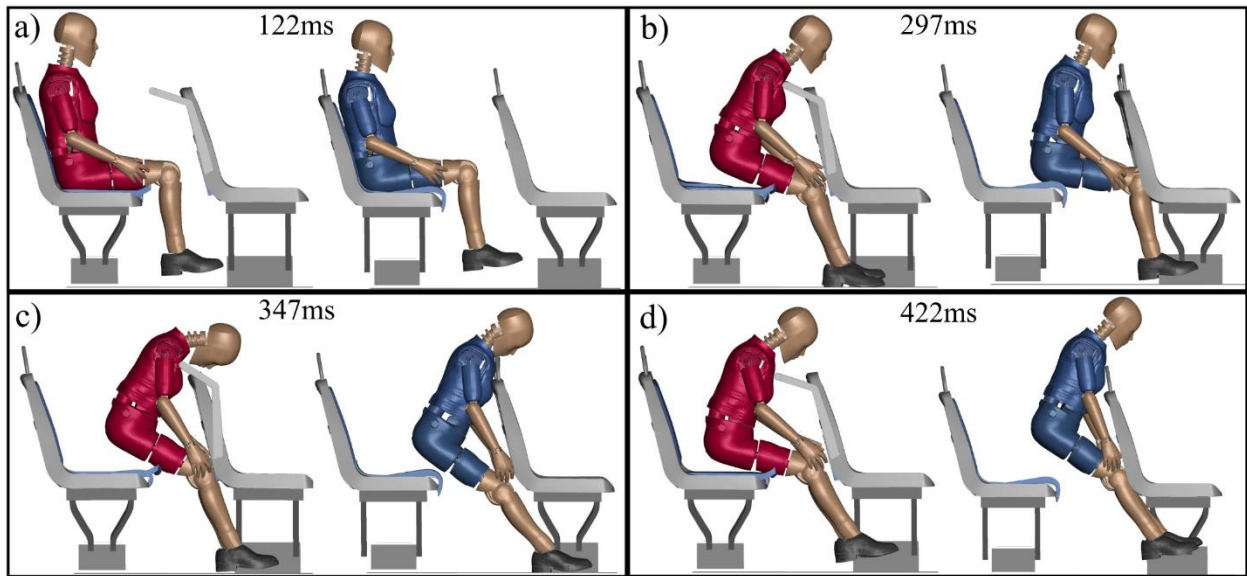


**Figure 112: HIII F05 Motion in proposed seat design (left) compared with motions in experimental test buck model for test case #1 (right)**

The F05 HIII in the proposed seat design impacted the lowered handrail on the thorax and eliminated all contact with the face. The F05 HIII ended the sequence (422 ms) still partially seated compared with the elevated pelvis of the F05 HIII in the experimental test buck.

### **5.5.1.3. GHBMCM50 Motion in Proposed Seat Design**

The motion of the M50 HBM was compared between the proposed seat design and experimental test buck model (Figure 113).

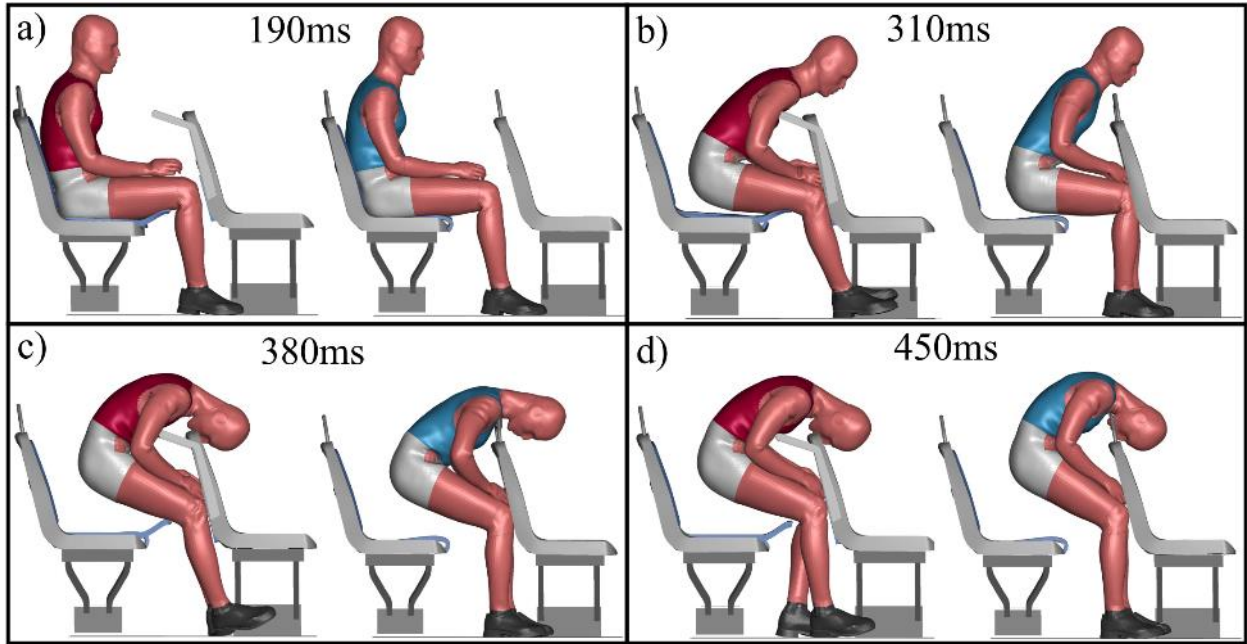


**Figure 113: Comparison of the motion of the M50 HBM in the proposed seat design and experimental test buck model**

The M50 HBM contacted the lowered handrail at the mid thorax. The handrail pivoted forward as it slowed the forward motion of the HBM. At 380 ms, the handrail lost contact with the thorax and pivoted back to its original position. The HBM remained positioned over the handrail at the end of the simulation (450 ms) with the spine in flexion. The face of the M50 HBM impacted the top of the forward seat in the proposed seat design (450 ms), similar to the results of the experimental test buck model.

#### **5.5.1.4. GHBMC F05 Motion in Proposed Seat Design**

The motion of the F05 HBM was compared between the proposed seat design and the experimental test buck model (Figure 114).

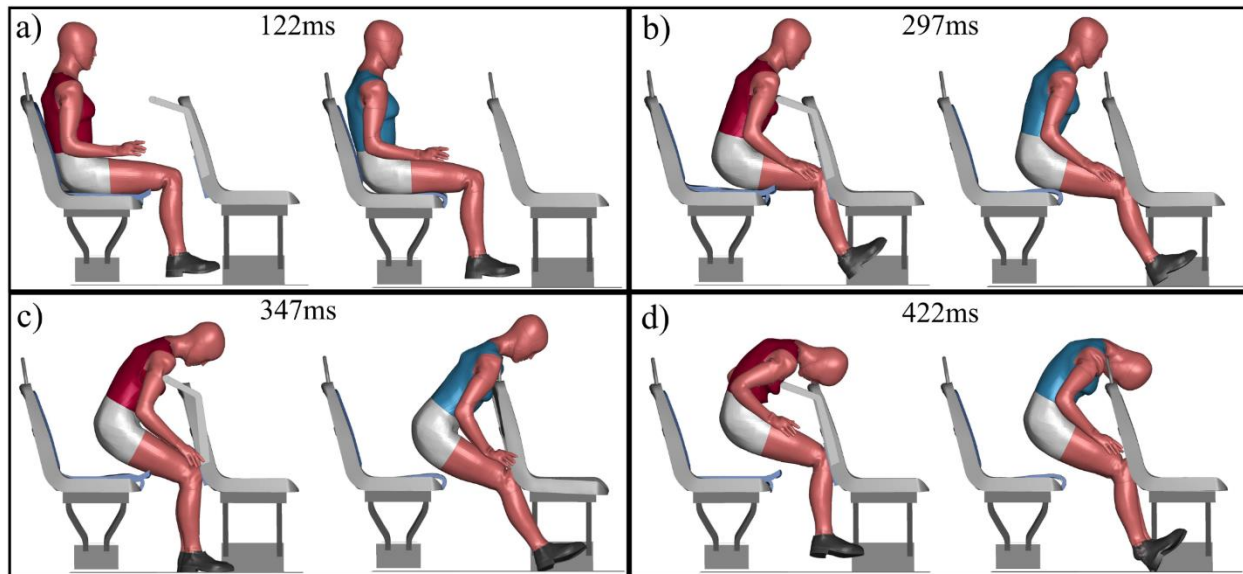


**Figure 114: Comparison of the F05 motion between the proposed seat design and experimental test buck model**

The upper thorax of the F05 HBM impacted the lowered handrail in the proposed seat design. Contact between the handrail and the thorax was maintained throughout the duration of the simulation. As the lowered handrail stopped the forward motion of the HBM, it caused the spine to flex, which resulted in the face of the F05 impacting the top of the forward seat frame (422 ms).

### **5.5.2. Injury Metrics Comparison Between Proposed Seat Design and Experimental Test Buck Model**

This section presents the comparison of the injury metrics of each occupant surrogate in the experimental test buck model and the proposed seat design with the test configuration of 6.5g pulse, upright posture, and inboard seating location.

#### **5.5.2.1. M50 and F05 HIII Injury Metrics in Proposed Seat Design**

The injury metrics were calculated for the M50 and F05 HIIIs in the proposed seat design and compared with the results from the experimental test buck model (Table 34).

In general, the injury metrics were reduced in the proposed seat design when compared with the experimental test buck model. The focal loading on the anterior neck for the M50 and the lower face for the F05 was eliminated which prevented the most injurious sources of loading.

The elimination of the focal impact on the lower face of the F05 in the proposed seat design resulted in the  $N_{ij}$  being lowered to 0.48 from 1.24. The value for  $N_{ij}$  in the proposed seat design was below the IARV of 1 for the F05 HIII which corresponded to an 8% risk of an AIS 3 neck injury compared with

34% in the experimental test buck model. The peak flexion moment in the neck of the F05 was lowered to 25 Nm in the proposed seat design which brought it below the IARV of 95 Nm and predicted a <5% risk of an AIS 4 neck injury.

The M50 chest deflection was 19 mm in the proposed seat design, compared with 1 mm in the experimental test buck model. The probability of an AIS 3 thoracic injury for the M50 due to the increased deflection was 6% for the M50, compared with 2% in the experimental test buck model. The 17 mm chest deflection with the F05 in the proposed seat design resulted in a 7% probability of an AIS 3 thoracic injury, compared with a 2% risk in the experimental test buck model.

The M50 showed a 50% decrease in femur loading with the proposed seat design whereas the F05 showed a 33% increase in femur loading. The increase in femur loading for the F05 raised the risk for an AIS 2 femur injury from 0% in the experimental test buck model to 1% in the proposed seat design.

**Table 34: M50 and F05 injury metric comparison between proposed seat design (PD) and experimental test buck model (Exp.)**

Injury Metrics	M50					F05				
	IARV M50	Exp.	Injury Risk (Exp.)	PD	Injury Risk (PD)	IARV F05	Exp.	Injury Risk (Exp.)	PD	Injury Risk (PD)
<b>Head</b>										
HIC <sub>15</sub>	700	35.5	0%	9.7	0%	700	25.8	0%	14.3	0%
BrIC	1	0.87	1%	0.64	0%	1	0.89	1%	0.82	1%
<b>Neck</b>										
Nij	1	0.38	8%	0.20	6%	1	1.21	34%	0.48	8%
Pk. Upper Neck Moment, Extension (Nm)	96	39	0%	12	0%	49	5	0%	22	0%
Pk. Upper Neck Moment, Flexion (Nm)	190	40	<5%	17	<5%	95	183	>5%	25	<5%
Pk. Upper Neck Axial Force, Tension (N)	4170	978	0%	515	0%	2620	538	0%	518	0%
Pk. Upper Neck Axial Force, Compression (N)	4000	234	0%	136	0%	2520	366	0%	80	0%
Pk. Upper Neck Shear Force (N)	3100	726	<5%	427	<5%	1950	1648	<5%	352	<5%
Pk. Lower Face Force	1779	0	0%	0	0%	1779	2404	31%	0	0%
Pk. Larynx Force (Cricoid, Thyroid)	248, 180	920	Fracture	150	No Fr.	248, 180	0	No Fr.	43	No Fr.
<b>Thorax</b>										
CTI	1	0.15	0%	0.10	0%	1	0.2	0%	0.3	0%
Pk. Chest Acceleration (g)	60	11.6	7%	8.6	7%	60	19.1	13%	9.9	7%
Pk. Chest Deflection (mm)	50	1.0	2%	19.1	6%	41	3.0	2%	16.6	7%
VC	1	0.0	0%	0.0	0%	1	0.0	0%	0.0	0%
Pk. Chest Deflection Rate (m/s)	8.2	0.4	0%	0.3	0%	8.2	0.2	0%	0.3	0%
<b>Lower Extremity</b>										
Pk. Left Femur Axial Force (N)	1	2722	0%	1336	0%	6800	1543	0%	1992	1%
Pk. Right Femur Axial Force (N)	1	2529	0%	1256	0%	6800	1563	0%	2139	1%

### 5.5.2.2. GHBMC M50 Injury Metrics in Proposed Seat Design

Injury metrics for the M50 HBM were calculated and tabulated for comparison between the proposed seat design and experimental test buck model (Table 35).

The values of  $N_{ij}$  for the M50 HBM saw an average reduction of 45% at the OC, C1, C4, and C7 cross-section levels, and an increase of 40% at the C2 cross section in the proposed seat design compared with the experimental test buck model. None of the injury metrics measured at the cross-section levels of the neck met the thresholds to predict a high probability of a neck injury with the proposed seat design.

The maximum larynx cartilage compression for the M50 saw a reduction from 75% in the experimental test buck model to 34% in the proposed seat design. The larynx compression in the proposed seat design was below the threshold for cartilage fracture (50% strain).

The thorax compression of the M50 peaked at 32.5 mm for the upper chest band compared with 0.56 mm in the experimental test buck model. A 32.5 mm peak thorax compression corresponded to a 10% probability of an AIS 3 thorax injury, which was an increase from the 0% probability with the experimental test buck model. The values for VC (max. 0.13 m/s) and peak thorax deflection rate (max. 0.72 m/s) in the proposed seat design did not increase the probability of a thoracic injury.

The femur axial force with the M50 HBM was 65% lower in the proposed seat design. The peak forces dropped from an average of 2430 N in the experimental test buck model to 740 N with the proposed seat design.

**Table 35: HBM M50 injury metric comparison between experimental test buck model (Exp.) and proposed seat design (PD)**

Injury Metrics	IARV M50	Experimental Test Buck Model					Proposed Seat Design				
Head											
HIC <sub>15</sub>	700	23.2	/	/	/	/	7	/	/	/	/
BrIC	1	0.81	/	/	/	/	0.77	/	/	/	/
Neck		OC	C1	C2	C4	C7	OC	C1	C2	C4	C7
Nij	1	0.19	0.26	0.30	0.42	0.55	0.11	0.13	0.42	0.24	0.30
Pk. Upper Neck Moment, Extension (Nm)	96	14	18	8	19	29	6	5	8	8	12
Pk. Upper Neck Moment, Flexion (Nm)	190	6	8	18	32	60	0	1	27	3	2
Pk. Upper Neck Axial Force, Tension (N)	4170	454	663	224	981	626	347	425	288	992	1046
Pk. Upper Neck Axial Force, Compression (N)	4000	130	239	897	234	348	14	33	975	169	214
Pk. Upper Neck Shear Force (N)	3100	129	345	383	356	639	76	221	222	195	243
Pk. Larynx Force, Cricoid, Thyroid	248, 180	75%	/	/	/	/	34%	/	/	/	/
Thorax		Upper	Middle	Lower			Upper	Middle	Lower		
Pk. Chest Deflection (mm)	50	0.56	1.04	5.03	/	/	32.51	25.99	0.00	/	/
VC	1	0.03	0.05	0.05	/	/	0.13	0.09	0.01	/	/
Pk. Chest Deflection Rate (m/s)	8.2	0.52	0.54	0.55	/	/	0.72	0.46	0.36	/	/
Lower Extremity											
Pk. Left Femur Axial Force (N)	1	2440	/	/	/	/	882	/	/	/	/
Pk. Right Femur Axial Force (N)	1	2420	/	/	/	/	779	/	/	/	/



### **5.5.2.3. GHBMC F05 Injury Metrics in Proposed Seat Design**

Injury metrics for the F05 HBM were calculated and tabulated for comparison between the proposed seat design and experimental test buck model (Table 36).

In general, the F05 HBM saw a reduction in injury potential with the proposed seat design. The peak larynx compression was reduced from 80% in the experimental test buck model to 14% in the proposed seat design, which brought it below the threshold for larynx cartilage fracture (50% compression). The proposed seat design resulted in a general decrease in forces and moments throughout the neck cross-sections.

The peak thorax compression increased from 25.7 mm in the experimental test buck model to 29.4 mm in the proposed seat design. The increase in thorax compression resulted in a <1% increase in the probability of a thoracic injury for the F05 in the proposed seat design. The femur axial loads of the F05 were comparable between the test buck models, with an average of 1439 N in the experimental test buck model and an average 1406 N in the proposed seat design.

**Table 36: HBM F05 injury metric comparison between experimental test buck model and proposed seat design**

Injury Metrics	IARV F05	Experimental Test Buck Model				Proposed Seat Design			
Head									
HIC <sub>15</sub>	700	58.6	/	/	/	14.0	/	/	/
BrIC	1	0.76	/	/	/	0.76	/	/	/
Neck		C1	C2	C4	C7	C1	C2	C4	C7
N <sub>ij</sub>	1	0.15	0.20	0.30	0.27	0.11	0.15	0.19	0.20
Pk. Upper Neck Moment, Extension (Nm)	49	13	13	34	23	3	4	16	17
Pk. Upper Neck Moment, Flexion (Nm)	95	1	1	23	6	8	10	9	9
Pk. Upper Neck Axial Force, Tension (N)	2620	92	96	160	111	91	100	106	123
Pk. Upper Neck Axial Force, Compression (N)	2520	605	625	1026	1110	336	437	549	593
Pk. Upper Neck Shear Force (N)	1950	305	157	180	439	97	81	72	118
Pk. Lower Face Force	1779		/	/	/		/	/	/
Pk. Larynx Force (Cricoid, Thyroid)	248, 180	80%	/	/	/	14%	/	/	/
Thorax		Upper	Middle	Lower		Upper	Middle	Lower	
Pk. Chest Deflection (mm)	41	4.5	25.7	17.8	/	11.2	29.4	18.4	/
VC	1	0.0	0.1	0.1	/	0.0	0.1	0.1	/
Pk. Chest Deflection Rate (m/s)	8.2	0.5	1.1	1.1	/	0.5	0.9	0.6	/
Lower Extremity									
Pk. Left Femur Axial Force (N)	6800	1352	/	/	/	1475	/	/	/
Pk. Right Femur Axial Force (N)	6800	1526	/	/	/	1338	/	/	/

### 5.5.3. Tissue Level Injury Assessment and Comparison with HBMs in the Experimental Test Buck Model and Proposed Seat Design

This section presents the results of the tissue level injury assessment with the M50 and F05 HBMs seated in the experimental test buck model (section 5.3) and the proposed seat design. The tissue level injury assessment was used as a biofidelic method of comparing the potential for injury between the proposed seat design and the experimental test buck model. Tissue level injuries were assessed for each body region of the HBM by extracting the applicable element metrics (strains, stresses, pressures, displacements), and comparing with the associated injury thresholds as listed in table 3.

#### 5.5.3.1. Diffuse Axonal Injury (Maximum Principal Strains in Brain Regions of Interest)

The 95<sup>th</sup> percentile maximum principal strain (logarithmic strain) was calculated for each region of interest in the brain (Table 37).

**Table 37: 95<sup>th</sup> percentile MPS per brain region for the experimental test buck model (Exp.) and proposed seat design (PD)**

Brain Region	M50			F05		
	95 <sup>th</sup> MPS		Ratio (PD/Exp.)	95 <sup>th</sup> MPS		Ratio (PD/Exp.)
	Exp.	PD		Exp.	PD	
Cerebellum	0.080	0.069	0.850	0.052	0.052	1.000
Cerebrum Gray	0.197	0.184	0.940	0.196	0.158	0.805
Corpus Callosum	0.174	0.170	0.980	0.195	0.095	0.490
Thalamus	0.158	0.135	0.850	0.176	0.133	0.750
Brainstem Midbrain	0.243	0.227	0.940	0.169	0.134	0.790
Brainstem	0.124	0.099	0.800	0.113	0.096	0.860
Basal Ganglia	0.209	0.190	0.910	0.143	0.116	0.810
Cerebrum White	0.189	0.173	0.900	0.150	0.121	0.805

The 95<sup>th</sup> MPS throughout the brain regions of the HBMs followed a similar trend, as observed in the Corpus Callosum (Figure 115). The first spike in MPS occurred when the HBM thorax or neck impacted the forward handrail. This caused the head to abruptly stop forward motion and resulted in large inertial forces, and subsequently increased strains in the brain tissue. The second spike in MPS coincided with the face impacting the top of the forward seatback. The F05 seated in the new design exhibited a much lower second peak in MPS due to the impact between the face and seat frame (0.08 vs. 0.195 occurring from 400-450 ms).

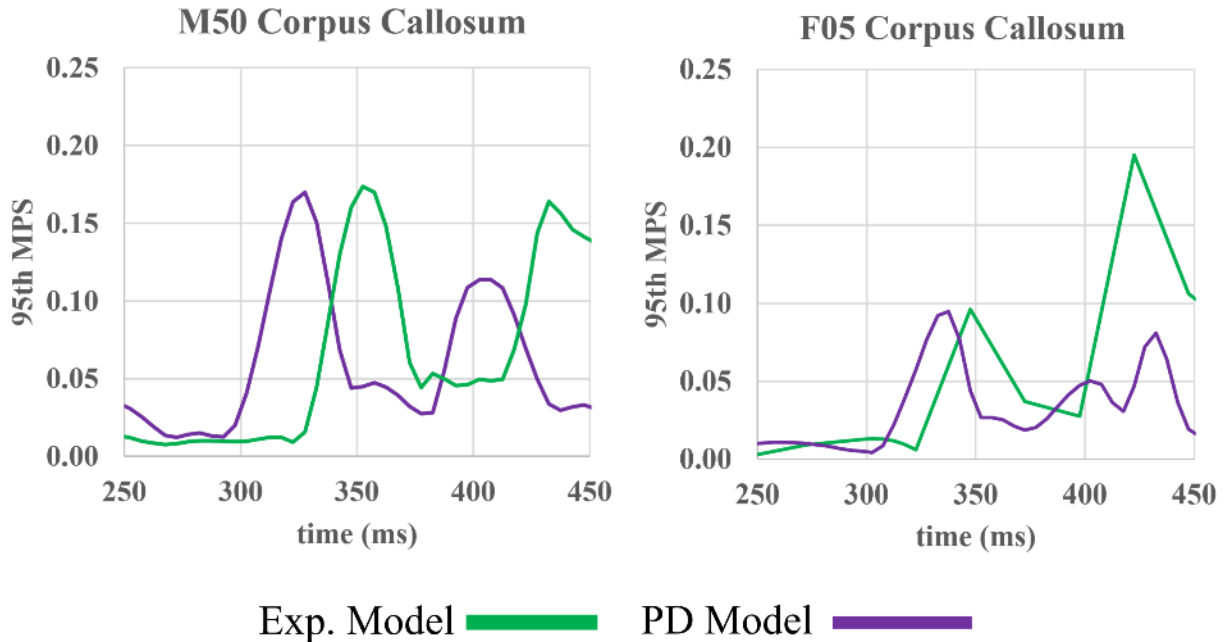


**Figure 115: Comparison of the MPS trend through the duration of the simulation in the Corpus Callosum of the M50 and F05 model in the experimental test buck model (Exp.) and the proposed seat design (PD)**

The proposed seat design resulted in an average reduction in 95<sup>th</sup> MPS of 10% for the M50 and 21% for the F05. Neither the M50 or F05 reported strains in any brain region that met the threshold of 0.48 for a diffuse axonal injury in either test buck model. The largest strains for the M50 occurred in the brainstem (midbrain) for both the proposed seat design and experimental test buck model. The largest strains in the F05 occurred in the cerebrum (gray) for both the proposed seat design and experimental test buck model. The results for the MPS throughout the brain regions of interest demonstrated a low probability of diffuse axonal injury.

#### **5.5.3.2. Cerebral Contusion (Peak Pressures in Brain Regions of Interest)**

None of the peak average pressures in the brain regions of interest surpassed the coup/countrecoup pressure thresholds (237 kPa/-104 kPa) for a cerebral contusion (Table 38).

The responses of the HBMs in the proposed seat design and experimental test buck model were comparable. The proposed seat design did not result in any substantial reduction in average brain pressures in both the M50 and F05 models.

**Table 38: Peak average coup and countercoup pressures by brain region of interest**

Brain Region	M50				F05			
	Exp.	PD	Exp.	PD	Exp.	PD	Exp.	PD
	Peak coup (kPa)		Peak countercoup (kPa)		Peak coup (kPa)		Peak countercoup (kPa)	
Cerebellum	5.2	9.4	-16.7	-21.4	5.0	2.5	-3.2	-3.8
Cerebrum	5.6	7.6	-8.8	-10.3	10.3	7.5	-0.7	-0.9
Corpus Callosum	6.0	7.2	-7.4	-7.0	9.5	7.6	-0.6	-0.8
Thalamus	5.4	7.7	-8.3	-10.6	7.1	7.1	-0.4	-0.4
Brainstem Midbrain	5.0	8.1	-9.4	-14.2	7.8	6.8	-0.1	-0.2
Brainstem	5.1	9.2	-17.3	-20.3	7.4	4.1	-5.1	-3.9
Basal Ganglia	5.3	7.6	-7.1	-9.7	10.0	9.6	-0.5	-0.6
Cerebrum White	6.1	7.2	-7.9	-7.4	10.8	7.0	-0.7	-0.9

**5.5.3.3. Subdural Hematoma (Bridging Veins Axial Strains)**

The peak bridging vein strains were comparable for the M50 model in the proposed seat design and experimental test buck model (Figure 116). The M50 had peak strains in the experimental test buck model of 0.095, which occurred at 345 ms, and peak strains of 0.08 which occurred at 320 ms in the proposed seat design. The F05 showed a higher peak strain of 0.08 in the proposed seat design compared with a peak of 0.02 in the experimental test buck model. Neither HBM showed bridging vein strains that surpassed the threshold for a subdural hematoma (0.25) seated in either test buck model.

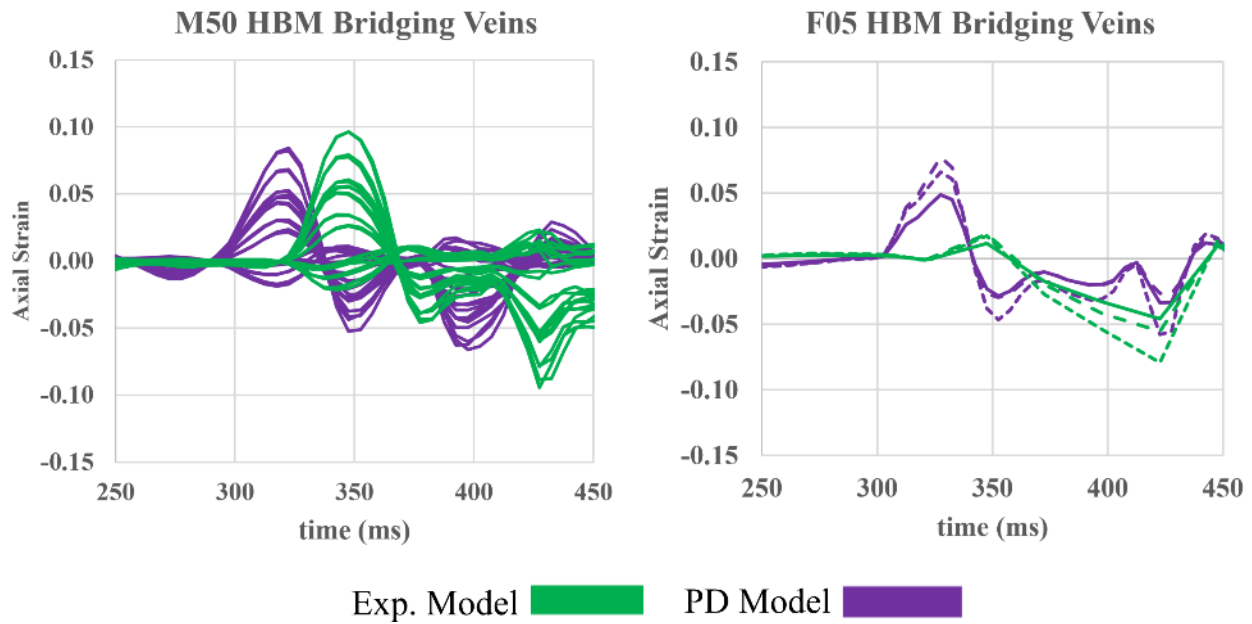


**Figure 116: Bridging veins axial strains comparison between the experimental test buck model (Exp.) and proposed seat design (PD) with the M50 and F05 HBMs**

#### 5.5.3.4. Neck Ligament Distractions (Beam Element Change in Length)

The peak change in length of all the ligaments in the cervical spine were compared with the force displacement curves to determine the whether they peaked in the toe region, linear region, traumatic region, or failure region (Figure 117, Figure 118).

The results for the M50 showed that the ligaments located on the posterior side of the cervical spine ISL, PLL, and CL were more likely to have peak strains in the traumatic region. The proposed seat design demonstrated an increase the degree of ligament distraction over the experimental test buck model. There was no ligament failure predicted with the M50 HBM.

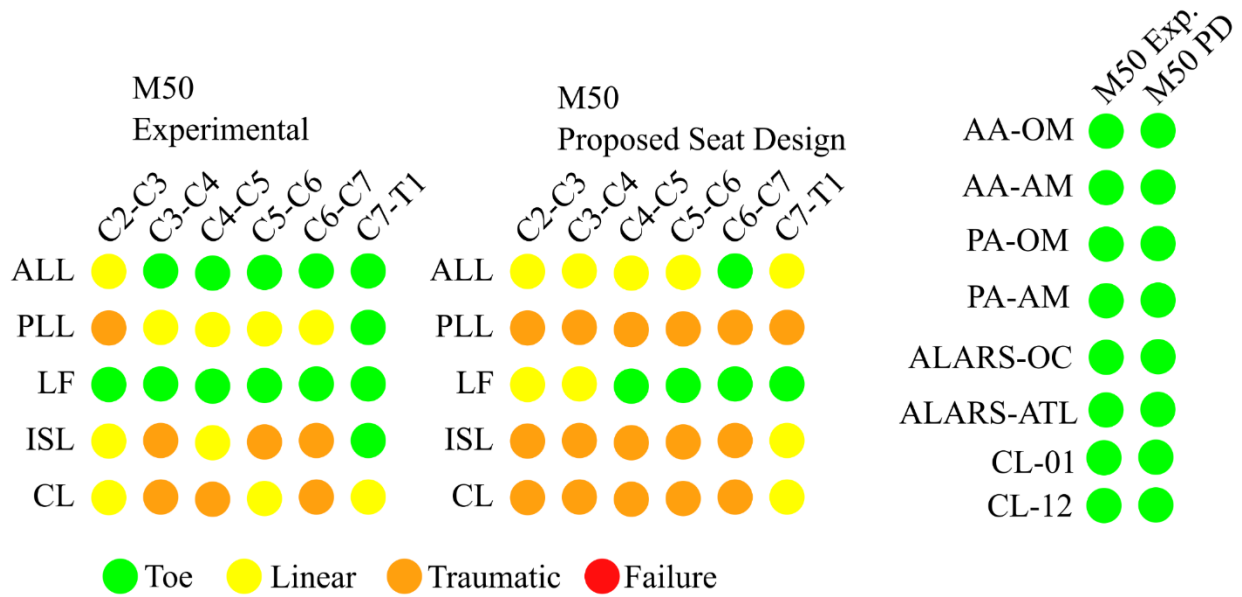


**Figure 117: M50 cervical spine ligament distraction comparison between experimental test buck model (Exp.) and proposed seat design (PD)**

The F05 HBM showed minimal ligament distractions in the cervical spine, with most ligaments having peak distraction in the toe region, and none entering the traumatic region. The F05 seated in the proposed seat design also demonstrated increased ligament distraction in the ISL, PLL, and CL when compared with the experimental test buck model.

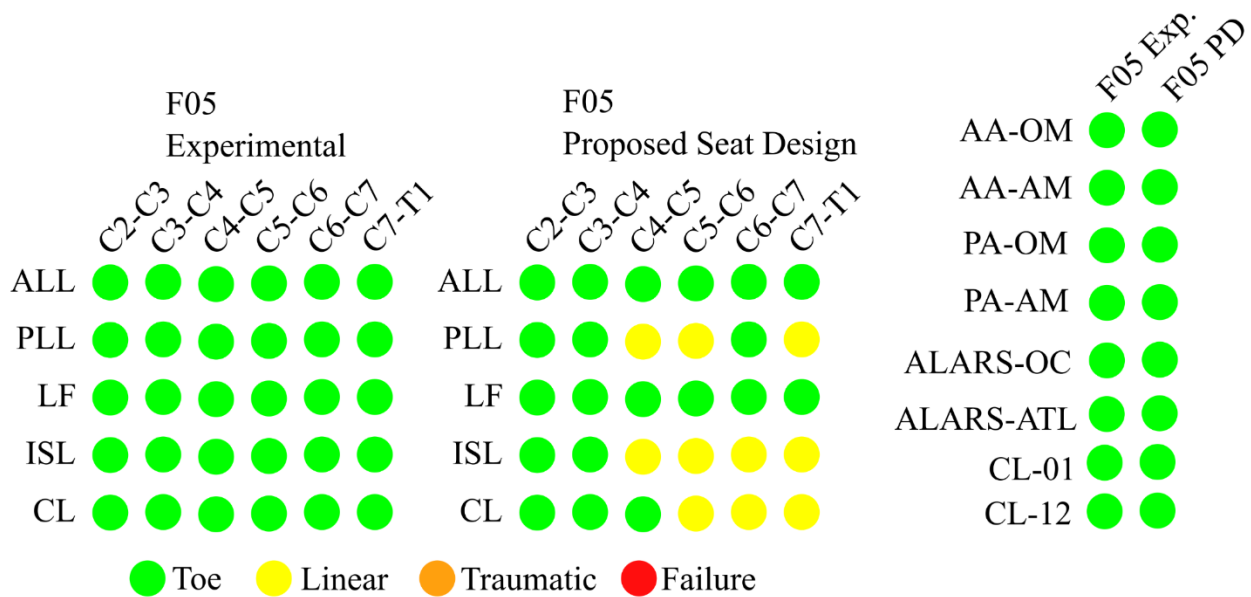


**Figure 118: F05 cervical spine ligament distraction comparison between experimental test buck model (Exp.) and proposed seat design (PD)**

### 5.5.3.5. Intervertebral Disc Avulsion (Tensile Stress in Cervical Spine Endplates)

Results for the intervertebral disc avulsion showed that there was no failure in the M50 and the F05 seated in either the experimental test buck model or the proposed seat design.

### 5.5.3.6. Cervical Spine Fracture (Effective Plastic Strain in the Cervical Spine)

None of the elements in the cervical spine of the M50 seated in either test buck model achieved the EPS threshold for bone failure (0.0178 Cortical / 0.095 Trabecular). The F05 model also did not exhibit any fracture at any level of the cervical spine in both the proposed seat design and the experimental test buck model.

### 5.5.3.7. Ribs & Sternum Fracture (Effective Plastic Strain)

There was no predicted fracture in any of the ribs or sternum of the M50 in either test buck model. The F05 predicted fracture at the sternum both in the experimental test buck model and the proposed seat design (Table 39). There was also fracture predicted at the 8<sup>th</sup> and 10<sup>th</sup> rib on the left side for the F05 in the experimental test buck model.

**Table 39: F05 Rib and sternum EPS and potential for fracture in the experimental test buck model (Exp.) and the proposed seat design (PD)**

Part	F05	
	Exp.	PD
Rib 8 Left (Cortical)	2	0
Rib 10 Left (Cortical)	5	0
Sternum (Cortical)	0	0
Sternum (Trabecular)	17	32

### 5.5.3.8. Pelvis Fracture (Effective Plastic Strain)

Hard tissue failure was predicted in the sacrum and coxal bones of the M50 when seated in the experimental test buck and the proposed seat design (Table 40).

There was a 72% reduction in the amount of fracture for the sacrum and an 82% reduction for the coxal with the proposed seat design and the M50. The F05 resulted in 5 total elements in the cortical sacrum bone fracturing.



**Table 40: Effective plastic strain in the pelvis region for M50 HBM in experimental test buck (Exp.) and proposed seat design (PD)**

Part Name	M50		F05	
	Exp.	PD	Exp.	PD
Sacrum (Cortical)	140	38	5	0
Sacrum (Trabecular)	0	0	0	0
Coxal (Cortical)	191	33	0	0
Coxal (Trabecular)	0	0	0	0

### 5.5.3.9. Leg Fracture (Effective Plastic Strain)

The GHBMC leg model was only capable of predicting cortical bone fracture. The M50 predicted fracture in both the left and right femur neck in the experimental design, 4 elements both sides. A single element failed each side in the proposed seat design for the M50 (Table 41). The F05 showed fracture in the tibia ends, fibula ends, femur neck, and femur head in both the experimental and proposed seat design. The amount of fracture was comparable in the experimental test buck and the proposed seat design with the F05.

**Table 41: Fracture in the legs of the M50 and F05 HBMs seated in the experimental test buck model (Exp.) and proposed seat design (PD)**

Part	M50				F05			
	Right Leg EPS		Left Leg EPS		Right Leg		Left Leg	
	Exp.	PD	Exp.	PD	Exp.	PD	Exp.	PD
Kneecap	0	0	0	0	0	0	0	0
Tibia Shaft	0	0	0	0	0	0	0	0
Tibia Top/Bottom Ends	0	0	0	0	53	30	49	30
Fibula Shaft (Cortical)	0	0	0	0	0	0	0	0
Fibula Top/Bottom Ends	0	0	0	0	5	5	3	3
Femur Shaft	0	0	0	0	0	0	0	0
Femur Condyle	0	0	0	0	0	0	0	0
Femur Neck	4	1	4	1	43	42	35	39
Femur Head	0	0	0	0	3	9	5	8

## 6. Discussion

In 2013, a transit bus collided with a passenger train at a rail crossing in Ottawa, resulting in multiple bus passenger fatalities. The ensuing investigation by the Transportation Safety Board of Canada (TSB) found that a lack of transit bus crashworthiness standards contributed to the number of fatalities [4]. The TSB recommended that Transport Canada (TC) develop crashworthiness standards applicable to transit buses. The first step in developing transit bus crashworthiness standards was investigating the injury mechanisms of passengers during an impact. TC initiated a research program that included full-scale transit bus impacts and deceleration sled experiments [10]. The experiments showed how ATDs impacted surrounding structures inside the bus and the resulting injury mechanisms.

The current study was a collaboration with TC, using numerical modelling to expand on the findings from the deceleration sled experiments. Numerical modelling allows for the use of biofidelic Human Body Models (HBM), which incorporate active musculature and tissue level injury prediction that is unavailable with the use of ATDs. The objective of this study was to assess the response of a HBM in a transit bus frontal impact to evaluate the effect of occupant surrogate biofidelity, occupant stature, and seat design on passenger kinematics and injury potential.

The first objective of this study was to develop and validate a model of the experimental test buck used by TC. Validating the test buck model involved comparing the kinematics and forces of the HIII model with the physical HIII in the eight experimental test configurations. Numerical models require validation to ensure that the model response accurately represents the physical experiment.

The second objective of this study was to assess passenger injury with the four occupant surrogates (50<sup>th</sup> and 5<sup>th</sup>, HBM and HIII) seated in the test buck with the 6.5g pulse, upright posture, and inboard seating location. Injury metrics ( $HIC_{15}$ ,  $N_{ij}$ , CTI, LE, etc.) were used as criteria for assessing passenger injury for all occupant surrogates, followed by the tissue-level injury assessment for the HBMs only.

As part of the second objective, the response of the biofidelic HBMs was compared with the HIII ATDs to assess any differences in response. The HIII ATD has been shown to lack biofidelity in crashworthiness testing due to the overly stiff neck and thorax [49]. The visual motion of the HBMs and HIIs in the test buck model were compared using highspeed video, which was followed by comparing kinematic traces. The geometry and material characterization of the HBM tissues resulted in different kinematics and injury predictions compared with the ATD.

The effect of passenger stature on injury potential was also assessed as part of the second objective. Smaller stature passengers are at an increased risk of injury and fatality in automobile crashes [40]. The

mid-sized and small stature occupant surrogates used in this study provided a means of assessing the effect of passenger size on injury potential in a transit bus impact.

The third objective of this study was to investigate passive safety design features that could be implemented in a transit bus without requiring the use of seat belts. Passive safety reduces the potential for passenger injury by modifying the spacing, orientation, and design of seats to minimize impact injuries. The HIII M50 ATD was used as the occupant surrogate for a parametric analysis with the experimental test buck that modified seat pitch, seat height, and ATD seating location, and measured the effect on injury metrics ( $HIC_{15}$ ,  $N_{ij}$ , CTI, and LE). In addition, three alternative seat geometry models were assessed with the M50 HIII to determine the effect of a lowered handrail, raised seat pan lip, and a raised headrest on injury metrics ( $HIC_{15}$ ,  $N_{ij}$ , CTI, and LE).

The fourth objective of this study was to create and assess a proposed seat design based on the findings from the sensitivity analysis and the alternative seat geometries. The proposed seat design was assessed for passenger injury using all four occupant surrogates and following the same procedure used with the experimental test buck model (objective #2). The results with the proposed seat design were compared with those from the experimental test buck to determine if there was a reduction in injury potential. The responses of the occupant surrogates seated in the proposed seat design was used to assess the effectiveness of passive safety design changes that could be implemented in a transit bus.

## **6.1. HIII Test Buck Model Validation**

The test buck model replicated the geometry of the physical test buck seats, handrails, and seat cushions. The HIII 50<sup>th</sup> and 5<sup>th</sup> percentile ATD models (HIII) were positioned in the test buck model to match the initial positioning of the ATDs in the experiments. The eight test configurations from the TC experiments were replicated in the model by configuring the ATD posture, ATD seating location, and acceleration pulse magnitude.

The validation process used in this study followed industry standard procedures involving qualitative and quantitative assessment [34]. The qualitative assessment compared the highspeed video from the experiment with the HIII model motion in the simulation. The quantitative assessment used cross-correlation to objectively compare the kinematic, force, and displacement traces between the experiment and the model.

### **6.1.1. M50 HIII Test Buck Model Validation**

Overall, the response of the M50 HIII test buck was very good, which provided confidence that the model was an accurate representation of the experiments. An accurate model was important for having

confidence in the injury assessment, which was done using the same kinematics evaluated during the validation.

The highest average rated metric for the M50 HIII was the femur force (0.871), which showed good agreement between the model and experiment for the impact timing, ramp up in force, and peak force. Cao et al. detailed the improvement of the HIII knee model by implementing an improved knee material model, which could have contributed to the excellent response of the femur load of the 50<sup>th</sup> percentile HIII model in the current study [156].

The head acceleration, upper neck moment, and upper neck shear force were the lowest average rated metrics with the M50 HIII. The low CORA ratings resulted from a different impact location of the HIII with the handrail between the model and experiment for test configurations #2b, #7, and #8. For example, test case #8 resulted in the HIII M50 model impacting the handrail on the anterior neck, while the physical HIII impacted the handrail on the chin (Figure 119a). The torso of the physical HIII tended to tilt forward more as the knees impacted the forward seatback, which placed the chin closer to the handrail and resulted in a higher probability of impact on the chin. The different impact locations with the handrail resulted in significant differences for the head kinematics and neck forces between the model and experiment, causing the poor CORA ratings.

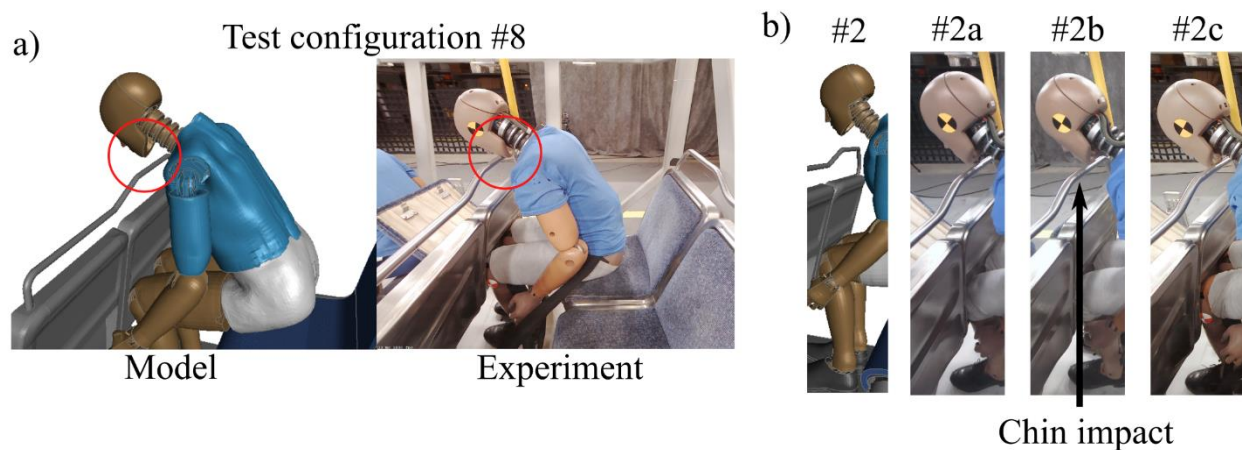


**Figure 119: a) Test configuration #8, the HIII model chin misses the handrail while the physical HIII impacts it due to a more forward tilt of the torso; b) #2a, #2b, and #2c configurations show enough variation in head motion to cause the chin to impact the handrail in one case, and not in the other two cases**

The three repeated experimental tests with configuration #2 demonstrated a difference in head trajectory, and chin impact location for the physical HIII, despite near identical initial positioning. Test case #2b had chin contact with the handrail while #2a and #2c did not (Figure 119b). Like test case #8, the physical HIII showed a tendency to tilt forward at the pelvis more than the HIII model, making it more likely for

the physical HIII to impact the handrail with its chin. For test case #2b the physical HIII tilted forward enough to result in chin impact, likely due to the variation in initial positioning of the physical ATDs. The CORA assessment of test case #2b had a poor CORA rating for the head and neck metrics as a result.

In general, the response of the M50 HIII model showed good agreement with the experiments. A slight change in the head trajectory and the resulting chin impact discrepancy between the model and experiment accounted for the lowest CORA ratings.

### 6.1.2. F05 HIII Test Buck Model Validation

The highest-rated metrics with the F05 HIII were the neck shear force and bending moment, which was a direct measurement of the resulting kinematics from the face of the HIII impacting the handrail. The good agreement between the model and the experiment provided confidence in the injury assessment at the head and neck using the same kinematics.

The lowest CORA ratings for the F05 HIII were the chest displacement, pelvis acceleration, and femur loads. Two issues caused the low CORA rating for the chest deflection response. First, in test configurations #1, #2, #3, and #8, the face of the F05 HIII in the model and experiment impacted the handrail, preventing chest compression. The lack of direct impact on the HIII thorax resulted in the thorax displacement sensor only measuring inertial effects, which were not comparable between the model and experiment (Figure 120a).

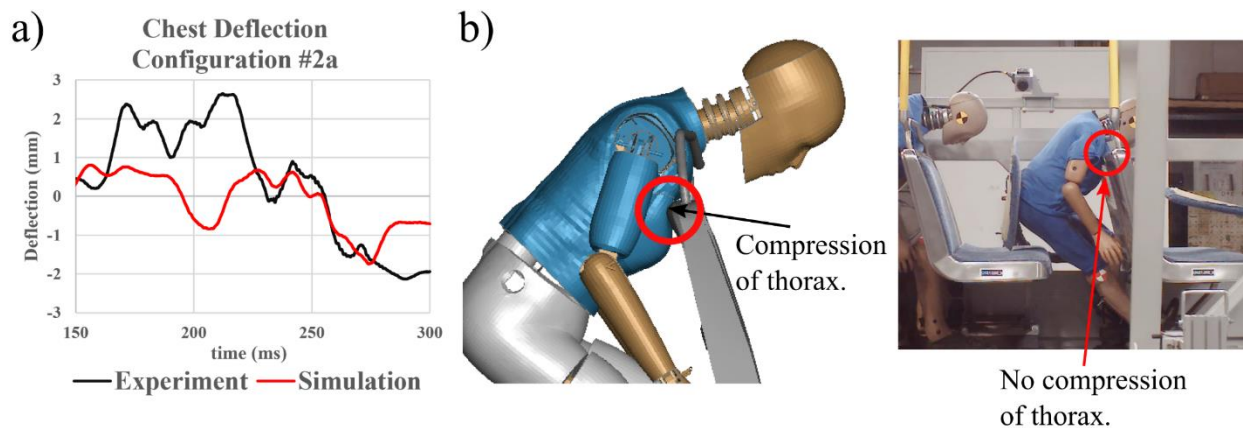


**Figure 120: a) Fluctuations in chest displacement caused by inertia; b) Chest deflection of the F05 HIII in the model, F05 HIII does not exhibit any chest deflection in the experiment**

Conversely, test configurations #4, #5, #6, and #7 resulted in significantly more chest compression in the model than in the experiment, leading to low CORA ratings. There was an average of 8.5% total thorax compression of the F05 model in test configurations #4, #5, #6, and #7, compared with an average of 1.5% total thorax compression in the experiments (Figure 120b). The motion of the HIII model resulted in

contact with the top edge of the forward seat frame, leading to thorax compression. A difference in ATD positioning between the physical HIII and the model likely caused the slight change in motion that resulted in the chest impacting the frame in the model and not in the experiment.

The F05 HIII model also demonstrated smaller peak femur forces and pelvis accelerations than the physical ATD. Since the M50 HIII model demonstrated excellent correlation of the femur loads between the model and physical test; the poor correlation with the F05 HIII model is unlikely to be due to the seat model. A potential explanation for the difference in lower extremity response between the model and physical ATD could be how the knees extended post impact with the forward seatback (Figure 121). The separation between the F05 feet and the floor of the test buck allowed the legs to extend after impacting the forward seat in both the experiment and model. A slightly different impact location with the knees could result in more knee extension and less femur axial loading for the model. The rapid knee extension could explain the lower femur forces, as the kinetic energy from the impact was directed at flexing the knee joint instead of femur axial compression. The different knee impact kinematics of the model could be a result of slight differences in initial positioning of the HIII model compared with the physical ATD.

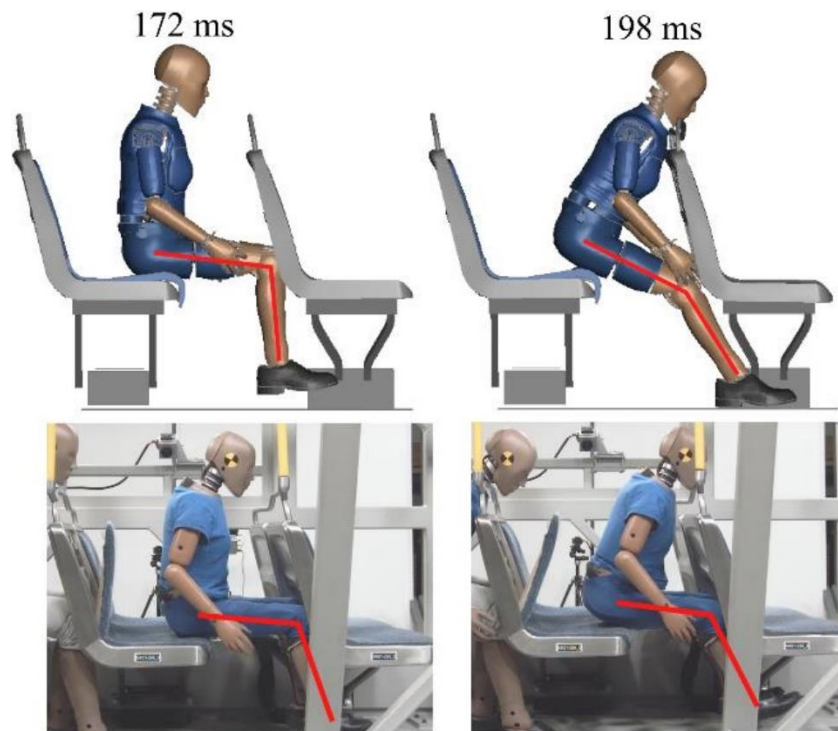


**Figure 121: Knee extension of the F05 HIII upon impacting the forward seatback, the legs of the HIII model appear to extend faster, due to the impact location with the forward seatback favoring extension of the knee instead of higher femur loads as observed with the physical HIII**

Overall, the F05 HIII coupled test buck model agreed well with the experiment. The impact on the lower face with the handrail was very similar between the model and the experiment regarding ATD motion and kinematics. The lowest rated metrics with the F05 were at the lower extremities which did not pertain to the primary sources of injury and were of less consequence in the overall objective of the study.

## **6.2. Potential for Injury in the Experimental Test Buck Model Using Injury Metrics and Tissue Level Assessment**

This study assessed injury with the HBMs and HIII ATDs using a combination of injury metrics (HIC<sub>15</sub>, Nij, CTI, LE, etc.) and HBM tissue level injury assessment. The injury metrics utilized the kinematics measured with the HIII instrumentation at the head, neck, chest, and femur. The injury metrics were also calculated with the HBMs using equivalent outputs, directly comparing the response of the two occupant surrogates. The HBMs provided a direct measurement of the larynx tissue deformation, which was compared with experimental thresholds to assess the potential for larynx cartilage fracture. In contrast, the HIIs measured the contact force on the anterior neck and compared it with experimental force thresholds for larynx cartilage fracture. As an added level of injury assessment, the HBMs were used to predict localized tissue injury at the thorax and pelvis, which was otherwise unavailable with the ATDs.

The impact with the forward handrail on the anterior surface of the neck showed a potential crushing injury to the thyroid and cricoid cartilages, which could be an AIS-5 injury resulting in obstruction of the airways. The impact forces along the anterior neck of the M50 HIII surpassed the experimental thresholds developed by Melvin et al. for larynx cartilage fracture of cadavers [72]. The anterior-posterior compression of the larynx cartilage of the M50 and F05 HBMs surpassed the 50% compression threshold for fracture, also reported by Melvin et al. (Figure 122a). The test buck handrail is thin and rigid to provide passengers a sturdy handhold while riding the bus. Consequently, the rigidity of the handrail results in little to no impact compliance, causing a focal injury potential. This study showed that the placement of rigid handrails that have a small surface area pose a high risk of localized tissue injury for an unrestrained transit bus passenger.

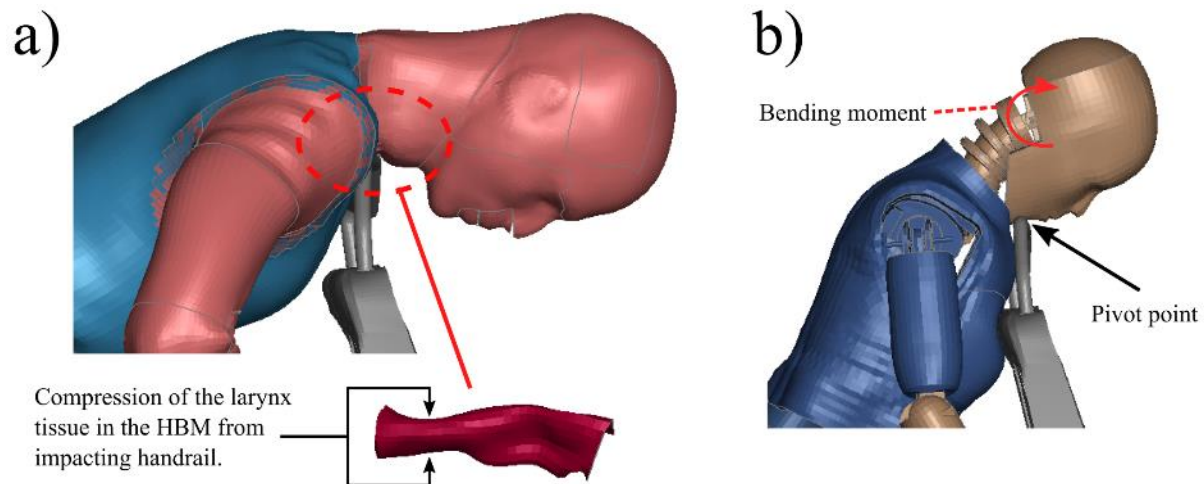


**Figure 122: a) Larynx tissue compression for the HBM; b) Pivot point between chin and handrail of the F05 results in a significant bending moment in the upper neck**

The impact between the chin of the F05 HIII and the handrail created a pivot point that led to a potential neck and mandible injury (Figure 122b). The forward momentum of the unrestrained passenger caused the head to rotate about the pivot point, resulting in large shear and bending forces in the upper neck. Olivares et al. also demonstrated a high potential for neck injury for the F05 HIII from impacting the forward handrail on the face [118]. The handrail impact on lower face of the F05 HIII demonstrated that regardless of the impact location of the handrail, it is likely to cause injury.

In the case of the focal impact on the anterior neck, none of the industry standard injury metrics ( $HIC_{15}$ , CTI,  $N_{ij}$ , LE, etc.) captured the potential for localized injury. Even the shear force in the upper neck load cell of the HIII and at every cross section of HBM cervical spine did not measure shear forces, axial forces, or bending moments that were in the range of predicting injury. This result highlighted the limitations of the standard HIII instrumentation and the ability for injury risk prediction resulting from focal loading on the anterior neck. The ability for direct measurement of contact forces in the numerical models provided insight not available with the physical ATDs. Additionally, numerical models allowed for the implementation of biofidelic tissue models designed to capture localized tissue injury, including direct measurement of the larynx tissue deformation to assess injury. Such a tissue level assessment in an experimental setting would only be possible with PMHS, which are difficult to obtain and labour intensive to use.

The tissue level assessment with the HBMs showed that the M50 predicted fracture predominantly in the pelvic region. PMHS testing has shown that pelvic fracture is possible via axial loading of the femur with a range of 4-7 kN [157]. The axial loading of the M50 HBM femurs in the current study was 2.5 kN, considerably lower than the experimental threshold. Without experimental data using PMHS in the test



buck, the response of the HBMs is only predictive; thus, the potential for pelvic fracture remains in question.

The F05 HBM predicted a fracture at the manubrium joint of the sternum due to the focal loading from the top of the forward seat frame. Fracture at the manubrium joint can occur in automotive crashes, referred to as "steering wheel injury" [158], [159]. PMHS can exhibit sternum fractures from belt loading in frontal impacts as well, with peak chest deflections of 30-50 mm causing fracture [160]. The peak chest deflection with the F05 HBM in the experimental test buck model was 25 mm, which places it slightly below the experimental range. Another contributing factor is the rigidity of the metal seat frame, which could cause high bending stresses in the sternum when impacting it directly. The results with the F05 demonstrated that not only is the handrail a potential source of injury, but also the seat frame itself, due to its rigid structure and height relative to small stature passengers. An added issue is that older adults have a reduced capacity to sustain focal loading on the thorax [161], which could place older transit passengers at risk of a more severe thorax injury under the loading conditions observed in this study.

In summary, the most severe injury in the experimental test buck model was the focal impact on the anterior neck from the handrail. A crushing injury of the larynx cartilages would be an AIS-5 injury, the most severe type of injury on the AIS scale and the only injury of that severity occurring with the experimental test buck model.

### **6.3. Effect of Occupant Surrogate Biofidelity on Kinematics and Injury Potential**

This section will identify differences in the response of the HBM and HIII, and will primarily focus on the M50, as the findings were generally the same with the F05. Section 6.5.2 will address the observations specific to the F05, related primarily to the difference in impact location with the forward handrail.

The further excursion and sagittal plane rotation of the HBM head caused the face to impact the top of the forward seat frame, which did not occur with the HIII (Figure 123). Previous studies have demonstrated that PMHS have increased head excursion in frontal impact experiments compared with the HIII due to the increased compliance of the biological tissues of the thorax [162]. Similar to a PMHS, the material characterization of the HBM neck is more compliant than the HIII, which contributes to the increased head excursion in the model [163].

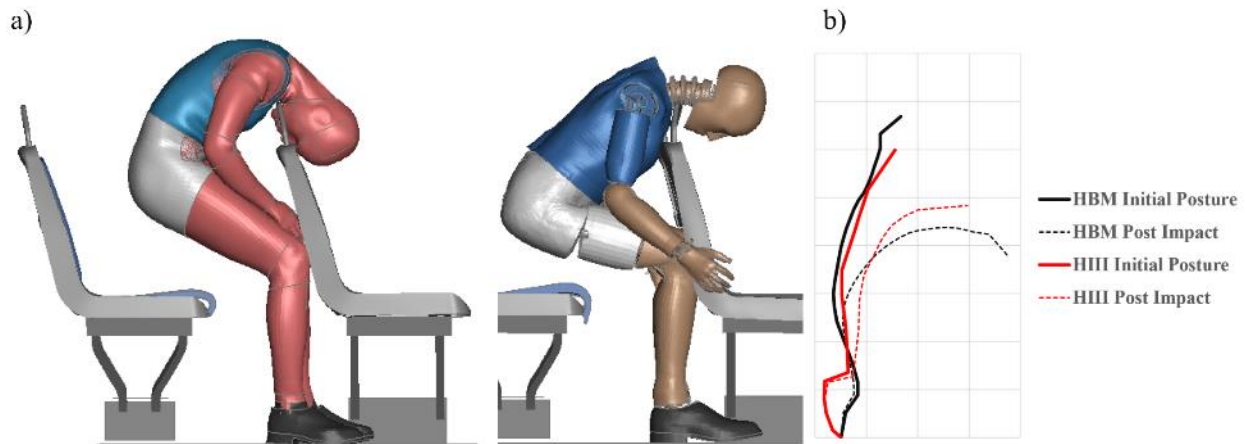


**Figure 123: a) The face of the HBM impacts the top of the forward seat frame due to the increased head excursion, which does not occur with the HIII; b) Comparison of the flexion of the spine-head complex of the HBM with the HIII showing the further forward and vertical excursion of the head**

The lower neck structure of the HIII also contributed to the limited forward flexion motion of the head (Figure 124) [49]. The HIII lower neck bracket attached rigidly to the thorax, preventing any further flexion that would increase the sagittal plane rotation of the HIII head. The cervical and thoracic spine of the HBM behaved as a continuous flexible member, allowing for the additional sagittal plane rotation of the head from the flexion contribution of the thoracic spine. The HBMs utility in predicting motion and injury was demonstrated in this study, such as the face impacting the seat frame, that was otherwise not observed with the HIII ATD.

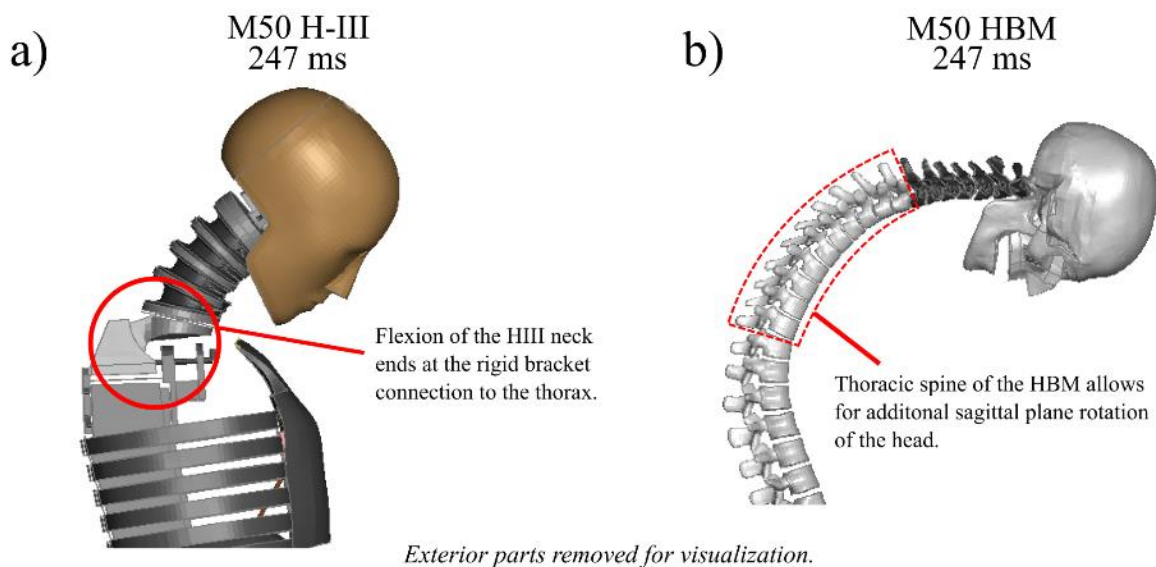


**Figure 124: a) Lower neck bracket of HIII prevents further flexion of the neck; b) thoracic spine of HBM allows for a full range of spinal flexion in a biofidelic manner**

The peak forces and moments measured with the neck cross-sections of the HBM increased when descending the cervical spine. White et al. attributed the larger moments in the lower cervical spine to the increasing moment arm due to each subsequent cross-section being further away from the head CG (Figure 125) [164]. The lower reaction forces in the OC cross-section led to a lower  $N_{ij}$  with the HBM than the HIII and thus a lower predicted probability of neck injury. Johnson et al. suggested that critical intercepts be explicitly developed for HBMs to accurately capture the potential for a neck injury at each cross-section [165]. The overly stiff neck of the HIII demonstrated the potential to overestimate injury at the upper neck level compared with response of the HBM, due to artificially high reaction forces at the upper neck load cell.

Despite the difference in upper neck reaction forces between the GHBM HBM and HIII ATD, the value of BrIC was comparable between the models, which agrees with previous findings in the literature [166]. Calculating BrIC requires using peak angular velocities of the head CG, which in this case were relatively close in magnitude between the HBM and HIII (Figure 125b). The plot of the head CG angular velocity also demonstrated the longer duration of negative angular velocity of the head, which corresponds to the increased sagittal plane rotation.

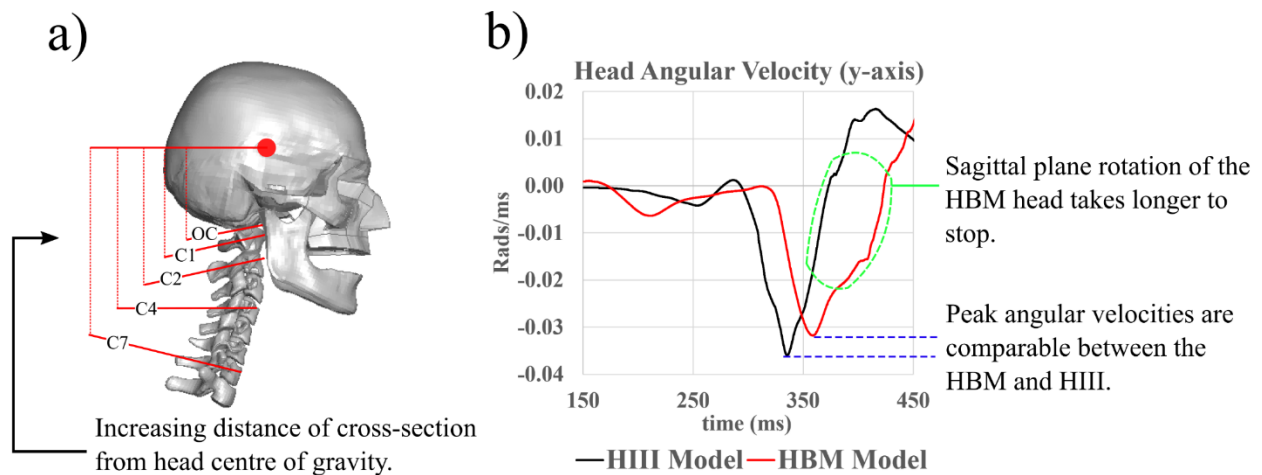


**Figure 125 a) Distance from head CG to the cross-section increases further down the cervical spine, causing increased bending moment arm; b) Peak angular velocities of the HBM and HIII head are similar in magnitude, which results in a similar value of BrIC, while the longer duration of sagittal plane rotation of the HBM head contributed to the face impacting the seat frame**

The impact between the thorax and the lowered handrail in the proposed seat design resulted in a larger normalized chest deflection for the HBM than for the HIII. The M50 HBM exhibited 14.0% normalized peak chest deflection, compared with 8.2% for the M50 HIII. Holmqvist et al. demonstrated that a HBM predicted a greater peak chest deflection than the HIII from a steering wheel focal impact, similar to the impact with the lowered handrail in the current study [167], [168]. In the current study, an

underestimation of the chest deflection sensor and a stiffer thorax structure reduced peak chest deflection for the HIII. The single-point deflection measurement of the HIII thorax sensor can fail to capture peak compression if a load is applied above or below the sensor. In addition, The HIII thorax was developed to replicate the response corridors of a cadaver thorax subjected to high-rate (6.7 m/s) and low-rate (4.3 m/s) pendulum impacts [51]. During the initial development of the HIII ATD, the accuracy of thorax compression under high-rate loading was prioritized, which led to an overly stiff response of the HIII thorax under the low-rate loading [52]. In the current study, the impact of the lowered handrail on the thorax was 4.8 m/s, placing it closer to the low-rate loading corridor, which explains the stiffer response of the HIII thorax and the lower peak deflection. Conversely, the GHBM thorax response was validated for focal pendulum impacts (4.3 m/s frontal and oblique, 2.5 m/s lateral) and 3-point belt loading, demonstrating a high level of biofidelity for the model under various loading conditions [84]. This study demonstrated the potential for an under prediction of thorax injury by the HIII ATD when compared with the response of the more biofidelic passenger surrogate (HBM).

### **6.3.1. F05 HBM and HIII Comparison**

The F05 HIII impacted the forward handrail on the chin, while the F05 HBM impacted the handrail on the anterior neck. The difference in handrail impact location was partially due to the difference in head form geometry between the models. The HBM chin/jaw geometry was smaller than the HIII by 20 mm, which caused the HBM chin to clear the handrail by 14 mm, demonstrating that if the HBM had a chin similar in size to that of the HIII, it potentially could have impacted the handrail on the chin as well. (Figure 126a,b) [169]. An additional contributor to the different impact locations is the error in matching the posture and limb positioning of the HBM with the HIII. White et al. described the discrepancies in matching the initial positioning of the HBM limbs and joints to that of the HIII as a potential source of error that can contribute to different kinematics between the models [170]. The initial seating phase of the simulation caused slight differences in the positioning of the F05 HBM and HIII, which could result in slight differences in limb trajectory. In the current study, even a slight difference in head trajectory can be the difference between the chin clearing or impacting the forward handrail. A side-by-side comparison between the models shows that after the seating phase, the head of the F05 HBM was slightly higher than the HIII (Figure 126c). The result with the F05 HIII and HBM demonstrated how a biofidelic model can result in significantly different kinematics caused by tissue geometry discrepancies and initial positioning errors.

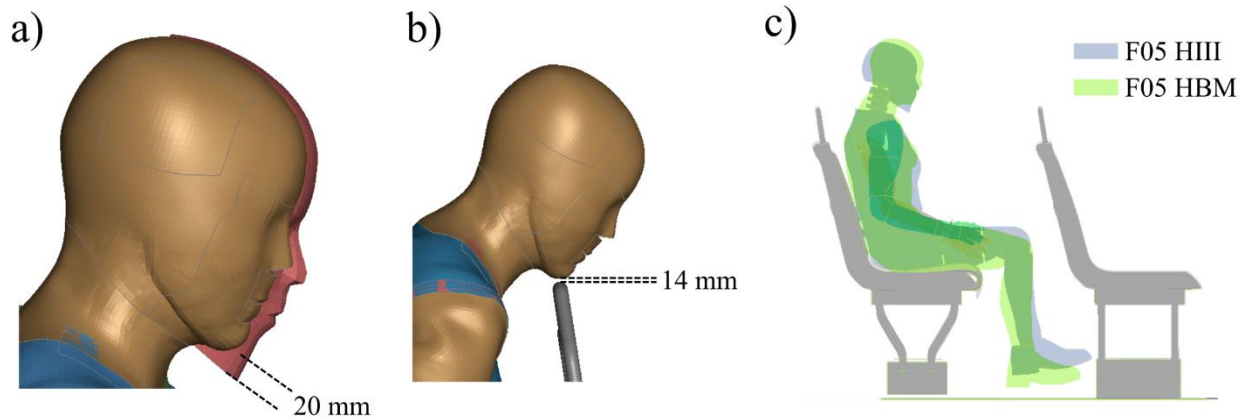


**Figure 126: a) Side-by-side comparison of F05 HBM and HIII head form showing that the HIII chin protrudes down 20 mm further than the HBM; b) The HBM chin clearance with the handrail is less than the additional size of the HIII chin c) Positioning of the F05 HBM and HIII after 125 ms seating phase of the simulation**

#### 6.4. Effect of Passenger Stature on Injury Potential

One of the objectives of this study was to assess the effect of passenger stature on kinematics and injury potential using a 5<sup>th</sup> and 50<sup>th</sup> percentile version of the HIII ATD models and the GHBMC HBMs.

This study demonstrated that smaller passengers are at an increased risk of face and neck injury in a transit bus frontal impact due to the potential for focal impact of the face on the forward handrail. The forward handrail was higher relative to the head of the F05 HIII, making impact on the face more likely (Figure 127). As the occupant was thrown forward, the higher relative height of the handrail for the F05 resulted in a smaller clearance between the chin and handrail for the F05 when compared with the M50 (Figure 127b).

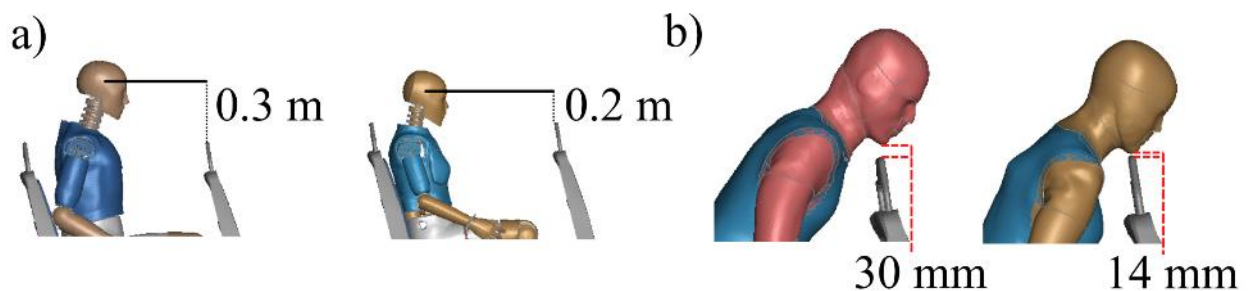


**Figure 127: a) The head of the F05 is closer to the handrail vertically due to the shorter seated stature; b) F05 HBM misses the handrail by a smaller margin than the M50**

In addition, the F05 exhibited chest compression from impacting the top of forward seat frame, which the M50 did not (Figure 128). The chest impact of the F05 appeared to be due to the more upright posture of the F05 as it impacted the forward handrail when compared with the M50. This was due to the smaller

upper leg limb length, which limited the torso of the F05 HBM from pitching forward before it impacted the forward handrail.

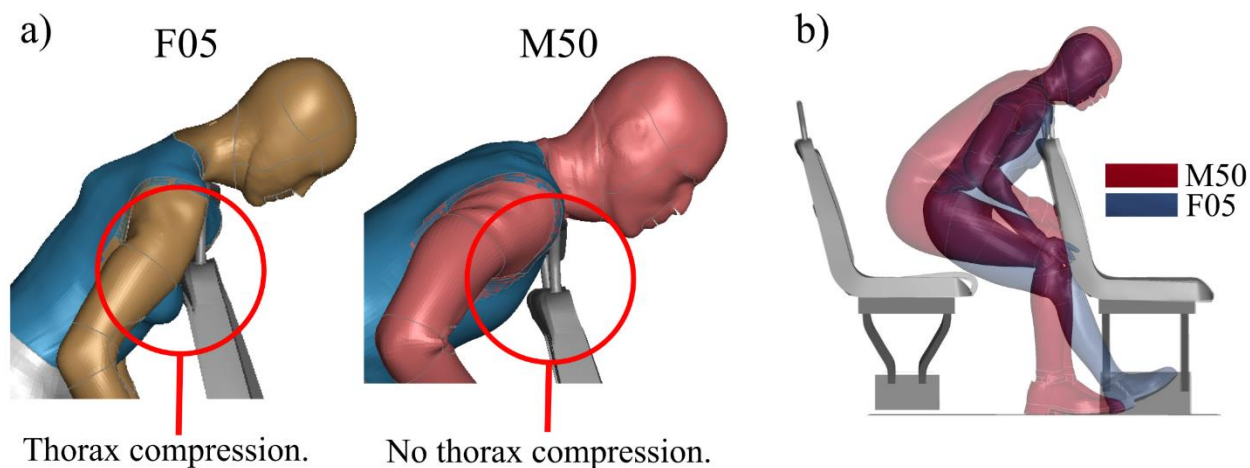


**Figure 128: a) F05 HBM has thorax compression due to impacting the top of the seat frame, not observed with the M50; b) the F05 has a more upright posture as it impacts the forward seat, resulting in chest compression on the top of the seat frame**

The lowered handrail impact on the thorax in the proposed seat design posed a greater risk of injury for the F05 HBM than for the M50. The F05 predicted sternum and rib fracture from impacting the lowered handrail, whereas the M50 did not predict any fracture. The F05 and M50 both had peak normalized thorax compressions of 14%. The current IARV states that a 23% normalized thorax compression with the F05 is equivalent in injury risk to 29% thorax compression with the M50, showing that the F05 can withstand less normalized chest compression before injury than the M50 [56]. Kemper et al. demonstrated that small female PMHS were at increased risk of thorax fracture as they could initiate rib fractures at 11% normalized thorax compression, compared with 14% for male PMHS [171]. The normalized thorax compression of the F05 in the current study placed it above the minimum threshold for PMHS rib fracture from the experiment. This study demonstrated that the normalized thorax compression of the small stature passenger from impacting a lowered handrail places them at an increased risk of fracture injury compared with the mid sized male.

This study demonstrated that the 30 mm reduction in seat pitch with the proposed seat design was less effective at reducing the secondary impact velocity and femur loads of the F05 HBM compared with the M50 HBM (Figure 129a). Reducing the secondary impact velocity is crucial for minimizing secondary impact injuries of passengers [172]. All things being equal with the test buck model, the smaller leg size of the F05 resulted in a greater free flight distance and subsequently a greater femur load resulting from the secondary impact (Figure 129b). Although this study showed that the small stature passenger received

less of a benefit from the seat pitch reduction compared with the mid sized passenger, both passengers were at a very low risk of lower extremity injury from impacting the forward seatback with the knees.

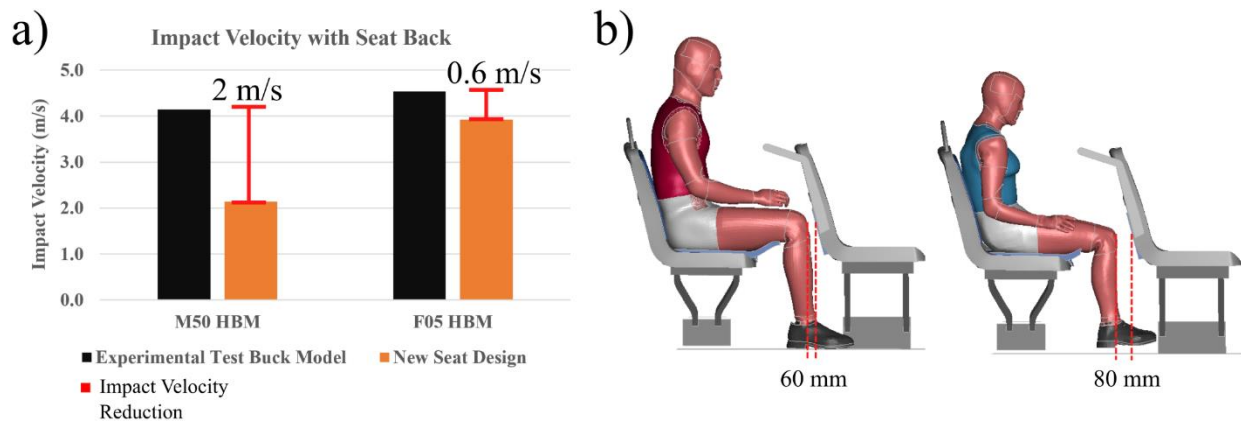


**Figure 129: a) Secondary impact velocity reduction is smaller for the F05 HBM compared with the M50 HBM; b) Initial separation between the knees and forward seatback is greater for the F05 HBM, resulting in greater secondary impact velocity**

### 6.5. Effective Passive Safety Measures Found Through Parametric Analysis and Alternative Seat Geometries using the HIII M50

The third objective of this study was to investigate passive safety measures that reduce passenger injury on transit buses. The passive safety studies included a parametric analysis using the experimental test buck seats and three alternative seat and handrail designs. The passenger surrogate used for both studies was the M50 HIII due to its computational efficiency compared with the HBM. The most significant risk of injury in the experimental test buck was the focal impact with the handrail on the neck and face. Thus, any potential new designs were required to eliminate the face or neck impact to be considered an improvement. In addition, the injury metrics  $HIC_{15}$ ,  $N_{ij}$ , CTI, and LE, were used to assess the head, neck, thorax, and lower extremity injury potential with the new designs/configurations.

The parametric analysis and alternative seat geometries demonstrated three successful passive safety methods for the HIII M50. The first method was reducing the seat pitch to lower the femur loads. A lower seat pitch reduced the free flight distance of the ATD, limiting the free flight velocity when the knees impacted the forward seatback. Reducing the secondary impact velocity has been identified as a crucial measure in other forms of mass transit to improve passive safety [140]. The second method of passive safety in this study was the raised seat pan lip, which limited the forward sliding of the HIII M50 on the seat and prevented the knees from impacting the forward seatback.

The third method of passive safety was when the forward handrail was lowered relative to the passenger, causing the impact with the handrail to occur on the upper chest instead of the anterior neck. The impact on the upper chest eliminated the anterior neck injury potential and lowered the  $HIC_{15}$ ,  $N_{ij}$  and CTI injury metrics. The handrail was lower relative to the passenger in the parametric analysis when the forward seat was lowered or when the ATD was seated in the outboard seat, due to the handrail curving down lower on that side. The alternative design with the lowered handrail showed an even greater improvement in protection, as the handrail was even lower relative to the passenger compared with the parametric analysis. Having the handrail lower relative to the passenger was a method of compartmentalizing the upper body of the HIII ATD by preventing focal impact on the head and neck. The impact on the thorax was preferable over the anterior neck or face impact as the thorax tissues can withstand more loading prior to injury [173]. Loading the thorax with the handrail is similar in function to that of 3-point belts, which engage the thorax to limit the passenger forward excursion and prevent the head from impacting surrounding structures, thereby limiting severe injury [174].

In addition, the three alternative seat designs provided insight into potential seat designs that should be avoided in a frontal impact scenario. It was demonstrated that a raised headrest could cause more injury to a passenger in a frontal impact when compared with lower seat back. The raised headrest caused dangerous levels of neck bending moment and shear force due to the face directly impacting the forward seatback (Figure 130). The potential for a neck injury was similar to that observed with high-backed seats in school buses and motorcoaches [126], [136]. The rigidity of transit bus seats exacerbated the potential for injury by not allowing for seat deformation upon impact as seen on school buses [130]. The results with the headrest model contradicted the recommendations by Olivares and Martinez, who suggested implementing raised headrests in transit buses to eliminate neck hyperextension injuries in a rear impact [116], [119]. While the raised headrest could potentially reduce or eliminate the potential for injury in a rear impact, this study demonstrated that it comes at a cost of increased injury in a frontal impact. In addition, the statistics reported by the NIAR study [29] showed that frontal impacts were more prevalent for fatal injuries of passengers on transit buses, suggesting that design improvements should favor mitigating injury in a frontal impact scenario.



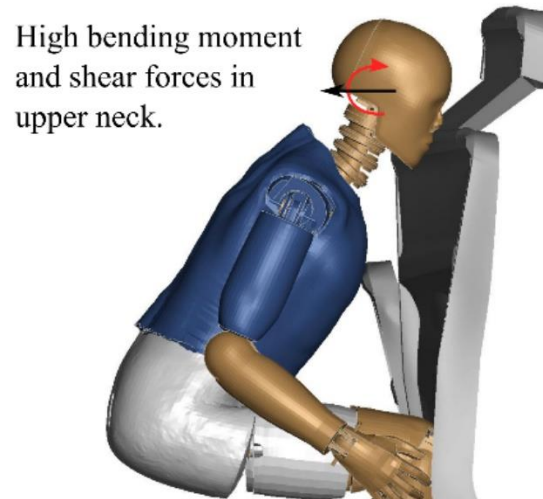


**Figure 130: Focal impact of the face on raised headrest causes high bending moment and shear forces in the upper neck and a high probability of neck injury**

### **6.6. Potential for Injury in Proposed Seat Design in Comparison with Experimental Test Buck Model**

The proposed seat design incorporated a lowered handrail, increased seat pan lip, and reduced seat pitch. The response of the M50 HBM in the proposed seat design primarily agreed with the findings from the sensitivity analysis and alternative geometries using the HIII M50. The compartmentalization provided by the seat pitch and seat pan lip reduced the femur loads of the M50 HBM, which reduced the severity of the lower extremity fracture prediction. The proposed seat design demonstrated effective compartmentalization and injury reduction potential for both the 50<sup>th</sup> percentile HIII and HBM.

The F05 HBM predicted a more severe sternum fracture due to the increased thorax loading from the lowered handrail in the proposed seat design (Figure 131). The thorax loading could present an even greater risk of thoracic injury for older passengers who have a lower tolerance for thorax loading due to decreased bone strength with aging [160]. The fracture due to the lowered handrail would be an AIS-3 thorax injury, which would still be less severe than the AIS-5 larynx crush injury caused by the handrail impact on the anterior neck in the experimental test buck [54].

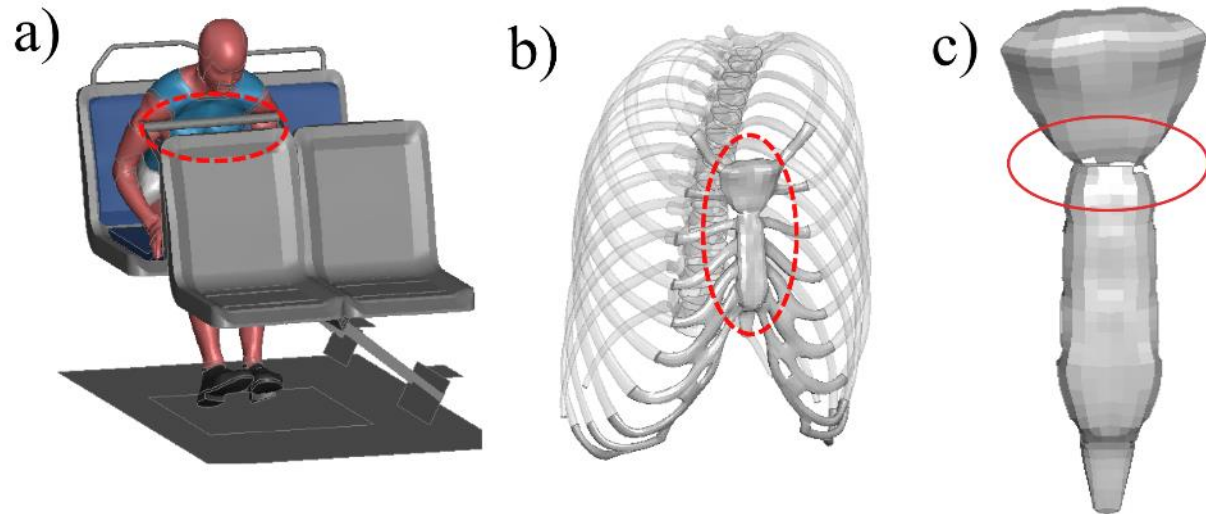


**Figure 131: a) Focal impact of the lowered handrail on the thorax of F05 HBM; b) Isolated sternum and ribs of the F05 HBM; c) Close up of sternum with fracture along the manubrium joint**

This study demonstrated that a lowered handrail was an effective method at reducing the potential for injury, primarily by eliminating the focal impact on the anterior neck and lower face. While there was a predicted sternum fracture for female passengers, it would still be preferable to the injuries caused by the anterior neck impact from the poor handrail placement in the experimental test buck.

## 7. Conclusions

### 7.1. Study Limitations and Recommendations

The TC sled experiments were limited to a 6.5 g and 5.7 g pulse; both scaled down from the original 7 g pulse corresponding to the 40 kph impact speed. Impacts at a higher velocity could result in more severe injury due to greater secondary impact velocities, and therefore should also be investigated.

The impacts with the test buck were also limited to forward-facing seats. The full-scale bus impacts demonstrated that the side-facing seats on transit buses present a unique safety risk for passengers as they are ejected sideways into the surrounding structures. Further investigation with the physical test buck and test buck model looking into the potential for injury in side-facing seats is required.

The TC test buck experiments were limited to HIII ATDs; thus, only the ATD model responses in the test buck were validated. PMHS experiments would be required to validate the responses of the HBMs in the test buck model. The responses of all occupant surrogates in the proposed seat design were not validated because no experimental data was available with either the ATDs or PMHS seated in the proposed seat design.

The sled experiments were limited to the 5<sup>th</sup> and 50<sup>th</sup> percentile passenger statures. Physical and numerical ATDs and HBMs range from child sizes to a 95<sup>th</sup> percentile male adult stature. As the current study demonstrated that small stature adult passengers were at an increased risk of injury, investigating the kinematics of small children in an unrestrained transit bus impact scenario is essential to determine the risk for children. Martinez et al. found that child passengers were at a high risk of head and neck injury due to the relative size of the forward seat [119]. The relative size of the seat for a child is large enough to cause a focal impact on the front of the face, which could result in serious head and neck injury as demonstrated with the M50 HIII seated in the raised headrest design.

This study demonstrated a potential for tissue fracture in a transit bus impact. Future work could investigate the potential for fracture using aged HBM models with tissue material properties reflecting the decrease in bone strength as people age. Investigating the injury risk posed to the elderly would be useful as it has already been shown that they comprise a considerable portion of the public transit injuries despite their relatively low usage [26], [175].

The HBMs were repositioned via a simulation in this study, developing stresses in the elements of the tissues. The repositioned HBMs were then initiated in a zero-stress state for the proceeding simulations which was a potential source of error.

The GHBMC HBM implements bone fracture via element erosion once it surpasses the failure criteria. The surrounding elements absorb the load previously supported by the deleted element, which can cause surrounding elements to fail prematurely, resulting in an overestimated fracture in the model.

The GHBMC HBMs in this study implemented activation of the neck and upper back muscles using a startle response load curve, which can affect the head kinematics during impact. The load curves used in the models to define the ramp-up and release of muscle contraction corresponded to a startle response of a human volunteer. They were not specific to the muscle activation that might occur in a transit bus impact.

This study utilized a seat/handrail design from a previously in-service transit bus. Interior designs vary between bus manufacturers, model type, and year. The different seat and handrail designs used on other bus models could result in different kinematics and injury potential for passengers.

## **7.2. Concluding Remarks**

The aim of this study was to assess passenger injury in a transit bus frontal impact using HIII ATDs and the GHBMC HBMs (50<sup>th</sup> and 5<sup>th</sup> percentile) seated in two different test buck models.

The first test buck model replicated a sled buck used by TC to conduct a series of frontal impact experiments. The test buck model was validated using the responses of small and mid-sized HIII ATDs in eight test configurations. The experimental test buck model assessed the potential for passenger injury using a seat and handrail design typical of transit buses currently in use.

The primary mechanism of injury for passengers in the experimental test buck model was from impacting the forward handrail located along the top of the seat frame. The M50 HIII, M50 HBM, and the F05 HBM all impacted the handrail on the anterior neck. The impact force on the anterior neck measured with the M50 HIII and the larynx tissue compression measured with the HBMs surpassed the threshold to predict a crushing injury to the larynx cartilages. A crushing injury to the larynx would be a potentially fatal AIS-5 injury due to airway obstruction. The F05 HIII impacted the forward handrail on the face, resulting in a high probability of mandible fracture and upper neck injury. The experimental test buck model demonstrated that the placement of handrails could put passengers at serious risk of focal impact injuries. The inability of the industry standard injury metrics to capture the larynx crush injury highlighted their limitations when analyzing focal impact injuries. The utility of the HBM provided the ability to measure the deformation of the larynx cartilage tissue directly.

Smaller passengers were at a greater risk of injury due to the relative size of the surrounding seats and handrails. The relative size and height difference between the small stature passenger and the forward seat led to chest deflection when seated in the experimental test buck model, which did not occur with the

mid-sized passenger. The chest deflection resulted in a predicted sternum fracture with the F05 HBM. The findings demonstrated that standard seat sizes and handrail placements on transit buses could result in different impact locations and injuries depending on passenger stature. Minimizing injury requires that the seat and handrail placement be compatible with all passenger statures.

The second test buck model incorporated passive safety design improvements based on findings from a parametric analysis and three alternative seat geometry models. The proposed seat design implemented a lowered handrail which impacted the small and mid-sized passenger surrogates on the thorax. The lower handrail eliminated the potential for anterior neck, lower face, and upper neck injury while increasing thorax compression. The F05 HBM predicted a more severe sternum fracture due to the increased chest compression from the lower handrail. The sternum fracture was preferable to the focal impact injuries of the larynx, face, and upper neck observed in the experimental test buck model. The findings from the proposed seat design demonstrated that lowering the handrail is a simple yet effective means of reducing injury for passengers of small and mid-sized statures.

# Letters of Copyright Permissions

4/28/22, 1:51 PM

<https://marketplace.copyright.com/rs-ui-web/mp/license/cb099238-bcf7-4df6-b03e-a656f9f3a638/c0a97759-f5be-4ab1-b1f2-49a5e...>



This is a License Agreement between University of Waterloo ("User") and Copyright Clearance Center, Inc. ("CCC") on behalf of the Rightsholder identified in the order details below. The license consists of the order details, the CCC Terms and Conditions below, and any Rightsholder Terms and Conditions which are included below. All payments must be made in full to CCC in accordance with the CCC Terms and Conditions below.

Order Date	17-Feb-2022	Type of Use	Republish in a thesis/dissertation
Order License ID	1190344-1	Publisher Portion	SAE International Image/photo/illustration
System ID	730967		

## LICENSED CONTENT

Publication Title	Response of Human Larynx to Blunt Loading	Country	United States of America
Author/Editor	Melvin, J. W.	Rightsholder	SAE International
Date	12/31/1972	Publication Type	Report

## REQUEST DETAILS

Portion Type	Image/photo/illustration	Distribution	Worldwide
Number of images / photos / illustrations	3	Translation	Original language of publication
Format (select all that apply)	Electronic	Copies for the disabled?	No
Who will republish the content?	Academic institution	Minor editing privileges?	No
Duration of Use	Life of current edition	Incidental promotional use?	No
Lifetime Unit Quantity	Up to 499	Currency	CAD
Rights Requested	Main product		

## NEW WORK DETAILS

Title	Assessment of Human Body Model Response in Frontal Bus Crash Scenarios to Improve Public Transportation Safety	Institution name	University of Waterloo
Instructor name	Duane Cronin	Expected presentation date	2022-07-20

## ADDITIONAL DETAILS

Order reference number	N/A	The requesting person / organization to appear on the license	University of Waterloo
------------------------	-----	---	------------------------

## REUSE CONTENT DETAILS

<https://marketplace.copyright.com/rs-ui-web/mp/license/cb099238-bcf7-4df6-b03e-a656f9f3a638/c0a97759-f5be-4ab1-b1f2-49a5eaf5a2cc>

1/4

Title, description or numeric reference of the portion(s)	Fig 1. Fig 3B, Fig 5	Title of the article/chapter the portion is from	Response of Human Larynx to Blunt Loading
Editor of portion(s)	N/A	Author of portion(s)	Melvin, J. W.
Volume of serial or monograph	N/A	Issue, if republishing an article from a serial	N/A
Page or page range of portion	3-9	Publication date of portion	1973-01-01

## CCC Terms and Conditions

1. **Description of Service; Defined Terms.** This Republication License enables the User to obtain licenses for republication of one or more copyrighted works as described in detail on the relevant Order Confirmation (the "Work(s)"). Copyright Clearance Center, Inc. ("CCC") grants licenses through the Service on behalf of the rightsholder identified on the Order Confirmation (the "Rightsholder"). "Republication", as used herein, generally means the inclusion of a Work, in whole or in part, in a new work or works, also as described on the Order Confirmation. "User", as used herein, means the person or entity making such republication.
2. The terms set forth in the relevant Order Confirmation, and any terms set by the Rightsholder with respect to a particular Work, govern the terms of use of Works in connection with the Service. By using the Service, the person transacting for a republication license on behalf of the User represents and warrants that he/she/it (a) has been duly authorized by the User to accept, and hereby does accept, all such terms and conditions on behalf of User, and (b) shall inform User of all such terms and conditions. In the event such person is a "freelancer" or other third party independent of User and CCC, such party shall be deemed jointly a "User" for purposes of these terms and conditions. In any event, User shall be deemed to have accepted and agreed to all such terms and conditions if User republishes the Work in any fashion.
3. **Scope of License; Limitations and Obligations.**
  - 3.1. All Works and all rights therein, including copyright rights, remain the sole and exclusive property of the Rightsholder. The license created by the exchange of an Order Confirmation (and/or any invoice) and payment by User of the full amount set forth on that document includes only those rights expressly set forth in the Order Confirmation and in these terms and conditions, and conveys no other rights in the Work(s) to User. All rights not expressly granted are hereby reserved.
  - 3.2. **General Payment Terms:** You may pay by credit card or through an account with us payable at the end of the month. If you and we agree that you may establish a standing account with CCC, then the following terms apply: Remit Payment to: Copyright Clearance Center, 29118 Network Place, Chicago, IL 60673-1291. Payments Due: Invoices are payable upon their delivery to you (or upon our notice to you that they are available to you for downloading). After 30 days, outstanding amounts will be subject to a service charge of 1-1/2% per month or, if less, the maximum rate allowed by applicable law. Unless otherwise specifically set forth in the Order Confirmation or in a separate written agreement signed by CCC, invoices are due and payable on "net 30" terms. While User may exercise the rights licensed immediately upon issuance of the Order Confirmation, the license is automatically revoked and is null and void, as if it had never been issued, if complete payment for the license is not received on a timely basis either from User directly or through a payment agent, such as a credit card company.
  - 3.3. Unless otherwise provided in the Order Confirmation, any grant of rights to User (i) is "one-time" (including the editions and product family specified in the license), (ii) is non-exclusive and non-transferable and (iii) is subject to any and all limitations and restrictions (such as, but not limited to, limitations on duration of use or circulation) included in the Order Confirmation or invoice and/or in these terms and conditions. Upon completion of the licensed use, User shall either secure a new permission for further use of the Work(s) or immediately cease any new use of the Work(s) and shall render inaccessible (such as by deleting or by removing or severing links or other locators) any further copies of the Work (except for copies printed on paper in accordance with this license and still in User's stock at the end of such period).

- 3.4. In the event that the material for which a republication license is sought includes third party materials (such as photographs, illustrations, graphs, inserts and similar materials) which are identified in such material as having been used by permission, User is responsible for identifying, and seeking separate licenses (under this Service or otherwise) for, any of such third party materials; without a separate license, such third party materials may not be used.
- 3.5. Use of proper copyright notice for a Work is required as a condition of any license granted under the Service. Unless otherwise provided in the Order Confirmation, a proper copyright notice will read substantially as follows: "Republished with permission of [Rightsholder's name], from [Work's title, author, volume, edition number and year of copyright]; permission conveyed through Copyright Clearance Center, Inc. " Such notice must be provided in a reasonably legible font size and must be placed either immediately adjacent to the Work as used (for example, as part of a by-line or footnote but not as a separate electronic link) or in the place where substantially all other credits or notices for the new work containing the republished Work are located. Failure to include the required notice results in loss to the Rightsholder and CCC, and the User shall be liable to pay liquidated damages for each such failure equal to twice the use fee specified in the Order Confirmation, in addition to the use fee itself and any other fees and charges specified.
- 3.6. User may only make alterations to the Work if and as expressly set forth in the Order Confirmation. No Work may be used in any way that is defamatory, violates the rights of third parties (including such third parties' rights of copyright, privacy, publicity, or other tangible or intangible property), or is otherwise illegal, sexually explicit or obscene. In addition, User may not conjoin a Work with any other material that may result in damage to the reputation of the Rightsholder. User agrees to inform CCC if it becomes aware of any infringement of any rights in a Work and to cooperate with any reasonable request of CCC or the Rightsholder in connection therewith.
4. Indemnity. User hereby indemnifies and agrees to defend the Rightsholder and CCC, and their respective employees and directors, against all claims, liability, damages, costs and expenses, including legal fees and expenses, arising out of any use of a Work beyond the scope of the rights granted herein, or any use of a Work which has been altered in any unauthorized way by User, including claims of defamation or infringement of rights of copyright, publicity, privacy or other tangible or intangible property.
5. Limitation of Liability. UNDER NO CIRCUMSTANCES WILL CCC OR THE RIGHTSHOLDER BE LIABLE FOR ANY DIRECT, INDIRECT, CONSEQUENTIAL OR INCIDENTAL DAMAGES (INCLUDING WITHOUT LIMITATION DAMAGES FOR LOSS OF BUSINESS PROFITS OR INFORMATION, OR FOR BUSINESS INTERRUPTION) ARISING OUT OF THE USE OR INABILITY TO USE A WORK, EVEN IF ONE OF THEM HAS BEEN ADVISED OF THE POSSIBILITY OF SUCH DAMAGES. In any event, the total liability of the Rightsholder and CCC (including their respective employees and directors) shall not exceed the total amount actually paid by User for this license. User assumes full liability for the actions and omissions of its principals, employees, agents, affiliates, successors and assigns.
6. Limited Warranties. THE WORK(S) AND RIGHT(S) ARE PROVIDED "AS IS". CCC HAS THE RIGHT TO GRANT TO USER THE RIGHTS GRANTED IN THE ORDER CONFIRMATION DOCUMENT. CCC AND THE RIGHTSHOLDER DISCLAIM ALL OTHER WARRANTIES RELATING TO THE WORK(S) AND RIGHT(S), EITHER EXPRESS OR IMPLIED, INCLUDING WITHOUT LIMITATION IMPLIED WARRANTIES OF MERCHANTABILITY OR FITNESS FOR A PARTICULAR PURPOSE. ADDITIONAL RIGHTS MAY BE REQUIRED TO USE ILLUSTRATIONS, GRAPHS, PHOTOGRAPHS, ABSTRACTS, INSERTS OR OTHER PORTIONS OF THE WORK (AS OPPOSED TO THE ENTIRE WORK) IN A MANNER CONTEMPLATED BY USER; USER UNDERSTANDS AND AGREES THAT NEITHER CCC NOR THE RIGHTSHOLDER MAY HAVE SUCH ADDITIONAL RIGHTS TO GRANT.
7. Effect of Breach. Any failure by User to pay any amount when due, or any use by User of a Work beyond the scope of the license set forth in the Order Confirmation and/or these terms and conditions, shall be a material breach of the license created by the Order Confirmation and these terms and conditions. Any breach not cured within 30 days of written notice thereof shall result in immediate termination of such license without further notice. Any unauthorized (but licensable) use of a Work that is terminated immediately upon notice thereof may be liquidated by payment of the Rightsholder's ordinary license price therefor; any unauthorized (and unlicensable) use that is not terminated immediately for any reason (including, for example, because materials containing the Work cannot



reasonably be recalled) will be subject to all remedies available at law or in equity, but in no event to a payment of less than three times the Rightsholder's ordinary license price for the most closely analogous licensable use plus Rightsholder's and/or CCC's costs and expenses incurred in collecting such payment.

#### 8. Miscellaneous.

- 8.1. User acknowledges that CCC may, from time to time, make changes or additions to the Service or to these terms and conditions, and CCC reserves the right to send notice to the User by electronic mail or otherwise for the purposes of notifying User of such changes or additions; provided that any such changes or additions shall not apply to permissions already secured and paid for.
- 8.2. Use of User-related information collected through the Service is governed by CCC's privacy policy, available online here:<https://marketplace.copyright.com/rs-ui-web/mp/privacy-policy>
- 8.3. The licensing transaction described in the Order Confirmation is personal to User. Therefore, User may not assign or transfer to any other person (whether a natural person or an organization of any kind) the license created by the Order Confirmation and these terms and conditions or any rights granted hereunder; provided, however, that User may assign such license in its entirety on written notice to CCC in the event of a transfer of all or substantially all of User's rights in the new material which includes the Work(s) licensed under this Service.
- 8.4. No amendment or waiver of any terms is binding unless set forth in writing and signed by the parties. The Rightsholder and CCC hereby object to any terms contained in any writing prepared by the User or its principals, employees, agents or affiliates and purporting to govern or otherwise relate to the licensing transaction described in the Order Confirmation, which terms are in any way inconsistent with any terms set forth in the Order Confirmation and/or in these terms and conditions or CCC's standard operating procedures, whether such writing is prepared prior to, simultaneously with or subsequent to the Order Confirmation, and whether such writing appears on a copy of the Order Confirmation or in a separate instrument.
- 8.5. The licensing transaction described in the Order Confirmation document shall be governed by and construed under the law of the State of New York, USA, without regard to the principles thereof of conflicts of law. Any case, controversy, suit, action, or proceeding arising out of, in connection with, or related to such licensing transaction shall be brought, at CCC's sole discretion, in any federal or state court located in the County of New York, State of New York, USA, or in any federal or state court whose geographical jurisdiction covers the location of the Rightsholder set forth in the Order Confirmation. The parties expressly submit to the personal jurisdiction and venue of each such federal or state court. If you have any comments or questions about the Service or Copyright Clearance Center, please contact us at 978-750-8400 or send an e-mail to [support@copyright.com](mailto:support@copyright.com).



This is a License Agreement between Christopher Pastula ("User") and Copyright Clearance Center, Inc. ("CCC") on behalf of the Rightsholder identified in the order details below. The license consists of the order details, the Marketplace Order General Terms and Conditions below, and any Rightsholder Terms and Conditions which are included below.

All payments must be made in full to CCC in accordance with the Marketplace Order General Terms and Conditions below.

<b>Order Date</b>	20-Jun-2022	<b>Type of Use</b>	Republish in a thesis/dissertation
<b>Order License ID</b>	1238294-1	<b>Publisher</b>	OXFORD UNIVERSITY PRESS
<b>ISSN</b>	0141-5387	<b>Portion</b>	Image/photo/illustration

## LICENSED CONTENT

<b>Publication Title</b>	European journal of orthodontics	<b>Rightsholder</b>	Oxford University Press - Journals
<b>Article Title</b>	The microstructural and biomechanical development of the condylar bone: a review.	<b>Publication Type</b>	Journal
<b>Author/Editor</b>	EUROPEAN ORTHODONTIC SOCIETY.	<b>Start Page</b>	479
<b>Date</b>	01/01/1979	<b>End Page</b>	485
<b>Language</b>	English, English	<b>Issue</b>	4
<b>Country</b>	United Kingdom of Great Britain and Northern Ireland	<b>Volume</b>	36

## REQUEST DETAILS

<b>Portion Type</b>	Image/photo/illustration	<b>Distribution</b>	Worldwide
<b>Number of images / photos / illustrations</b>	1	<b>Translation</b>	Original language of publication
<b>Format (select all that apply)</b>	Electronic	<b>Copies for the disabled?</b>	No
<b>Who will republish the content?</b>	Academic institution	<b>Minor editing privileges?</b>	No
<b>Duration of Use</b>	Life of current edition	<b>Incidental promotional use?</b>	No
<b>Lifetime Unit Quantity</b>	Up to 499	<b>Currency</b>	USD
<b>Rights Requested</b>	Main product		

## NEW WORK DETAILS

6/22/22, 10:05 AM

<https://marketplace.copyright.com/rs-ui-web/mp/license/a4bb8e91-d889-4f1a-ad46-288afee0c95b/c2ff51c1-3de4-41aa-8424-47b...>

<b>Title</b>	Assessment of Human Body Model Response in Frontal Bus Crash Scenarios to Improve Public Transportation Safety	<b>Institution name</b>	University of Waterloo
		<b>Expected presentation date</b>	2022-07-28
<b>Instructor name</b>	Duane Cronin		

### ADDITIONAL DETAILS

<b>Order reference number</b>	N/A	<b>The requesting person / organization to appear on the license</b>	Christopher Pastula
-------------------------------	-----	--	---------------------

### REUSE CONTENT DETAILS

<b>Title, description or numeric reference of the portion(s)</b>	Figure 2	<b>Title of the article/chapter the portion is from</b>	The microstructural and biomechanical development of the condylar bone: a review.
<b>Editor of portion(s)</b>	Willems, Nop M B K; Langenbach, Geerling E J; Everts, Vincent; Zentner, Andrej	<b>Author of portion(s)</b>	Willems, Nop M B K; Langenbach, Geerling E J; Everts, Vincent; Zentner, Andrej
<b>Volume of serial or monograph</b>	36	<b>Issue, if republishing an article from a serial</b>	4
<b>Page or page range of portion</b>	479-485	<b>Publication date of portion</b>	2014-07-31

## Marketplace Order General Terms and Conditions

The following terms and conditions ("General Terms"), together with any applicable Publisher Terms and Conditions, govern User's use of Works pursuant to the Licenses granted by Copyright Clearance Center, Inc. ("CCC") on behalf of the applicable Rightsholders of such Works through CCC's applicable Marketplace transactional licensing services (each, a "Service").

1) **Definitions.** For purposes of these General Terms, the following definitions apply:

"License" is the licensed use the User obtains via the Marketplace platform in a particular licensing transaction, as set forth in the Order Confirmation.

"Order Confirmation" is the confirmation CCC provides to the User at the conclusion of each Marketplace transaction. "Order Confirmation Terms" are additional terms set forth on specific Order Confirmations not set forth in the General Terms that can include terms applicable to a particular CCC transactional licensing service and/or any Rightsholder-specific terms.

"Rightsholder(s)" are the holders of copyright rights in the Works for which a User obtains licenses via the Marketplace platform, which are displayed on specific Order Confirmations.

"Terms" means the terms and conditions set forth in these General Terms and any additional Order Confirmation Terms collectively.

"User" or "you" is the person or entity making the use granted under the relevant License. Where the person accepting the Terms on behalf of a User is a freelancer or other third party who the User authorized to accept the General Terms on the User's behalf, such person shall be deemed jointly a User for purposes of such Terms.

"Work(s)" are the copyright protected works described in relevant Order Confirmations.

2) **Description of Service.** CCC's Marketplace enables Users to obtain Licenses to use one or more Works in accordance with all relevant Terms. CCC grants Licenses as an agent on behalf of the copyright rightsholder identified in the relevant Order Confirmation.

3) **Applicability of Terms.** The Terms govern User's use of Works in connection with the relevant License. In the event of any conflict between General Terms and Order Confirmation Terms, the latter shall govern. User acknowledges that Rightsholders have complete discretion whether to grant any permission, and whether to place any limitations on any grant, and that CCC has no right to supersede or to modify any such discretionary act by a Rightsholder.

4) **Representations; Acceptance.** By using the Service, User represents and warrants that User has been duly authorized by the User to accept, and hereby does accept, all Terms.

5) **Scope of License; Limitations and Obligations.** All Works and all rights therein, including copyright rights, remain the sole and exclusive property of the Rightsholder. The License provides only those rights expressly set forth in the terms and conveys no other rights in any Works

6) **General Payment Terms.** User may pay at time of checkout by credit card or choose to be invoiced. If the User chooses to be invoiced, the User shall: (i) remit payments in the manner identified on specific invoices, (ii) unless otherwise specifically stated in an Order Confirmation or separate written agreement, Users shall remit payments upon receipt of the relevant invoice from CCC, either by delivery or notification of availability of the invoice via the Marketplace platform, and (iii) if the User does not pay the invoice within 30 days of receipt, the User may incur a service charge of 1.5% per month or the maximum rate allowed by applicable law, whichever is less. While User may exercise the rights in the License immediately upon receiving the Order Confirmation, the License is automatically revoked and is null and void, as if it had never been issued, if CCC does not receive complete payment on a timely basis.

7) **General Limits on Use.** Unless otherwise provided in the Order Confirmation, any grant of rights to User (i) involves only the rights set forth in the Terms and does not include subsequent or additional uses, (ii) is non-exclusive and non-transferable, and (iii) is subject to any and all limitations and restrictions (such as, but not limited to, limitations on duration of use or circulation) included in the Terms. Upon completion of the licensed use as set forth in the Order Confirmation, User shall either secure a new permission for further use of the Work(s) or immediately cease any new use of the Work(s) and shall render inaccessible (such as by deleting or by removing or severing links or other locators) any further copies of the Work. User may only make alterations to the Work if and as expressly set forth in the Order Confirmation. No Work may be used in any way that is defamatory, violates the rights of third parties (including such third parties' rights of copyright, privacy, publicity, or other tangible or intangible property), or is otherwise illegal, sexually explicit, or obscene. In addition, User may not conjoin a Work with any other material that may result in damage to the reputation of the Rightsholder. User agrees to inform CCC if it becomes aware of any infringement of any rights in a Work and to cooperate with any reasonable request of CCC or the Rightsholder in connection therewith.

8) **Third Party Materials.** In the event that the material for which a License is sought includes third party materials (such as photographs, illustrations, graphs, inserts and similar materials) that are identified in such material as having been used by permission (or a similar indicator), User is responsible for identifying, and seeking separate licenses (under this Service, if available, or otherwise) for any of such third party materials; without a separate license, User may not use such third party materials via the License.

9) **Copyright Notice.** Use of proper copyright notice for a Work is required as a condition of any License granted under the Service. Unless otherwise provided in the Order Confirmation, a proper copyright notice will read substantially as follows: "Used with permission of [Rightsholder's name], from [Work's title, author, volume, edition number and year of copyright]; permission conveyed through Copyright Clearance Center, Inc." Such notice must be provided in a reasonably legible font size and must be placed either on a cover page or in another location that any person, upon gaining access to the material which is the subject of a permission, shall see, or in the case of republication Licenses, immediately adjacent to the Work as used (for example, as part of a by-line or footnote) or in the place where substantially all other credits or notices for the new work containing the republished Work are located. Failure to include the required notice results in loss to the Rightsholder and CCC, and the User shall be liable to pay liquidated damages for each such failure equal to twice the use fee specified in the Order Confirmation, in addition to the use fee itself and any other fees and charges specified.

10) **Indemnity.** User hereby indemnifies and agrees to defend the Rightsholder and CCC, and their respective employees and directors, against all claims, liability, damages, costs, and expenses, including legal fees and expenses, arising out of any use of a Work beyond the scope of the rights granted herein and in the Order Confirmation, or any use of a Work

which has been altered in any unauthorized way by User, including claims of defamation or infringement of rights of copyright, publicity, privacy, or other tangible or intangible property.

**11) Limitation of Liability.** UNDER NO CIRCUMSTANCES WILL CCC OR THE RIGHTSHOLDER BE LIABLE FOR ANY DIRECT, INDIRECT, CONSEQUENTIAL, OR INCIDENTAL DAMAGES (INCLUDING WITHOUT LIMITATION DAMAGES FOR LOSS OF BUSINESS PROFITS OR INFORMATION, OR FOR BUSINESS INTERRUPTION) ARISING OUT OF THE USE OR INABILITY TO USE A WORK, EVEN IF ONE OR BOTH OF THEM HAS BEEN ADVISED OF THE POSSIBILITY OF SUCH DAMAGES. In any event, the total liability of the Rightsholder and CCC (including their respective employees and directors) shall not exceed the total amount actually paid by User for the relevant License. User assumes full liability for the actions and omissions of its principals, employees, agents, affiliates, successors, and assigns.

**12) Limited Warranties.** THE WORK(S) AND RIGHT(S) ARE PROVIDED "AS IS." CCC HAS THE RIGHT TO GRANT TO USER THE RIGHTS GRANTED IN THE ORDER CONFIRMATION DOCUMENT. CCC AND THE RIGHTSHOLDER DISCLAIM ALL OTHER WARRANTIES RELATING TO THE WORK(S) AND RIGHT(S), EITHER EXPRESS OR IMPLIED, INCLUDING WITHOUT LIMITATION IMPLIED WARRANTIES OF MERCHANTABILITY OR FITNESS FOR A PARTICULAR PURPOSE. ADDITIONAL RIGHTS MAY BE REQUIRED TO USE ILLUSTRATIONS, GRAPHS, PHOTOGRAPHS, ABSTRACTS, INSERTS, OR OTHER PORTIONS OF THE WORK (AS OPPOSED TO THE ENTIRE WORK) IN A MANNER CONTEMPLATED BY USER; USER UNDERSTANDS AND AGREES THAT NEITHER CCC NOR THE RIGHTSHOLDER MAY HAVE SUCH ADDITIONAL RIGHTS TO GRANT.

**13) Effect of Breach.** Any failure by User to pay any amount when due, or any use by User of a Work beyond the scope of the License set forth in the Order Confirmation and/or the Terms, shall be a material breach of such License. Any breach not cured within 10 days of written notice thereof shall result in immediate termination of such License without further notice. Any unauthorized (but licensable) use of a Work that is terminated immediately upon notice thereof may be liquidated by payment of the Rightsholder's ordinary license price therefor; any unauthorized (and unlicensable) use that is not terminated immediately for any reason (including, for example, because materials containing the Work cannot reasonably be recalled) will be subject to all remedies available at law or in equity, but in no event to a payment of less than three times the Rightsholder's ordinary license price for the most closely analogous licensable use plus Rightsholder's and/or CCC's costs and expenses incurred in collecting such payment.

**14) Additional Terms for Specific Products and Services.** If a User is making one of the uses described in this Section 14, the additional terms and conditions apply:

**a) *Print Uses of Academic Course Content and Materials (photocopies for academic coursepacks or classroom handouts).*** For photocopies for academic coursepacks or classroom handouts the following additional terms apply:

i) The copies and anthologies created under this License may be made and assembled by faculty members individually or at their request by on-campus bookstores or copy centers, or by off-campus copy shops and other similar entities.

ii) No License granted shall in any way: (i) include any right by User to create a substantively non-identical copy of the Work or to edit or in any other way modify the Work (except by means of deleting material immediately preceding or following the entire portion of the Work copied) (ii) permit "publishing ventures" where any particular anthology would be systematically marketed at multiple institutions.

iii) Subject to any Publisher Terms (and notwithstanding any apparent contradiction in the Order Confirmation arising from data provided by User), any use authorized under the academic pay-per-use service is limited as follows:

A) any License granted shall apply to only one class (bearing a unique identifier as assigned by the institution, and thereby including all sections or other subparts of the class) at one institution;

B) use is limited to not more than 25% of the text of a book or of the items in a published collection of essays, poems or articles;

C) use is limited to no more than the greater of (a) 25% of the text of an issue of a journal or other periodical or (b) two articles from such an issue;

D) no User may sell or distribute any particular anthology, whether photocopied or electronic, at more than one institution of learning;

E) in the case of a photocopy permission, no materials may be entered into electronic memory by User except in order to produce an identical copy of a Work before or during the academic term (or analogous period) as

to which any particular permission is granted. In the event that User shall choose to retain materials that are the subject of a photocopy permission in electronic memory for purposes of producing identical copies more than one day after such retention (but still within the scope of any permission granted), User must notify CCC of such fact in the applicable permission request and such retention shall constitute one copy actually sold for purposes of calculating permission fees due; and

F) any permission granted shall expire at the end of the class. No permission granted shall in any way include any right by User to create a substantively non-identical copy of the Work or to edit or in any other way modify the Work (except by means of deleting material immediately preceding or following the entire portion of the Work copied).

iv) Books and Records; Right to Audit. As to each permission granted under the academic pay-per-use Service, User shall maintain for at least four full calendar years books and records sufficient for CCC to determine the numbers of copies made by User under such permission. CCC and any representatives it may designate shall have the right to audit such books and records at any time during User's ordinary business hours, upon two days' prior notice. If any such audit shall determine that User shall have underpaid for, or underreported, any photocopies sold or by three percent (3%) or more, then User shall bear all the costs of any such audit; otherwise, CCC shall bear the costs of any such audit. Any amount determined by such audit to have been underpaid by User shall immediately be paid to CCC by User, together with interest thereon at the rate of 10% per annum from the date such amount was originally due. The provisions of this paragraph shall survive the termination of this License for any reason.

**b) Digital Pay-Per-Uses of Academic Course Content and Materials (e-coursepacks, electronic reserves, learning management systems, academic institution intranets).** For uses in e-coursepacks, posts in electronic reserves, posts in learning management systems, or posts on academic institution intranets, the following additional terms apply:

i) The pay-per-uses subject to this Section 14(b) include:

A) **Posting e-reserves, course management systems, e-coursepacks for text-based content**, which grants authorizations to import requested material in electronic format, and allows electronic access to this material to members of a designated college or university class, under the direction of an instructor designated by the college or university, accessible only under appropriate electronic controls (e.g., password);

B) **Posting e-reserves, course management systems, e-coursepacks for material consisting of photographs or other still images not embedded in text**, which grants not only the authorizations described in Section 14(b)(i)(A) above, but also the following authorization: to include the requested material in course materials for use consistent with Section 14(b)(i)(A) above, including any necessary resizing, reformatting or modification of the resolution of such requested material (provided that such modification does not alter the underlying editorial content or meaning of the requested material, and provided that the resulting modified content is used solely within the scope of, and in a manner consistent with, the particular authorization described in the Order Confirmation and the Terms), but not including any other form of manipulation, alteration or editing of the requested material;

C) **Posting e-reserves, course management systems, e-coursepacks or other academic distribution for audiovisual content**, which grants not only the authorizations described in Section 14(b)(i)(A) above, but also the following authorizations: (i) to include the requested material in course materials for use consistent with Section 14(b)(i)(A) above; (ii) to display and perform the requested material to such members of such class in the physical classroom or remotely by means of streaming media or other video formats; and (iii) to "clip" or reformat the requested material for purposes of time or content management or ease of delivery, provided that such "clipping" or reformatting does not alter the underlying editorial content or meaning of the requested material and that the resulting material is used solely within the scope of, and in a manner consistent with, the particular authorization described in the Order Confirmation and the Terms. Unless expressly set forth in the relevant Order Confirmation, the License does not authorize any other form of manipulation, alteration or editing of the requested material.

ii) Unless expressly set forth in the relevant Order Confirmation, no License granted shall in any way: (i) include any right by User to create a substantively non-identical copy of the Work or to edit or in any other way modify the Work (except by means of deleting material immediately preceding or following the entire portion of the Work copied or, in the case of Works subject to Sections 14(b)(1)(B) or (C) above, as described in such Sections) (ii) permit "publishing ventures" where any particular course materials would be systematically marketed at multiple institutions.

iii) Subject to any further limitations determined in the Rightsholder Terms (and notwithstanding any apparent contradiction in the Order Confirmation arising from data provided by User), any use authorized under the electronic course content pay-per-use service is limited as follows:

- A) any License granted shall apply to only one class (bearing a unique identifier as assigned by the institution, and thereby including all sections or other subparts of the class) at one institution;
- B) use is limited to not more than 25% of the text of a book or of the items in a published collection of essays, poems or articles;
- C) use is limited to not more than the greater of (a) 25% of the text of an issue of a journal or other periodical or (b) two articles from such an issue;
- D) no User may sell or distribute any particular materials, whether photocopied or electronic, at more than one institution of learning;
- E) electronic access to material which is the subject of an electronic-use permission must be limited by means of electronic password, student identification or other control permitting access solely to students and instructors in the class;
- F) User must ensure (through use of an electronic cover page or other appropriate means) that any person, upon gaining electronic access to the material, which is the subject of a permission, shall see:
  - o a proper copyright notice, identifying the Rightsholder in whose name CCC has granted permission,
  - o a statement to the effect that such copy was made pursuant to permission,
  - o a statement identifying the class to which the material applies and notifying the reader that the material has been made available electronically solely for use in the class, and
  - o a statement to the effect that the material may not be further distributed to any person outside the class, whether by copying or by transmission and whether electronically or in paper form, and User must also ensure that such cover page or other means will print out in the event that the person accessing the material chooses to print out the material or any part thereof.
- G) any permission granted shall expire at the end of the class and, absent some other form of authorization, User is thereupon required to delete the applicable material from any electronic storage or to block electronic access to the applicable material.

iv) Uses of separate portions of a Work, even if they are to be included in the same course material or the same university or college class, require separate permissions under the electronic course content pay-per-use Service. Unless otherwise provided in the Order Confirmation, any grant of rights to User is limited to use completed no later than the end of the academic term (or analogous period) as to which any particular permission is granted.

v) Books and Records; Right to Audit. As to each permission granted under the electronic course content Service, User shall maintain for at least four full calendar years books and records sufficient for CCC to determine the numbers of copies made by User under such permission. CCC and any representatives it may designate shall have the right to audit such books and records at any time during User's ordinary business hours, upon two days' prior notice. If any such audit shall determine that User shall have underpaid for, or underreported, any electronic copies used by three percent (3%) or more, then User shall bear all the costs of any such audit; otherwise, CCC shall bear the costs of any such audit. Any amount determined by such audit to have been underpaid by User shall immediately be paid to CCC by User, together with interest thereon at the rate of 10% per annum from the date such amount was originally due. The provisions of this paragraph shall survive the termination of this license for any reason.

c) *Pay-Per-Use Permissions for Certain Reproductions (Academic photocopies for library reserves and interlibrary loan reporting) (Non-academic internal/external business uses and commercial document delivery).* The License expressly excludes the uses listed in Section (c)(i)-(v) below (which must be subject to separate license from the applicable Rightsholder) for: academic photocopies for library reserves and interlibrary loan reporting; and non-academic internal/external business uses and commercial document delivery.

- i) electronic storage of any reproduction (whether in plain-text, PDF, or any other format) other than on a transitory basis;
- ii) the input of Works or reproductions thereof into any computerized database;
- iii) reproduction of an entire Work (cover-to-cover copying) except where the Work is a single article;
- iv) reproduction for resale to anyone other than a specific customer of User;
- v) republication in any different form. Please obtain authorizations for these uses through other CCC services or directly from the rightsholder.

Any license granted is further limited as set forth in any restrictions included in the Order Confirmation and/or in these Terms.

d) *Electronic Reproductions in Online Environments (Non-Academic-email, intranet, internet and extranet)*. For "electronic reproductions", which generally includes e-mail use (including instant messaging or other electronic transmission to a defined group of recipients) or posting on an intranet, extranet or Intranet site (including any display or performance incidental thereto), the following additional terms apply:

- i) Unless otherwise set forth in the Order Confirmation, the License is limited to use completed within 30 days for any use on the Internet, 60 days for any use on an intranet or extranet and one year for any other use, all as measured from the "republication date" as identified in the Order Confirmation, if any, and otherwise from the date of the Order Confirmation.
- ii) User may not make or permit any alterations to the Work, unless expressly set forth in the Order Confirmation (after request by User and approval by Rightsholder); provided, however, that a Work consisting of photographs or other still images not embedded in text may, if necessary, be resized, reformatted or have its resolution modified without additional express permission, and a Work consisting of audiovisual content may, if necessary, be "clipped" or reformatted for purposes of time or content management or ease of delivery (provided that any such resizing, reformatting, resolution modification or "clipping" does not alter the underlying editorial content or meaning of the Work used, and that the resulting material is used solely within the scope of, and in a manner consistent with, the particular License described in the Order Confirmation and the Terms.

#### 15) Miscellaneous.

- a) User acknowledges that CCC may, from time to time, make changes or additions to the Service or to the Terms, and that Rightsholder may make changes or additions to the Rightsholder Terms. Such updated Terms will replace the prior terms and conditions in the order workflow and shall be effective as to any subsequent Licenses but shall not apply to Licenses already granted and paid for under a prior set of terms.
- b) Use of User-related information collected through the Service is governed by CCC's privacy policy, available online at [www.copyright.com/about/privacy-policy/](http://www.copyright.com/about/privacy-policy/).
- c) The License is personal to User. Therefore, User may not assign or transfer to any other person (whether a natural person or an organization of any kind) the License or any rights granted thereunder; provided, however, that, where applicable, User may assign such License in its entirety on written notice to CCC in the event of a transfer of all or substantially all of User's rights in any new material which includes the Work(s) licensed under this Service.
- d) No amendment or waiver of any Terms is binding unless set forth in writing and signed by the appropriate parties, including, where applicable, the Rightsholder. The Rightsholder and CCC hereby object to any terms contained in any writing prepared by or on behalf of the User or its principals, employees, agents or affiliates and purporting to govern or otherwise relate to the License described in the Order Confirmation, which terms are in any way inconsistent with any Terms set forth in the Order Confirmation, and/or in CCC's standard operating procedures, whether such writing is prepared prior to, simultaneously with or subsequent to the Order Confirmation, and whether such writing appears on a copy of the Order Confirmation or in a separate instrument.
- e) The License described in the Order Confirmation shall be governed by and construed under the law of the State of New York, USA, without regard to the principles thereof of conflicts of law. Any case, controversy, suit, action, or proceeding arising out of, in connection with, or related to such License shall be brought, at CCC's sole discretion, in any federal or state court located in the County of New York, State of New York, USA, or in any federal or state court



6/22/22, 10:05 AM <https://marketplace.copyright.com/rs-ui-web/mp/license/a4bb8e91-d889-4f1a-ad46-288afee0c95b/c2ff51c1-3de4-41aa-8424-47b...>

whose geographical jurisdiction covers the location of the Rightsholder set forth in the Order Confirmation. The parties expressly submit to the personal jurisdiction and venue of each such federal or state court.

Re: Mass transit report figures copyright permission

 Gerardo Olivares  
To: Chris Pastula

Hello Chris

That should be fine just make sure you reference the source documents. Once you have your thesis report published let me know I am still interested in the topic

Best regards

Gerardo

Hi Dr. Olivares,


I am a masters level student at the University of Waterloo and am doing research into transit bus crashworthiness.

I am emailing you to request copyright permission to use some of the figures from your 2012 report "Crashworthiness Evaluation of Mass Transit Buses" in my thesis as part of my literature review, as it is very similar to the work I am currently doing.

I apologize for emailing you directly, but I have been unable to get a response via contacting the FTA or the NIAR directly concerning this.

Any help would be greatly appreciated,  
Chris Pastula  
University of Waterloo

Re: Copyright Request

 Luis Martinez  
To: Chris Pastula

Hello Chris,

By this email I provide you with requested permission.

Best regards,

Luis

Hi Dr. Martinez,

I am a masters level student at the University of Waterloo working on a dissertation related to public transit safety.

I am emailing you to request copyright permission to include some figures from your 2017 conference proceeding "ADULT AND CHILD DUMMIES TESTS FOR SAFETY ASSESSMENT OF SEATED OCCUPANTS IN URBAN BUS COLLISIONS" in my thesis, in the literature review section. I would very much like to include some figures from your work as it is very related to the work I am doing.

Thanks for your time,

Chris



**COPYRIGHT RELEASE FORM**

Humanetics Innovative Solutions Inc., the copyright owner, acknowledges and grants to University of Waterloo the one-time usage of requested photos/illustrations/images/logo in masters dissertation that was requested by Christopher Pastula following that:

- 1) Humanetics logo/trademark is visibly embedded in the requested photos/illustrations/images/logo

OR

- 2) Clearly reference Humanetics as the credit for the photos/illustrations/images/logo used.

These photos/illustrations/images/logo maybe only be used for the purpose requested. Use of the Humanetics images or logo is prohibited without prior written permission from the Marketing Department of Humanetics.

Print Name: Christopher Pastula Date: June 19, 2022

Signature: 

[humaneticsatd.com](http://humaneticsatd.com)

Humanetics Headquarters  
23300 Haggerty Road | Farmington Hills | MI 48335 USA  
T +1 248 778 2000 | F +1 248 778 2001

**HUMANETICS GROUP**

## References

- [1] Statistics Canada, "Monthly Passenger Bus and Urban Transit Survey (MBUS)," North American Industry Classification System (NAICS), [Online]. Available: <https://www23.statcan.gc.ca/imdb/p2SV.pl?Function=getSurvey&SDDS=2745>.
- [2] U.S. Department of Transportation Federal Transit Administration, *Public Transportation's Role in Responding to Climate Change*, 2010.
- [3] Clean Energy Canada, the David Suzuki Foundation, Environmental Defence, Équiterre, Pembina Institute, *Reducing GHG Emissions in Canada's Transportation Sector*, 2016.
- [4] Transportation Safety Board of Canada, "Railway Investigation Report R13T0192," Ottawa, 2015.
- [5] Ottawa Police, "OC Transpo Bus Crash," 2021. [Online]. Available: <https://www.ottawapolice.ca/en/annual-report-2019/oc-transpo-bus-crash.aspx>.
- [6] G. C. Giovanni Belingardi, "Vehicle Crashworthiness Design-General Principles and Potentialities of Composite Material Structures," in *Impact Engineering of Composite Structures*, 2011.
- [7] World Health Organization, "Global Status Report on Road Safety," 2018.
- [8] "Government of Canada Justice Laws Website," [Online]. Available: [https://laws-lois.justice.gc.ca/eng/regulations/c.r.c.,\\_c.\\_1038/FullText.html](https://laws-lois.justice.gc.ca/eng/regulations/c.r.c.,_c._1038/FullText.html).
- [9] U. S. G. P. Office, "Nat'l Highway Traffic Safety Admin., DOT, 571.208 Standard No. 208; Occupant crash protection".
- [10] K. T. A. B. M. D. F. G. Suzanne Tylko, "Interim Report Transit Bus Research," Transport Canada, 2020.
- [11] A. D. G. G. P. Salvatore Cafiso, "Using the Delphi method to evaluate opinions of public transport managers on bus safety," *Safety Science*, 2012.
- [12] J. A. Sgro, "Bus Passenger Safety," 2019.

- [13] Center for Urban Transportation Research, "Crashworthiness/Crash Energy Management for Bus," Federal Transit Administration.
- [14] T. F. London, "The Mayor's Transport Strategy," [Online]. Available: <https://tfl.gov.uk/corporate/about-tfl/the-mayors-transport-strategy#on-this-page-0>.
- [15] N. C. Database, "Canada Road User Fatalities 2016 2017," [Online]. Available: <https://wwwapps2.tc.gc.ca/Saf-Sec-Sur/7/NCDB-BNDC/p.aspx?l=en&wk=12#o106>.
- [16] Transport Canada, "Canadian Motor Vehicle Traffic Collision Statistics: 2019," 2019.
- [17] F. T. Administration, "Federal Transit Administration Safety and Security Time Series Data," [Online]. Available: <https://www.transit.dot.gov/ntd/data-product/safety-security-time-series-data>.
- [18] I. Savage, "Comparing the fatality risks in United States transportation across modes and over time," *Research in Transportation Economics*, vol. 43, pp. 9-22, 2013.
- [19] International Railway Safety Council, "Safety Statistics," [Online]. Available: <https://international-railway-safety-council.com/safety-statistics/>.
- [20] New York City Department of Transportation, "Pedestrian Safety Study & Action Plan," 2010.
- [21] A. B. S. O. V. K. R. K. N. H. M. M. S. H. I. K. Alix Edwards, "Analysis of bus collisions and identification of countermeasures," Transport for London, 2018.
- [22] E. Hildebrand, "Benchmarking Canadian, American and Australian Bus Safety," in *Canadian Multidisciplinary Road Safety Conference*, London, Ontario, 2001.
- [23] P. O. Noah Goodall, "Evaluation of a Transit Bus Collision Avoidance Warning System in Virginia," 2022.
- [24] A. D. P. L. J. B. E. W. Denise Kendrick, "Systematic review of the epidemiology of non-collision injuries occurring to older people during use of public buses in high income countries," *Journal of Transport and Health*, 2015.
- [25] The Federal Transit Administration, "Bus Occupant Safety: A Synthesis of Transit Practice (TCRP Synthesis 18)," 1996.

- [26] M. S. D. A. P. S. R. B. P Halpern, "Non-collision injuries in public buses: a national survey of a neglected problem," *Emergency Medicine*, pp. 108-110, 2005.
- [27] R. G. R. B. Alan Kirk, "Passenger Casualties in Non-Collision Incidents on Buses and Coaches in Great Britain".
- [28] A. E. J. A. D. B. Mervyn Edwards, "Banging heads onboard buses: Assessment scheme to improve injury mitigation for bus passengers," *Traffic Injury Prevention*, vol. 20, pp. 571-577, 2019.
- [29] National Institute for Aviation Research, "Mass Transit Crashworthiness Statistical Data Analysis," 2005.
- [30] Transport For London, *Bus Safety Roadmap for New Build Buses*.
- [31] Transport For London, "Bus Safety Standard Executive Summary," London, 2018.
- [32] L. B. N. S. A. M. Jo Barnes, "Research into the safety of London Bus Passengers," Transport Safety Research Centre, 2019.
- [33] S. R. K. R. D. V. Gulshan Noorumar, "Mathematical models for assessment of vehicle crashworthiness: a review," *International Journal of Crashworthiness*, 2021.
- [34] National Academies of Sciences, Procedures for verification and validation of computer simulations used to roadside safety applications, Washington DC: The National Academies Press.
- [35] C. Thunert, *CORApus Release 4.0.4 User's Manual*, 2017.
- [36] J. K. M. W. J Foster, "Hybrid III- A Biomechanically Based Crash Test Dummy 770938".
- [37] Ansys, "Download LST, LLC Barrier, Dummy, and Tire Models for LS-DYNA," 2020. [Online]. Available: [https://www.lstc.com/download/dummy\\_models](https://www.lstc.com/download/dummy_models).
- [38] S. Guha, *LSTC Detailed Hybrid III 5th Dummy Positioning & Post-Processing*, 2011.
- [39] Humanetics, "Hybrid III 50th Male," 2020. [Online]. Available: <https://humanetics.humaneticsgroup.com/products/anthropomorphic-test-devices/frontal-impact/hybrid-iii-50th-male/hybrid-iii-50th-male>.

- [40] M. S.-G. J. C. Dipan Bose, "Vulnerability of Female Drivers Involved in Motor Vehicle Crashes: An Analysis of US Population at Risk," *American Journal of Public Health*, 2011.
- [41] T. B. E. O. Anne Looker, "Does Body Size Account for Gender Differences in Femur Bone Density and Geometry?," *Journal of Bone and Mineral Research*, 2001.
- [42] K. Z. M. R. J.-T. W. M. N. C.-H. L. Jingwen Hu, "Frontal crash simulations using parametric human models representing a diverse population," *Traffic Injury Prevention*, 2019.
- [43] J. M. Craig Newgard, "Differences in the Effectiveness of Frontal Air Bags by Body Size Among Adults Involved in Motor Vehicle Crashes," *Traffic Injury Prevention*.
- [44] D. R. Bruce Donnelly, "Comparison of Cadaver and Hybrid III Dummy Response to Axial Impacts of the Femur," 872204.
- [45] H. Mertz, "Biofidelity of the Hybrid III Head," *SAE Technical Paper Series*, 851245.
- [46] A. R. K. M. L. M. C. T. F. C. L. Stephanie M. Beeman, "Occupant kinematics in low-speed frontal sled tests: Human volunteers, Hybrid III ATD, and PMHS," *Accident Analysis and Prevention*, pp. 128-139, 2012.
- [47] J. K. G. N. G. K. Venkatesh Agaram, "Hybrid III Dummy Neck Response to Air Bag Loading".
- [48] J. M. Alan Nahum, *Accidental Injury Biomechanics and Prevention Second Edition*.
- [49] A. R. R. M. Dimitrios Kallieris, "The Biofidelity of Hybrid III Dummies".
- [50] D. S. A. N. Charles Kroell, "Impact Tolerance and Response of the Human Thorax," 710851.
- [51] R. Neathery, "Analysis of Chest Impact Response Data and Scaled Performance Recommendations".
- [52] D. L. R. K. J. C. Greg Shaw, "Dummy Torso Response to Anterior Quasi-Static Loading".
- [53] J. M. D. V. H. M. John Horsch, "Thoracic Injury Assessment of Belt Restraint Systems Based on Hybrid III Chest Compression," *Stapp Car Crash Journal* 912895.
- [54] Association for the Advancement of Automotive Medicine, "Abbreviated Injury Scale 2005 Update 2008," Barrington, 2008.

- [55] H. M. Priya Prasad, "The position of the United States Delegation to the ISO Working Group 6 on the Use of HIC in the Automotive Environment," 1985.
- [56] A. L. I. P. P. Harold J. Mertz, "Biomechanical and Scaling Basis for Frontal and Side Impact Injury Assessment Reference Values," *Stapp Car Crash Journal*, vol. 60, 2003.
- [57] S. G. V. N. F. C. G Virzi Mariotti, "Head Injury Criterion: Mini Review," *American Journal of Biomedical Science & Research*, 2019.
- [58] V. H. L. M. T. G. N. H.J. Mertz, "An assesment of Compressive Neck Loads Under Injury-Producing COnditions," *The Physician and SPortsmedicine*, 1978.
- [59] L. P. H.J. Mertz, "Strength and Response of the Human Neck," *Fifteenth Stapp Car Crash Conference*, 1971.
- [60] E. S. F. B. M. H. N. K. M. M. Rolf Eppinger, "Development of Improved Injury Criteria for the Assesment of Advanced Automotive Restraint Systems-II," 1999.
- [61] B. F. David Meckman, "Mechanics of Cardiothoracic Injury in Primates," *The Journal of Trauma*, 1972.
- [62] I. L. David Viano, "A Viscous Tolerance Criterion for SOft Tissue Injury Assessment," 1987.
- [63] M. C. K. M. J. M. V. H. Erik Takhounts, "Development of Brain Injury Criteria (BrIC)," *Stapp Car Crash Journal*, 2013.
- [64] S. H. K. P. G. L. M. F. P. W. Tony Laituri, "New Risk Curves for NHTSA's Brai Injury Criterion (BrIC): Derivations and Assessments," *Stapp Car Crash Journal*, vol. 60, pp. 301-362, 2016.
- [65] D. Hampson, "Facial Injury: A Review of Biomechanical Studies and Test Precedures for Facial Injury Assessment," *Journal of Biomechanics*, vol. 28, pp. 1-7, 1995.
- [66] J. C. S. G. A. K. Gerald Nyquist, "Facial Impact Tolerance and Response".
- [67] C. W. M. W. D. S. A. N. Douglas Allsop, "Facial Impact Responses-A Comparison of the Hybrid III Dummy and Human Cadaver".



- [68] A. N. D. Schneider, "Impact Studies of Facial Bones and Skull," in *Sixteenth Stapp Car Crash Conference*, 1972.
- [69] C. W. S. M. T. R. V. C. F. B. Ray Daniel, "Fracture Injury Risk of the Restrained Mandible to Anterior-Posterior Blunt Impacts," *Journal of Biomechanical Engineering*, 2021.
- [70] F. P. W. S. O. K. Norbert Kleinsasser, "External trauma to the larynx: classification, diagnosis, therapy," *Laryngology*, vol. 257, pp. 439-444, 2000.
- [71] G. W. S. C. N. M. Jeff Mandel, "Transglottic high frequency jet ventilation for management of laryngeal fracture associated with air bag deployment injury," *Journal of Clinical Anesthesia*, vol. 20, pp. 369-371, 2008.
- [72] R. S. L. T. N. O. J.W. Melvin, "Response of Human Larynx to Blunt Loading," *STAPP*, 1973.
- [73] F. M. Melvin Butler, "The Padded Dash Syndrome: Blunt Trauma to the Larynx and Trachea," in *Meeting of the Western Section, American Laryngological Rhinological and Otolological Society*, Pomona, California, 1968.
- [74] A. S. Alan Nahum, "Biodynamics of Injury to the Larynx in Automobile Collisions," 1968.
- [75] J. M. Donald Huelke, "Anatomy, Injury Frequency, Biomechanics, and Human Tolerance," 1979.
- [76] M. H. H. M. Britta Bockholdt, "Experimental investigations of fracture of the upper thyroid horns," *Legal Medicine*, pp. 252-255, 2003.
- [77] J. G. C. G. J. D. Alan Nahum, "Impact Tolerance of the Skull and Face".
- [78] C. C. C. A. M. N. C. W. Gadd, "A Study of Responses and Tolerances of the Neck".
- [79] M. C. K. M. Daniel Parent, "Biofidelity Evaluation of the THOR and Hybrid III 50th Percentile Male Frontal Impact Anthropomorphic Test Devices," *Stapp Car Crash Journal*, vol. 61, pp. 227-276, 2017.
- [80] S. H. K. Y. M. G. Yuichi Kitagawa, "Occupant Kinematics in Simulated Autonomous Driving Vehicle Collisions: Influence of Seating Position, Direction and Angle," *Stapp Car Crash Journal*, vol. 61, pp. 101-155, 2017.

- [81] Leanport, "Global Human Body Models Consortium," 2016. [Online]. Available: <http://www.ghbmc.com/>.
- [82] D. M. N. V. A. R. J. S. Scott Gayzik, "Development of the Global Human Body Models Consortium Mid-Sized Male Full Body Model," in *Injury Biomechanics Research*.
- [83] G. T. D. O. C. S. Alejandro Palacio, "Non-collision injuries in urban buses-Strategies for prevention," *Accident Analysis and Prevention*, 2007.
- [84] L. Global Human Body Models Consortium, *User Manual: M50 Occupant Version 4.3 for LS-DYNA*, Winston-Salem: Elemence, 2014.
- [85] T. G. Ayub Ommaya, "Cerebral Concussion and Traumatic Unconsciousness," *Brain*, 1974.
- [86] E. C. A. B. E. C. G. A. Dominique Debanne, "Axon Injury," *Physiol Rev*, pp. 555-602, 2011.
- [87] D. M. W. S. Douglas Smith, "Diffuse Axonal Injury in Head Trauma," *J Head Trauma Rehabil*, pp. 307-316, 2003.
- [88] I. C. E. P. L. Z. A. K. K. Y. David Viano, "Concussion in Professional Football: Brain Responses By Finite Element Analysis: Part 9," *Neurosurgery*, 2005.
- [89] L. C. W. M. C. Y. K. L. a. R. H. J. R. L. G. A. G. S. K. D. C. Fidel Hernandez, "Six Degree-of-Freedom Measurements of Human Mild Traumatic Brain Injury," *Annals of Biomedical Engineering*, 2014.
- [90] W. Z. S. J. A. G. A. R. P. B. J. J. C. T. W. M. J. J. C. S. M. D. S. R. S. P. B. K. M. G. J. P. M. S. A. B. S. Jonathan G. Beckwith, "Estimated Brain Tissue Response Following Impacts Associated With and Without Diagnosed Concussion," *Annals of Biomedical Engineering*, vol. 46, pp. 819-830, 2018.
- [91] A. S. M. S. K. Declan A. Patton, "The Biomechanical Determinants of COncussion: Finite Element Simulations to Investigate Brain Tissue Deformation During Sporting Impacts to the Unprotected Head," *Journal of Applied Biomechanics*, pp. 721-730, 2013.
- [92] Z. Y. C. G. U. M. J. I. B. D. E. V. J. V. S. Nele Famaey, "Structural and mechanical characterisation of bridging veins: A review," *Journal of the Mechanical Behaviour of Biomedical Materials*, 2014.

- [93] L. T. Thomas Gennarelli, "Biomechanics of Acute Subdural Hematoma," *The Journal of Trauma*, 1982.
- [94] J. G. P. V. J. V. S. G. V. d. P. H. A. I. V. D. B. Hans Delye, "Biomechanical Properties of the Superior Sagittal Sinus-Bridging Vein Complex," *Stapp Car Crash Journal*, vol. Vol. 50, pp. 625-636, 2006.
- [95] G. U. M. A. M. P.-W. H. R. S. P. D. N. F. J. V. S. a. B. D. Dries De Kegel, "Investigation of tissue level tolerance for cerebral contusion in a controlled cortical impact porcine model," *Traffic Injury Prevention*, vol. 22, pp. 616-622, 2021.
- [96] R. W. S. Alan M. Nahum, "An Experimental Model for Closed Head Impact Injury".
- [97] R. S. C. W. Alan Nahum, "Intracranial Pressure Dynamics During Head Impact".
- [98] M. C. A. N. Carley Ward, "Intracranial Pressure-A Brain Injury Criterion," 1980.
- [99] S. K. F. P. Narayan Yoganandan, "Biomechanics of the cervical spine Part 2. Cervical spine soft tissue responses and biomechanical modeling," *Clinical Biomechanics*, 2001.
- [100] J. M. N. C. D. C. Stephen Mattucci, "Strain rate dependent properties of younger human cervical spine ligaments," *Journal of the Mechanical Behaviour of Biomedical Materials*, 2012.
- [101] D. C. Stephen Mattucci, "A method to characterize average cervical spine ligament response based on raw data sets for implementation into injury biomechanics models," *Journal of Mechanical Behaviour of Biomedical Materials*, 2014.
- [102] D. S. C. Jennifer A. DeWit, "Cervical spine segment finite element model for traumatic injury prediction," *Journal of The Mechanical Behaviour of Biomedical Materials*, pp. 138-150, 2012.
- [103] P. D. Ego Seeman, "Bone Quality - The Material and Structural Basis of Bone Strength and Fragility," *The New England Journal of Medicine*, 2006.
- [104] G. L. V. E. A. Z. Nop Willems, "The microstructural and biomechanical development of the condylar bone: a review," *European Journal of Orthodontics*, 2014.
- [105] MORR Transportation Consulting Ltd., "An Analysis of Transit Bus Axle Weight Issues," Winnipeg, 2014.

- [106] Official Journal of the European Union, "Regulation No. 80 of the Economic Commission for Europe of the United Nations (UN/ECE)," 2013.
- [107] Z. T. Sandor Vineze-Pap, "Simulations of bus-seat impact tests according to ECE regulations".
- [108] L. R. Catherine Marciniak, "Grafton and Kempsey bus crashes remembered 30 years after the tragedies," ABC North Coast, 19 October 2019. [Online]. Available: <https://www.abc.net.au/news/2019-10-20/kempsey-and-grafton-bus-crashed-30-years-on/11614914>. [Accessed 2022].
- [109] Federal Register of Legislative Instruments, "Vehicle Standard (Australian Design Rule 68/00-Occupant Protection in Buses) 2006," 2006.
- [110] American Public Transit Association, *Standard Bus Procurement Guidelines*.
- [111] Bus Testing and Research Center, "Altoona Bus Testing and Research Center Test Bus Procedure: Safety-A Double-Lane Change (Obstacle Avoidance Test)".
- [112] Bus Testing and Research Center, "Altoona Bus Testing and Research Center Test Bus Procedure," [Online]. Available: <https://www.altoonabustest.psu.edu/bus-tests/Safety.aspx>.
- [113] S. S. Kumbhar, *Development of a finite element model and analysis of a rear impact scenario of a low floor mass transit bus*, MASC Thesis, Wichita State University, 2002.
- [114] A. U. Joshi, *Finite Element Modeling of Low Floor Mass Transit Bus and Analysis of Frontal Impact Scenarios*, MASC Thesis, Whichita State University, 2003.
- [115] H. S. H. H. Erich Mayrhofer, "Enhanced Coach and Bus Occupant Safety".
- [116] G. Olivares, "Crashworthiness Evaluation of Mass Transit Buses," 2012.
- [117] S. Thokade, *Passenger Safety in Real-Life Crash Scenarios of Mass Transit Buses*, 2004.
- [118] V. Y. Gerardo Olivares, "Injury Mechanisms to Mass Transit Bus Passengers During Frontal, Side and Rear Impact Crash Scenarios," *NIAR, Wichita State University*, 2009.
- [119] M. E. M. d. L.-O. E. A. R. T. Luis Martinez, "Adult and Child dummies test for safety assesment of occupants in urban bus collisions," 2017.

- [120] J. B. Linda McCray, "Child Safety Research in School Buses".
- [121] National Safety Council, "School Bus," [Online]. Available: <https://injuryfacts.nsc.org/motor-vehicle/road-users/school-bus/>.
- [122] D. N. M. L. Peter Lapner, "Analysis of a school bus collision: mechanism of injury in the unrestrained child," *Canadian Journal of Surgery*, p. 269, 2003.
- [123] Task Force on School Bus Safety, "Strengthening School Bus Safety in Canada," 2020.
- [124] F. M. V. S. Standards, "49 CFR § 571.222 - Standard No. 222; School bus passenger seating and crash protection.," [Online]. Available: <https://www.law.cornell.edu/cfr/text/49/571.222>.
- [125] C. V. B. S. Kevin Chang, "Schhol Bus Safety: Evaluating the Evolution of Compartmentalization and Seat Belt Restraints," *Journal of the Transportation Research Board*.
- [126] L. S. L. M. Jeffrey Elias, "Large school bus safety restraint evaluation," National Highway Traffic Safety Administration.
- [127] L. S. L. M. Jeffrey C. Elias, "Large school bus safety restraint evaluation-Phase II," National Highway Traffic Safety Administration.
- [128] L. J. B. C. S. L. A. B. S. S. Kristin Bolte, "Simulations of Large School Bus Crashes," *SAE Technical Paper Series*, 2000.
- [129] H. G. J. Z. Y. Z. Zhigang Li, "The necessity of evaluating child neck injury in frontal collision of school bus for transportation safety," *Safety Science*, 2013.
- [130] R. L. H. Z. N. J. G. F. X. Q. Zhigang Li, "Development of a school bus restraint system model and its application in the evaluation of designed protective strategies on child neck injury in front-end crash," *International Journal of Crashworthiness*, 2020.
- [131] National Traffic Highway Safety Administration, "NHTSA's Approach to Motorcoach Safety," 2007.
- [132] I. T. Anton Kuznetcov, "Influence of non-standard seating postures on safety of motorcoach," *Safety Science*, 2019.

- [133] I. T. Anton Kuznetcov, "Effect of acceleration pulse shape on the safety of unbelted motorcoach passengers in frontal collision under uncertainty of their seating posture," *International Journal of Crashworthiness*, vol. 25, pp. 231-241, 2020.
- [134] I. T. C. Q. W. Anton Kuznetov, "Numerical parametric study affecting passenger safety in motorcoach frontal collision," *International Journal of Crashworthiness*, pp. 214-226, 2017.
- [135] T. S. P. Z. F. H. E. M. M. R. Qian Peng, "Occupant injury risk assesment and protective measures in frontal collision of a bus," *Interantional Journal of Crashworthiness*, vol. 24, pp. 429-441, 2019.
- [136] National Highway Traffic Safety Administration, "NHTSA's Motorcoach Safety Research Crash, Sled, and Static Tests," 2010.
- [137] Department of Transportation, National Highway Traffic Safety Administration, "49 CFR Part 571 Docket No. NHTSA-2010-0112 RIN 2127-AK56 Federal Motor Vehicle Safety Standards; Motorcoach Definition; Occupant Crash Protection," 2009.
- [138] Government of Canada, "Transport Canada to make seat belts mandatory on highway buses," 11 July 2018. [Online]. Available: <https://www.canada.ca/en/transport-canada/news/2018/07/transport-canada-to-make-seat-belts-mandatory-on-highway-buses.html>. [Accessed 2022].
- [139] International Transit Studies Program, "Rail Passenger Safety: Equipment and technologies," 2006.
- [140] S. W. Guangjun Gao, "Crashworthiness of passenger rail vehicles: a review," *International Journal of Crashworthiness*, vol. 24, pp. 664-676, 2019.
- [141] H. T. Suchao Xie, "Dynamic simulation of railway vehicle occupants under secondary impact," *Vehicle System Dynamics*, 2013.
- [142] J. A. J. M. M. Carvalho, "Implications of the inline seating layout on the protection of occupants of railway coach interiors," 2011.
- [143] G. L. A. S. Francesco Caputo, "On the evaluation of the overloads coming from the use of seat-belts on a passenger railway seat," *International Journal Mechanical Material Description*, 2012.

- [144] L. Z. Liang Wei, "Evaluation and improvement of crashworthiness for high-speed train seats," *Interantional Journal of Crashworthiness*, 2018.
- [145] F. R. P. D. H. M. C. L. Audrey Hault-Dubrulle, "Analysis of train driver protection in rail collisions: Part I. Evaluation of injury outcome for train driver in desk impact," 2013.
- [146] F. R. P. D. H. M. C. L. L. Audrey Hault-Dubrulle, "Analysis of train driver protection in rail collisions: Part II. Design of a desk with improved crashworthiness performance," 2013.
- [147] US Department of Transportation Federal Railroad Administration, "Single Passenger Rail Car Impact Test Volume II: Summary of Occupant Protection Program," 2000.
- [148] K. Krishan, *Occupant-Seat Contact Pressure Characteristics of Polyurethane Foam Seats using Explicit Finite-Element Analyses*, 2017.
- [149] A. S. W. A. E.-M. M. Mohamed, *Friction Coefficient of Rubber Shoe Soles Sliding Against Ceramic Flooring*, KGK Rubberpoint, 2011.
- [150] G. O. V. C. B. B. Jeremy Cummings, "Occupant Friction Coefficients on Various COmbinations of Seat and Clothing," *SAE International*, 2009.
- [151] SAE, "Instrumentation for impact test-Part 1-Electronin Instrumentation," 2007.
- [152] A. C. S. M. R. G. V. N. Dhaval Jani, "Repositioning Human Body Lower Extremity FE Model," *SAE International*, 2009.
- [153] L. Zhu, *Development of Guidelines for Deformable and Rigid Switch in Ls-Dyna Simulation*, 2009.
- [154] D. M. S. G. J. S. Nicholas White, "Cross-sectional neck response of a total human body FE mdoel during simulated frontal and side automobile impacts," *Computer methods in Biomechanics and Biomedical Engineering*, vol. 18, pp. 293-315, 2013.
- [155] D. C. Donata Gierczycka, "Occupant thorax response variations due to arm position and restraint systems in side impact crash scenarios," *Accident Analysis and Preventuon*, vol. 106, pp. 173-180, 2017.
- [156] K. Z. X. L. L. Y. Libo Cao, "Improvement and Validation of Hybrid III Dummy Knee Finite Element Model," *SAE International*, 2015.

- [157] C. B. R. K. S. M. M. D. S. L. R. R. B. F. L. D. Robert Salzar, "Development of Injury Criteria for Pelvis Fracture in Frontal Crashes," *Traffic Injury Prevention*, pp. 299-305, 2006.
- [158] S. K. P. O. S. G. M. S.-D. F. H. A. L. Stefan Schulz-Drost, "Fractures of the manubrium sterni: treatment options and a possible classification of different types of fractures," *Journal of Thoracic Disease*, 2018.
- [159] S. Z. S. B. H.-P. S. G. W. C. W. Max Scheyerer, "Location of Sternal Fractures as a Possible Marker for Associated Injuries," *Emergency Medicine International*, 2013.
- [160] D. L. J. A. J. P. T. M. M. S. J. C. Greg Shaw, "Small female rib cage fracture in frontal sled tests," *Traffic Injury Prevention*, 2017.
- [161] C. C. D. C. G. T. R. C. Vishal Bansal, "Rib and sternum fractures in the elderly and extreme elderly following motor vehicle crashes," *Accident Analysis and Prevention*, 2010.
- [162] F. P. M. S. J. M. D. M. Narayan Yognandan, "Comparison of Head-Neck Responses in Frontal Impacts Using Restrained Human Surrogates," *Annals of Advances in Automotive Medicine*, 2011.
- [163] D. C. M. P. Jason Fice, "Cervical Spine Model to Predict Capsular Ligament Response in Rear Impact," *Annals of Biomedical Engineering*, pp. 2152-2162, 2011.
- [164] D. M. S. G. J. S. Nicholas White, "Cross-sectional neck response of a total human body FE model during simulated frontal and side automobile impacts," *Computer Methods in Biomechanics and Biomedical Engineering*, 2015.
- [165] B. K. S. G. Dale Johnson, "Comparison of Neck Injury Criteria Values Across Human Body Models of Varying Complexity," *frontiers in Bioengineering and biotechnology*, 2020.
- [166] J. G. J. S. S. G. A. W. J. S. Derek Jones, "Head injury metric response in finite element ATDs and a human body in multidirectional loading regimes," *Traffic Injury Prevention*, 2019.
- [167] S. T. P. R. F. T. M. S. Kristian Holmqvist, "Heavy vehicle frontal sled crash test analysis-chest deflection response in the Hybrid III dummy," *International Journal of Crashworthiness*, 2013.
- [168] J. D. M. M.-V. P. R. M. S. S. T. F. T. Kristian Holmqvist, "Improving Hybrid III Injury Assessment in Steering Wheel Rim to Chest Impacts Using Responses from Finite Element Hybrid III and Human Model," *Traffic Injury Prevention*, 2014.



- [169] B. K. J. S. S. G. Mathew Davis, "Development and Full Body Validation of a 5th Percentile Female Finite Element Model," *Stapp Car Crash Journal*, 2016.
- [170] K. D. S. G. J. S. Nicholas White, "Head and Neck Response of a Finite Element Anthropomorphic Test Device and Human Body Model During a Simulated Rotary-Wing Aircraft Impact," *Journal of Biomechanical Engineering*, 2014.
- [171] E. K. C. M. S. M. J. S. S. D. A. Kemper, "Reducing Chest Injuries in Automobile Collisions: Rib Fracture Timing and Implications for Thoracic Injury Criteria," *Journal of Biomedical Engineering*, 2011.
- [172] H. T. Suchao Xie, "Dynamic simulation of railway vehicle occupants under secondary impacts," *Vehicle System Dynamics*, 2013.
- [173] D. V. A. K. Cynthia Bir, "Development of biomechanical response corridors of the thorax to blunt ballistic impacts," *Journal of Biomechanics*, 2004.
- [174] D. P. S. P. D. L. J. C. R. K. H. G. Greg Shaw, "Impact Response of Restrained PMHS in Frontal Sled Tests: Skeletal Deformation Patterns Under Seat Belt Loading," *Stapp Car Crash Journal*, 2009.
- [175] American Public Transportation Association, "Who Rides Public Transportation," 2017.

# Appendices

## Appendix A: Highspeed Video Comparison with Models for Test Cases #2 - #8 Test Case #2a (6.5g Pulse, Reclined Posture, Inboard Seat)

50<sup>th</sup> Percentile HIII

122 ms



197 ms



272 ms



347 ms



5<sup>th</sup> Percentile HIII

122 ms



197 ms



272 ms



347 ms



**Test Case #2b (6.5g Pulse, Reclined Posture, Inboard Seat)**

**50<sup>th</sup> Percentile HIII**

122 ms



197 ms



272 ms



347 ms



**5<sup>th</sup> Percentile HIII**

122 ms



197 ms



272 ms



347 ms



**Test Case #2c (6.5g Pulse, Reclined Posture, Inboard Seat)**

50<sup>th</sup> Percentile HIII

5<sup>th</sup> Percentile HIII

122 ms

122 ms



197 ms

197 ms



272 ms

272 ms



347 ms

347 ms



**Test Case #3 (5.7g Pulse, Upright Posture, Inboard Seat)**

**50<sup>th</sup> Percentile HIII**

122 ms



197 ms



272 ms



347 ms



**5<sup>th</sup> Percentile HIII**

122 ms



197 ms



272 ms



347 ms



**Test Case #4 (6.5g Pulse, Upright Posture, Outboard Seat)**

**50<sup>th</sup> Percentile HIII**

**5<sup>th</sup> Percentile HIII**

122 ms

122 ms



197 ms

197 ms



272 ms

272 ms



347 ms

347 ms



**Test Case #5 (6.5g Pulse, Reclined Posture, Outboard Seat)**

**50<sup>th</sup> Percentile HIII**

**5<sup>th</sup> Percentile HIII**

122 ms

122 ms



197 ms

197 ms



272 ms

272 ms



347 ms

347 ms



# Test Case #6 (5.7g Pulse, Upright Posture, Outboard Seat)

## 50<sup>th</sup> Percentile HIII

122 ms



197 ms



272 ms



347 ms



## 5<sup>th</sup> Percentile HIII

122 ms



197 ms



272 ms



347 ms





**Test Case #7 (5.7g Pulse, Reclined Posture, Outboard Seat)**

**50<sup>th</sup> Percentile HIII**

122 ms



197 ms



272 ms



347 ms



**5<sup>th</sup> Percentile HIII**

122 ms



197 ms



272 ms



347 ms



**Test Case #8 (5.7g Pulse, Reclined Posture, Inboard Seat)**

**50<sup>th</sup> Percentile HIII**

122 ms



197 ms



272 ms



347 ms



**5<sup>th</sup> Percentile HIII**

122 ms



197 ms



272 ms



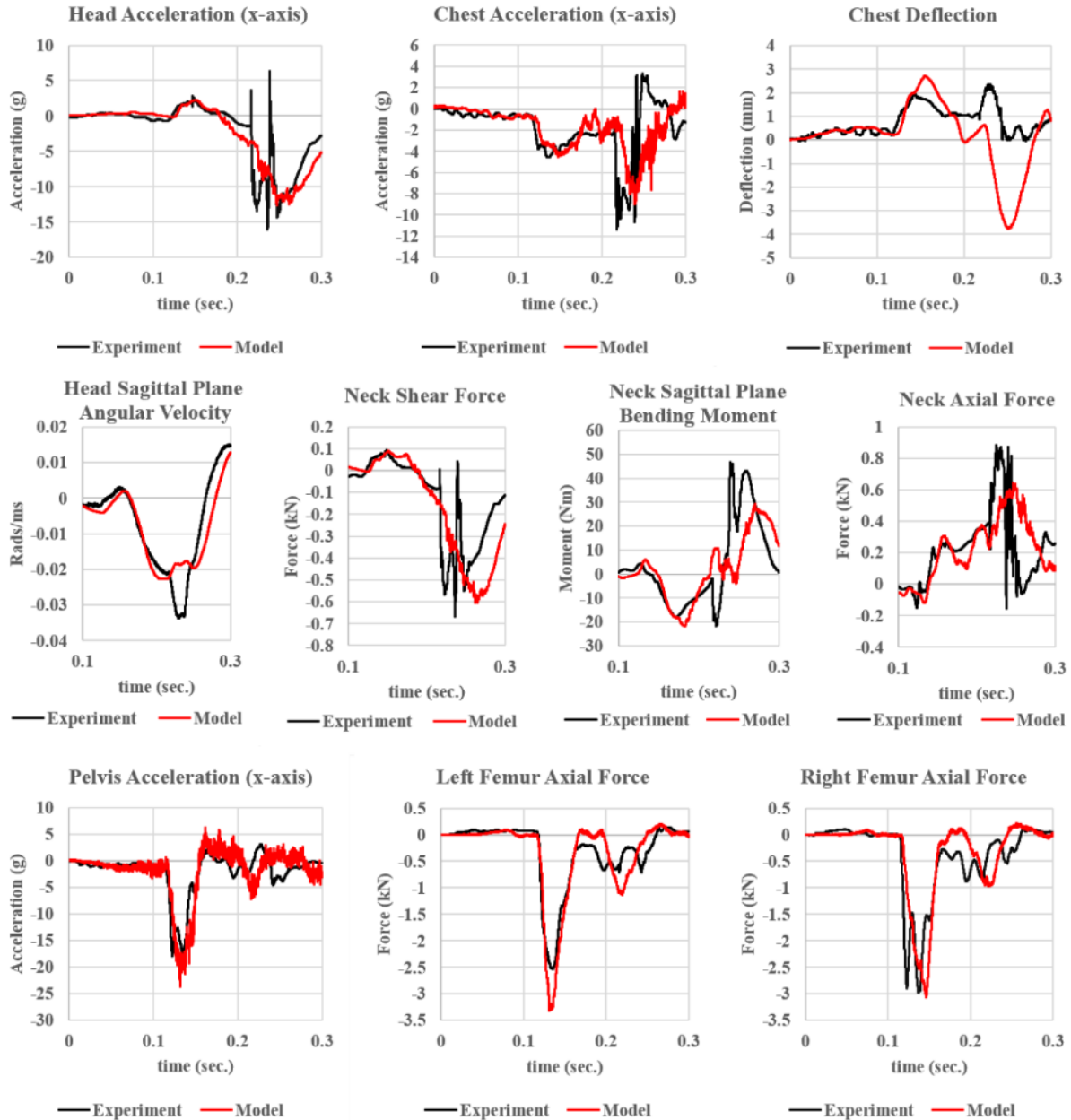
347 ms



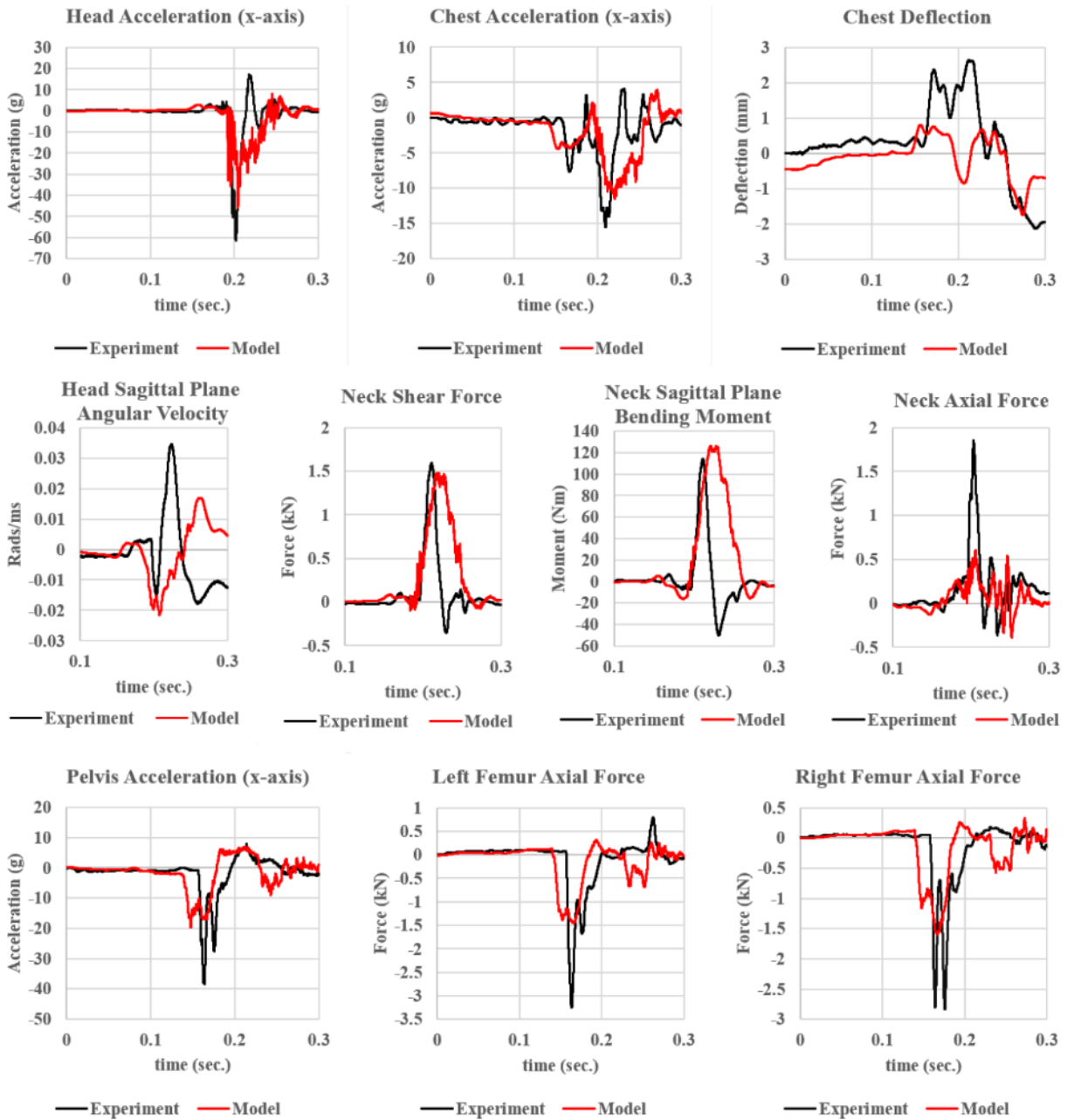
## Appendix B: Kinematic Trace Comparison Between Experiments and Models for Test Cases #2 - #8

### Test Case #2a (6.5g Pulse, Reclined Posture, Inboard Seat)

#### 50<sup>th</sup> Percentile HIII

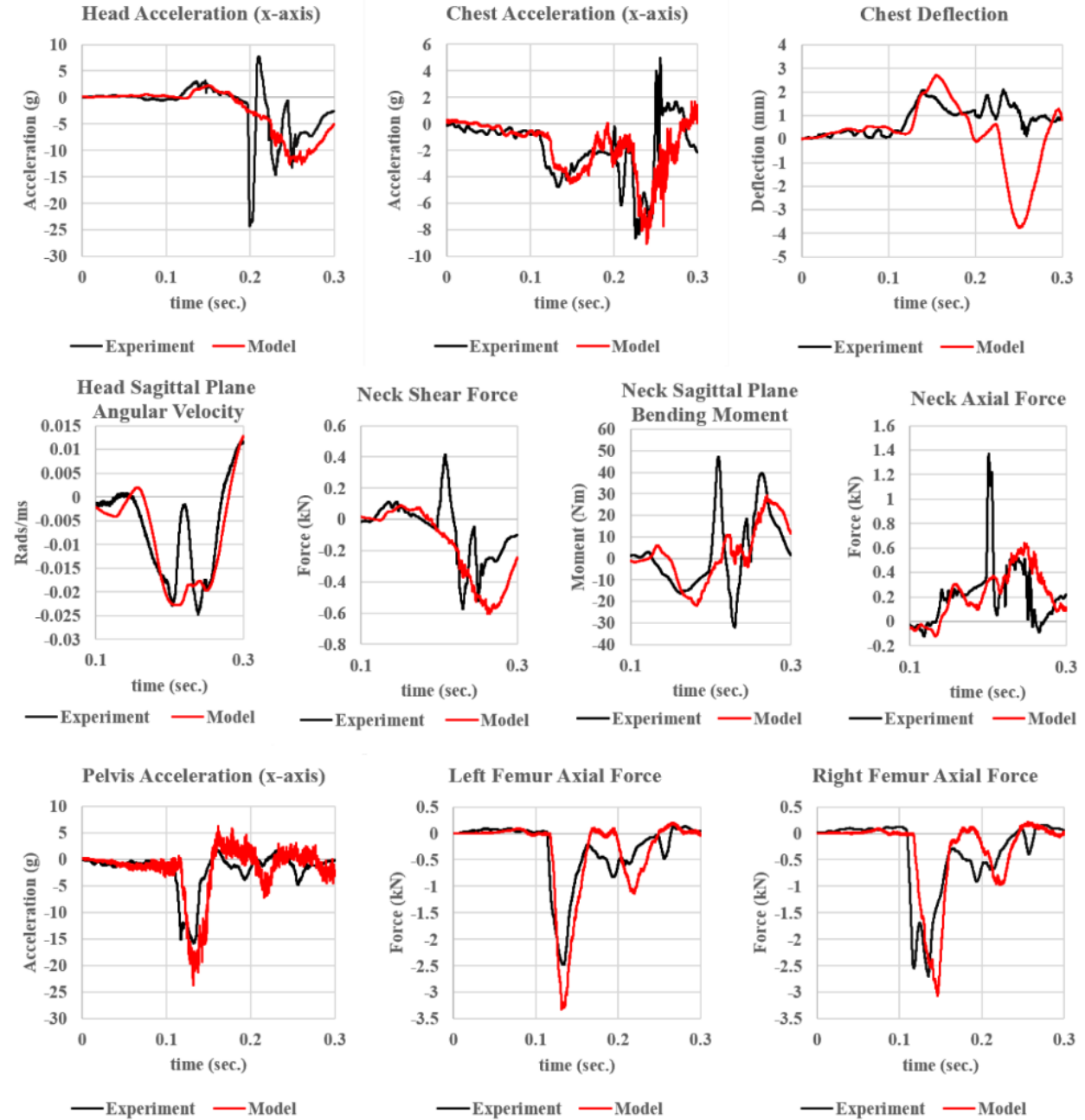


## 5<sup>th</sup> Percentile HIII

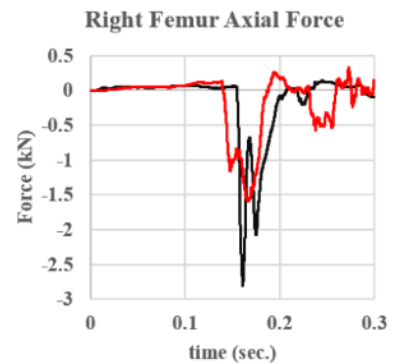
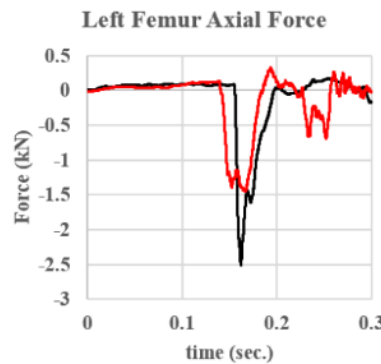
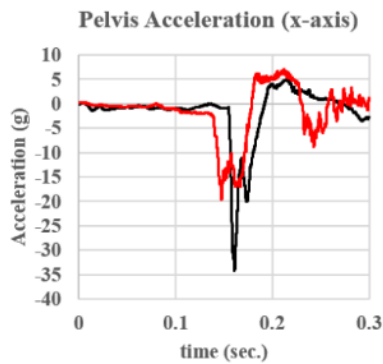
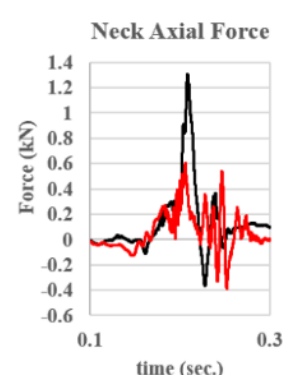
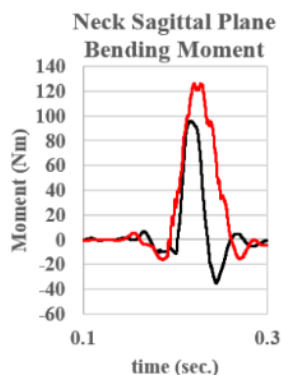
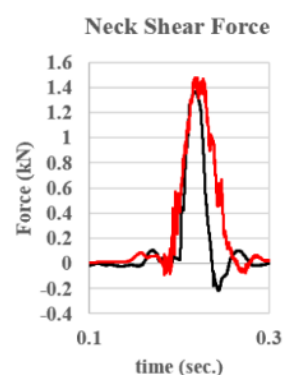
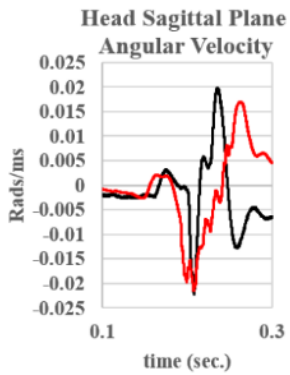
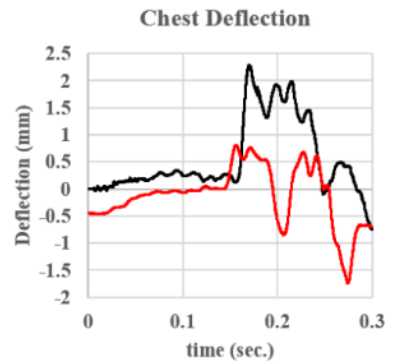
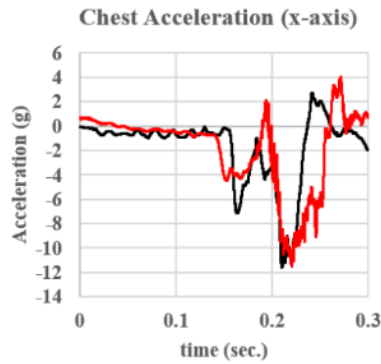
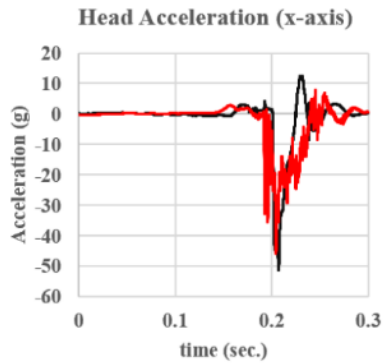


# Test Case #2b (6.5g Pulse, Reclined Posture, Inboard Seat)

## 50<sup>th</sup> Percentile HIII

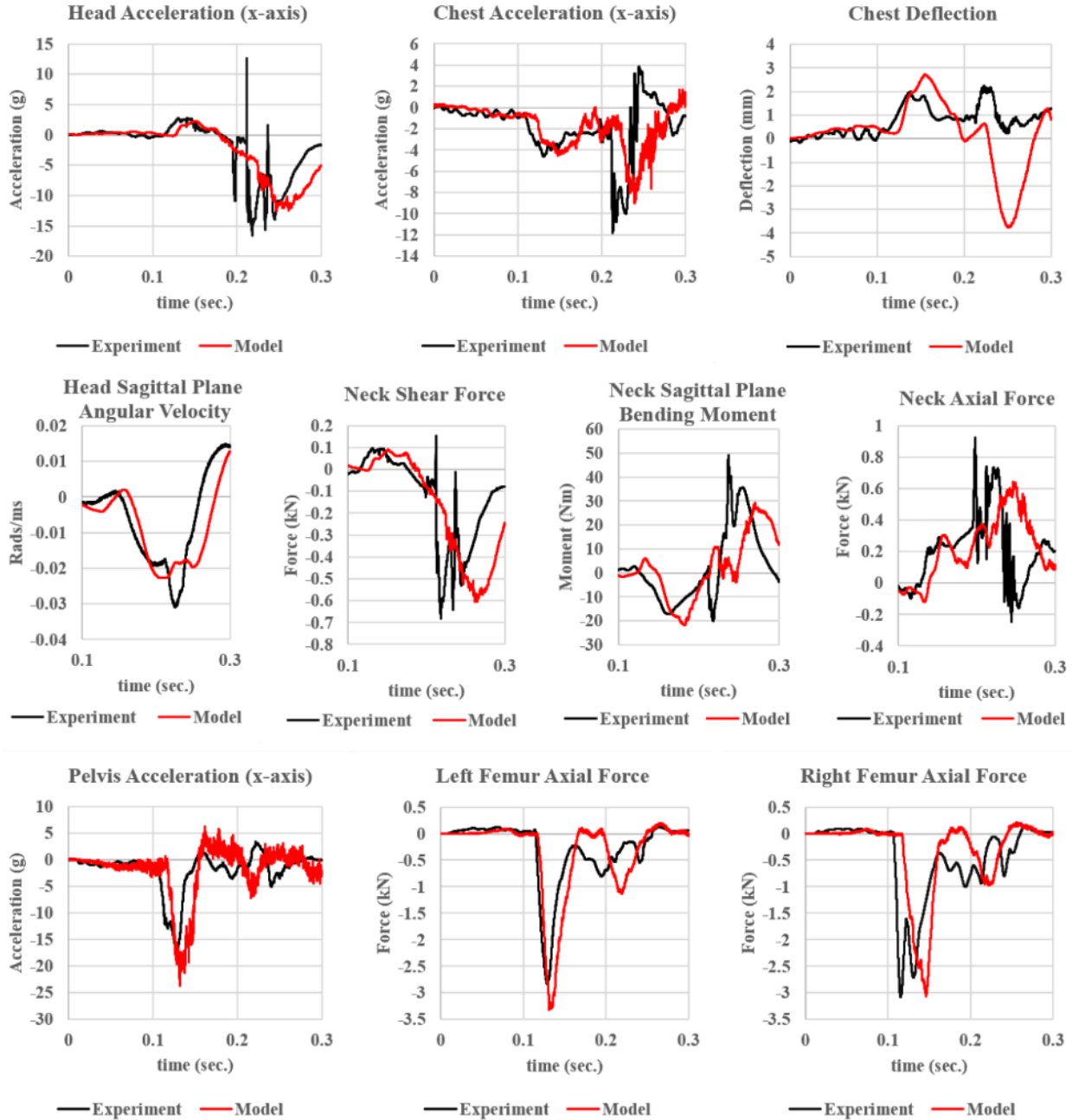


# 5<sup>th</sup> Percentile HIII

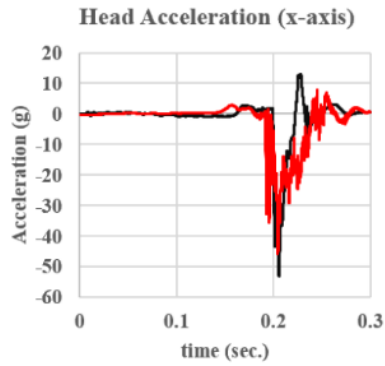


# Test Case #2c (6.5g Pulse, Reclined Posture, Inboard Seat)

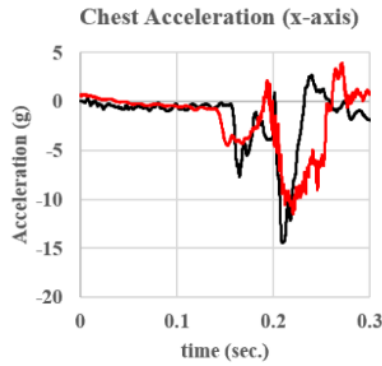
## 50<sup>th</sup> Percentile HIII



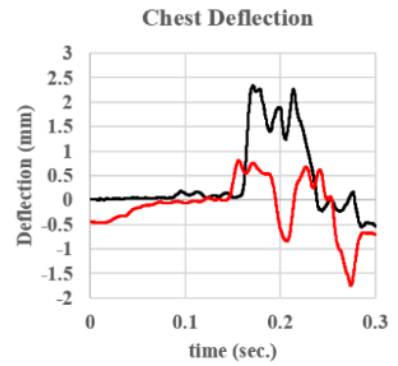
# 5<sup>th</sup> Percentile HIII



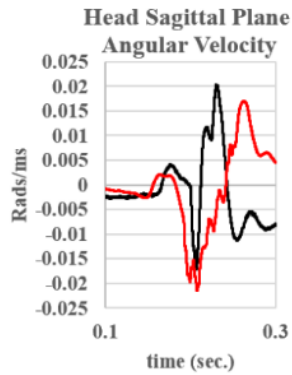
— Experiment — Model



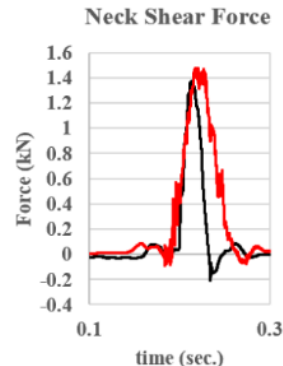
— Experiment — Model



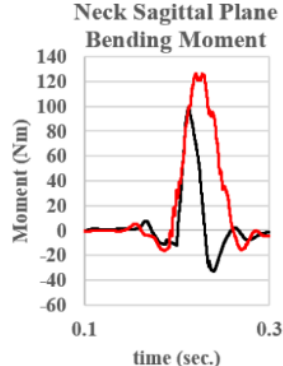
— Experiment — Model



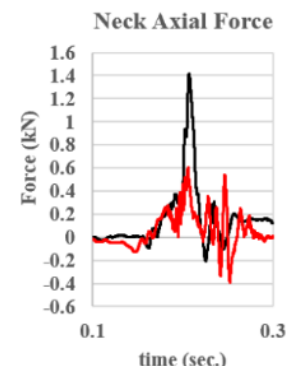
— Experiment — Model



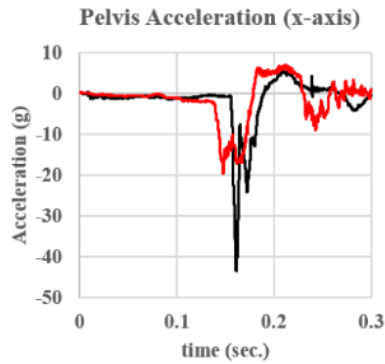
— Experiment — Model



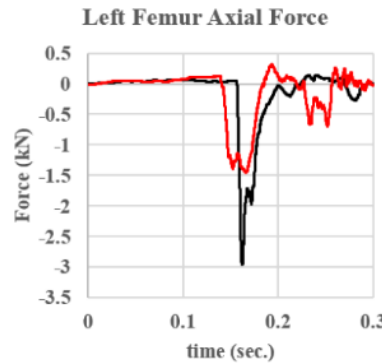
— Experiment — Model



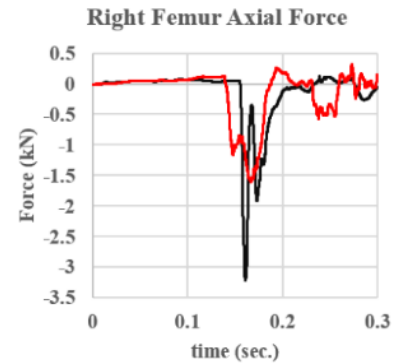
— Experiment — Model



— Experiment — Model



— Experiment — Model

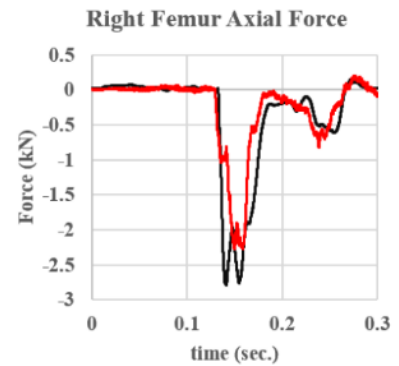
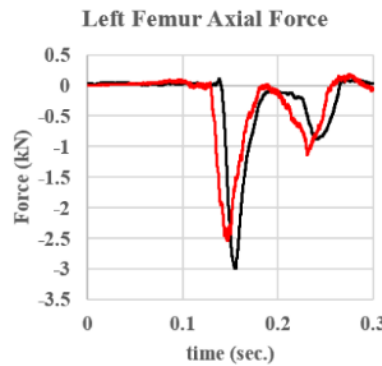
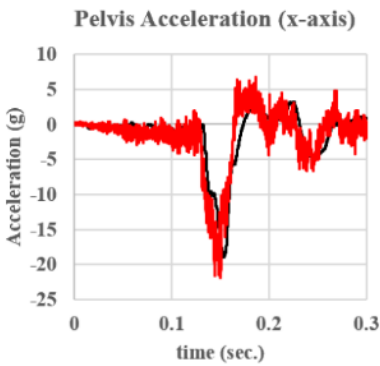
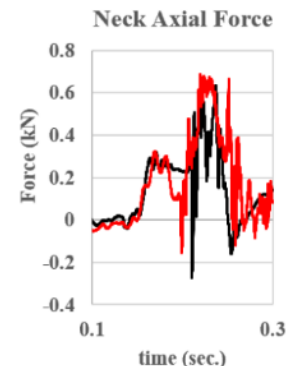
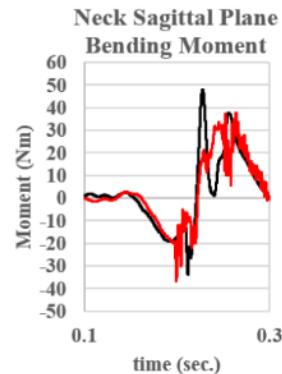
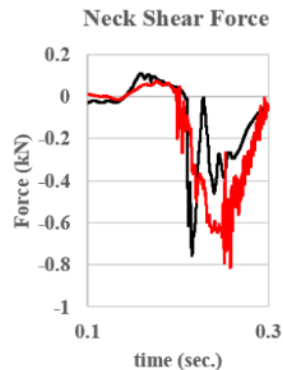
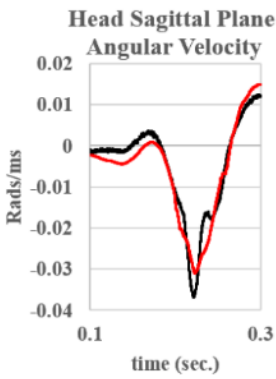
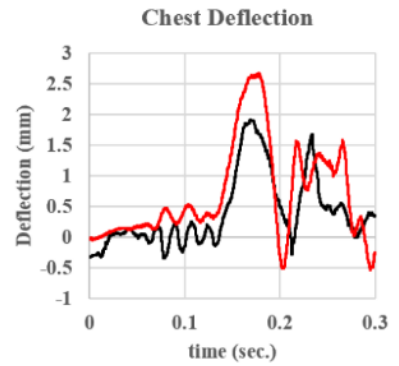
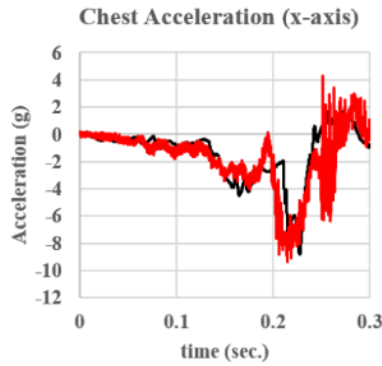
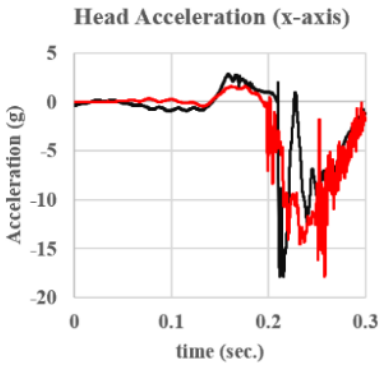


— Experiment — Model

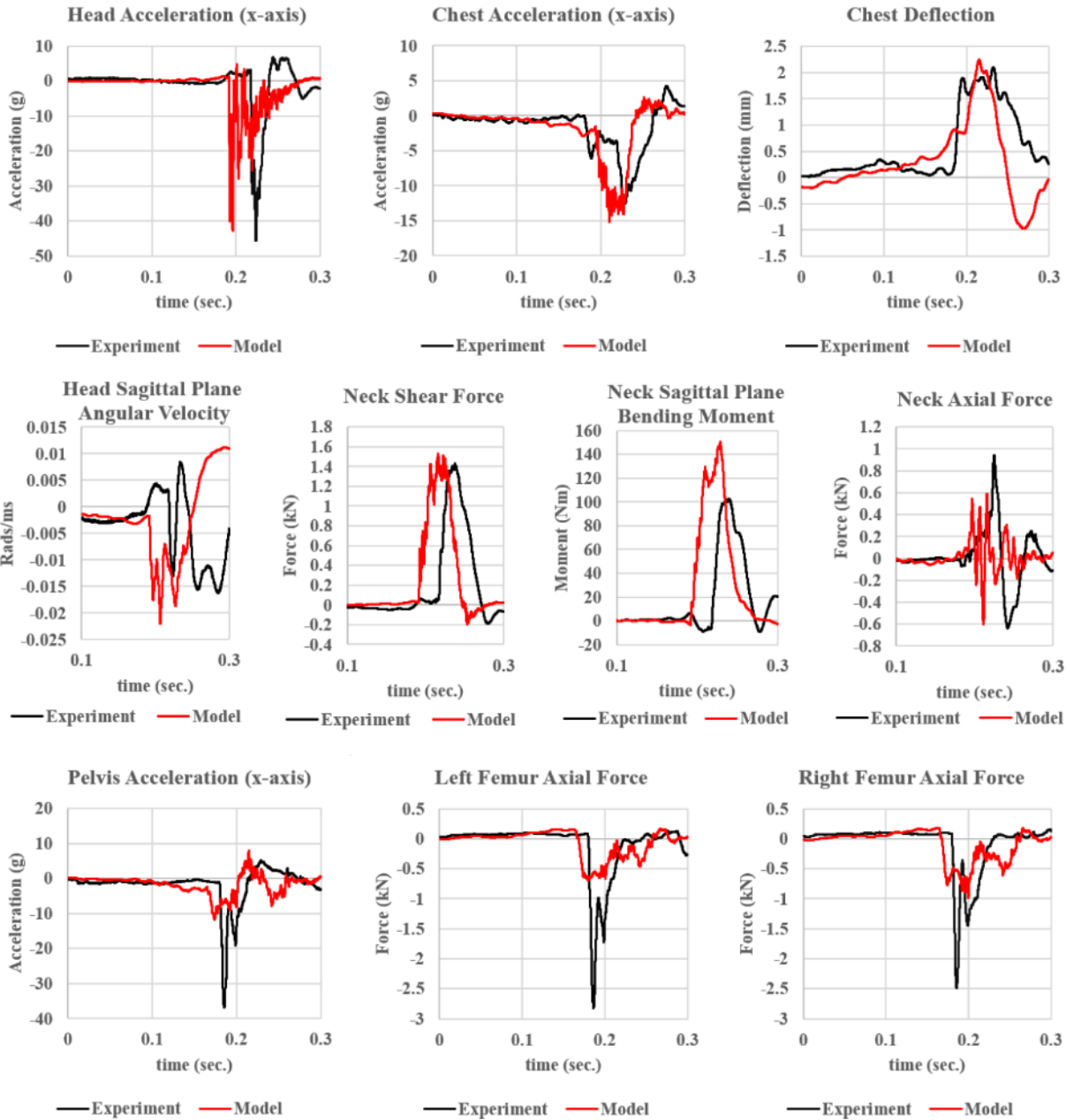


# Test Case #3 (5.7g Pulse, Upright Posture, Inboard Seat)

## 50<sup>th</sup> Percentile HIII

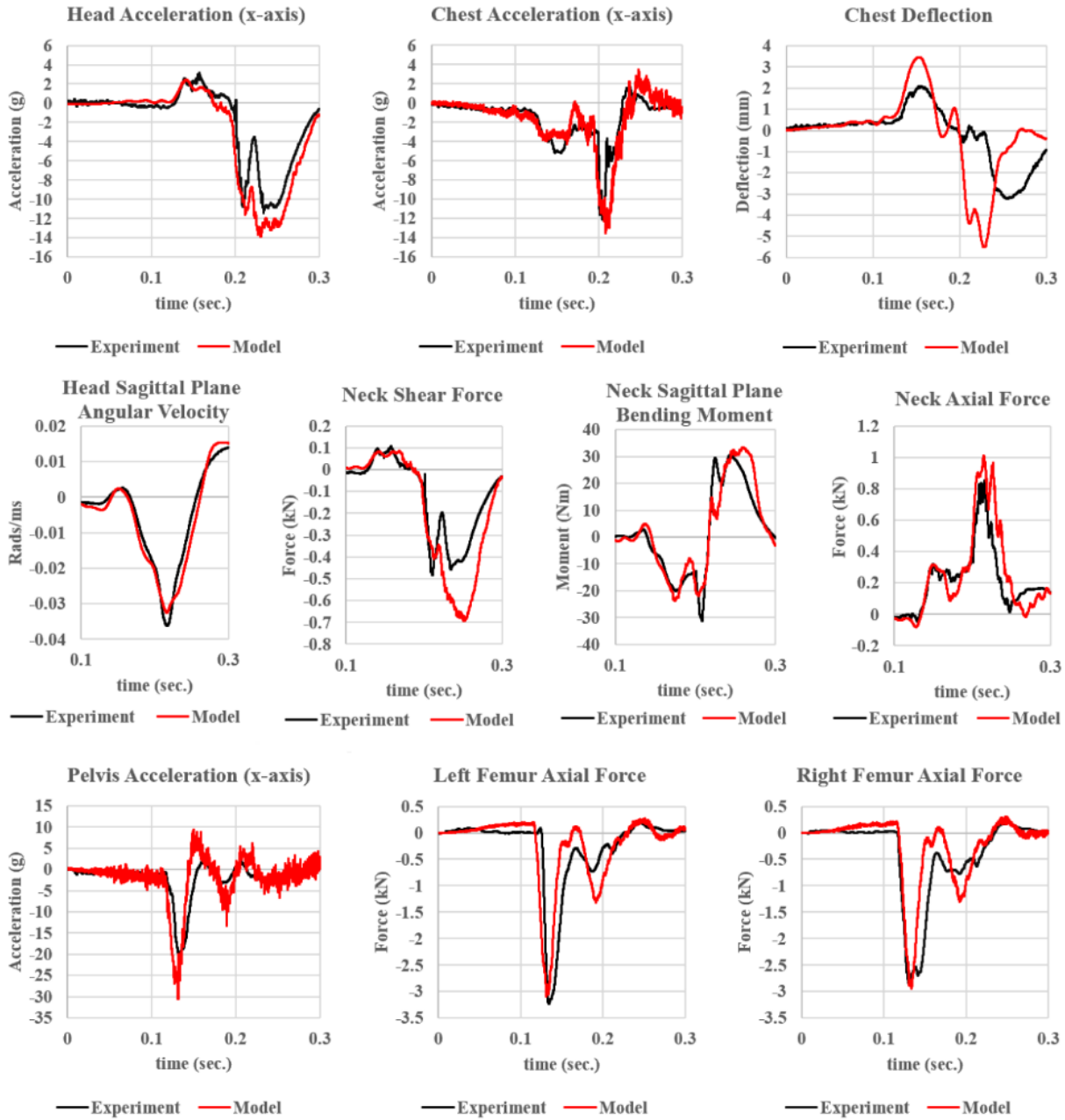


# 5<sup>th</sup> Percentile HIII

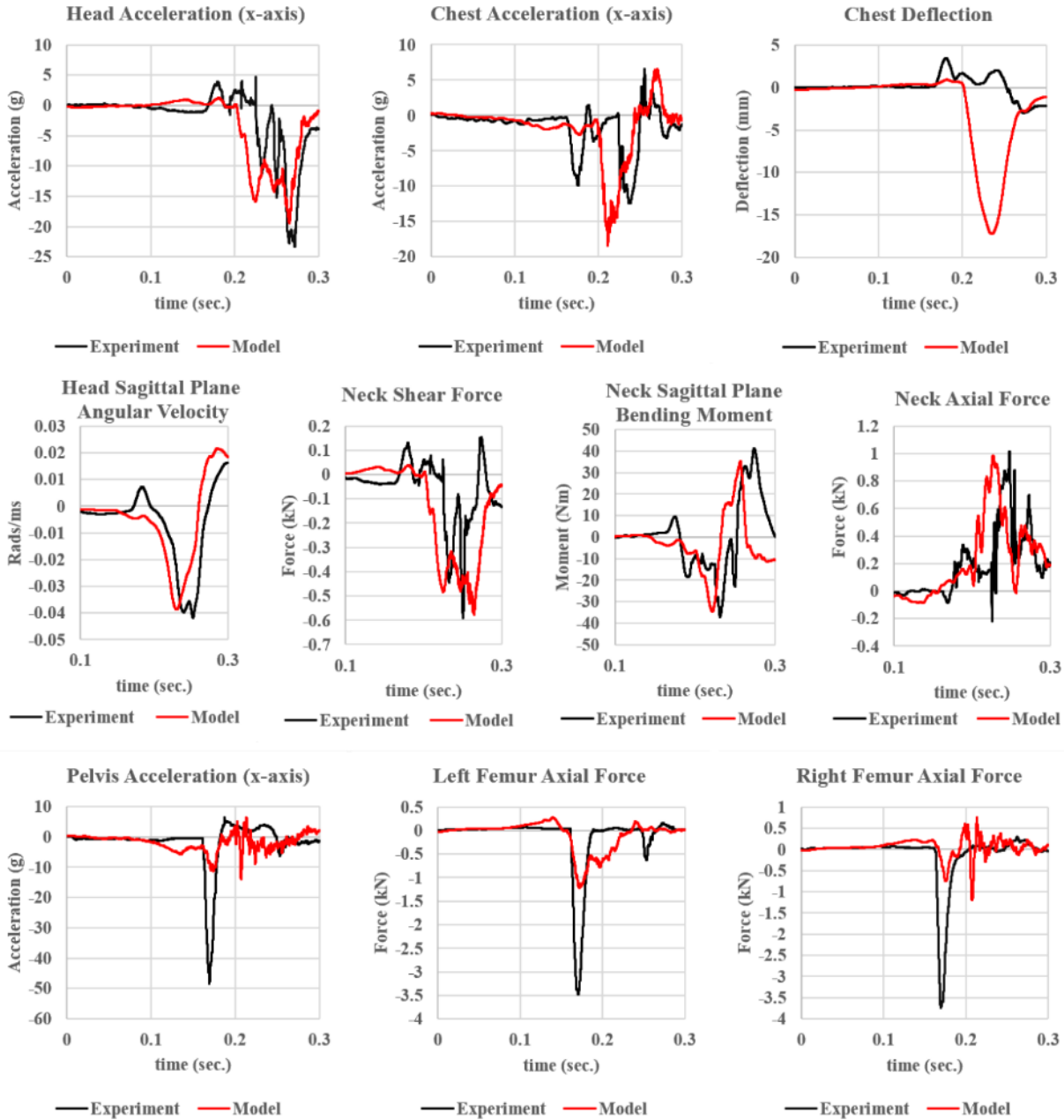


# Test Case #4 (6.5g Pulse, Upright Posture, Outboard Seat)

## 50<sup>th</sup> Percentile HIII

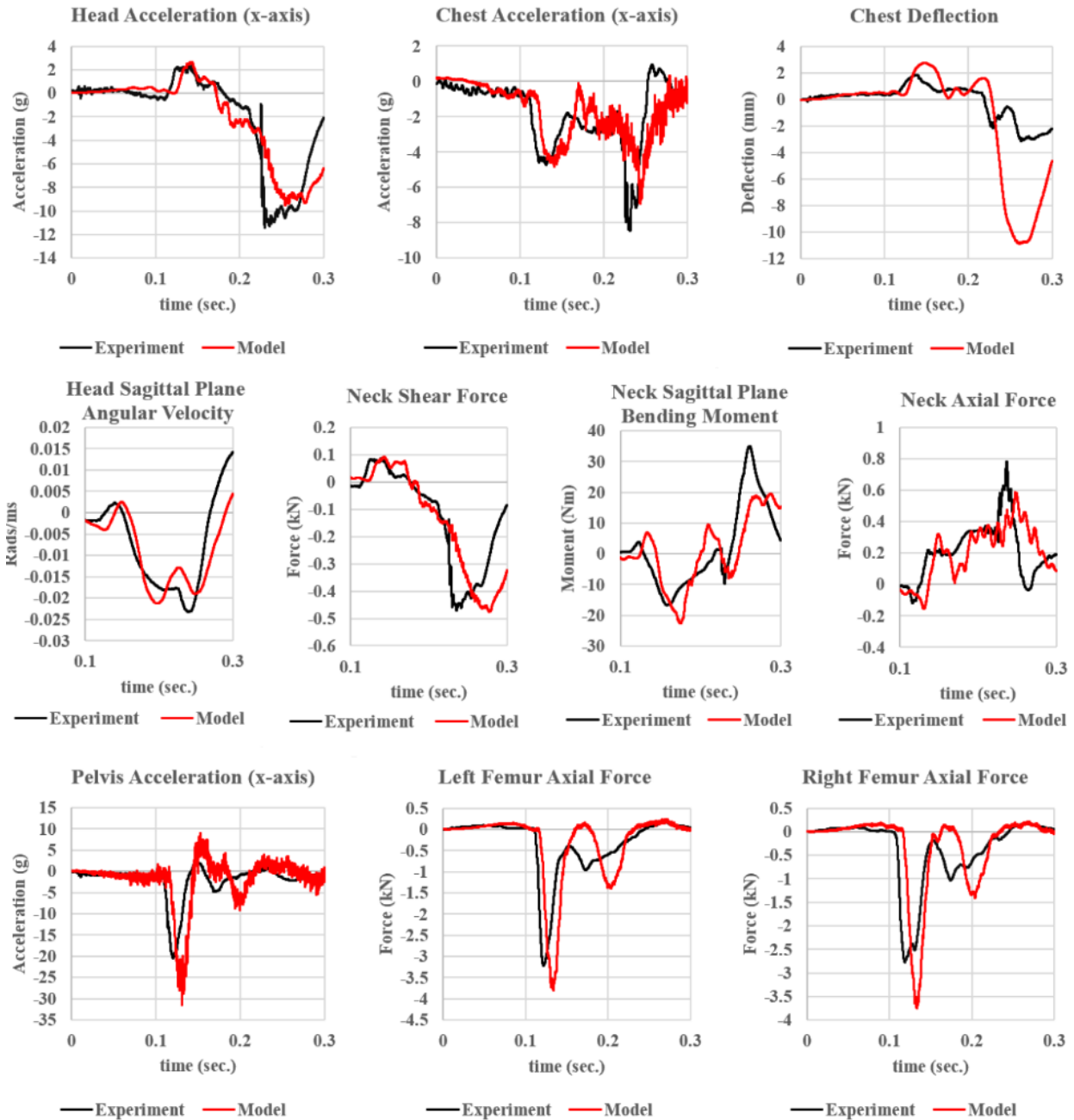


# 5<sup>th</sup> Percentile HIII

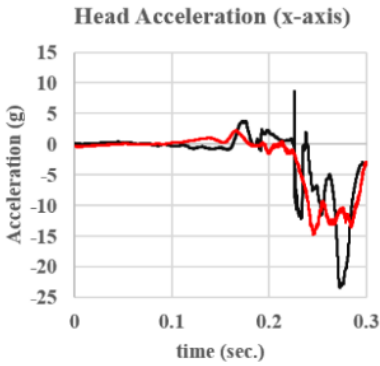


# Test Case #5 (6.5g Pulse, Reclined Posture, Outboard Seat)

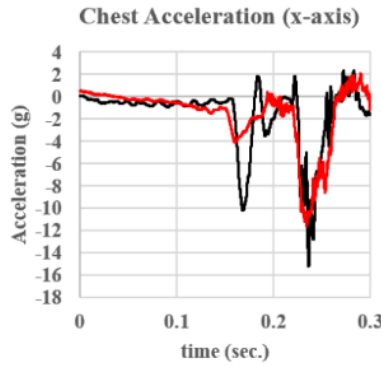
## 50<sup>th</sup> Percentile HIII



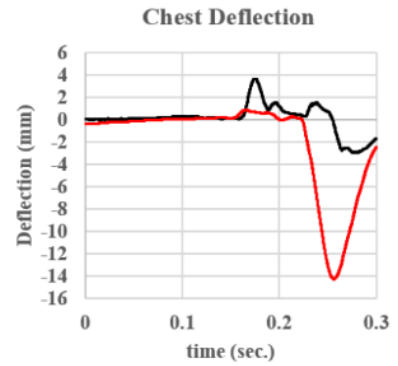
# 5<sup>th</sup> Percentile HIII



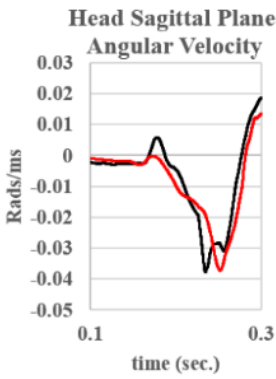
— Experiment — Model



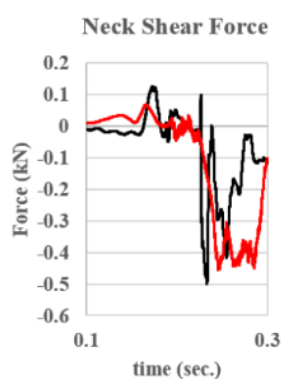
— Experiment — Model



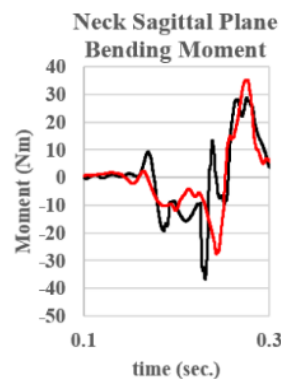
— Experiment — Model



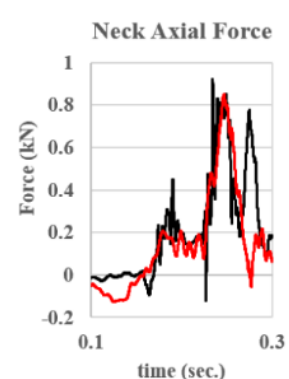
— Experiment — Model



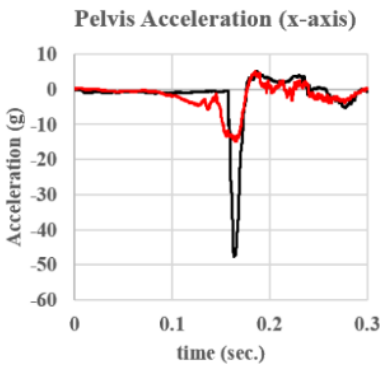
— Experiment — Model



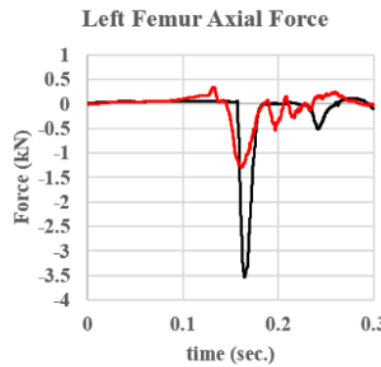
— Experiment — Model



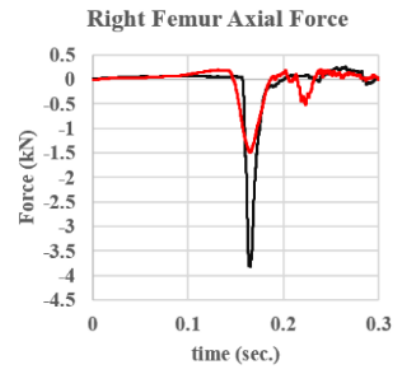
— Experiment — Model



— Experiment — Model



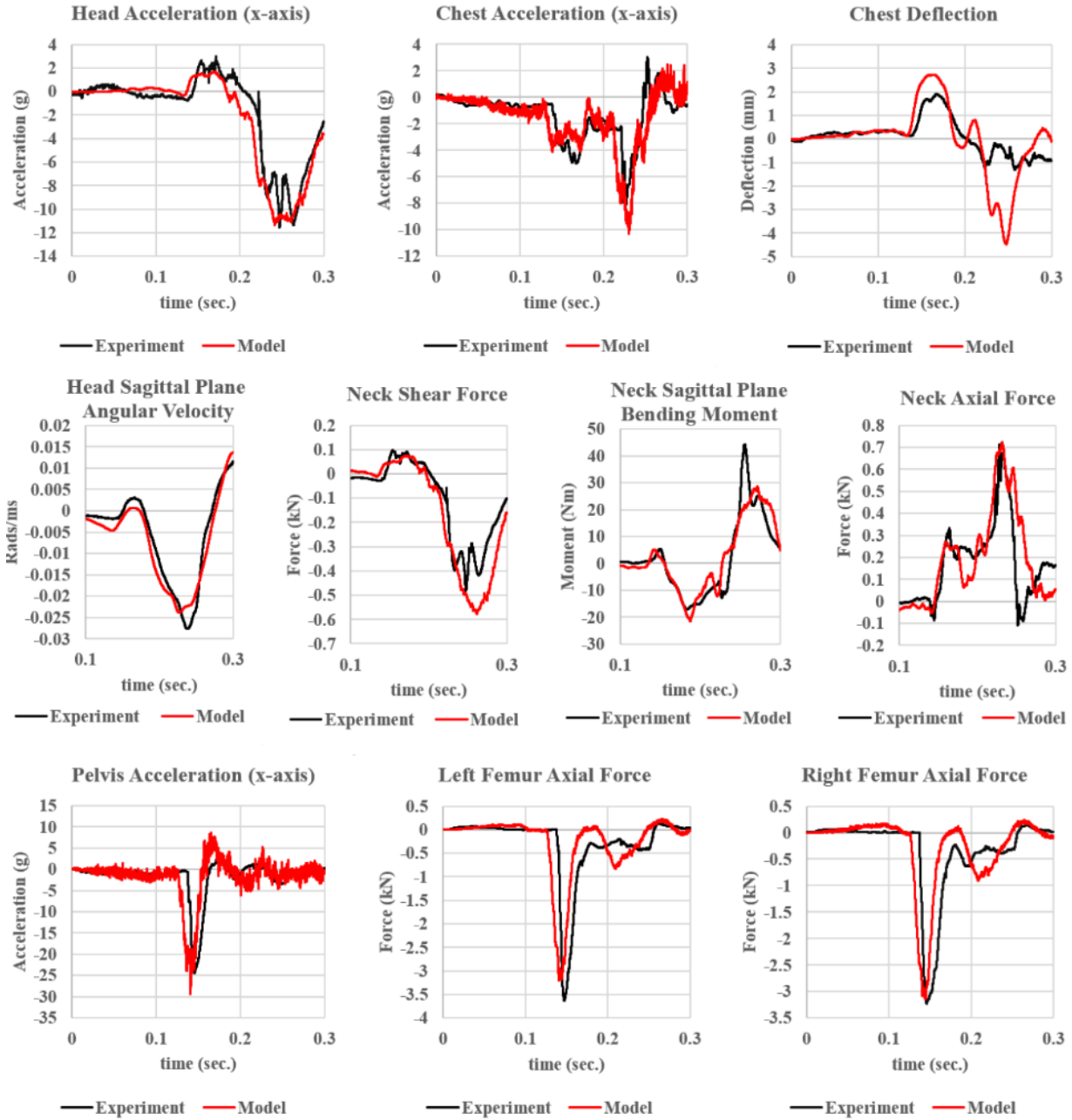
— Experiment — Model



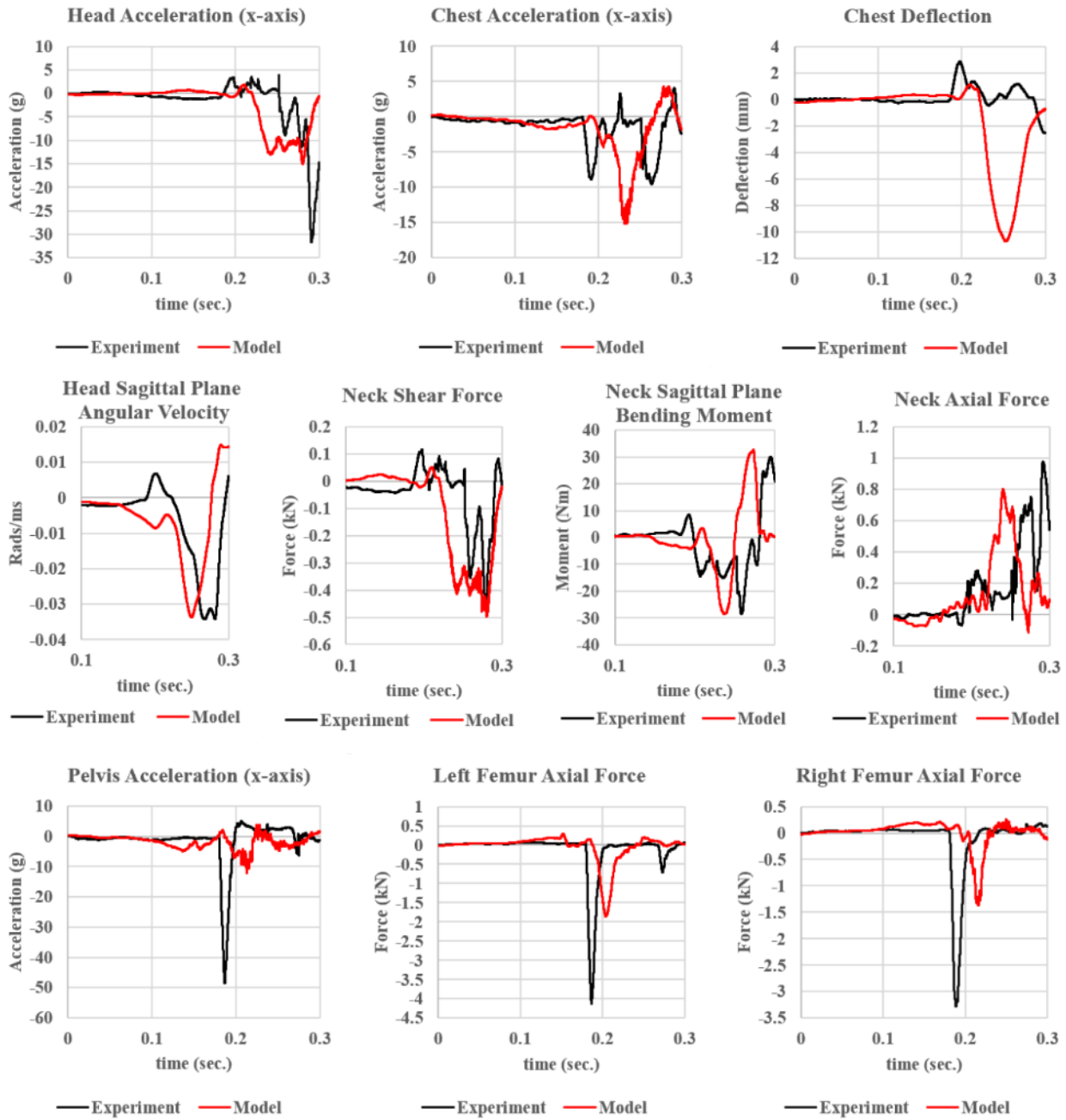
— Experiment — Model

# Test Case #6 (5.7g Pulse, Upright Posture, Outboard Seat)

## 50<sup>th</sup> Percentile HIII



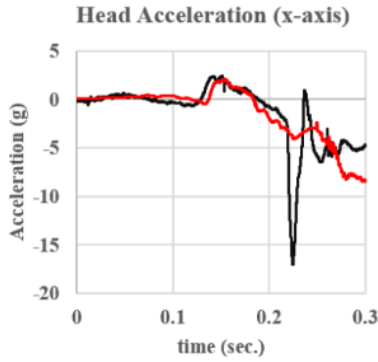
# 5<sup>th</sup> Percentile HIII



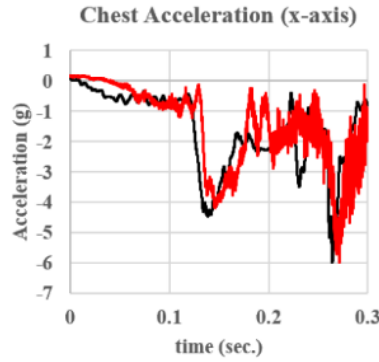


# Test Case #7 (5.7g Pulse, Reclined Posture, Outboard Seat)

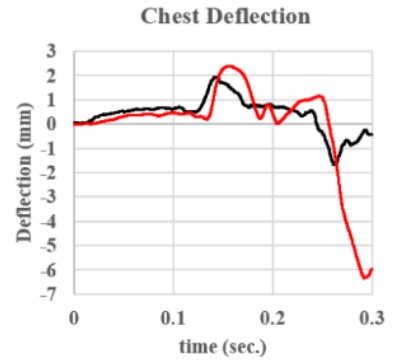
## 50<sup>th</sup> Percentile HIII



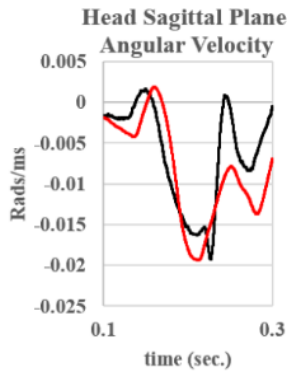
— Experiment — Model



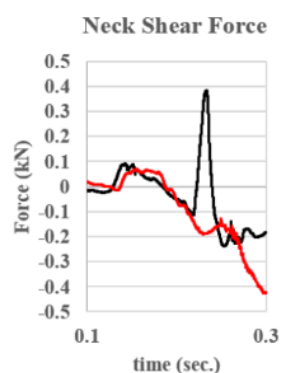
— Experiment — Model



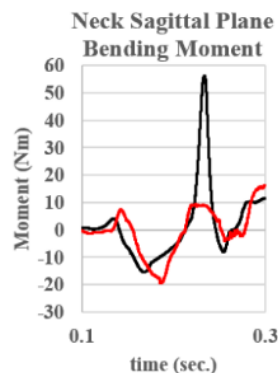
— Experiment — Model



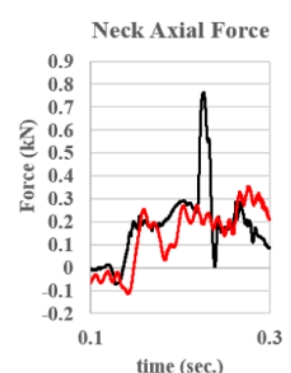
— Experiment — Model



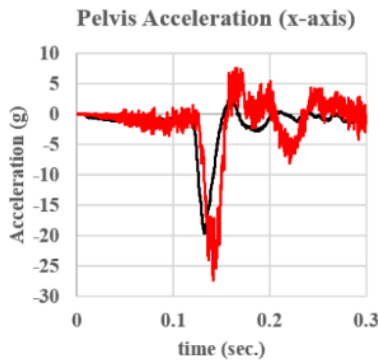
— Experiment — Model



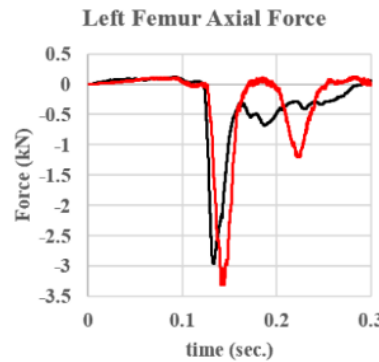
— Experiment — Model



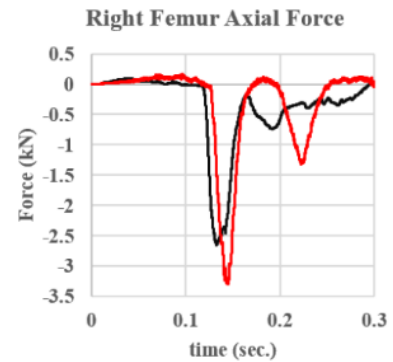
— Experiment — Model



— Experiment — Model

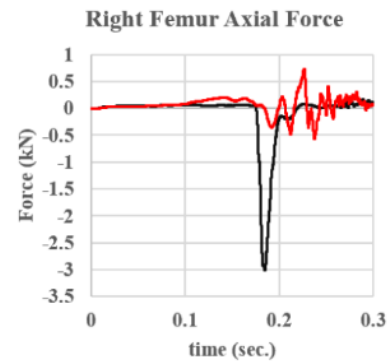
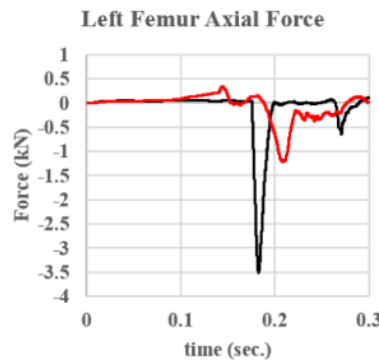
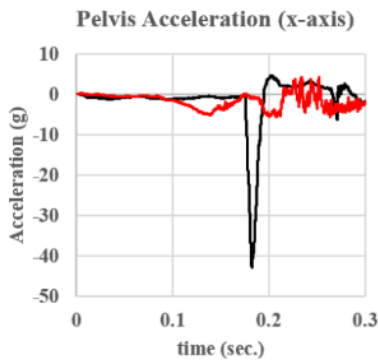
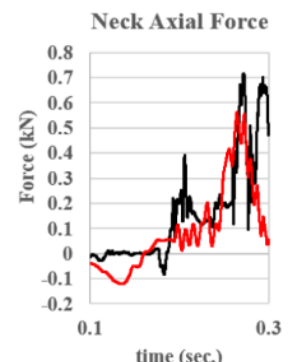
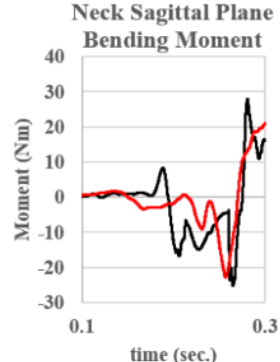
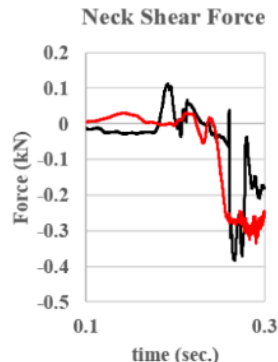
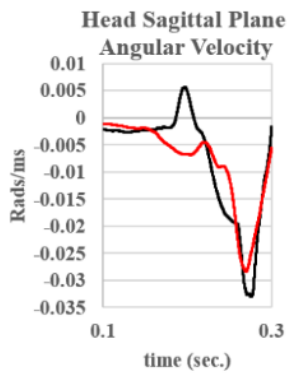
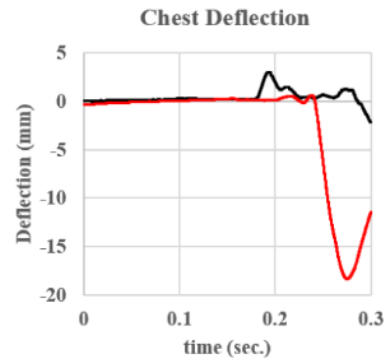
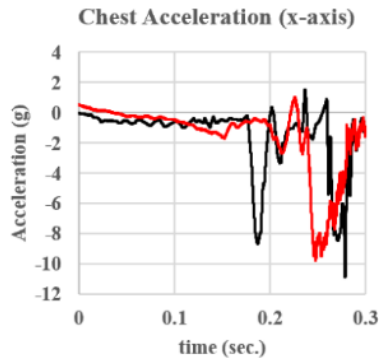
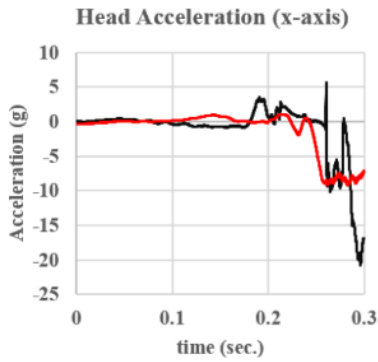


— Experiment — Model



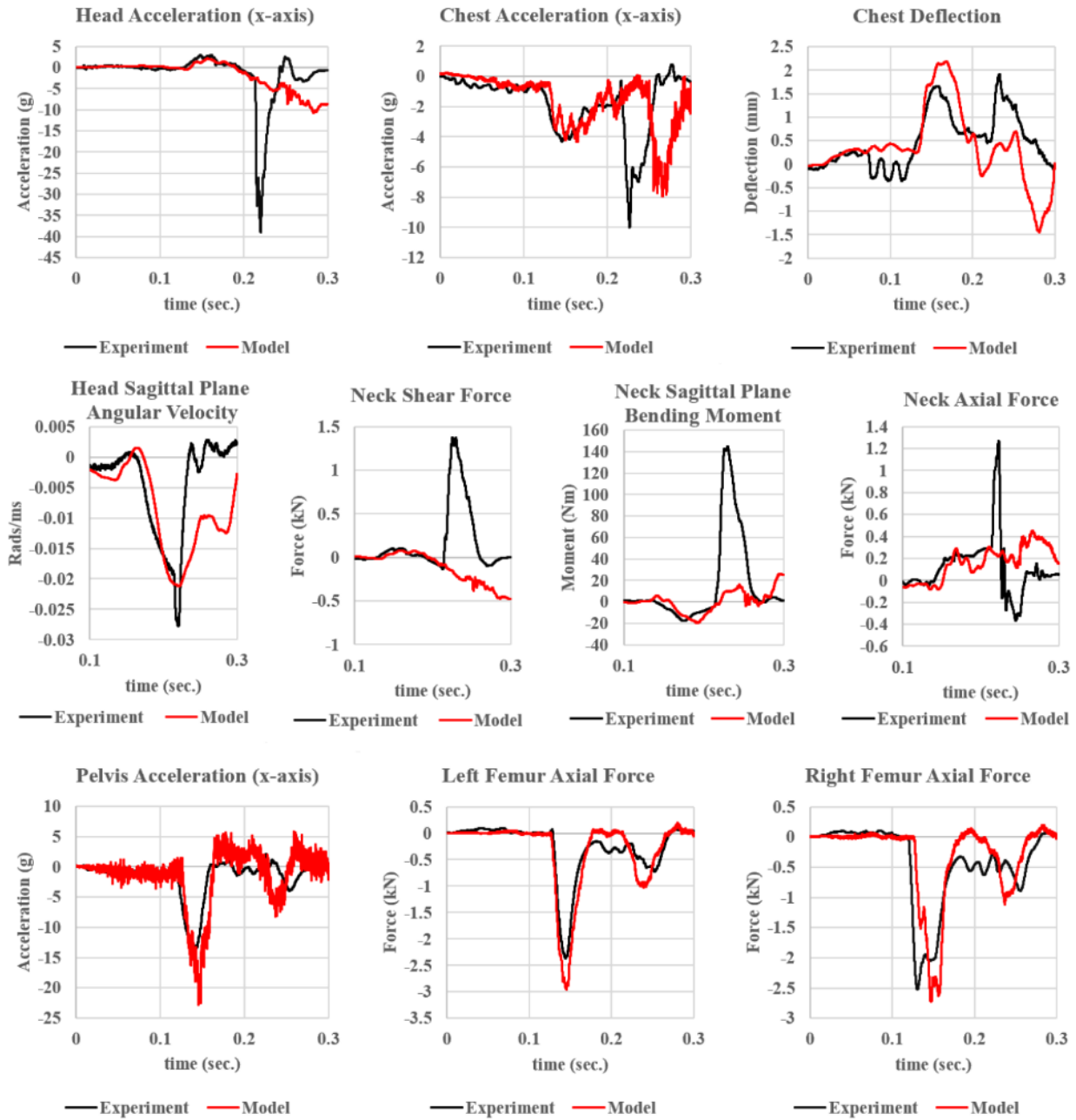
— Experiment — Model

# 5<sup>th</sup> Percentile HIII



# Test Case #8 (5.7g Pulse, Reclined Posture, Inboard Seat)

## 50<sup>th</sup> Percentile HIII



# 5<sup>th</sup> Percentile HIII

